

**UNIVERSITY OF QUEBEC AT CHICOUTIMI**

**THESIS PRESENTED TO THE  
UNIVERSITY OF QUEBEC AT CHICOUTIMI  
IN PARTIAL FULFILLMENT OF  
THE REQUIREMENTS FOR THE DEGREE OF  
DOCTOR OF PHILOSOPHY IN ENGINEERING**

**BY**

**HANY AMMAR**

**INFLUENCE OF METALLURGICAL PARAMETERS ON  
THE MECHANICAL PROPERTIES AND QUALITY INDICES OF Al-Si-Cu-Mg  
AND Al-Si-Mg CASTING ALLOYS**

**MAY 2010**

**UNIVERSITÉ DU QUÉBEC À CHICOUTIMI**

**THÈSE**

**PRÉSENTÉ À**

**L'UNIVERSITÉ DU QUÉBEC À CHICOUTIMI**

**COMME EXIGENCE PARTIELLE**

**DU DOCTORAT EN INGÉNIERIE**

**PAR**

**HANY AMMAR**

**INFLUENCE DES PARAMÈTRES MÉTALLURGIQUES SUR LES  
PROPRIÉTÉS MÉCANIQUES ET L'INDICE DE QUALITÉ POUR LES  
ALLIAGES COULÉS Al-Si-Cu-Mg ET Al-Si-Mg**

**MAI 2010**

*Dedicated to my parents, my wife Basma,  
and to my children Hala and Ahmed.*

## RÉSUMÉ

La présente étude a été réalisée en vue d'enquêter sur l'influence d'un certain nombre de paramètres métallurgiques sur les propriétés de traction et les indices de qualité de deux alliages de fonderie à haute résistance Al-9%Si, à savoir les alliages 354 et 359, contenant respectivement 1,8% Cu-0,5 % Mg et 0,5% Mg. Ces alliages ne sont que très peu utilisés par les fondeurs malgré le fait qu'ils sont prometteurs dans plusieurs domaines d'applications d'ingénierie en raison de leur résistance supérieure. Afin de valider leur utilisation dans des applications industrielles, une solide base de données a été créée grâce à la présente étude. De plus, une corrélation entre les propriétés de traction, les indices de qualité et les paramètres métallurgiques les plus communs affectant et contrôlant les propriétés de ces alliages a été réalisée. Les variables étudiées sont notamment le niveau de fer, la teneur en cuivre, le niveau de magnésium, la teneur en strontium, le taux de solidification, les températures et les temps des traitements thermiques (mise en solution et le vieillissement). Les chartes d'indice de qualité ont été utilisées comme outil d'évaluation pour sélectionner les conditions optimales à appliquer dans afin de développer une résistance élevée et une qualité optimale des alliages de fonderie 354 et 359.

Une analyse des résultats montre que l'addition de fer a des effets délétères sur la force et la qualité des alliages 354 et 359. Ces effets sont liés à la taille et à la morphologie des phases contenant du fer, en particulier les phases  $\beta$ -Al<sub>3</sub>FeSi et  $\pi$ -Al<sub>8</sub>Mg<sub>3</sub>FeSi<sub>6</sub>. L'addition de cuivre aux alliages de type 359 joue un rôle important dans l'amélioration de la résistance, cette amélioration se produit cependant au détriment de la ductilité et ainsi une faible influence sur l'indice de qualité est noté. L'ajout jusqu'à 0,6% de magnésium à l'alliage 359 améliore considérablement la résistance sans affecter l'indice de qualité. L'augmentation du niveau de Mg au-delà 0,6% se traduit par une légère augmentation de la résistance de l'alliage avec une réduction notable de la ductilité et de l'indice de qualité due à la formation d'une fraction volumique importante de la phase  $\pi$ -Al<sub>8</sub>Mg<sub>3</sub>FeSi<sub>6</sub>.

Un taux de solidification rapide améliore les propriétés de traction et les indices de qualité des deux alliages 354 et 359. L'amélioration de ces propriétés des indices de qualité sont liés à l'amélioration des caractéristiques des microstructures qui accompagne le taux de solidification rapide, à savoir: le raffinement de la structure dendritique (c'est à dire une fine DAS), la modification des particules de silicium eutectique, la réduction du niveau de porosité et de la taille des pores, la réduction de la taille et de la fraction volumique des phases intermétalliques formées.

Une augmentation de la température de mise en solution améliore la résistance et la qualité des pièces moulées par rapport à la condition telle que coulée. Conformément à ces constatations, les températures maximales sécuritaires de mise en solution de 520°C et de 537°C sont respectivement recommandées pour le traitement thermique de pièces moulées pour les alliages 354 et 359 afin de produire une résistance et un indice de qualité optimaux. Une mise en solution à ces températures produit un certain nombre des

changements bénéfiques dans la microstructure ce qui se traduit par une amélioration importante de la résistance et de l'indice de qualité. Une mise en solution à des températures supérieures à 525°C entraîne la fonte naissante des phases  $Al_2Cu$  dans les alliages 354 et la formation d'un niveau élevé de porosité lors du retrait des pièces coulées après trempe. En conséquence de la fonte naissante, les particules de silicium dans la microstructure montrent une morphologie polygonale dans les régions où la fonte de la phase  $Al_2Cu$  s'est produite.

Une augmentation du temps de mise en solution améliore encore les propriétés de traction et les valeurs de l'indice de qualité des alliages 354 et 359. Douze heures a été jugé comme temps optimal pour le traitement thermique des pièces coulées. Le temps de mise en solution nécessaire pour obtenir des propriétés de traction et des indices de qualité spécifiques pour les alliages 354 et 359 non modifiés peut être raccourci en modifiant ces alliages avec le strontium. Toutefois, l'effet bénéfique de l'addition du Sr sur la réponse des alliages 354 et 359 diminue à mesure que le temps de mise en solution augmente.

Un vieillissement à 155°C permet de produire une plus grande résistance et un indice de qualité optimal pour les deux alliages 354 et 359 par rapport à un vieillissement à des températures plus élevées. Le pic de résistance observée pour les alliages 354 et 359 peut être atteint après un temps de vieillissement plus court, à condition que la température de vieillissement soit accrue. Les temps de vieillissement nécessaire pour atteindre la résistance maximale pour l'alliage 354 sont de 72 heures, 40 heures, 8 heures, 1 heure et 15 minutes à des températures de vieillissement de 155°C, 170°C, 195°C, 220°C et 245°C respectivement, tandis que les temps de vieillissement nécessaires pour atteindre la résistance maximale dans l'alliage 359 sont de 32 heures, 24 heures, 1 heure, 30 minutes et 10 minutes respectivement, aux mêmes températures de vieillissement.

Un traitement de vieillissement à haute température est accompagné d'une réduction des propriétés de traction et de la valeur de l'indice de qualité. D'autre part, ce traitement introduit aussi la possibilité de réaliser des gains économiques importants en diminuant le temps et le coût du traitement. Un vieillissement à basse température (155°C) produit des précipités fins et denses ayant un espacement plus petit entre les particules, tandis qu'à une température plus élevée (245°C par exemple), les précipités sont moins denses, leur taille est plus grossière et ceux-ci sont dispersés plus largement dans la matrice. Il a été observé que les alliages 354 ont affichés des niveaux de résistance plus élevés, comparé aux alliages 359 et ce, pour tous les traitements de vieillissement. Cependant, cette haute résistance a été obtenue au détriment de la ductilité, entraînant de légères variations dans les valeurs de l'indice de qualité des pièces coulées à partir de l'alliage 354.

Les chartes des indices de qualité développées dans le cadre de cette recherche facilitent l'interprétation et l'évaluation des propriétés de traction des alliages 354 et 359 en vertu d'une variation des éléments d'alliage ajoutés, de la solidification et des conditions de traitement thermique étudiées. L'utilisation de ces chartes pour l'interprétation des

propriétés en traction fournit un moyen précis et logique pour déduire l'influence de ces paramètres métallurgiques sur ces alliages. Basée sur les chartes de qualité développées, il est possible de faire une sélection précise des conditions les plus appropriées requises pour obtenir le meilleur compromis possible entre la résistance d'un alliage, son indice de qualité et le coût de production.

## ABSTRACT

The current study was carried out with a view to investigating the influence of a number of metallurgical parameters on the tensile properties and quality indices of two high strength Al-9%Si casting alloys, namely, 354 and 359, containing 1.8%Cu-0.5%Mg and 0.5%Mg, respectively. These alloys are still not widely used by most foundrymen in spite of the fact that they are extremely promising for several fields of engineering applications because of their superior strength. For the purposes of validating their use in industrial applications, a solid data base was created, based on the present study, correlating the tensile properties and the quality indices of these alloys with the most common metallurgical parameters affecting and controlling the properties. The variables investigated include iron level; copper content; magnesium level; strontium content; solidification rate; solution heat treatment temperatures and times; and aging temperatures and times. Quality charts were used as an evaluation tool for selecting the optimum conditions to be applied in practice in order to develop high strength and optimum quality in 354 and 359-type castings.

An analysis of the results shows that the addition of iron has deleterious effects on both the strength and the quality of these alloys. These effects are related to the size and morphology of the iron-containing phases, specifically,  $\beta$ -Al<sub>5</sub>FeSi and  $\pi$ -Al<sub>8</sub>Mg<sub>3</sub>FeSi<sub>6</sub> present in the alloys. The addition of copper to 359-type alloys plays a significant role in improving the alloy strength; this improvement occurs, however, at the expense of ductility and therefore only a slight effect on the quality index is noted. The addition of up to 0.6% magnesium to 359-type alloys considerably improves their strength without affecting the quality. Increasing the Mg-level beyond 0.6% results in a slight increase in the alloy strength with a noticeable reduction in ductility and quality index due to the formation of a large volume fraction of the  $\pi$ -Al<sub>8</sub>Mg<sub>3</sub>FeSi<sub>6</sub> phase.

A rapid solidification rate enhances the tensile properties and quality indices of both 354 and 359 alloys. Such enhanced properties and indices are related to the refinement of the microstructural features which accompanies the high solidification rate, namely, refinement of the dendritic structure (i.e. a finer SDAS); modification of the eutectic silicon particles; reduced porosity levels and pore size; and reduced sizes and volume fractions of the intermetallic phases formed.

An increase in the solutionizing temperature improves the strength and quality of the castings compared to the as-cast condition. In accordance with these findings, maximum safe solutionizing temperatures of 520°C and 537°C are respectively recommended for heat treating 354 and 359-type castings to produce superior strength and optimum quality. Solution treatment at these temperatures is observed to bring about a number of improvements in the microstructure by which the strength and the quality are thereby enhanced. Solution treatment at temperatures above 525°C results in the incipient melting of the Al<sub>2</sub>Cu phases in the 354 alloys and the formation of high levels of shrinkage porosity after quenching. As a consequence of the incipient melting, silicon particles in the

microstructure exhibit a polygonal morphology in areas where the melting of the  $Al_2Cu$  phase has occurred.

An increase in the solution heat treatment time further enhances the tensile properties and the quality index values of the 354 and 359 alloys. Twelve hours was judged as the optimum solution heat treatment time for these castings. The solution time required to obtain a specific level of tensile properties and quality index in the unmodified 354 and 359 alloys may be shortened by modifying these alloys with strontium. However, the beneficial effect of Sr-addition on the response of the 354 and 359 alloys to solution treatment diminishes as the solution heat treatment time is increased.

Aging at  $155^\circ C$  is observed to produce the highest strength and optimum quality in both 354 and 359-type castings compared to aging at higher temperatures. The peak-strength observed for 354 and 359 alloys may be attained after shorter aging times on condition that the aging temperature is increased. The aging times required for reaching peak-strength in 354 alloys are 72 hours, 40 hours, 8 hours, 1 hour, and 15 minutes at aging temperatures of  $155^\circ C$ ,  $170^\circ C$ ,  $195^\circ C$ ,  $220^\circ C$ , and  $245^\circ C$ , respectively, while the aging times required for reaching peak-strength in 359 alloys are 32 hours, 24 hours, 1 hour, 30 minutes, and 10 minutes, respectively, at these same aging temperatures.

Aging at higher temperatures is accompanied by a reduction in the tensile properties and quality index value. On the other hand, it also introduces the possibility of achieving significant economic gains by minimizing the time and cost of the treatment. Aging treatment at the lower temperature of  $155^\circ C$  produces fine and dense precipitates having smaller inter-particle spacings, while at a higher aging temperature such as  $245^\circ C$ , the precipitates are coarser in size, less dense, and more widely dispersed in the matrix. The 354 alloys were observed to display higher strength levels when compared to the 359 alloys for all aging treatments. This high strength, however, was obtained at the expense of ductility, resulting in slight variations in the quality index values of the 354 castings.

The quality charts developed in the course of the current research facilitate the interpretation and evaluation of the tensile properties of the 354 and 359 alloys under the various alloying, solidification, and heat treatment conditions studied. The use of these charts in the interpretation of the tensile properties provides an accurate and logical means to deduce the influence of such metallurgical parameters on these alloys. Based on the quality charts developed, it is possible to make an accurate selection of the most suitable conditions required to obtain the best compromise between alloy strength, quality and cost-effectiveness.

## ACKNOWLEDGEMENTS

I am profoundly grateful to my supervisors, Prof Fawzy H. Samuel and Prof Agnes M. Samuel, for their supervision, guidance, and support from the initial to the final stages of this study.

I am indebted to Dr. Geoffrey K. Sigworth and Dr. Jen C. Lin for proposing the work plan for the current study, for constructive discussion, and for invaluable comments provided throughout the duration of this study.

Financial support received from Alcoa Canada Ltd, General Motors Powertrain Group (USA), Natural Sciences and Engineering Research Council of Canada (NSERC), Egyptian Bureau of Cultural and Educational Affairs in Canada, and the Fonds québécois de la recherche sur la nature et les technologies (FQRNT) through the intermediary of the Aluminum Research Centre (REGAL) is gratefully acknowledged.

It is a pleasure to thank all those who have contributed in any way to the completion of this study: Mr Alain Bérubé from TAMLA Group for carrying out the foundry work; Mme Helen Campbell from McGill University for assistance in using the electron microscope facilities; and Mme Marion Sinclair for revising the text of my thesis.

I am grateful to my wife Basma Khattab for providing me with a harmonious atmosphere so conducive to study; I would like to take this opportunity to express my profound gratitude to her for her moral support and patience.

## PUBLICATIONS

Eleven publications in the form of journal articles, conference papers and posters were prepared from the current Ph.D. study. Seven of these have been published or are in press; the remaining four are articles which will be submitted shortly to referred journals.

Full details are provided below.

### Refereed Journal Papers

1. H.R. Ammar, F.H. Samuel, A.M. Samuel, G.K. Sigworth and J.C. Lin, "Appropriate Heat Treatment for Improving Strength and Quality of 354-Type Casting Alloys," *AFS Transactions*, Vol. 118, 2010, in Press.
2. H.R. Ammar, F.H. Samuel, A.M. Samuel, G.K. Sigworth and J.C. Lin, "Developing Superior Strength and Optimum Quality in Al-9%Si-0.5%Mg Casting Alloys for Structural Applications," *AFS Transactions*, Vol. 117, 2009, pp. 149-168.
3. H.R. Ammar, F.H. Samuel, A.M. Samuel, G.K. Sigworth and J.C. Lin, "Optimum Conditions for Precipitation Hardening in Al-9%Si-1.8%Cu-0.5%Mg Casting Alloys," Prepared for Submission to *Metallurgical & Materials Transactions A*, 2010.
4. H.R. Ammar, F.H. Samuel, A.M. Samuel, G.K. Sigworth and J.C. Lin, "Strengthening of Al-9%Si-0.5%Mg Casting Alloys through an Adequate Aging Treatment," Prepared for Submission to *Metallurgical & Materials Transactions A*, 2010.
5. H.R. Ammar, F.H. Samuel, A.M. Samuel, G.K. Sigworth and J.C. Lin, "Effects of Cooling Rate, Mg-Addition, Sr-Modification on the Mechanical Properties and the Quality of 359-Type Al-Si-Mg Casting Alloys," Prepared for Submission to *Materials Science & Engineering A*, 2010.
6. H.R. Ammar, F.H. Samuel, A.M. Samuel, G.K. Sigworth and J.C. Lin, "Age Hardening Behavior of 354- and 359-Type Casting Alloys," Prepared for Submission to *Materials Science & Engineering A*, 2010.

### Conference Presentations / Proceedings

7. H.R. Ammar, F.H. Samuel, A.M. Samuel, G.K. Sigworth and J.C. Lin, "Improved Strength and Quality of 354-Al-Si-Cu-Mg Alloys," *The 8th Arab Foundry Symposium*, 05-08 November 2010, Sharm El-Sheikh, Egypt.
8. H.R. Ammar, F.H. Samuel, A.M. Samuel, G.K. Sigworth and J.C. Lin, "Appropriate Heat Treatment for Improving Strength and Quality of 354-Type Casting Alloys," *114<sup>th</sup> Metalcasting Congress*, March 19-23, 2010, Orlando, Florida, USA.
9. H.R. Ammar, F.H. Samuel, A.M. Samuel, G.K. Sigworth and J.C. Lin, "Developing Superior Strength and Optimum Quality in Al-9%Si-0.5%Mg Casting Alloys for Structural Applications," *113<sup>th</sup> Metalcasting Congress*, April 7-10, 2009, Las Vegas, Nevada, USA.

### Scientific Posters

10. H.R. Ammar, F.H. Samuel, A.M. Samuel, G.K. Sigworth, J.C. Lin, E. Simielli and G. Dufour, "Premium Strength and Optimum Quality Al-Si-Cu-Mg Casting Alloys for Structural Applications," Poster presented at "Journée des Etudiants du REGAL" (REGAL Students Day), October 21, 2009, ETS, Montreal; Published in *The Encyclopaedia of Research on Aluminium in Quebec – 2009 Edition* (Strategic Aluminium Research Network), October 21, 2009, ETS, Montreal, Les Presses de l'Aluminium (PRAL), Chicoutimi, QC, Canada, 2010, Axis II – New Aluminium Products and Materials, in Press – **Winner of the CQRDA Award.**
11. H.R. Ammar, F.H. Samuel, A.M. Samuel, G.K. Sigworth, J.C. Lin and G. Dufour, "Developing Premium Strength and Superior Quality in Al-Si-Mg Castings for High-Strength Applications," Poster presented at "Journée des Etudiants du REGAL" (REGAL Students Day), November 28, 2008, McGill University, Montreal; Published in *The Encyclopaedia of Research on Aluminium in Quebec – 2008 Edition* (Strategic Aluminium Research Network), November 28, 2008, McGill University, Montreal, Les Presses de l'Aluminium (PRAL), Chicoutimi, QC, Canada, 2009, Axis II – New Aluminium Products and Materials, p. 44 – **Winner of the Alcoa Award.**

## TABLE OF CONTENTS

<b>RÉSUMÉ</b> .....	<b>i</b>
<b>ABSTRACT</b> .....	<b>iv</b>
<b>ACKNOWLEDGEMENTS</b> .....	<b>vi</b>
<b>PUBLICATIONS</b> .....	<b>vii</b>
<b>TABLE OF CONTENTS</b> .....	<b>ix</b>
<b>LIST OF FIGURES</b> .....	<b>xi</b>
<b>LIST OF TABLES</b> .....	<b>xviii</b>
<b>CHAPTER 1</b> .....	<b>1</b>
<b>INTRODUCTION AND OBJECTIVES</b> .....	<b>1</b>
1.1. INTRODUCTION .....	2
1.2. OBJECTIVES .....	4
<b>CHAPTER 2</b> .....	<b>6</b>
<b>SURVEY OF THE LITURATURE</b> .....	<b>6</b>
2.1. INTRODUCTION .....	7
2.2. ALUMINUM CASTINGS.....	7
2.3. ALUMINUM-SILICON CASTINGS .....	9
2.3.1. 354-Type Castings .....	13
2.3.2. 359-Type Castings .....	13
2.4. THE CONCEPT OF QUALITY INDICES AND QUALITY CHARTS FOR Al-Si CASTING ALLOYS.....	14
2.4.1. Quality Index (Q) Proposed by Drouzy <i>et al.</i> .....	15
2.4.2. Quality Index (Q <sub>N</sub> ) Proposed by Din <i>et al.</i> .....	17
2.4.3. Quality Index (Q <sub>C</sub> ) Proposed by Cáceres.....	19
2.4.4. Quality Index (Q <sub>D</sub> ) Proposed by Alexopoulos and Pantelakis.....	24
2.4.5. Quality Index (Q <sub>E</sub> ) Proposed by Tiryakioğlu <i>et al.</i> .....	27
2.5. METALLURGICAL FACTORS .....	28
2.5.1. Influence of Impurity Elements .....	29
2.5.2. Influence of Hardening Elements .....	32
2.5.3. Influence of Modification.....	36
2.5.4. Influence of Solidification Conditions .....	40
2.5.5. Influence of Heat Treatment.....	42
2.5.5.1. Solution Heat Treatment.....	42
2.5.5.2. Quenching .....	46

2.5.5.3. Aging Treatment .....	48
<b>CHAPTER 3.....</b>	<b>57</b>
<b>METHODOLOGY AND EXPERIMENTAL TECHNIQUES .....</b>	<b>57</b>
3.1. INTRODUCTION.....	58
3.2. MELTING AND CASTING PROCESSES.....	58
3.3. HEAT TREATMENT.....	64
3.4. MECHANICAL TESTING .....	66
3.5. MICROSTRUCTURAL CHARACTERIZATION .....	67
<b>CHAPTER 4.....</b>	<b>74</b>
<b>INFLUENCES OF ALLOY COMPOSITION, SOLIDIFICATION RATE, AND SOLUTIONIZING PARAMETERS.....</b>	<b>74</b>
4.1. INTRODUCTION.....	75
4.2. CHARACTERIZATION OF THE MICROSTRUCTURE.....	75
4.2.1. Characteristics of Intermetallic Phases .....	76
4.2.2. Characteristics of Eutectic Silicon Particles.....	85
4.2.3. Characteristics of Secondary Dendrite Arm Spacing (SDAS).....	93
4.3. EVALUATION OF TENSILE PROPERTIES AND QUALITY INDEX.....	96
4.3.1. Influence of Iron .....	97
4.3.2. Effects of Copper .....	107
4.3.3. Influence of Magnesium.....	111
4.3.4. Effects of Solidification Rate .....	120
4.3.5. Influence of Solution Heat Treatment Parameters.....	130
4.3.5.1. Influence of Solutionizing Temperature.....	130
4.3.5.2. Influence of Solution Heat Treatment Time.....	143
<b>CHAPTER 5.....</b>	<b>151</b>
<b>INFLUENCE OF AGING PARAMETERS.....</b>	<b>151</b>
5.1. INTRODUCTION.....	152
5.2. AGING BEHAVIOR OF 354 CASTING ALLOYS .....	153
5.3. AGING BEHAVIOR OF 359 CASTING ALLOYS .....	177
5.4. COMPARISON BETWEEN AGING BEHAVIOR OF 354 AND 359 ALLOYS.. .....	191
<b>CHAPTER 6.....</b>	<b>199</b>
<b>CONCLUSIONS AND RECOMMENDATIONS.....</b>	<b>199</b>
<b>RECOMMENDATIONS FOR FUTURE WORK.....</b>	<b>206</b>
<b>REFERENCES.....</b>	<b>207</b>
<b>APPENDIX.....</b>	<b>226</b>

## LIST OF FIGURES

### CHAPTER 2

Figure 2.1.	The growing trend of sharing aluminum alloys in the automotive industry, as seen over 50 years in North America. <sup>21,22</sup> .....	9
Figure 2.2.	Al-Si casting alloys: (a) Al-Si binary system; (b) microstructure of hypoeutectic alloys; (c) microstructure of eutectic alloys; (d) microstructure of hypereutectic alloys. <sup>32</sup> .....	12
Figure 2.3.	Example of the quality chart proposed by Drouzy <i>et al.</i> <sup>41</sup> generated using Equations 1 and 2.....	17
Figure 2.4.	Example of the quality chart proposed by Din <i>et al.</i> generated using Equation 3 for Al-Si-Mg casting alloys with $K = 50$ MPa.....	18
Figure 2.5.	A log-log plot of true stress versus true strain for calculating $n$ and $K$ values in Equation 4. <sup>46,47</sup> .....	19
Figure 2.6.	Determining the beginning of necking based on the true-stress/true-strain curve during tensile testing. <sup>46,47</sup> .....	20
Figure 2.7.	Example of the quality chart proposed by Cáceres illustrating <i>iso-flow</i> and <i>iso-q</i> lines generated using Equations 8 and 9, respectively, with $K = 511$ MPa. ....	23
Figure 2.8.	Two models of quality charts for the A356 alloy; the dashed lines are <i>iso-Q</i> and <i>iso-YS</i> lines calculated with Equations 1 and 2, respectively. The solid lines are <i>iso-flow</i> lines and <i>iso-q</i> lines calculated with Equations 8 and 9, respectively, with $K = 430$ MPa. <sup>44,45,48,49,51,53</sup> .....	25
Figure 2.9.	Example of the quality chart proposed by Alexopoulos and Pantelakis, as generated using Equation 16 with a $K_D$ value of unity.....	27
Figure 2.10.	Influence of Fe-level on the ductility of modified and unmodified 356-T6 alloys. <sup>72</sup> .....	30
Figure 2.11.	Tensile properties and quality index values of 356 alloys as a function of aging time at 155°C and iron content. <sup>72-74</sup> .....	31
Figure 2.12.	Effects of Mg-content on tensile properties and quality index of Al-7%Si alloy castings. <sup>72,74</sup> .....	33
Figure 2.13.	A quality index chart illustrating the effects of Mg-content, Fe-level, solidification rate, and heat treatment on the tensile properties and quality index of Al-7Si-Mg alloys. Under-aging and peak-aging conditions are indicated by solid symbols and open symbols, respectively. <sup>50</sup> .....	34
Figure 2.14.	Tensile properties of permanent mold Al-9%Si-0.5%Mg casting alloys having various Cu contents and subjected to T6- and T62-tempers. <sup>1</sup> .....	35
Figure 2.15.	Quality chart illustrating the influence of the content of Cu and other elements (Mg, Si, Fe, and Mn) as well as cooling rate, as indicated by arrows, on the strength and quality index of Al-Si-Cu-Mg alloys. The numbers 1 through 21 located in the chart represent various alloy compositions. <sup>2</sup> .....	37

Figure 2.16.	The quality index $Q$ as a function of the level of Sr for A356-T6 casting alloys subjected to three solidification rates. <sup>8, 89</sup> .....	39
Figure 2.17.	Quality chart illustrating the effects of solidification rate on the tensile properties and quality of A356-T6 alloy castings. The numerical values give the SDAS in microns. <sup>72</sup> .....	41
Figure 2.18.	The balance of forces between a moving dislocation and a precipitate resisting its motion. <sup>131</sup> .....	53
Figure 2.19.	Effects of aging temperature and time on the tensile properties and quality index of the sand-cast 356 Al-7%Si-0.3%Mg alloy. <sup>41</sup> .....	55
Figure 2.20.	Effects of aging temperature and aging time as a function of Mg-content on the probable yield strength and hardness of sand cast 356 Al-7%Si-0.3%Mg and 357 Al-7%Si-0.6%Mg alloys, for each temperature, using only the portion of the curves corresponding to the graduated part of the time scale. <sup>41</sup> .....	56

### CHAPTER 3

Figure 3.1.	Spectrolab Jr CCD Spark Analyzer used in the current study.....	60
Figure 3.2.	(a) ASTM B-108 permanent mold used for casting; and (b) schematic representation of the permanent mold casting used to prepare the tensile test specimens. <sup>133</sup> .....	61
Figure 3.3.	A schematic representation of (a) the end-chill mold casting block used to prepare the tensile test specimens; (b) the blank used to machine the test specimen; and (c) the dimensions of test specimens prepared according to ASTM E8M-04 standards. <sup>134</sup> .....	63
Figure 3.4.	The MTS Servohydraulic mechanical testing machine used in the current study.....	67
Figure 3.5.	Clemex Vision PE4 image analysis system used for the present work. ....	69
Figure 3.6.	The electron probe microanalyzer (EPMA) system used in the current study. ....	71
Figure 3.7.	Scanning electron microscope system used in this work.....	73
Figure 3.8.	Field emission scanning electron microscopy used in the current study. ....	73

### CHAPTER 4

Figure 4.1.	Volume fraction of intermetallic phases observed in the 354 and 359 alloys which were cast using a graphite mold preheated to 600°C: (a) soluble Al <sub>2</sub> Cu phase, and (b) partially soluble Fe- and Cu-bearing phases. (It should be noted that the maximum solutionizing temperature applied to alloys coded 10S through 12S is 520°C.).....	78
Figure 4.2.	Morphology of the intermetallic phases observed in 9S alloy samples: (a) as-cast; (b) after solutionizing at 490°C; (c) and (d) after solutionizing at 537°C (samples were obtained from the gauge length of B108 test bars).....	83
Figure 4.3.	The intermetallic phases observed in 12S alloy samples: (a) $\beta$ -Al <sub>3</sub> FeSi and $\pi$ -Al <sub>8</sub> Mg <sub>3</sub> FeSi <sub>6</sub> phases in the as-cast condition; (b) backscattered image showing partially soluble phases remaining after solutionizing at 520°C; (c)	

	fragmentation of $\beta$ -Al <sub>5</sub> FeSi phase after solutionizing at 520°C (samples were obtained from the gauge length of B108 test bars).....	84
Figure 4.4.	Morphology of eutectic silicon particles observed in non-modified and modified 359 casting alloys under the following conditions: (a) and (c) non-modified and modified alloys in the as-cast conditions, respectively; (b) and (d) non-modified and modified alloys after applying solutionizing treatment at 537°C for 24 h, respectively (samples were obtained from the gauge length of B108 test bars). .....	88
Figure 4.5.	Morphology of eutectic silicon particles observed in non-modified and modified 354 casting alloys under the following conditions: (a) and (c) non-modified and modified alloys in the as-cast conditions, respectively; (b) and (d) non-modified and modified alloys after applying solutionizing treatment at 520°C for 24 h, respectively (samples were obtained from the gauge length of B108 test bars). .....	90
Figure 4.6.	Characteristics of eutectic silicon particles, average area, and average aspect ratio, as functions of solutionizing temperature applied for 12 h to (a) alloy 1S from the 359-type castings; and (b) alloy 10S from the 354-type castings (samples were obtained from the gauge length of B108 test bars).....	91
Figure 4.7.	Characteristics of eutectic silicon particles, average area, and average aspect ratio, as functions of solutionizing time applied at 537°C to (a) alloys 1S and 1N from 359-type castings; and at 520°C to (b) alloys 10S and 10N from 354-type castings (samples were obtained from the gauge length of B108 test bars). .....	92
Figure 4.8.	Optical micrographs showing the size of the $\alpha$ -Al dendrites in the 359 alloys produced using an end-chill mold (a) Level I; (b) Level II; and (c) Level III (samples were obtained from the gauge length of the E8M-04 test bars).....	95
Figure 4.9.	Quality chart generated using Equations 1 and 2 showing the influence of iron and copper on the tensile properties and the quality indices of 359- and 354-type B108 test bar castings under the specified conditions. It should be noted that the maximum solutionizing temperature applied to alloys coded 10S through 12S is 520°C. ....	98
Figure 4.10.	Quality chart generated using Equations 8 and 9 showing the influence of iron and copper on the tensile properties and the quality of the 359- and 354-type B108 test bar castings ( $K = 520$ MPa) under the specified conditions. It should be noted that the maximum solutionizing temperature applied to alloys coded 10S through 12S is 520°C. ....	99
Figure 4.11.	Porosity formation due to obstruction of liquid metal feeding by the $\beta$ -Fe phase.....	101
Figure 4.12.	Scatterplots correlating iron content in 359- and 354-type castings with: (a) quality index values ( $Q$ ) calculated using Equation 1; (b) ultimate tensile strength ( $UTS$ ); (c) yield strength ( $YS$ ); and (d) elongation to fracture ( $E_f$ ). .....	106

- Figure 4.13. Scatterplots correlating copper content in Al-9%Si-0.5%Mg casting alloys with: (a) quality index values ( $Q$ ) calculated using Equation 1; (b) ultimate tensile strength ( $UTS$ ); (c) yield strength ( $YS$ ); and (d) elongation to fracture ( $E_f$ )..... 110
- Figure 4.14. Quality chart generated using Equations 1 and 2 illustrating the influence of magnesium content on the tensile properties and the quality of the 359-type B108 test bar castings containing 0.07%Fe. (These castings were subjected to solutionizing treatment at 537°C for 12 hours followed by aging treatment at 170°C for 8 hours.)..... 113
- Figure 4.15. Quality chart generated using Equations 8 and 9 illustrating the influence of magnesium content on the tensile properties and the quality of the 359-type B108 test bar castings containing 0.07%Fe ( $K = 507$  MPa). (These castings were subjected to solutionizing treatment at 537°C for 12 hours followed by aging treatment at 170°C for 8 hours.)..... 114
- Figure 4.16. Optical micrographs showing (a)  $\pi$ -phases remaining in the 6SM alloy (1%Mg) after applying solutionizing treatment at 537°C for 12 h followed by aging treatment at 170°C for 8 h; (b) and (c) longitudinal sections beneath the fracture surface of 6SM alloy; (d) longitudinal section beneath the fracture surface of 1SM alloy (samples were obtained from the gauge length of B108 test bars). ..... 116
- Figure 4.17. Scatterplots correlating Mg-content in 359-type B108 test bar castings containing 0.07%Fe with: (a) quality index values ( $Q$ ) calculated using Equation 1; (b) ultimate tensile strength ( $UTS$ ); (c) yield strength ( $YS$ ); and (d) elongation to fracture ( $E_f$ ). ..... 119
- Figure 4.18. Quality chart generated using Equations 1 and 2 showing the influence of solidification rate on the tensile properties and the quality indices of the 1S-359 and 10S-354-type E8M-04 test bar castings containing 0.07%Fe. The 359 and 354 castings were subjected to solutionizing treatment at 537°C and 520°C, respectively, for 12 h followed by aging treatment at 170°C for 8h. .... 121
- Figure 4.19. Quality chart generated using Equations 8 and 9 showing the influence of solidification rate on the tensile properties and the quality indices of the 1S-359 and 10S-354-type E8M-04 test bar castings containing 0.07%Fe ( $K = 472$  MPa). The 359 and 354 castings were subjected to solutionizing treatment at 537°C and 520°C, respectively, for 12 h followed by aging treatment at 170°C for 8 h. .... 122
- Figure 4.20. Optical micrographs illustrating the microstructural features in the 359 castings produced using an end-chill mold at (a) Level I; and (b) Level III (samples were obtained from the gauge length of E8M-04 test bars). ..... 124
- Figure 4.21. (a) and (c) are backscattered images showing the size of the  $\beta$ -Al<sub>5</sub>FeSi phase observed at the fracture surface (arrowed) of 1S-359 alloy samples containing 0.07%Fe and obtained from Levels I and III, respectively; (b) and

- (c) are the EDX spectra corresponding to the phases in the images shown in (a) and (c), respectively (the fractographs were obtained from the fracture surface of the E8M-04 test bars)..... 126
- Figure 4.22. Scatterplots correlating solidification rate in terms of SDAS in 359 castings with: (a) quality index values ( $Q$ ) calculated using Equation 1; (b) ultimate tensile strength ( $UTS$ ); (c) yield strength ( $YS$ ); and (d) elongation to fracture ( $E_f$ )..... 129
- Figure 4.23. Quality chart generated using Equations 1 and 2 showing the influence of solutionizing temperatures on the properties of 354-type B108 test bar castings containing three levels of iron. All samples were solutionized for 12 h followed by aging treatment at 170°C for 8 h. The two additional points represent the 10S alloy solutionized at 530°C and 537°C for 12 h each followed by the same aging treatment. .... 131
- Figure 4.24. Quality chart generated using Equations 8 and 9 showing the influence of solutionizing temperatures on the properties of 354-type B108 test bar castings containing three levels of iron ( $K = 617$  MPa). All samples were solutionized for 12 h followed by aging treatment at 170°C for 8 h. The two additional points represent the 10S alloy solutionized at 530°C and 537°C for 12 h each followed by the same aging treatment. .... 132
- Figure 4.25. Backscattered images showing the matrix of the 10S-354 alloy in (a) the as-cast condition containing a large volume fraction of  $Al_2Cu$  phases; and (b) where, after applying solutionizing treatment at 520°C for 12 h, a complete dissolution of the same phases may be observed..... 134
- Figure 4.26. Contour plots correlating the dual effects of solutionizing temperature (ST) and Fe-levels in 354 castings: (a) with quality index values ( $Q$ ) calculated using Equation 1; (b) with ultimate tensile strength ( $UTS$ ); and (c) with yield strength ( $YS$ ). .... 138
- Figure 4.27. Microstructure of 354 castings subjected to solutionizing temperatures of (a) 525°C; (b) 530°C; and (c) 537°C for 12 h each (samples were obtained from the gauge length of B108 test bars)..... 141
- Figure 4.28. SEM images of the fracture surface of 354 alloy samples (a) solutionized at 525°C; (b) solutionized at 537°C; and (c) a high magnification image of the circled area in (b) showing enhanced detail of the polygonal Si particles (fractographs were obtained from the fracture surface of B108 test bars)..... 142
- Figure 4.29. Quality chart generated using Equations 1 and 2 illustrating the influence of solution heat treatment times and Sr-modification on the tensile properties and quality index of 354- and 359-type B108 test bars castings. The 354 samples were solutionized at 520°C for the specified time durations, while the 359 samples were solutionized at 537°C for the same time periods. .... 144
- Figure 4.30. Tensile properties (ultimate tensile strength,  $UTS$ ; yield strength,  $YS$ ; and elongation to fracture,  $E_f$ ) and quality index ( $Q$ ) correlated to the solution heat treatment times (SHt) of the 1N-359 alloys. .... 145

Figure 4.31.	Tensile properties (ultimate tensile strength, $UTS$ ; yield strength, $YS$ ; and elongation to fracture, $E_f$ ) and quality index ( $Q$ ) correlated to the solution heat treatment times (SHt) of the 10N-354 alloys. ....	146
Figure 4.32.	Quality index values shown as a function of solutionizing time and Sr-modification of the 354 alloys. ....	148

## CHAPTER 5

Figure 5.1.	The tensile properties of the 354 alloy (10N) under various aging temperatures and aging times. ( <i>Note: "m" and "h" on the X-axis indicate minutes and hours, respectively.</i> ) .....	158
Figure 5.2.	Quality chart generated using Equations 1 and 2 illustrating (a) the strength and quality of the 354 alloy under all aging temperatures and times applied; and (b) a simplified chart of (a) showing the strength and quality of the 354 alloy under the three specified aging temperatures. ....	160
Figure 5.3.	Matrix plots correlating the quality index ( $Q$ ), ultimate tensile strength ( $UTS$ ) and yield strength ( $YS$ ) with aging temperature for 354 (10N) alloy aged at 155°C and 245°C. ....	165
Figure 5.4.	Size and density of precipitates formed at various aging temperatures in 10N-354 alloy: (a) optical micrographs showing the dendrite regions from which the SEM images were taken; (b) SEM image, as-cast condition; (c) SEM image after aging at 155°C for 72 h; (d) SEM image after aging at 195°C for 72 h; (e) SEM image after aging at 245°C for 72 h; and (f) EDX spectrum corresponding to the precipitates observed (samples were obtained from the gauge length of B108 test bars). ....	168
Figure 5.5.	SEM images taken from dendrite regions showing the effects of aging time on the size and density of the precipitates in 10N-354 alloy corresponding to: (a) as-cast condition, 20000x; (b) after aging at 245°C for 1 h; (c) after aging at 245°C for 72 h; and (d) EDX spectrum corresponding to the precipitates observed (samples were obtained from the gauge length of B108 test bars). ....	170
Figure 5.6.	SEM images of the fracture surface of the 354 alloy, or 10N casting; (a) and (b) cleavage facets and cleavage cracks which are characteristic of the mixed fracture mode observed upon aging at 155°C for 72 h; (c) and (d) deep shear dimples which are features of the ductile fracture mode observed upon aging at 245°C for 72 h (fractographs were obtained from the fracture surface of B108 test bars). ....	176
Figure 5.7.	The tensile properties of the 359 alloy (1N) under various aging temperatures and aging times. ( <i>Note: "m" and "h" on the X-axis indicate minutes and hours, respectively.</i> ) .....	180
Figure 5.8.	Quality chart generated using Equations 1 and 2 illustrating (a) the strength and quality of the 359 alloy under all aging temperatures and times applied; and (b) a simplified chart of (a) showing the strength and quality of the 359 alloy under the three specified aging temperatures. ....	182

Figure 5.9. Schematic representation showing the influence of increasing aging temperature on the size, density, and inter-particle spacing of the hardening precipitates: (a) at a low aging temperature, and (b) at a high aging temperature. (L1 and L2 indicate the inter-particle spacing in each case.)..... 184

Figure 5.10. SEM images of the fracture surface of the 359 alloy or 1N casting (a) and (b) cleavage cracking which characterizes the mixed fracture mode observed upon aging at 155°C for 72 h; and (c) deep shear dimples which are features of the ductile fracture mode observed upon aging at 245°C for 72 h (fractographs were obtained from the fracture surface of B108 test bars)..... 187

Figure 5.11. Matrix plots correlating the quality index (*Q*), ultimate tensile strength (*UTS*) and yield strength (*YS*) with aging temperature for 359 (1N) alloy aged at 155°C and 245°C. .... 188

Figure 5.12. FESEM analysis of the precipitates observed in the 359 or 1N alloy (a) SEM image taken from the dendrite region of the 1N alloy aged at 220°C for 72 h; (b) EDX spectrum corresponding to the gray particles in the SEM image; (c) EDX spectrum corresponding to the bright precipitates in the SEM image (samples were obtained from the gauge length of B108 test bars)..... 191

Figure 5.13. Quality chart generated using Equations 1 and 2 to compare the strength and quality of the 354 and 359 alloys or 10N and 1N castings, respectively, aged at 155°C for time durations of 1 hour - 72 hours, as labeled on the curves. .... 194

Figure 5.14. Quality chart generated using Equations 1 and 2 to compare the strength and quality of the 354 and 359 alloys or 10N and 1N castings, respectively, aged at 170°C for time durations of 1 hour - 72 hours, as labeled on the curves. .... 195

Figure 5.15. Quality chart generated using Equations 1 and 2 to compare the strength and quality of the 354 and 359 alloys or 10N and 1N castings, respectively, aged at 195°C for time durations of 5 minutes - 72 hours, as labeled on the curves. .... 196

Figure 5.16. Quality chart generated using Equations 1 and 2 to compare the strength and quality of the 354 and 359 alloys or 10N and 1N castings, respectively, aged at 220°C for time durations of 5 minutes - 72 hours, as labeled on the curves. .... 197

Figure 5.17. Quality chart generated using Equations 1 and 2 to compare the strength and quality of the 354 and 359 alloys or 10N and 1N castings, respectively, aged at 245°C for time durations of 5 minutes - 72 hours, as labeled on the curves. .... 198

## LIST OF TABLES

### CHAPTER 2

Table 2.1.	Chemical composition limits of 354- and 359-type casting alloys. <sup>23, 26, 40</sup> .....	14
Table 2.2.	Tensile properties of 354- and 359-type casting alloys. <sup>1, 23-26, 39, 40</sup> .....	14
Table 2.3.	Characteristics of Mg-Si phases formed during aging treatment. <sup>116, 117, 118, 119</sup> .....	49
Table 2.4.	Characteristics of Al-Cu phases formed during aging treatment. <sup>113, 115, 120</sup> .....	50
Table 2.5.	Characteristics of Al-Cu-Mg phases formed during aging treatment. <sup>113, 120, 125</sup> .....	51
Table 2.6.	Characteristics of <i>Q</i> -phase and its precursors formed during aging treatment of Al-Si-Cu-Mg alloys. <sup>126, 127, 129</sup> .....	52

### CHAPTER 3

Table 3.1.	Actual chemical composition of the alloys investigated for the current study. .	60
Table 3.2.	Aging temperature and time as applied to the 1N and 10N alloys in this study.	65

### CHAPTER 4

Table 4.1.	Volume fractions of the intermetallic phases observed in 1S through 12S alloys, which were cast using a graphite mold preheated to 600°C, for the as-cast condition and two solutionizing temperatures.....	79
Table 4.2.	Average SDAS measured for the alloys coded 1S and 10S corresponding to 359 and 354 alloys, respectively (samples were obtained from the gauge length of E8M-04 test bars).....	94

### APPENDIX

Table A.1.	Tensile properties and quality index values for the 359 alloys containing various levels of iron and copper, investigated in the as-cast condition and after applying two solution heat treatment temperatures for 12 h each.....	228
Table A.2.	Tensile properties and quality index values for the 354 alloys containing various levels of iron, investigated in the as-cast condition and after applying ten solution heat treatment temperatures for 12 h each.....	229
Table A.3.	Tensile properties and quality index values for the unmodified (1N) and modified (1S) 359 alloys investigated in the as-cast condition and after applying six solution heat treatment times at 537°C for each alloy.....	230

Table A.4.	Tensile properties and quality index values for the unmodified (10N) and modified (10S) 354 alloys investigated in the as-cast condition and after applying six solution heat treatment times at 520°C for each alloy.....	231
Table A.5.	Tensile properties and quality index values for the 359 alloys containing various levels of magnesium.....	232
Table A.6.	Tensile properties and quality index values for the 359 (1S) and 354 (10S) alloys investigated under different solidification rates.....	232
Table A.7.	Tensile properties and quality index values for the 354 (10N) alloy after applying aging treatment at 155°C for various aging times.....	233
Table A.8.	Tensile properties and quality index values for the 354 (10N) alloy after applying aging treatment at 170°C for various aging times.....	234
Table A.9.	Tensile properties and quality index values for the 354 (10N) alloy after applying aging treatment at 195°C for various aging times.....	235
Table A.10.	Tensile properties and quality index values for the 354 (10N) alloy after applying aging treatment at 220°C for various aging times.....	236
Table A.11.	Tensile properties and quality index values for the 354 (10N) alloy after applying aging treatment at 245°C for various aging times.....	237
Table A.12.	Tensile properties and quality index values for the 359 (1N) alloy after applying aging treatment at 155°C for various aging times.....	238
Table A.13.	Tensile properties and quality index values for the 359 (1N) alloy after applying aging treatment at 170°C for various aging times.....	239
Table A.14.	Tensile properties and quality index values for the 359 (1N) alloy after applying aging treatment at 195°C for various aging times.....	240
Table A.15.	Tensile properties and quality index values for the 359 (1N) alloy after applying aging treatment at 220°C for various aging times.....	241
Table A.16.	Tensile properties and quality index values for the 359 (1N) alloy after applying aging treatment at 245°C for various aging times.....	242
Table B.1.	Characteristics of eutectic silicon particles of 354 (10S) alloy as functions of solutionizing temperature applied for 12 h.....	244
Table B.2.	Characteristics of eutectic silicon particles of 359 (1S) alloy as functions of solutionizing temperature applied for 12 h.....	244
Table B.3.	Characteristics of eutectic silicon particles of unmodified 354 (10N) alloy as functions of solution heat treatment time applied at 520°C.....	245
Table B.4.	Characteristics of eutectic silicon particles of modified 354 (10S) alloy as functions of solution heat treatment time applied at 520°C.....	245
Table B.5.	Characteristics of eutectic silicon particles of unmodified 359 (1N) alloy as functions of solution heat treatment time applied at 537°C.....	246
Table B.6.	Characteristics of eutectic silicon particles of modified 359 (1S) alloy as functions of solution heat treatment time applied at 537°C.....	246

## **CHAPTER 1**

### **INTRODUCTION AND OBJECTIVES**

## CHAPTER 1

### INTRODUCTION AND OBJECTIVES

#### 1.1. INTRODUCTION

Aluminum-silicon casting alloys show great promise for several fields of engineering applications. The growing tendency towards the use of these casting alloys is directly related to the specific advantages they provide including their high strength-to-weight ratio which leads to reducing fuel consumption and improving mechanical performance. The permanent mold 354-type Al-9%Si-1.8%Cu-0.5%Mg and 359-type Al-9%Si-0.5%Mg casting alloys display superior strength and hardness values after the application of suitable heat treatment procedures as a result of the presence of hardening elements, namely, copper, magnesium, and silicon. The high 9% Si-content of these alloys enhances castability, reduces shrinkage, and improves both strength and ductility.<sup>1,2,3</sup>

The 354 and 359 casting alloys are, however, still not used by most foundrymen, in spite of the fact that they display a strong potential for several fields of industrial applications, specifically, when premium strength is a principle prerequisite. This study was carried out for the purposes of providing a solid foundation for both alloys when validating these alloys for industrial use. Such a background was created by correlating the tensile properties and the quality indices of these alloys with the most common metallurgical parameters affecting and controlling their tensile properties and quality index

values. The variables investigated here include iron level; copper content; magnesium level; strontium content; solidification rate; solution heat treatment temperatures; solution heat treatment times; aging temperatures; and aging times.

Alloy composition plays a critical role in determining the final tensile properties and quality index values of Al-Si casting alloys. This parameter includes either alloying elements or impurities. The alloying elements are usually added with the intention of improving a specific property of the casting. Copper and magnesium are the most common strengthening elements to be added to Al-Si casting alloys for the purposes of improving the strength and hardness of these alloys, specifically, after applying the appropriate heat treatments.<sup>4, 5, 6, 7</sup> Strontium is a well-known alloying element used as a chemical modifier. It is usually added to Al-Si alloys to transform the coarse acicular morphology of eutectic silicon particles into a fine fibrous form. Such modifications lead to improved mechanical properties of the castings.<sup>8, 9, 10</sup> The impurity elements, on the other hand, have a deleterious effect on the tensile properties and the quality of the casting, as a consequence, certain procedures should be applied to the casting to neutralize the deterioration caused by such impurity elements. Iron is considered to be the most prevalent impurity element in Al-Si casting alloys.<sup>11, 12</sup>

The solidification rate of the casting is considered to be a significant metallurgical parameter in determining the overall tensile properties and quality index values of an Al-Si casting. The application of appropriate heat treatment procedures to 354 and 359 castings will improve their tensile properties and quality. The treatment includes selecting the

adequate solution heat treatment temperature and time, as well as recommending a suitable aging temperature and time.

Quality charts were used as an evaluation tool for selecting the optimum conditions to be applied in practice in order to develop superior tensile properties and optimum quality in 354- and 359-type casting alloys. The right alloy quality in engineering applications involves reaching a suitable compromise between numerous factors so as to present the least possible risk and maximum performance combined with cost efficiency. Alloy composition, solidification rate, and heat treatment procedures are all parameters which closely affect alloy quality since they also influence the tensile properties of the casting. The quality of aluminum alloy castings may be defined using numerical values which correlate to their mechanical properties. Several models were proposed to correlate the quality of the Al-Si castings to the mechanical properties of these alloys, as will be discussed in the next chapter. In the present study, the results of the tensile tests will be presented in the form of quality charts which provide an accurate tool for evaluating the tensile properties and the quality of the 354- and 359-type castings under the various metallurgical conditions applied to these castings.

## **1.2. OBJECTIVES**

The current study was carried out with a view to developing a strong and a well-founded background for two high strength Al-9%Si casting alloys for the purposes of validating these alloys for industrial use. The alloys studied are the 354 (Al-9%Si-1.8%Cu-0.5%Mg) and the 359 (Al-9%Si-0.5%Mg) alloys. The objectives of this study were accomplished by carrying out the following tasks.

1. Investigating the influence of the following metallurgical variables on the tensile properties and the quality index values of the 354 and 359 alloys:
  - (i) iron (Fe) content;
  - (ii) copper (Cu) level;
  - (iii) magnesium (Mg) content;
  - (iv) strontium (Sr) level;
  - (v) solidification rate;
  - (vi) solution heat treatment temperature;
  - (vii) solution heat treatment time;
  - (viii) aging temperature; and
  - (ix) aging time.
2. Analyzing the quality of the alloys obtained under various conditions (variables i through ix in objective 1) by using the suitable proposed quality indices.
3. Applying the quality charts as a tool for evaluating the tensile properties and quality indices of the castings and for selecting the optimum metallurgical conditions for achieving superior strength and optimum quality in 354- and 359-type casting alloys.

## **CHAPTER 2**

### **SURVEY OF THE LITURATURE**

## CHAPTER 2

### 2. SURVEY OF THE LITURATURE

#### 2.1. INTRODUCTION

The current chapter will review aluminum-silicon casting alloys and their properties in relation to a number of metallurgical parameters. The concept of quality indices and quality charts with their practical applications in materials engineering will be also covered. Several metallurgical parameters will be covered in this survey of the related literature regarding their effects on the tensile properties and quality indices of these alloys. The metallurgical factors include (i) impurity elements; (ii) hardening elements; (iii) modification; (iv) solidification rate; (iv) solution heat treatment parameters; and (vi) age-hardening conditions.

#### 2.2. ALUMINUM CASTINGS

Aluminum casting alloys show great promise for several fields of application including transportation, and the automotive, aerospace and defence industries. The continuous and steady growth of aluminum alloy usage for industrial applications is directly related to the need for taking advantage of such specific assets as a high strength-to-weight ratio, and by so doing to enhance mechanical performance and to lessen energy consumption.<sup>13, 14, 15, 16, 17, 18, 19</sup> The reduction in fuel consumption is considered to be not

only a decisive economical factor but also a significant environmental advantage obtainable by decreasing the production of exhaust gases.<sup>20,21,22</sup>

With the intention of reducing vehicle weight in the automotive industry, several iron-based components are in the process of being replaced with lightweight parts made of aluminum-based alloys since the density of aluminum is known to be one-third that of steel. Figure 2.1 reveals the growing trend, over a 50-year period, of incorporating aluminum alloys in the automotive industry, where for the year 2009, aluminum shares 8.7% of the vehicle curb weight, a percentage which is expected to increase by up to 10.4% in the next eleven years.<sup>21,22</sup> Aluminum castings share either partially or entirely in several cast parts produced by the automotive industry including engine blocks, pistons, cylinder heads, intake manifolds, crankcases, carburetors, transmission housings, rocker arms, as well as numerous other components. The increasing demand for the use of aluminum alloys is related not only to their mechanical performance, economical efficiency, and environmental advantages but also to the fact that these alloys offer advantageous safety features whereby the ability of aluminum to absorb the energy of impact in case of accident is twice that of steel for the same weight.<sup>22</sup>

The properties of aluminum casting alloys can be improved upon through the appropriate control of several metallurgical factors involved in the production of these castings. One such parameter might involve the addition of suitable alloying elements. Silicon is one of the most common alloying elements and may be added to aluminum in order to produce a range of experimental and commercial Al-Si base alloys offering a wide

range of mechanical and physical properties. A brief description of Al-Si alloy characteristics and features will be presented in the next sections.

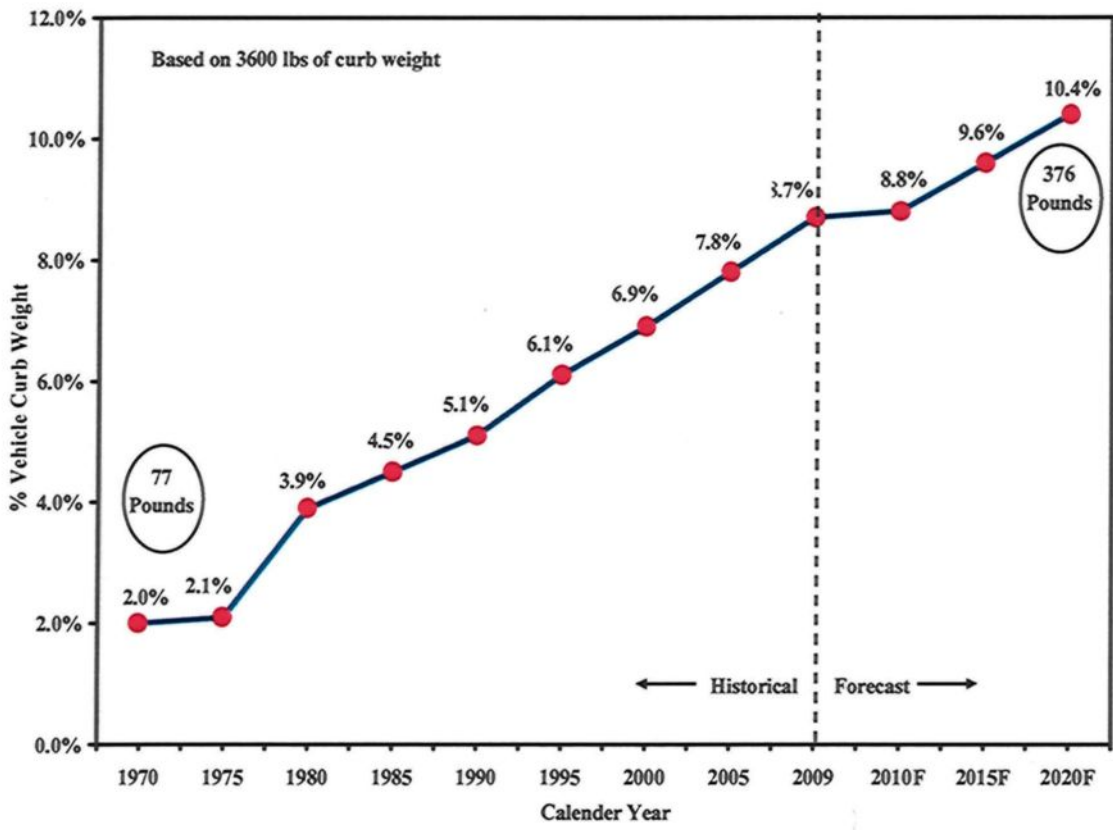


**Figure 2.1.** The growing trend of sharing aluminum alloys in the automotive industry, as seen over 50 years in North America.<sup>21,22</sup>

### 2.3. ALUMINUM-SILICON CASTINGS

The addition of silicon as a dominant alloying element produces castings with physical and mechanical properties which are of great pertinence to recent industrial requirements. These Al-Si casting alloys provide superior casting characteristics; low shrinkage; improved hot-tearing resistance; good wear and corrosion resistance; satisfactory weldability; a low thermal expansion coefficient and high thermal conductivity.

In addition to these advantages, a further range of mechanical properties for Al-Si castings may be attained by adding suitable hardening elements such as copper and magnesium and by applying adequate heat treatments. These characteristics of Al-Si castings are the main reason for their acknowledged versatility in several fields of industrial application where aluminum-silicon cast parts form as much as 90% of total aluminum castings.<sup>23, 24, 25, 26, 27, 28, 29, 30</sup>

Aluminum-silicon casting alloys may be subdivided into three groups according to their level of silicon-content as may be observed in Figure 2.2(a);<sup>31, 32</sup> these groups are (i) hypoeutectic alloys with a silicon content of 5-10%; (ii) eutectic alloys with a silicon level of 11-13%; and (iii) hypereutectic alloys containing 14-20% silicon. Thus, in accordance with the level of silicon to be observed, the microstructural features of each group differ from one another. Consequently, the mechanical properties of these groups of castings are directly related to the specific features of the microstructure in each case.

In hypoeutectic alloys, the  $\alpha$ -aluminum precipitates in the form of a dendritic network, followed by the precipitation of eutectic Al-Si in the interdendritic regions, as will be observed in Figure 2.2(b). In the case of eutectic alloys, the entire cast structure consists mainly of an Al-Si eutectic structure, as may be seen in Figure 2.2(c). Hypereutectic alloys are characterized by the precipitation of primary silicon cuboids followed by the solidification of the eutectic structure, as shown in Figure 2.2(d).<sup>31, 32</sup>

The Al-Si casting alloys, as mentioned earlier, have worthwhile physical and mechanical properties, a fact which is amply confirmed by their wide range of applications. Hypoeutectic and eutectic Al-Si casting alloys are the most commonly used in industrial

applications,<sup>33</sup> whereas hypereutectic alloys are used principally for high wear resistance applications.<sup>34, 35, 36, 37, 38</sup> The improved wear resistance of this latter group is a result of the high silicon content of the alloys ultimately leading to the precipitation of hard primary silicon particles, as may be seen in Figure 2.2(d), although the presence of these cuboid silicon particles has a deleterious effect on other mechanical properties, particularly on the machinability of these castings.<sup>34, 37, 38</sup>

Two hypoeutectic aluminum-silicon casting alloys will be investigated in the current study so as to correlate metallurgical parameters with their tensile properties and quality index values. The hypoeutectic 354- and 359-type castings are the backbone of this specific study since they reveal great promise for several fields of industrial applications as a result of their superior strength. An extensive investigation will be carried out subsequently regarding the effects of metallurgical factors on the properties of these particular castings so as to provide a solid and sufficient background for these casting alloys to be included in industrial and commercial applications. A discussion of the quality index concept in conjunction with quality charts as tools for material selection is also one of the objectives of this study. The evaluation and selection of the properties for the designated alloys can reliably be made based on these conceptual tools.

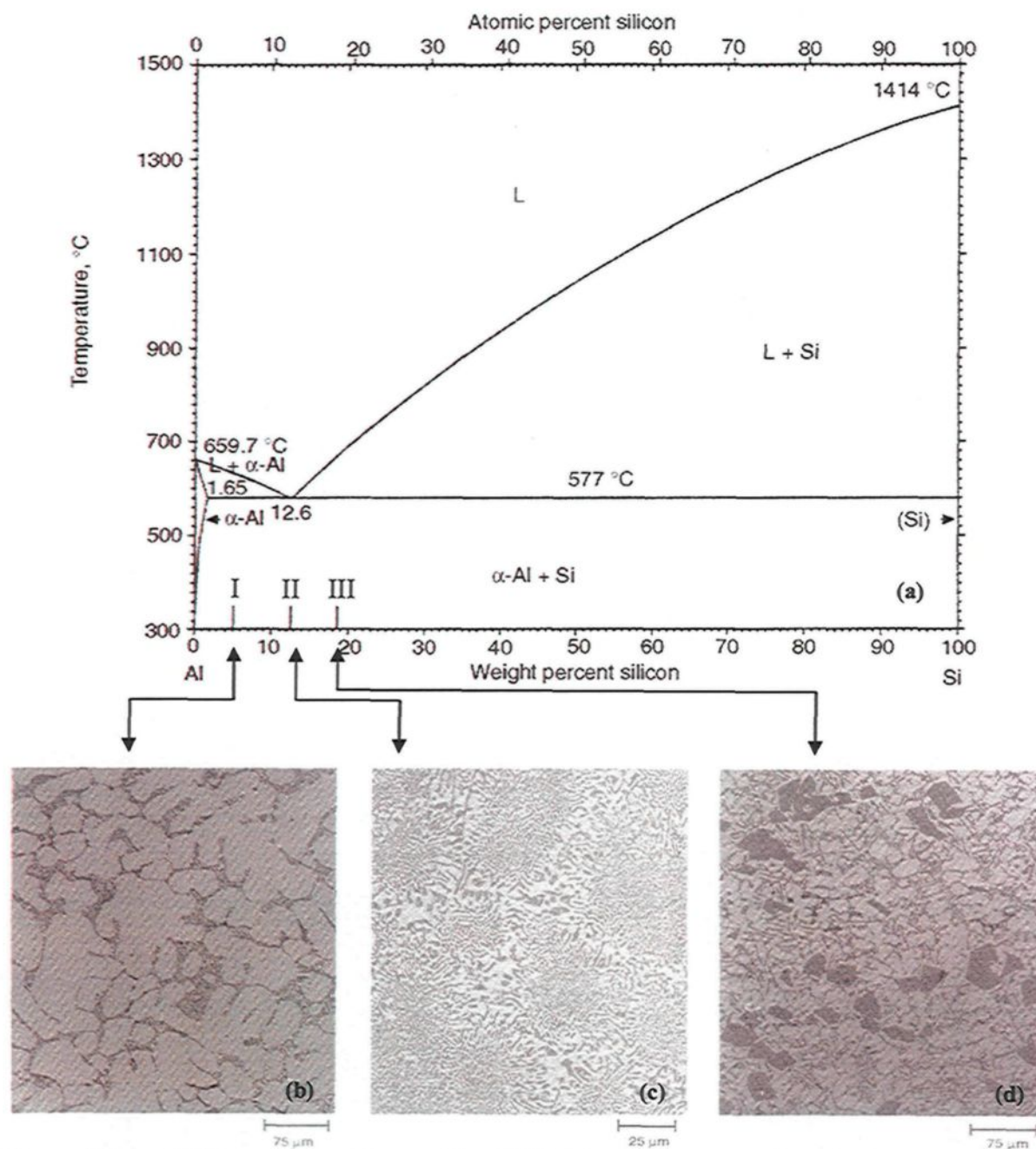


**Figure 2.2.** Al-Si casting alloys: (a) Al-Si binary system; (b) microstructure of hypoeutectic alloys; (c) microstructure of eutectic alloys; (d) microstructure of hypereutectic alloys.<sup>32</sup>

### **2.3.1. 354-Type Castings**

Permanent mold-cast 354-type Al-Si-Cu-Mg alloys display superior strength and hardness values after the application of a suitable heat treatment; this improvement is a result of the presence of the hardening elements, copper and magnesium. The high Si-content of this type of alloy enhances its castability and reduces shrinkage; the corrosion resistance and hot-tearing tendency of these castings, however, are affected as a consequence of the presence of copper. These specific castings hold great promise for structural applications because of the superior strength they attain after suitable heat treatment is applied. For this reason, 354-type castings have the potential for being used in the manufacture of several parts and components in the automotive and aerospace industries.<sup>1, 24, 26</sup> Table 2.1 shows the chemical composition limits of this alloy while Table 2.2 lists its tensile properties as observed after applying a T61-temper.<sup>1, 23-26, 39, 40</sup>

### **2.3.2. 359-Type Castings**

Permanent-mold cast 359-type Al-Si-Mg alloys are characterized by their superior casting characteristics and low shrinkage resulting from their high silicon content. Table 2.1 shows the chemical composition limits of the 359 casting alloys while their tensile properties under a T61-regime are listed in Table 2.2. This type of casting is of interest in structural applications to some extent because of the superior strength it acquires after the application of heat treatment. The higher tensile and fatigue strength of this particular type of casting, in conjunction with its high resistance to corrosion, results in expanding its range of application to include the aircraft and missile industries.<sup>1, 23-26, 40</sup>

**Table 2.1.** Chemical composition limits of 354- and 359-type casting alloys.<sup>23, 26, 40</sup>

Alloy	Elements, wt%								
	<i>Si</i>	<i>Cu</i>	<i>Mg</i>	<i>Fe</i>	<i>Mn</i>	<i>Zn</i>	<i>Ti</i>	<i>Others</i>	<i>Al</i>
<b>354</b>	8.6-9.5	1.6-2	0.4-0.6	0.2 max	0.1 max	0.1 max	0.2 max	0.15	Bal.
<b>359</b>	8.5-9.5	0.2 max	0.5-0.7	0.2 max	0.1 max	0.1 max	0.2 max	0.15	Bal.

**Table 2.2.** Tensile properties of 354- and 359-type casting alloys.<sup>1, 23-26, 39, 40</sup>

Alloy	Tensile Properties		
	Ultimate Tensile Strength (MPa)	Yield Strength (MPa)	Elongation to fracture (%)
<b>Permanent Mold 354</b>	380	285	6
<b>Permanent Mold 359</b>	325	255	7

The mechanical properties of aluminum-silicon casting alloys are related directly to various metallurgical parameters involved in production procedures. The quality of Al-Si castings may be expressed in terms of their mechanical properties, a concept known as quality index. Several quality indices have been proposed in the literature with the intention of evaluating the quality of aluminum-silicon castings as a function of their mechanical properties.

#### **2.4. THE CONCEPT OF QUALITY INDICES AND QUALITY CHARTS FOR Al-Si CASTING ALLOYS**

The quality of aluminum-silicon casting alloys is considered to be a key factor in selecting an alloy casting for a particular engineering application. Deciding upon the right alloy quality thus involves reaching a suitable compromise between numerous factors so as to present the least possible risk with maximum performance in combination with adequate

cost effectiveness. Alloy composition, solidification rate, heat treatment procedures, casting defects, and such microstructural features as grain size and intermetallic phases, are all parameters which closely affect alloy quality since they also influence the mechanical properties of the casting. The concept of quality indices and quality charts as well as their progress since 1980 will be reviewed in the following subsections.

#### 2.4.1. Quality Index (Q) Proposed by Drouzy *et al.*

The quality of aluminum alloy castings may be defined using numerical values which correlate to their mechanical properties. Drouzy *et al.*<sup>41</sup> first proposed these numerical values in 1980 and termed them quality indices; these may be represented by the following equation:

$$Q = \sigma_{uts} + d \log(E_f) \quad \text{Equation 1}$$

where  $Q$  is the quality index in *MPa*;  $\sigma_{uts}$  refers to the ultimate tensile strength in *MPa*;  $E_f$  refers to the percentage elongation to fracture; and  $d$  is a material constant equal to 150 *MPa* for Al-7Si-Mg alloys. The probable yield strength ( $\sigma_{P(YS)}$ ) for the same alloy may be proposed as:

$$\sigma_{P(YS)} = a \sigma_{UTS} - b \log(E_f) + c \quad \text{Equation 2}$$

where the coefficients  $a$ ,  $b$ , and  $c$  for Al-7Si-Mg were determined as 1, 60, and -13 respectively, while the constants  $b$  and  $c$  are expressed in units of *MPa*.

Equation 1 is used to generate the *iso-Q* lines in the quality charts proposed by Drouzy *et al.*,<sup>41, 42</sup> whereas Equation 2 is used to generate the *iso-probable yield strength* lines. The quality chart generated using Equations 1 and 2 is shown in Figure 2.3. These quality charts are generated for use as a simple method of evaluating, selecting, and also

predicting the most appropriate metallurgical conditions which may be applied to the castings so as to obtain the best possible compromise between tensile properties and casting quality. The quality index value ( $Q$ ) is intrinsically related to the level of the quality of the castings which are susceptible to improvement through adequate control of the impurity elements, casting defects, modification, solution heat treatment and solidification conditions. The probable yield strength ( $\sigma_{p(YS)}$ ) depends mainly on the hardening elements such as magnesium and copper and also on the age-hardening conditions applied to the castings.<sup>27, 41, 42</sup> The right selection of the factors mentioned earlier may increase both quality index values and the probable yield strength in the directions shown in Figure 2.3. The quality chart shown in this figure provides sufficient information for each point located on this type of plot. This information supports the use of these charts in the evaluation of the appropriate metallurgical conditions to be applied to Al-Si casting alloys in order to obtain the specific prerequisite properties. As may be seen in Figure 2.3, the properties which are known for each point located in the chart are the tensile strength ( $UTS$ ), elongation to fracture ( $E_f$ ), yield strength ( $YS$ ), and the quality index value ( $Q$ ).

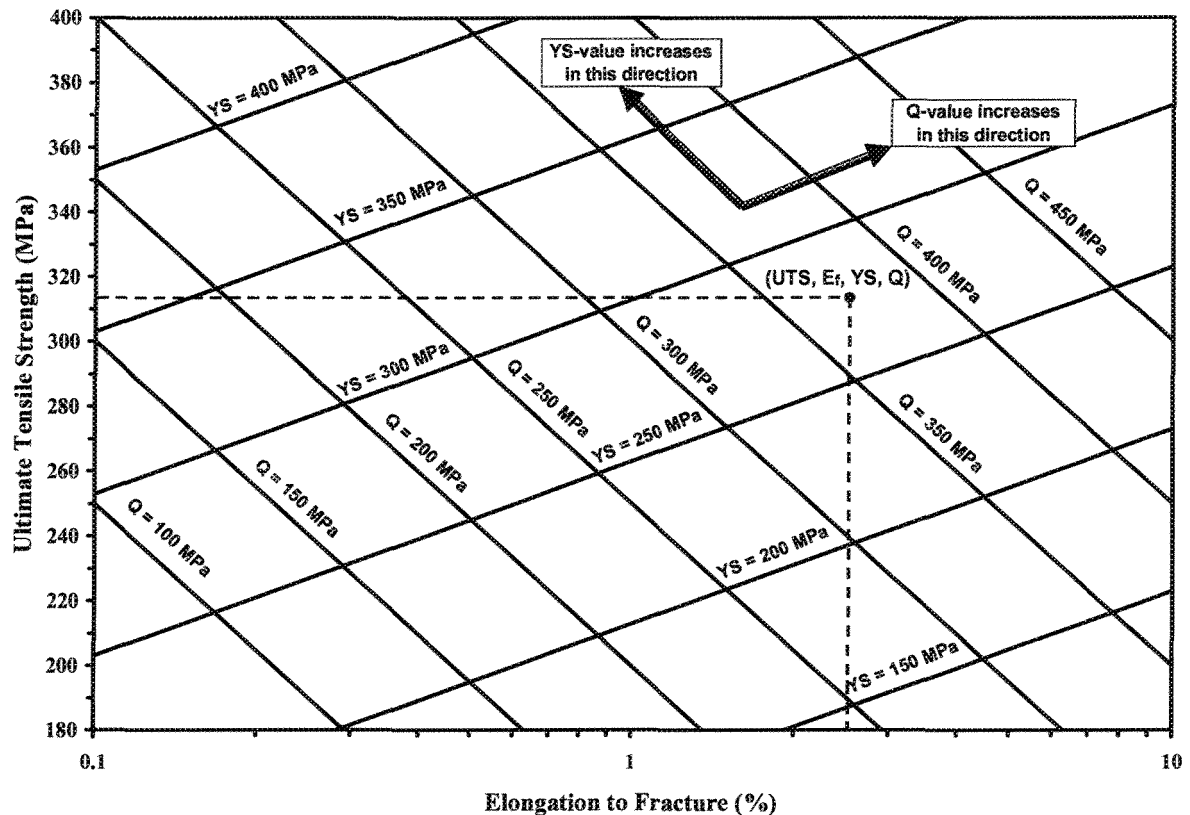


**Figure 2.3.** Example of the quality chart proposed by Drouzy *et al.*<sup>41</sup> generated using Equations 1 and 2.

#### 2.4.2. Quality Index ( $Q_N$ ) Proposed by Din *et al.*

The concept of a quality index, as proposed by Drouzy *et al.*,<sup>41</sup> is based on specific findings when applying aging treatment to Al-Si-Mg casting alloys. Upon applying peak-aging to these alloys, a linear relationship with a negative slope of 150 MPa was obtained between the tensile strength and the logarithm of elongation to fracture. Din *et al.*<sup>43</sup> observed that the aging results obtained from Al-Cu alloys display curvilinear behavior upon plotting tensile strength versus the logarithm of elongation to fracture. According to these findings, Din *et al.*<sup>43</sup> concluded that the concept described in Equations 1 and 2 is not

transferable to Al-Cu alloys. Thus, they proposed an alternative definition of the quality concept. This new definition of quality index has the form of:

$$Q_N = \sigma_{0.2} + K E_f \quad \text{Equation 3}$$

where  $\sigma_{0.2}$  is the 0.2% proof strength,  $E_f$  refers to the percentage elongation to fracture, and  $K$  is a material constant expressed in *MPa* which has the values of 7.5 for A206 alloys and 13 for A201 alloys in the under-aged conditions, and a value of 50 for the under-aged and over-aged properties of A356 and A357 alloys. Figure 2.4 shows the quality chart generated using Equation 3 and also illustrates the properties which may be obtained for each point located in this particular type of chart.

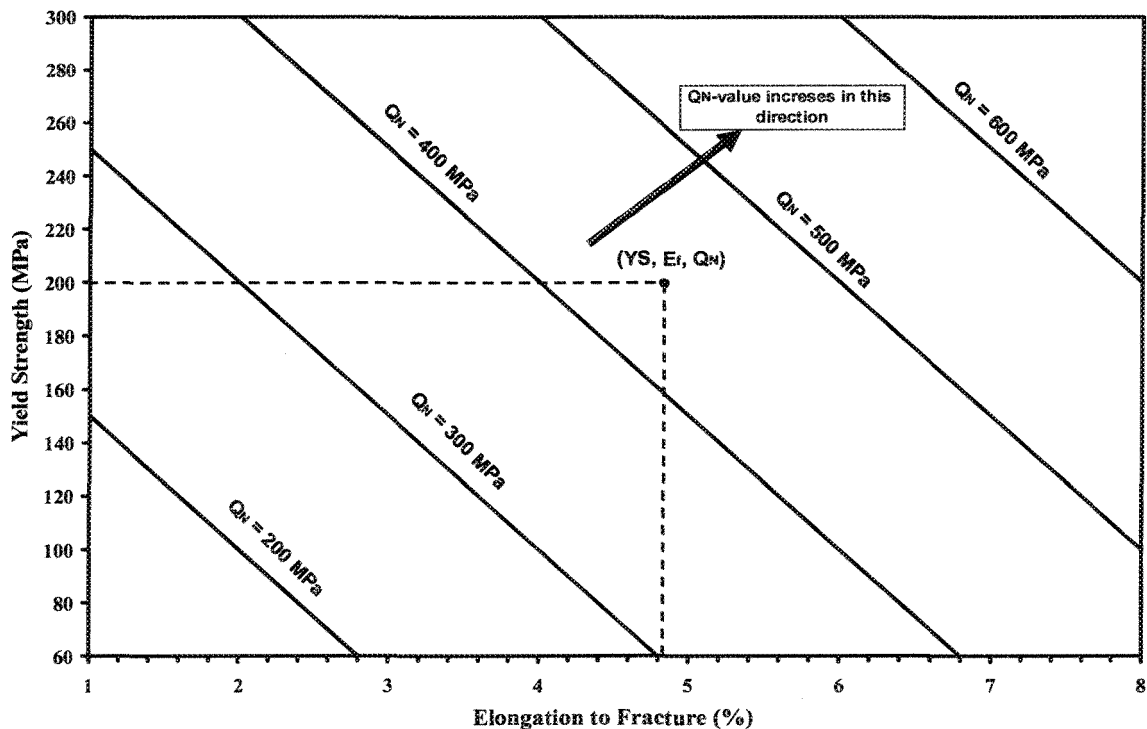


**Figure 2.4.** Example of the quality chart proposed by Din *et al.* generated using Equation 3 for Al-Si-Mg casting alloys with  $K = 50$  MPa.

### 2.4.3. Quality Index ( $Q_C$ ) Proposed by Cáceres

Although the quality index concept was first developed semi-empirically by Drouzy *et al.*,<sup>41, 42</sup> more recently Cáceres has developed a theoretical model which explains the physical significance of the quality index.<sup>42, 44, 45</sup> The model proposed by Cáceres is based on the assumption that the deformation curves of a material may be represented by the Holloman equation having the form<sup>46, 47</sup>

$$P = K S^n \quad \text{Equation 4}$$

where  $P$  is the true stress,  $S$  is the true plastic strain,  $n$  is the strain-hardening exponent, and  $K$  is the strength coefficient. The values of  $n$  and  $K$  may be calculated from a *log-log* plot of true stress versus true strain, as shown in Figure 2.5.<sup>46, 47</sup>

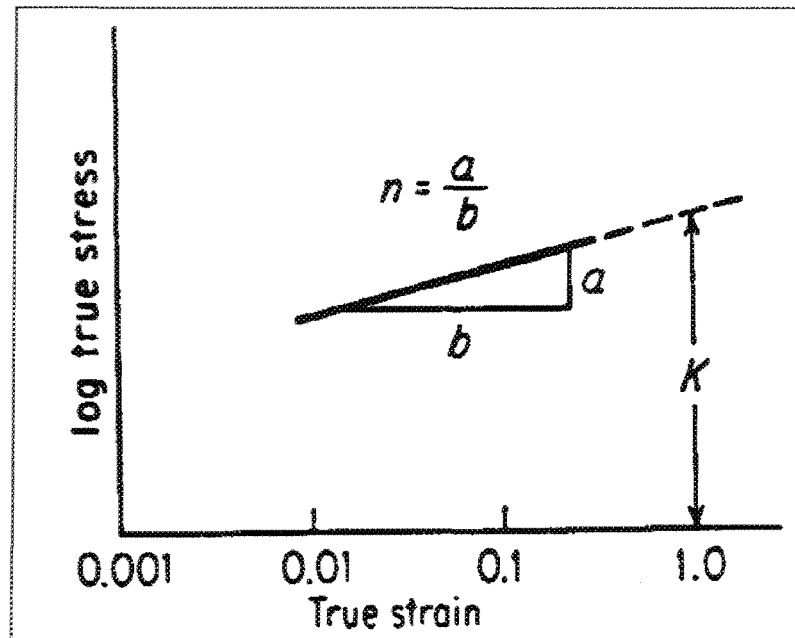


**Figure 2.5.** A log-log plot of true stress versus true strain for calculating  $n$  and  $K$  values in Equation 4.<sup>46, 47</sup>

The strain-hardening exponent  $n$  correlates to the rate of strain hardening  $\frac{dP}{dS}$  through the following correlation:<sup>46,47</sup>

$$n = \frac{d(\log P)}{d(\log S)} = \frac{d(\ln P)}{d(\ln S)} = \frac{S}{P} \times \frac{dP}{dS} \text{ or } \frac{dP}{dS} = n \frac{P}{S} \quad \text{Equation 5}$$

The samples which fracture under tensile testing may produce an amount of necking depending on their ductility. Necking usually starts at the point of tensile instability when the strain-hardening rate is equal to the true stress as described in Equation 6 and may be observed in Figure 2.6.

$$\frac{dP}{dS} = P \quad \text{Equation 6}$$

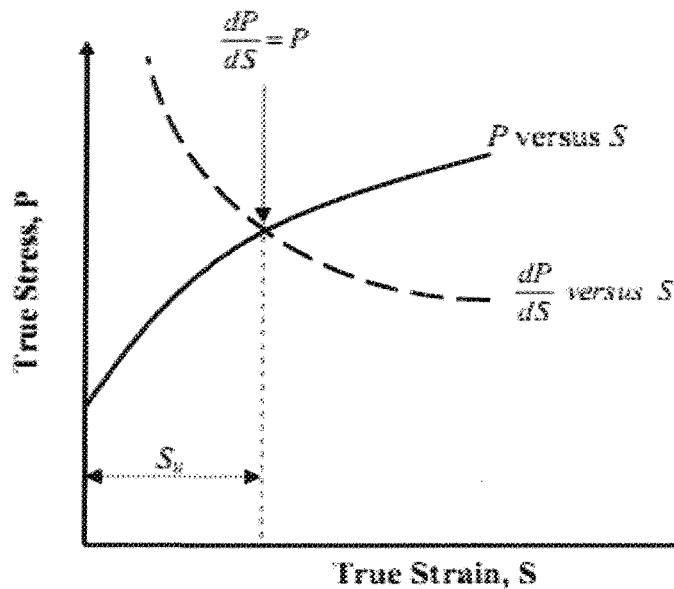


**Figure 2.6.** Determining the beginning of necking based on the true-stress/true-strain curve during tensile testing.<sup>46,47</sup>

From Equation 5 and Equation 6, it may be concluded that necking will begin when the strain-hardening exponent is equal to the true uniform plastic strain, *i.e.*  $n = S_u$ . More explicitly, under usual conditions the true uniform plastic strain  $S_u$  represents the critical strain at which the instability in tension or necking starts.<sup>46,47</sup>

These samples may attain maximum quality values, *i.e.* maximum elongation and tensile strength, when  $S_f = S_u = n$  where  $S_f$  is the strain at fracture. Lower quality values will be obtained in the case where the fracture strain  $S_f$  is lower than the critical strain  $S_u$ , *i.e.* when  $S_f < S_u$  or  $S_f < n$ . Cáceres identified a relative quality index based on the assumption that necking will occur when  $E_u \cong S_u = n$ , where  $E_u$  is the engineering strain at the onset of necking; based on the preceding he hypothesized that the maximum quality may be obtained when  $E_f/n \approx 1$  while the minimum quality will be reached when  $E_f \approx 0$ , which occurs when the specimen fractures at the yield point. The quality values between the maximum and minimum limits may be presented by *iso-lines* corresponding to the fraction of elongation to fracture,  $E_f$ , related to the critical strain,  $E_u$ , at which necking starts. On this basis, Cáceres proposed a relative quality index which has the form<sup>44, 45, 48, 49, 50, 51, 52, 53, 54, 55</sup>

$$q = \frac{E_f}{E_u} \cong \frac{E_f}{n} \quad \text{Equation 7}$$

By assuming that the true strain and engineering strain are equivalent, *i.e.*  $S \cong E$ , and by correlating the true values of stress and strain with the nominal values in Equation 4 (where true stress  $P = \sigma(1 + E)$  and true strain  $S = \ln(1 + E)$ ,  $\sigma$  and  $E$  being the engineering stress and strain, respectively), the equation would then be expressed as:<sup>44, 45, 48-55</sup>

$$\sigma = K [\ln(1 + E)]^n e^{-\ln(1+E)} \cong K E^n e^{-E} \quad \text{Equation 8}$$

By substituting the strain-hardening exponent  $n$  from Equation 7 in Equation 8, the relative quality index  $q$  may be expressed in terms of engineering stress and strain by the relation:<sup>44, 45, 48-55</sup>

$$\sigma = K E^{\frac{E}{q}} e^{-E} \quad \text{Equation 9}$$

Equation 8 and Equation 9 are used to generate the *iso-flow* lines and the *iso-q* lines, respectively, in the quality charts proposed by Cáceres. The quality chart generated using Equations 8 and 9 is shown in Figure 2.7 where the line  $q = 1$  represents the maximum quality, while the lines  $q < 1$  represent lesser quality values. Equation 9 does not, however, calculate the  $Q$ -values proposed in Equation 1. Cáceres correlated the relative quality index  $q$  with the quality index  $Q$  proposed by Drouzy *et al.* based on the observations that the *iso-q* lines generated by the former are roughly equivalent to the *iso-Q* lines generated by the latter, as may be seen in Figure 2.8. As a result, the slope of the *iso-q* lines is also roughly equivalent to the parameter  $d$  in Equation 1, and this slope may be determined by differentiating Equation 9 with respect to the strain  $E$  at  $q \rightarrow 1$  which results in the following correlation:

$$d = -\frac{d\sigma}{dE} \cong 0.4K \quad \text{Equation 10}$$

By correlating Equations 7, 8 and 10 with Equation 1, the quality index  $Q$  relates to the relative quality index  $q$  and the parameters  $n$  and  $K$  through the following equation:

$$Q = K [(qn)^n e^{-qn} + 0.4 \log(100qn)] \quad \text{Equation 11}$$

Equation 11 calculates the  $Q$ -values corresponding to each relative quality index value  $q$ , in such a way that each *iso-q* line represents two values identifying the material quality,

namely,  $Q$ - and  $q$ -values as shown in Figure 2.7. Equation 11 may be simplified into the following form:<sup>2, 48-50, 52, 55</sup>

$$Q \approx K [1.12 + 0.22 \times \ln(q)] \quad \text{where } q = 0.04 \sim 1. \quad \text{Equation 12}$$

Equation 12 is a simplified model used to correlate the quality index  $Q$  with the relative quality index  $q$ .

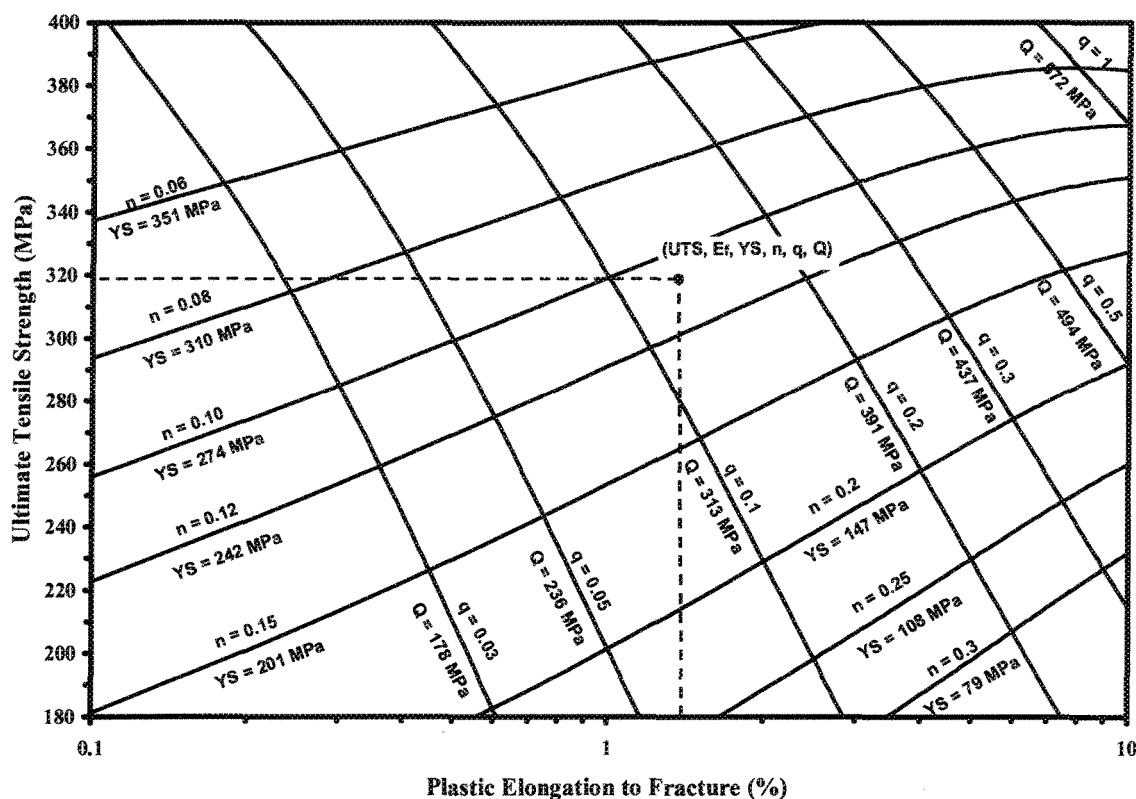


**Figure 2.7.** Example of the quality chart proposed by Cáceres illustrating *iso-flow* and *iso-q* lines generated using Equations 8 and 9, respectively, with  $K = 511$  MPa.

The quality chart shown in Figure 2.7 provides several significant properties for each point located in the chart such as tensile strength ( $UTS$ ), plastic elongation to fracture ( $E_f$ ), yield strength ( $YS$ ), relative quality index ( $q$ ) and quality index value ( $Q$ ). The

numerous properties available for each point in the quality chart proposed by Cáceres provide a significant tool for the evaluation, selection, and prediction of the appropriate metallurgical conditions to be applied for an aluminum silicon casting alloy so as to obtain certain properties for particular applications. Figure 2.8 shows the quality chart proposed by Cáceres, *i.e.* the solid-line curves superimposed on that of Drouzy *et al.*, represented by the dashed-line curves. It will be observed from this figure that the *iso-Q* lines are quasi-parallel to the *iso-q* lines. This relative relationship between *iso-Q* and *iso-q* lines provides a physical meaning for the *Q*-value since it is possible to describe it in terms of the relative quality index or relative ductility.<sup>44, 45, 48, 51, 53</sup> In the same way, the *iso-YS* and *iso-flow* lines are also virtually parallel, which means that the *iso-YS* lines may be described as *iso-flow* lines which adds a physical significance to the meaning of the *iso-YS* lines.

#### 2.4.4. Quality Index ( $Q_D$ ) Proposed by Alexopoulos and Pantelakis

Alexopoulos and Pantelakis<sup>56, 57, 58, 59, 60</sup> proposed a quality index with the intention of evaluating aluminum casting alloys for aircraft applications. The evaluation of the castings using  $Q_D$  is based on their yield strength and their strain energy density. Yielding in a material is critical for aeronautical design so that  $Q_D$  is correlated to the yield strength of aluminum castings instead of their tensile strength. Strain energy density serves as an indicator for the ductility and fracture toughness of the aluminum castings used in

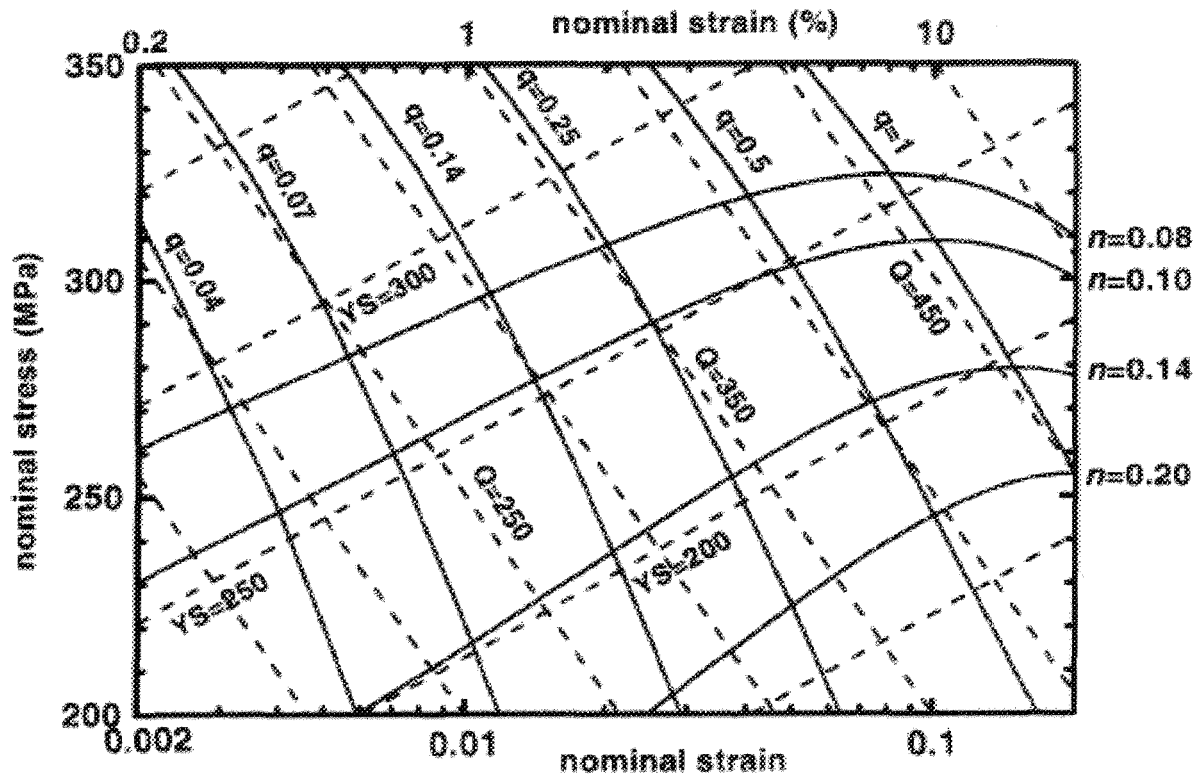


**Figure 2.8.** Two models of quality charts for the A356 alloy; the dashed lines are *iso-Q* and *iso-YS* lines calculated with Equations 1 and 2, respectively. The solid lines are *iso-flow* lines and *iso-q* lines calculated with Equations 8 and 9, respectively, with  $K = 430 \text{ MPa}$ .<sup>44, 45, 48, 49, 51, 53</sup>

aerospace applications. The correlation between the quality index  $Q_D$  and both the yield strength and fracture toughness of aluminum castings provides a tool for evaluating these castings and which may be used for damage tolerance applications. The proposed quality index  $Q_D$ , expressed in *MPa*, may be presented in the following form:<sup>56-60, 61</sup>

$$Q_D = K_D \times Q_0 \quad \text{Equation 13}$$

where  $Q_0$  characterizes the tensile properties of the material in question and  $K_D$  is a dimensionless factor which describes the scatter in the tensile properties. Based on the

same concept presented in Equation 1, the tensile properties may be correlated to  $Q_0$  through the following relation: <sup>56-61</sup>

$$Q_0 = [\sigma_p + (10 \times W)] \quad \text{Equation 14}$$

where  $\sigma_p$  is the yield strength and  $W$  refers to the strain energy density in energy per unit volume. The material toughness or the strain energy density may be calculated from the area under the stress-strain curve. <sup>46, 47, 56</sup>

The coefficient  $K_D$  may be determined using the following equation: <sup>56-61</sup>

$$K_D = \left( \frac{\sigma_{Pi}}{\sigma_{Pmax}} + \frac{W_i}{W_{max}} \right) \quad \text{Equation 15}$$

where  $i$  indicates the yield strength and strain energy values for a particular specimen  $i$  while  $max$  refers to the maximum values of  $\sigma$  and  $W$  out of a number of investigated specimens.

From Equations 13 through 15 the quality index  $Q_D$  may be formulated in the following relation: <sup>56-61</sup>

$$Q_D = \left( \frac{\sigma_{Pi}}{\sigma_{Pmax}} + \frac{W_i}{W_{max}} \right) \times (\sigma_{Pi} + 10 W_i) \quad \text{Equation 16}$$

The quality chart proposed by Alexopoulos and Pantelakis is shown in Figure 2.9. Equation 16 is used to generate this kind of chart in which each point represents three properties, namely, yield strength ( $YS$ ), strain energy density ( $W$ ), and the quality index value ( $Q_D$ ), as may be seen in Figure 2.9. These properties are used for the purpose of evaluating and selecting certain materials intended for a specific aeronautical application.

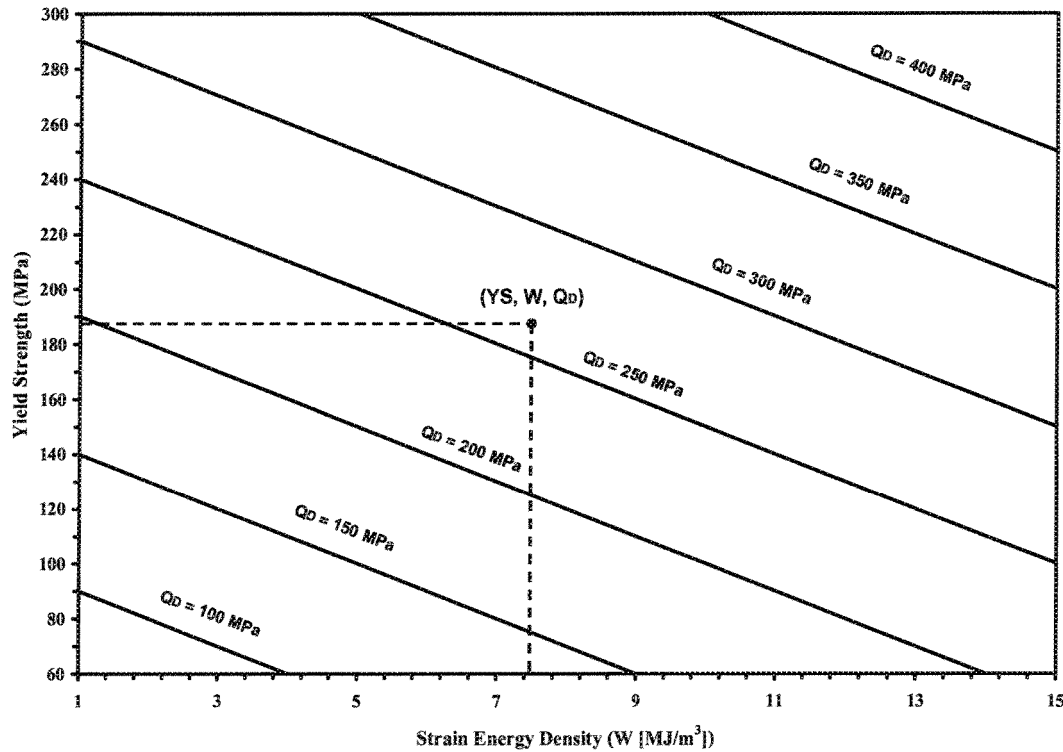


**Figure 2.9.** Example of the quality chart proposed by Alexopoulos and Pantelakis, as generated using Equation 16 with a  $K_D$  value of unity.

#### 2.4.5. Quality Index ( $Q_E$ ) Proposed by Tiryakioğlu *et al.*

Tiryakioğlu *et al.*<sup>62</sup> proposed a quality index based on the strain energy density, or toughness, of the specimen where the amount of the absorbed energy up to fracture is used as an indication of the material quality. The quality index proposed in this case represents the fraction of the target strain energy absorbed by the specimen where the energy absorbed is related to the presence of any structural discontinuity in the specimen under investigation. This quality index may be calculated by comparing the toughness of the specimen,  $W$ , with its threshold toughness,  $W_C$ , which represents the toughness of a

material free of major structural discontinuities. This index may hence be expressed by the following equation:

$$Q_E = \frac{W}{W_C} \quad \text{Equation 17}$$

The quality index, as expressed in Equation 17, is not usually recommended, however, since it does not include material strength as a parameter known to control alloy quality when combined with material toughness. For example, two specimens may have the same quality, *i.e.* the same toughness, in spite of the fact that their strength values are not equal.

With regard to the above-mentioned quality indices, it will be observed that the quality charts provided in Figure 2.3 and Figure 2.7 show all the tensile properties of the alloys, as discussed in sections 2.4.1 and 2.4.3. Therefore, this particular type of plot represents a significant tool for the purposes of evaluating, selecting, and predicting the most appropriate metallurgical conditions to be applied to Al-Si casting alloys when seeking specific properties. Accordingly, all the results emerging from the current study will be presented using these two types of charts, making use of the numerous tensile properties available for each point located in them. Generating such specific charts would provide a realistic and logical evaluation of the effects of various parameters on the tensile properties of the castings under study.

## **2.5. METALLURGICAL FACTORS**

Quality indices evaluate the quality of aluminum castings based on their mechanical properties so that any parameter affecting the properties of these alloys would also

necessarily influence their quality. The effects of metallurgical factors on the mechanical properties and quality of aluminum-silicon casting alloys will be reviewed in the following subsections. These parameters include: (i) impurity elements such as iron; (ii) hardening elements such as magnesium and copper; (iii) chemical modifiers such as strontium; (iv) solidification conditions; and (v) heat treatment procedures. To recapitulate, quality charts are used for the purpose of evaluating the mechanical properties and the quality of the castings under the influence of various metallurgical parameters; the quality chart concept has thus already been used as a selection tool for engineering materials in a wide range of studies.<sup>41-45, 48-61, 63, 64, 65, 66</sup>

### 2.5.1. Influence of Impurity Elements

Iron (Fe) is classified as an impurity element in aluminum-silicon casting alloys, and is considered to be the most prevalent in these alloys. The incidence of this particular impurity is due to the high solubility of Fe in liquid aluminum and the availability of numerous sources of iron during the casting process. On the other hand, iron displays limited solubility in solid aluminum where, at the eutectic temperature of 655°C, the solubility limit of iron in aluminum is ~0.04%; at 427°C, the solubility limit is less than 0.01%; while the solubility at room temperature would be even less than that.<sup>25, 67, 68, 69</sup> The amount of iron present in aluminum which exceeds the limit of solubility appears in the form of iron-bearing intermetallic phases such as  $\alpha$ -Al<sub>15</sub>Fe<sub>3</sub>Si<sub>2</sub>,  $\beta$ -Al<sub>5</sub>FeSi,  $\pi$ -Al<sub>8</sub>Mg<sub>3</sub>FeSi<sub>6</sub> and  $\delta$ -Al<sub>4</sub>FeSi<sub>2</sub>.<sup>70</sup> The detrimental influence of iron on the mechanical properties of aluminum casting alloys, specifically on ductility and fracture toughness, is

directly related to the volume fraction, size and morphology of the iron-containing phases formed in the metal matrix.<sup>67, 70, 71</sup>

The effects of Fe-content on the mechanical properties and the quality index of Al-Si casting alloys have been presented and discussed in a number of studies which, in principle, reported similar results regarding the deleterious effect of iron on the mechanical properties and the quality values of Al-Si casting alloys.<sup>41, 42, 48, 50, 72, 73, 74</sup> Whaler<sup>72</sup> observed that increasing the iron-content in modified and unmodified 356-T6 castings results in a considerable reduction in their ductility, as may be seen in Figure 2.10.

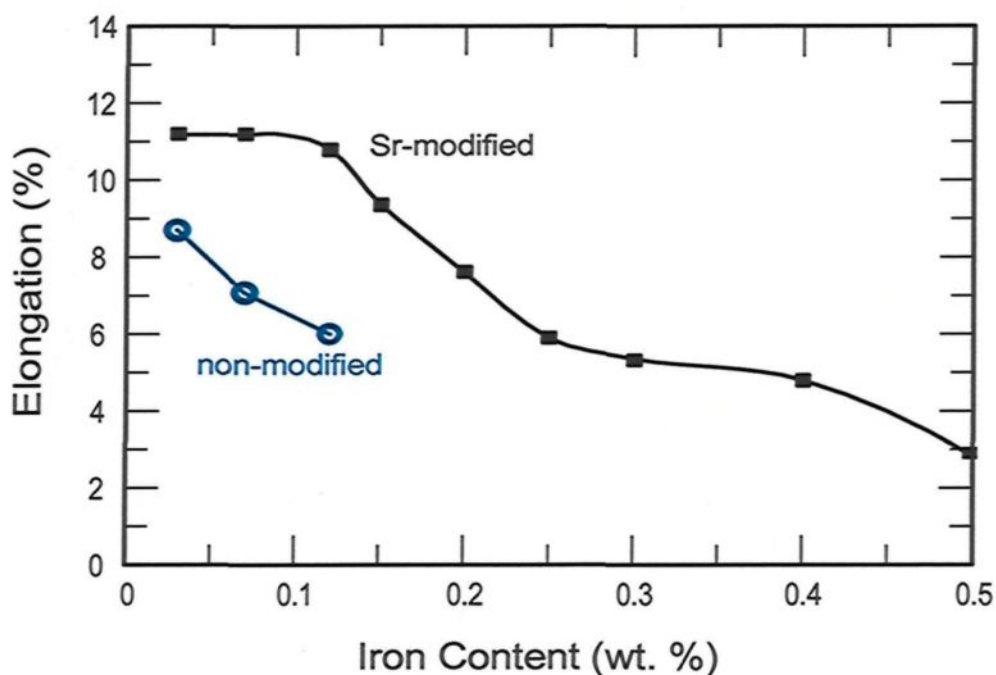


**Figure 2.10.** Influence of Fe-level on the ductility of modified and unmodified 356-T6 alloys.<sup>72</sup>

Another study<sup>72-74</sup> investigated the influence of iron-level on the quality index of 356 casting alloys aged at 155°C for various lengths of time. The results of this study are

shown in Figure 2.11 where it was observed that increasing the iron content reduces the tensile properties and quality index values of 356 castings under the various aging times applied. It was concluded that the alloys incorporating the best quality could be obtained by minimizing their iron content, as may be seen in Figure 2.11.

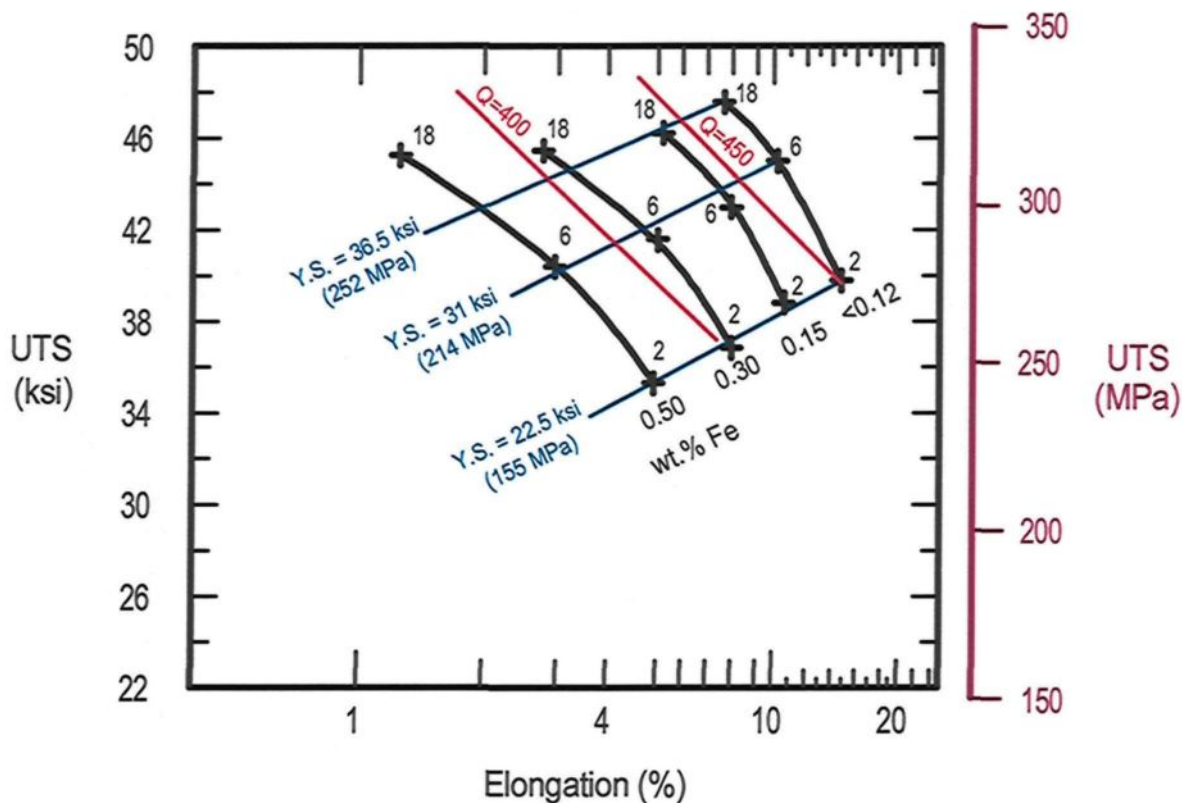


**Figure 2.11.** Tensile properties and quality index values of 356 alloys as a function of aging time at 155°C and iron content.<sup>72-74</sup>

### 2.5.2. Influence of Hardening Elements

Hardening elements are added to Al-Si casting alloys for the purpose of increasing their strength and hardness values. It is possible to further optimize the beneficial outcome of the addition of these strengthening elements by applying adequate heat treatment procedures. Magnesium (Mg) and copper (Cu) are the most common hardening elements to be added to Al-Si casting alloys.

The effects of Mg-content on the quality index and the mechanical properties of Al-Si casting alloys were examined in a number of studies. Drouzy *et al.*<sup>41</sup> reported that increasing the Mg content from 0.25% to 0.44% in a sand cast Al-7Si-Mg alloy results in increasing the strength of the alloy without any appreciable change being observed in its quality index.

A further study<sup>72, 74</sup> investigated the influence of Mg-content on the tensile properties and quality index of Al-7Si-Mg casting alloys containing Mg in the range of 0.06% to 0.44%. It was observed that increasing Mg-levels in the range mentioned results in increasing the strength and raising the quality index of the alloys, as may be observed in Figure 2.12. The improved quality of the casting, in this case, is related to the fact that the amount by which alloy ductility is decreased as a result of adding Mg is less than the amount by which the strength is increased; thus, the overall effect of increasing Mg from 0.06% to 0.044% is an increase in the quality index.

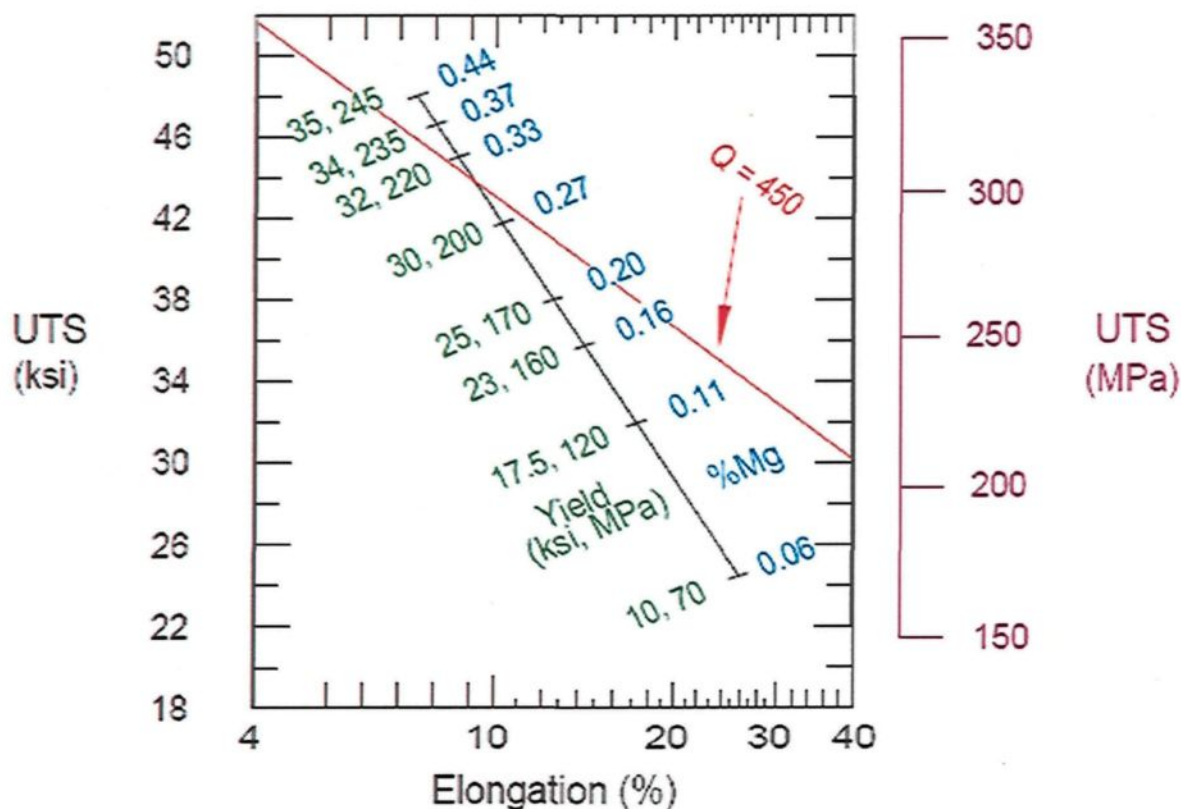


**Figure 2.12.** Effects of Mg-content on tensile properties and quality index of Al-7%Si alloy castings. <sup>72, 74</sup>

Cáceres and Barresi<sup>50</sup> studied the influence of Mg-content (0.3, 0.5, and 0.7%) on the quality index of Al-7Si-Mg casting alloys investigated under conditions of various iron levels, solidification rates, and heat treatments. It was concluded that the quality index value of 356/357 alloys may be optimized if the Mg-content does not exceed 0.5% in order to avoid the precipitation of the  $\pi$ -Al<sub>3</sub>Mg<sub>3</sub>FeSi<sub>6</sub> phase. Figure 2.13 shows that the best possible compromise between the strength, ductility, and quality of the alloys may be attained at an intermediate level of Mg-content, at a lower iron level, at a higher solidification rate, *i.e.* smaller dendrite arm spacing (DAS), and at the prevailing under-aged condition.

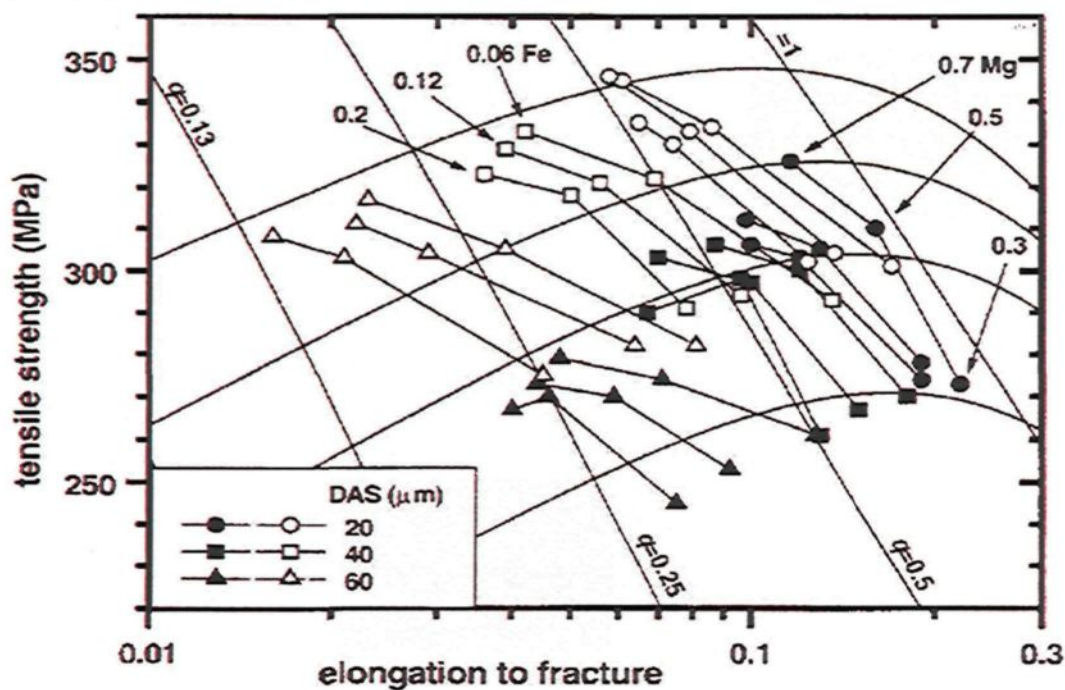


**Figure 2.13.** A quality index chart illustrating the effects of Mg-content, Fe-level, solidification rate, and heat treatment on the tensile properties and quality index of Al-7Si-Mg alloys. Under-aging and peak-aging conditions are indicated by solid symbols and open symbols, respectively.<sup>50</sup>

Copper (Cu) is a highly efficacious alloying element commonly added to aluminum alloys in order to improve their strength and hardness.<sup>6, 75, 76</sup> Lemon and Howle<sup>1</sup> investigated the influence of copper content (0, 0.4, 0.8, 1.2, 1.6, 2, 3, 4 wt% Cu) on the tensile properties of permanent mold Al-9%Si-0.5%Mg, in which the cast specimens were subjected to T6- and T62-heat treatments; the results of this study are presented in Figure 2.14. The straight lines shown in Figure 2.14 represent the range of tensile properties which may be obtained when connecting the results obtained from T6- and T62-tempers for each copper level. Lemon and Howle<sup>1</sup> observed that the optimum copper content is between 1.6 and 2 wt%. This copper concentration would provide the best compromise between

strength and ductility, and ultimately lead to the best quality in Al-9%Si-0.5%Mg casting alloys, as may be seen in Figure 2.14. Based on the results obtained, Lemon and Howle<sup>1</sup> selected two alloys having the optimum combination of strength and ductility accompanied by the ensuing quality. These are the 359-type Al-9%Si-0.5%Mg-0%Cu and the 354-type Al-9%Si-0.5%Mg-1.8%Cu alloys. Sigworth<sup>74</sup> re-plotted the results shown in Figure 2.14 using the quality index chart and he observed that copper concentrations of up to 1.8 wt% influence the quality index of Al-9%Si-0.5%Mg casting alloys advantageously as a result of the significant increase apparent in their tensile strength and the slight decrease in their ductility.

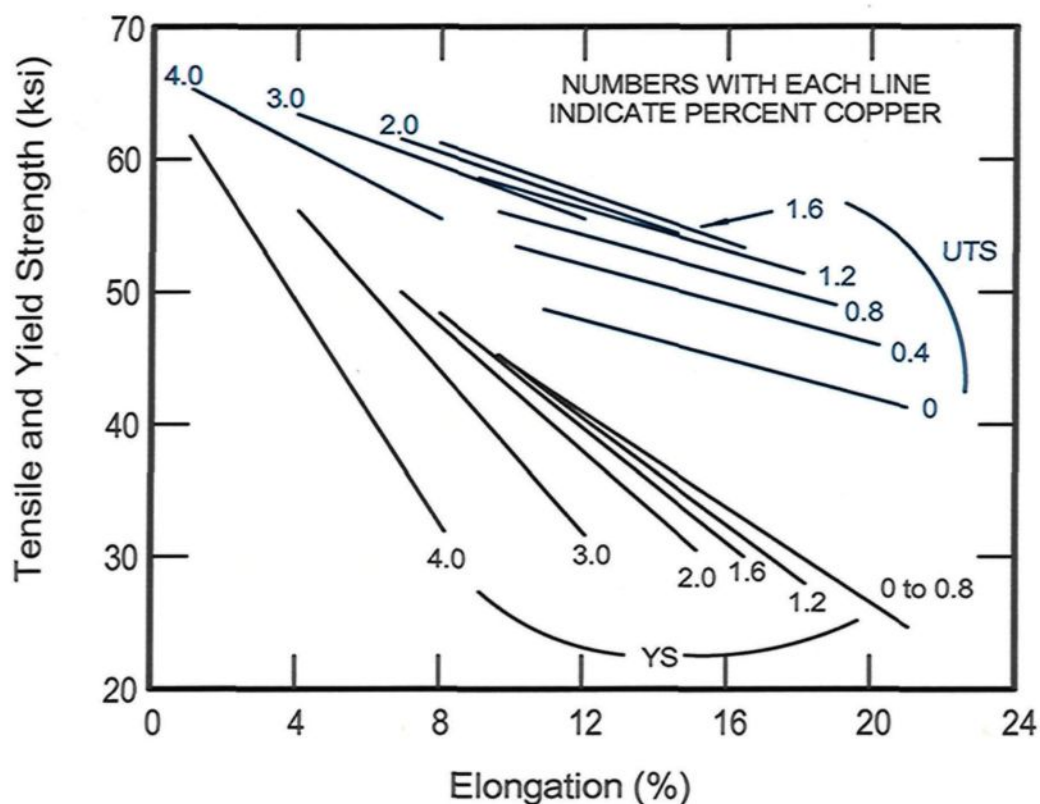


**Figure 2.14.** Tensile properties of permanent mold Al-9%Si-0.5%Mg casting alloys having various Cu contents and subjected to T6- and T62-temperatures.<sup>1</sup>

Cáceres *et al.*<sup>2</sup> studied the influence of the content of Cu and other elements, such as Mg, Si, Fe and Mn, as well as of the cooling rate on the mechanical properties and quality index of T6-tempered Al-Si-Cu-Mg casting alloys. They concluded that the overall effect of the strengthening elements such as Cu and Mg is the lessening of the quality index values of the alloys, as may be seen in the quality chart shown in Figure 2.15. The loss in quality in this case is directly related to the decreased ductility as a result of the cracking of second phase particles occurring in the strengthened alloys. It was also observed that the degree by which the quality index is affected upon the addition of copper depends not only on the copper-content itself but also on the presence of other elements existing with the copper such as Mg, Si, and Fe, as may be seen from Figure 2.15.

### **2.5.3. Influence of Modification**

Eutectic silicon particles play a critical role in determining the mechanical properties and the overall quality of an aluminum-silicon casting alloy. The size and morphology of the eutectic silicon particles are intrinsically responsible for the improved or the deteriorated mechanical properties of an Al-Si casting. Unmodified eutectic silicon particles are characterized by their coarse acicular plate-like form which diminishes the mechanical properties of the castings, in particular, ductility. The modification of Si particles aims at transforming their coarse acicular morphology into a fine fibrous form. These changes in the size and morphology of silicon particles results in enhanced ductility and strength, ultimately leading to improved quality.<sup>42, 77, 78, 79, 80</sup>

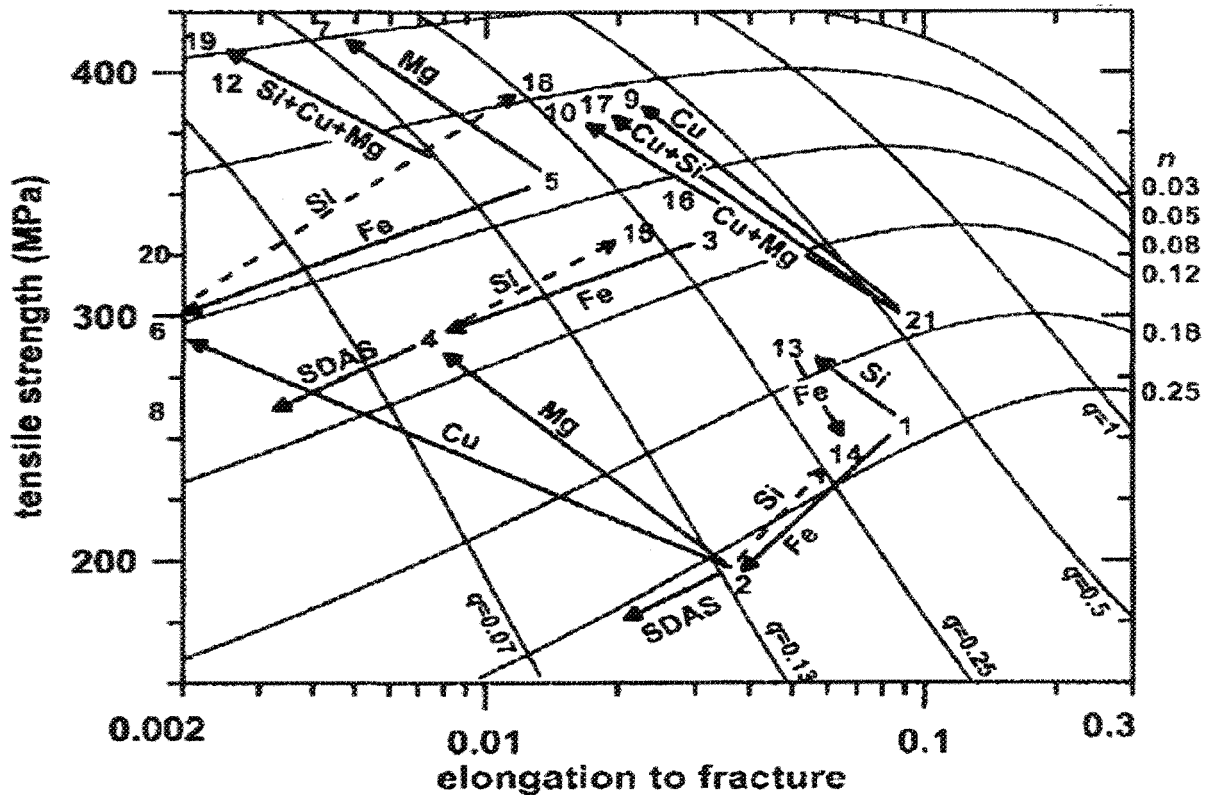


**Figure 2.15.** Quality chart illustrating the influence of the content of Cu and other elements (Mg, Si, Fe, and Mn) as well as cooling rate, as indicated by arrows, on the strength and quality index of Al-Si-Cu-Mg alloys. The numbers 1 through 21 located in the chart represent various alloy compositions.<sup>2</sup>

Several elements were observed to have a modifying effect on the eutectic silicon particles; these are sodium (Na), potassium (K), rubidium (Rb), cesium (Cs), strontium (Sr), calcium (Ca), barium (Ba), yttrium (Y), and lithium (La).<sup>8,9,81</sup> The value of  $\sim 1.64$  was proposed<sup>9,82,83,84</sup> as the ideal ratio of the atomic radius of a chemical modifier to that of silicon where twinning at the silicon-liquid interface is created when the ratio exceeds 1.65. This concept was introduced by Lu and Hellawell<sup>82</sup> where they proposed that the modifying agent is adsorbed at the silicon-liquid interface and results in growth twins and

branching of silicon particles. Sodium (Na) was used for many years as the optimum modifier for Al-Si alloys since it produces the greatest number of twins at the silicon interface. The selection of a modifying agent, however, is based on several factors including its ability to dissolve in the melt; its vapour pressure; its stability in the melt after dissolution; its affinity for oxidation; and the ability to adjust the amount of the additions.<sup>8, 9, 82, 84</sup>

Strontium replaced sodium as a preferred modifying agent since Na has several limitations when used as a modifier. Sodium (Na) has low solubility in molten aluminum, high vapour pressure, and a high affinity for oxidation. As a result of this, Na has a limited recovery rate of 20-30% of the amount added to the melt.<sup>8,9</sup> On the other hand, Sr addition is kept under satisfactory control by making use of master alloys such as Al-10%Sr. Strontium also has a low affinity for oxidation and its recovery reaches 90-100% of the amount added for which reason this element has become the most prevalent modifying agent in industrial applications.<sup>8, 9, 78, 85</sup> Several theories were proposed to facilitate understanding the mechanism of eutectic silicon modification.<sup>8, 9, 81, 82, 86</sup> The majority of these theories are based on two concepts, namely, the restricted nucleation and the restricted growth mechanisms of eutectic silicon particles in the presence of a modifying agent.

The addition of the appropriate amount of Sr improves the mechanical properties, specifically, the ductility and the quality index of Al-Si casting alloys.<sup>42, 79, 80, 87, 88</sup> Closset and Gruzleski<sup>89</sup> studied the influence of Sr-level on the quality index of A356-T6 casting alloys which had been subjected to three cooling rates. They observed that the strontium

range of 0.005%-0.015% is the optimum amount which may be added to A356 alloys to improve their mechanical properties and quality index values. The results of this investigation are presented in Figure 2.16 where it may be observed that inappropriate Sr-content may result in under-modification or over-modification of the alloys. Such effects are deleterious to the mechanical properties and the quality of the castings, as may be seen in Figure 2.16. The drop in the quality index of A356-T6 alloys in the case of an over-modified structure is related to the formation of Sr-containing phases such as  $Al_4SrSi_2$  and to the coarsening of silicon particles.<sup>8,27,90</sup>

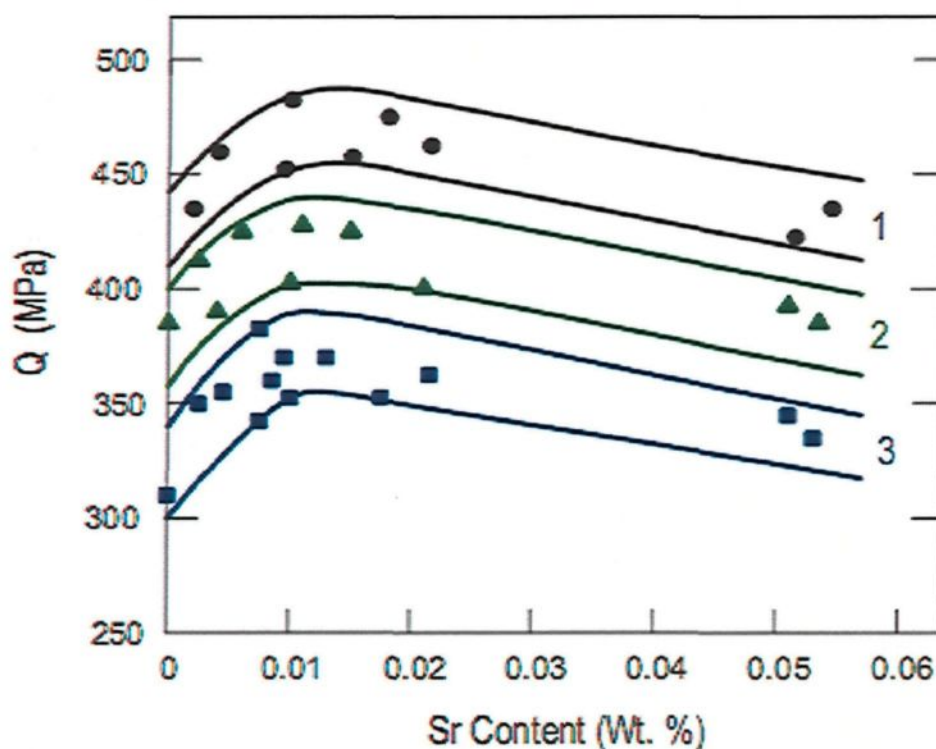


**Figure 2.16.** The quality index  $Q$  as a function of the level of Sr for A356-T6 casting alloys subjected to three solidification rates.<sup>8,89</sup>

#### 2.5.4. Influence of Solidification Conditions

The solidification rate has a considerable influence on the mechanical properties and the quality of Al-Si casting alloys where it affects the microstructural constituents of these castings. Secondary dendrite arm spacing (SDAS) is used to describe the solidification rate; thus a smaller SDAS is an indication of a rapid cooling rate while a larger SDAS refers to a slower solidification rate.

Boileau *et al.*<sup>91</sup> investigated the influence of various solidification times on the microstructure and mechanical properties of A356-T6 castings. A wedge-shaped mold was used to produce a casting which was designed for the specific purpose of providing a range of cooling rates or solidification times. It was observed, in this respect, that the fatigue strength, ultimate tensile strength, and the ductility of the castings were significantly enhanced when increasing the cooling rate, *i.e.* by reducing the solidification time. These improvements in the mechanical properties were related to the positive influence to be observed concerning the SDAS and porosity obtained by increasing the cooling rate. On the other hand, yield strength was observed to display negligible changes under the various solidification times applied. Oswalt and Misra<sup>92</sup> reported similar results in relation to the effect of solidification rate on the tensile properties of A356 and A357 Al-Si-Mg casting alloys.

Sigworth<sup>72</sup> collected and then collated data from a number of studies regarding the effects of solidification rate on the tensile properties of A356-T6 castings. The data were plotted in the form of a quality chart, as shown in Figure 2.17, where the tensile properties were plotted as a function of the SDAS. It was observed that the quality index values of the

castings were optimized by an increase in the solidification rate. The enhanced quality, in this case, results from the improved tensile strength and ductility of the castings. The highest quality was obtained for the shortest solidification time, *i.e.* the smallest SDAS. The code for each curve is an abbreviation used to identify the reference to the data used to generate each curve.<sup>72</sup>

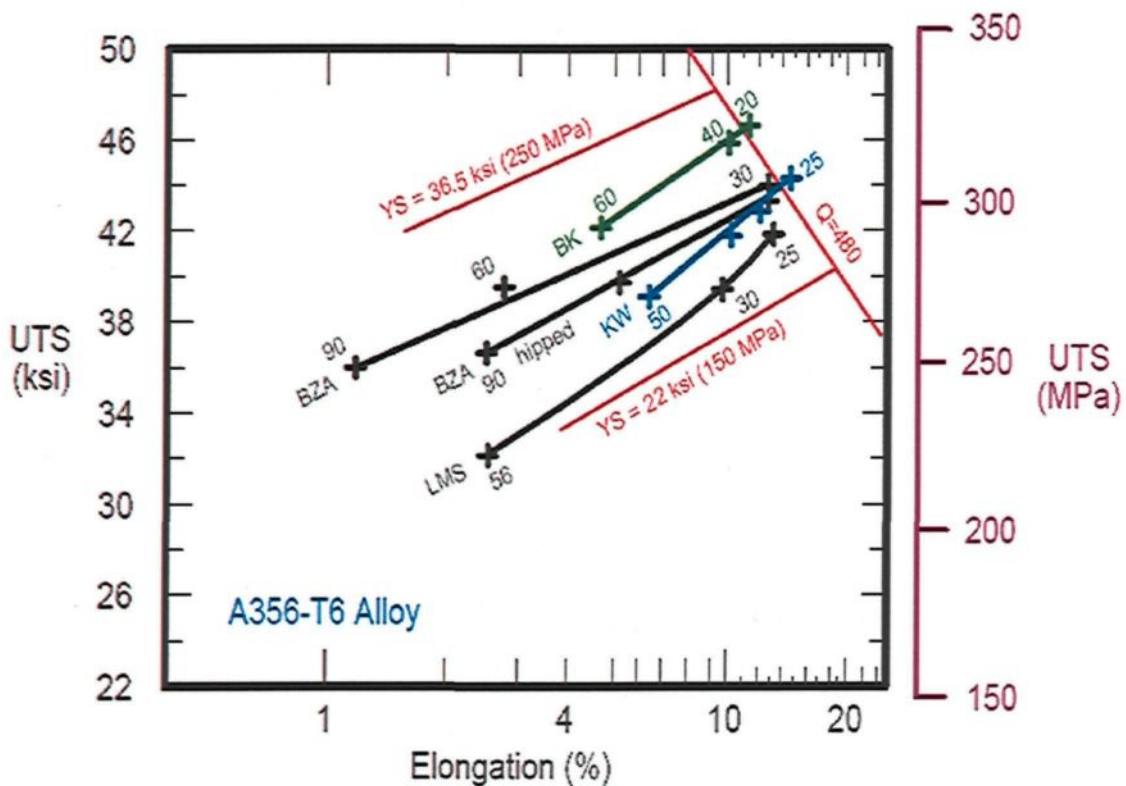


**Figure 2.17.** Quality chart illustrating the effects of solidification rate on the tensile properties and quality of A356-T6 alloy castings. The numerical values give the SDAS in microns.<sup>72</sup>

### **2.5.5. Influence of Heat Treatment**

Heat treatment may be applied to aluminum-silicon alloys for the purpose of improving their mechanical properties through a number of microstructural changes which take place as a function of the applied heat treatment regime and the designated thermal treatment parameters, *i.e.* temperature and time. The most prevalent complete thermal treatment for industrial applications is the T6-treatment. This technique comprises three stages: solution heat treatment, quenching, and aging, all of which will be introduced and discussed in the following subsections.

#### **2.5.5.1. Solution Heat Treatment**

Solution heat treatment includes the exposure of the casting to high temperatures for a certain length of time; the temperatures involved should correspond to the safety limits for the melting temperature expected for the phases in the cast structure so as to avoid the incipient melting of these same phases. Applying the appropriate solution heat treatment to Al-Si castings enhances the mechanical properties and quality index of these alloys as a result of the beneficial influence of this particular treatment on the microstructural features of these casting alloys. Several studies were carried out regarding the effects of solution heat treatment parameters, *i.e.* temperature and time, on the microstructure and mechanical properties of Al-Si casting alloys.

Taylor *et al.*<sup>93</sup> studied the influence of solution treatment on the microstructural characteristics of Al-Si-Mg alloys. It was observed that applying the solutionizing treatment at 540°C for 6 hours results in homogenizing the cast structure. The concentration profile of Mg was observed to have homogenous distribution over certain

selected dendrite arms. Regarding an Al-7%Si-0.5%Mg-0.12%Fe alloy, the matrix content of Mg was observed to increase from 0.44wt% to 0.49wt% upon increasing the solution temperature from 540°C to 555°C for either 1 or 6 hours. Similar observations were reported for the same alloy regarding the concentration profile of Si over the dendrite arms. In the same study, further observations were reported regarding the effects that solutionizing treatment may have on the microstructure of Al-Si-Mg alloys. Such observations as the dissolution of the Mg<sub>2</sub>Si phase, the spheroidization and coarsening of eutectic silicon particles, and the dissolution of the  $\pi$ -Al<sub>3</sub>Mg<sub>3</sub>FeSi<sub>6</sub> phase and its transformation into the  $\beta$ -Al<sub>5</sub>FeSi phase, particularly in the alloys containing 0.3wt% - 0.4wt% Mg.

Shivkumar *et al.*<sup>94</sup> investigated the effects of solution heat treatment parameters on the microstructural features and mechanical properties of A356.2 Al-Si-Mg alloys, and observed that 1-2 hours are the optimum solutionizing time at 540°C for permanent mold Sr-modified 356 alloys. Furthermore, increasing the solutionizing temperature to 550°C reduces the optimum time to a maximum of 1 hour and provides a further increase in the quality index values of the permanent mold Sr-modified alloys. The increased quality index values upon implementing this increase may be related to the increase in the dissolved Mg in the solid solution; to the reduction in the degree of heterogeneity of the cast structure; and to the increase in the rate of spheroidization of eutectic silicon particles. A further increase in the solutionizing temperature is not recommended since incipient melting of the eutectic structure was observed at a temperature range falling between 560°C and 563°C.

Several studies reported that the safest and most effective solution heat treatment of 356 Al-Si-Mg alloys is observably at 540°C for 4-12 hours.<sup>95</sup> On the other hand, the solutionizing temperature for these alloys was successfully increased experimentally to 550°C<sup>94, 96</sup> and 555°C.<sup>93</sup> Applying such high temperatures for industrial use, however, is not recommended in order to avoid any possibility of incipient melting of the microstructural constituents.

The solution heat treatment of Al-Si alloys containing copper requires a critical approach because of the lower melting point of the eutectic Al<sub>2</sub>Cu phase. Wang *et al.*<sup>97</sup> studied the influence of solutionizing temperatures on the microstructure and mechanical properties of 319.0 casting alloys with and without the addition of beryllium (Be). The selection of a solutionizing temperature for this particular alloy is of major importance since it contains 3.6% Cu. Three solutionizing temperatures of 490°C, 510°C, and 520°C were applied to the 319 castings for a period of 8 hours. For the Be-free samples, it was observed that raising the temperature from 490°C to 510°C results in a considerable improvement in the tensile properties, hardness, and quality index of the castings. These improvements in the mechanical properties were related to the microstructural changes occurring when increasing the temperature; they include the spheroidization of eutectic silicon; the dissolution and fragmentation of  $\beta$ -Al<sub>3</sub>FeSi platelets; and the reduction in the amount of blocklike Al<sub>2</sub>Cu phase. A further increase in the solution temperature to 520°C was observed to deteriorate the mechanical properties of the castings because of the local melting of the Al<sub>2</sub>Cu phase.

With regard to the Be-containing alloys, it was observed that the addition of beryllium increases the eutectic melting temperature of Al-Al<sub>2</sub>Cu from 515°C to 522°C; in this case, further improvements in the mechanical properties and quality index of the 319.0 alloys were observed even at a solutionizing temperature of 520°C. Samuel *et al.*<sup>98</sup> reported that increasing the solution temperature of 319.2 alloys in the range of 480°C to 515°C for 2 to 24 hours results in improving the ultimate tensile strength and elongation of the castings. This range of temperatures provides safe limits for the dissolution of the Al<sub>2</sub>Cu phases. The dissolution of these phases was observed to be further accelerated in the range of 505°C - 515°C. Any further increase in the solutionizing temperature to 540°C results in degraded tensile strength and elongation as a result of the melting of the eutectic copper phase.

Li<sup>99</sup> investigated suitable solution heat treatment parameters for 354 and 355 casting alloys as a function of eutectic silicon particle characteristics and mechanical properties. For the purpose of selecting suitable solutionizing temperatures, the castings were subjected to solutionizing temperatures in the range of 517°C - 547°C for 12 hours. It was observed, in this regard, that the optimum temperatures are 525°C and 535°C for 354 and 355 alloys, respectively. For selecting suitable solution heat treatment times, the castings were subjected to a solutionizing temperature of 527°C for a time range of 20 minutes to 48 hours. Taking into consideration the eutectic silicon particle characteristics and mechanical properties of 354 and 355 casting alloys, it was observed that 10-12 hours is the optimum solutionizing time for both alloys at 527°C. Similar results were reported<sup>100</sup> concerning the optimum solution heat treatment time for 354 alloys where the best

mechanical properties were obtained after solutionizing the 354 alloy at 525°C for 10-12 hours.

Solution heat treatment applied to Al-Si alloys results in improved microstructural characteristics, as well as enhanced mechanical properties and quality indices. Inappropriate solutionizing treatment, however, results in a number of drawbacks such as incipient melting;<sup>101, 102, 103</sup> surface blistering;<sup>104, 105</sup> and dimensional changes.<sup>25, 98</sup>

#### **2.5.5.2. Quenching**

The rapid cooling of the castings which follows the solution heat treatment step is known as quenching. The castings are quenched by rapid cooling to lower temperatures in water, oil, ambient air, or any other suitable quenching medium. This step aims at preventing the precipitation of equilibrium phases such as Al<sub>2</sub>Cu and Mg<sub>2</sub>Si while retaining the highest amount of solute atoms and vacancies in a supersaturated solid solution. Achieving these objectives during the quenching step provides optimum conditions for a successful precipitation process during the subsequent aging treatment. The time delay in quenching and the quenching rate are the major parameters controlling the mechanical properties in this particular heat treatment step.

It is always recommended, from a practical point of view, to perform quenching as soon as possible after the solution heat treatment for the purpose of minimizing the time delay in quenching.<sup>24, 106</sup> The quenching rate should be increased carefully to certain limits so as to avoid such problems as the formation of residual stresses and distortions of the castings which might accompany a very fast quenching rate.<sup>24, 25, 106</sup> Zhang and Zheng<sup>107</sup> applied quenching to A356 alloys using four quenching rates in still air and in water at

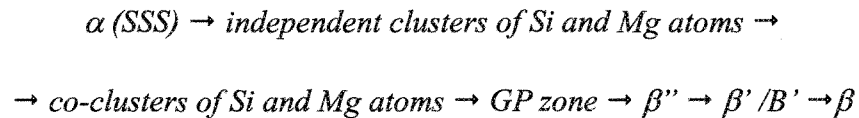
three temperatures, namely, 25°C, 60°C and 95°C each. It was observed that increasing the quenching rate from 0.5°C/s to 250°C/s, which corresponds to quenching in still air and water at 25°C, respectively, produces considerable improvement in the tensile properties of the A356 alloys.

Byczynski *et al.*<sup>108</sup> investigated the influence of quenching rates on the mechanical properties of 319 alloys. Five different quenching rates were applied to the 319 castings. These include: (i) quenching in warm water (65°C) at a quenching rate of 18.8°C/s; (ii) atomized water/air quenching at a rate of 5.5°C/s; (iii) high velocity air quenching at a rate of 3.8°C/s; (iv) still air quenching at a rate of 0.5°C/s; and (v) slow cooling at a rate of 0.02°C/s by quenching the samples in a heat treatment furnace at 505°C. The hardness was observed to increase steadily in the quenching rate ranging from 0.5°C/s to 18.8°C/s while in the range of 0.02°C/s to 0.5°C/s there was no significant change to be observed in the hardness of the alloys. The ultimate tensile strength was observed to increase in the quenching rate ranging from 0.02°C/s to 3.8°C/s while no significant change in strength was observed at quenching rates higher than 3.8°C/s. Elongation was observed to decrease upon increasing the quenching rate as a result of the increase in the strength and hardness of the alloys. Byczynski *et al.*<sup>108</sup> reported that quenching rate influences not only the mechanical properties of the 319 casting alloys but also the dimensions of the samples. A dimensional growth was observed from 0.03% at 0.5°C/s to 0.06% at 5.5°C/s which means that the dimensional growth increases by 100% in the quenching rate range of 0.5°C/s to 5.5°C/s.

### 2.5.5.3. Aging Treatment

The solution treatment and quenching process are followed by an aging treatment where the castings are subjected to a specified temperature for a certain period of time. Aging temperature and aging time are the two variables which control the characteristics of the phases precipitated during the aging treatment, and they ultimately also control the mechanical properties of the alloys.

The hardening effect which is an outcome of applying an aging treatment to Al-Si-Mg alloys is directly related to the precipitation of Mg-Si-containing phases. These phases have several different forms according to the phase transformation sequence occurring under the effects of temperature and time applied during the aging treatment. The most accepted precipitation sequence in Al-Mg-Si alloys was proposed as having the following phase transformation sequence: <sup>109, 110, 111, 112</sup>



This sequence represents various phases expected to form during aging treatment of an Al-Mg-Si alloy based on the aging parameters applied. Table 2.3 lists the main characteristics of these phases.

The aging treatment of an aluminum alloy containing copper as the alloying element results in the formation of various forms of Al-Cu-containing precipitates. The precipitation sequence of an Al-Cu alloy during the aging process has been proposed as follows: <sup>113, 114, 115</sup>



**Table 2.3.** Characteristics of Mg-Si phases formed during aging treatment. <sup>116, 117, 118, 119</sup>

Precipitated Phase	Unit Cell	Morphology
GP	Monoclinic, $a = 14.8 \text{ \AA}$ , $b = 4.05 \text{ \AA}$ , $c = 6.48 \text{ \AA}$ , $\beta = 105.3^\circ$	Spherical / Needles
$\beta''$	Monoclinic, $a = 15.16 \text{ \AA}$ , $b = 4.05 \text{ \AA}$ , $c = 6.74 \text{ \AA}$ , $\beta = 105.3^\circ$	Needles
$\beta'$	HCP, $a = 7.05 \text{ \AA}$ , $c = 4.05 \text{ \AA}$	Needles / Rods
$B'$	HCP, $a = 10.3 \text{ \AA}$ , $c = 4.05 \text{ \AA}$	Lath / Ribbons
$\beta$	FCC, $a = 6.39 \text{ \AA}$	Plates / Cubes

The coherent and semi-coherent phases,  $\theta''$  and  $\theta'$  respectively, contribute to increasing the strengthening level of the alloys. On the other hand, the incoherent equilibrium precipitate  $\theta$  ( $\text{Al}_2\text{Cu}$ ) results in diminishing the hardening level of the alloys because of the loss of coherency between the stable phases and the metal matrix. The main characteristics of the Al-Cu containing phases are listed in Table 2.4.

With regard to an aluminum alloy containing Cu and Mg as the hardening elements, the aging treatment results in the formation of a range of precipitates. In addition to forming  $\theta$ - $\text{Al}_2\text{Cu}$  precipitate and its precursors, other hardening phases are expected to form as well. The  $S$ - $\text{Al}_2\text{CuMg}$  phase and its precursors are further hardening precipitates which were observed to form during the aging treatment of an aluminum alloy containing Cu and

**Table 2.4.** Characteristics of Al-Cu phases formed during aging treatment. <sup>113, 115, 120</sup>

Precipitated Phase	Unit Cell	Morphology
GP	Cu-layer(s)	Disc
$\theta''$	Tetragonal, $a = 4.04\text{\AA}$ , $b = 4.04\text{\AA}$ , $c = 7.68\text{\AA}$	Plates
$\theta'$	Body-Centered Tetragonal $a = 4.04\text{\AA}$ , $b = 4.04\text{\AA}$ , $c = 5.80\text{\AA}$	Plates
$\theta$	Body-Centered Tetragonal $a = 6.066\text{\AA}$ , $b = 6.066\text{\AA}$ , $c = 4.874\text{\AA}$	Plates

Mg. The formation of the *S*-phases during aging treatment presents the following precipitation sequence: <sup>113, 120, 121, 122, 123, 124</sup>



This sequence starts as usual with the decomposition of the supersaturated solid solution (SSS) followed firstly by the formation of Guinier-Preston-Bagaryatsky (GPB) zones and then by the precipitation of the coherent  $S''$ , the semi-coherent  $S'$ , and finally the incoherent equilibrium  $S$  ( $\text{Al}_2\text{CuMg}$ ) phase.

The coherent  $S''$  and the semi-coherent  $S'$  precipitates are the main source of hardening in the aluminum alloy containing Cu and Mg and they are also responsible for increasing the strengthening level of this type of alloy, whereas overaging conditions result in the precipitation of the incoherent equilibrium  $S$  phase. For the same alloy with a high Cu-to-Mg ratio, a new phase designated as  $\Omega$  was observed to precipitate having a

composition close to the  $\text{Al}_2\text{Cu}$  phase,<sup>115, 120, 125</sup> although in the presence of silicon the  $\Omega$ -phase will not precipitate.<sup>120</sup> Another phase was also reported to form during the aging treatment of an Al-Cu-Mg alloy; this phase is designated as  $\sigma$  and has the composition of  $\text{Al}_5\text{Cu}_6\text{Mg}_2$ .<sup>120, 125</sup> Table 2.5 lists the crystal structure and morphology of the various phases reported to precipitate during the aging treatment of Al-Cu-Mg alloys.

**Table 2.5.** Characteristics of Al-Cu-Mg phases formed during aging treatment.<sup>113, 120, 125</sup>

Precipitated Phase	Unit Cell	Morphology
GPB	Orthorhombic, $a = 4.05\text{\AA}$ , $b = 9.05\text{\AA}$ , $c = 7.24\text{\AA}$	Laths / Rods
$S''$	Monoclinic, $a = 3.2\text{\AA}$ , $b = 4.04\text{\AA}$ , $c = 2.54\text{\AA}$	Laths / Rods
$S'$	Orthorhombic, $a = 4.04\text{\AA}$ , $b = 9.25\text{\AA}$ , $c = 7.17\text{\AA}$	Laths
$S$	Orthorhombic, $a = 4\text{\AA}$ , $b = 9.23\text{\AA}$ , $c = 7.14\text{\AA}$	Laths / Rods
$\Omega$	Tetragonal, $a = 6.066\text{\AA}$ , $c = 4.96\text{\AA}$ / Orthorhombic, $a = 4.96\text{\AA}$ , $b = 8.59\text{\AA}$ , $c = 8.48\text{\AA}$	Fine Plates
$\sigma$	Cubic, $a = 8.31\text{\AA}$	Cuboid Shape

Regarding the age-hardening of an aluminum alloy containing Si, Cu, and Mg as alloying elements, *i.e.* an Al-Si-Cu-Mg alloy, several precipitates may form in the Al-Si-Cu-Mg quaternary system based on the level of alloying elements contained in it, as well as on the aging temperatures and times applied. It was reported that a quaternary  $Q$ -phase and

its precursors precipitate during the age-hardening treatment of an Al-Si-Cu-Mg alloy.<sup>113, 126, 127, 128</sup> The precipitation sequence which leads finally to the formation of the stable  $Q$ -phase in Al-Si-Cu-Mg alloys may have the following form:<sup>126, 127, 129</sup>



Table 2.6 lists the crystal structure and morphology of the  $Q$ -phase and its precursors reported to precipitate during the aging treatment of Al-Si-Cu-Mg alloys.

**Table 2.6.** Characteristics of  $Q$ -phase and its precursors formed during aging treatment of Al-Si-Cu-Mg alloys.<sup>126, 127, 129</sup>

Precipitated Phase	Unit Cell	Morphology
$QP$	Hexagonal $a = 3.93\text{\AA}, c = 4.05\text{\AA}$	Rods
$QC$	Hexagonal $a = 6.7\text{\AA}, c = 4.05\text{\AA}$	Rods
$Q'$	Hexagonal	Laths
$Q$	Hexagonal $a = 10.4\text{\AA}, c = 4.05\text{\AA}$	Rods

The strengthening mechanism results from an age-hardening treatment which depends on the interaction between the moving dislocations and the precipitated phases.<sup>130,</sup>

<sup>131</sup> When a moving dislocation meets a precipitate, there is a balance of forces which results from the resistance exerted by the precipitate against the moving dislocation; this is shown

schematically in Figure 2.18. From this figure the balance of the forces between the moving dislocation and the precipitate may be described by the following equation:<sup>131</sup>

$$F = 2T \sin \theta \quad \text{Equation 18}$$

where  $F$  refers to the resistance force exerted by the precipitate against the moving dislocation and  $T$  indicates the line tension of the moving dislocation. The maximum line tension of the moving dislocation will be attained when  $\theta = 90^\circ$ . In the case of this kind of interaction, there exist two general conditions according to the nature of the precipitate itself. In the case of hard precipitates, the particle will not be deformed and the resistance force  $F$  can be greater than  $2T$  thus the dislocation will bypass the precipitate by cross-slip or by Orowan looping. In the case of soft particles, the precipitates will be sheared by the moving dislocation where  $2T$  can be greater than  $F$  and the dislocation will then pass through the particle itself.<sup>131</sup>

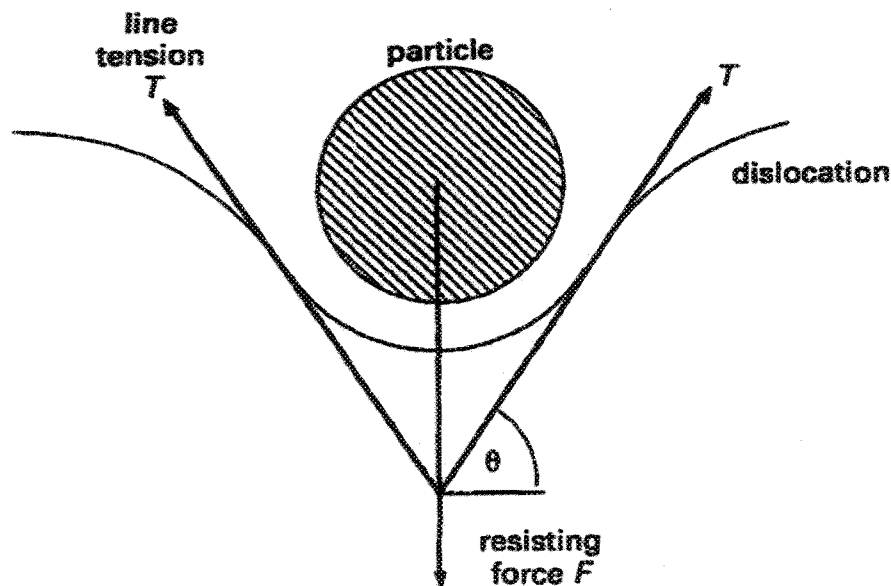


**Figure 2.18.** The balance of forces between a moving dislocation and a precipitate resisting its motion.<sup>131</sup>

The hard particles provide maximum hardening levels for the age-hardened alloys while the soft ones provide lower strength and hardness values. The strengthening effect which results from hard particles depends on the volume fraction and the size of these precipitates. In other words, the hardening level obtained in the case of hard particles depends on inter-particle spacing. The correlation between the yield strength and the inter-particle spacing, in the case of hard precipitates, is given by the Orowan relation:<sup>131, 132</sup>

$$\Delta\tau_y = Gb/L \quad \text{Equation 19}$$

where  $\Delta\tau_y$  is the increase in the yield strength as a result of resisting the dislocation motion by means of the hard particles,  $G$  is the shear modulus of the matrix,  $b$  is the Burger's vector of dislocation and  $L$  is the inter-particle spacing. The precipitation-hardening is more effective upon increasing the volume fraction of the precipitates and upon decreasing their size, in other words, the maximum hardening level will be attained upon decreasing the inter-particle spacing, as may be observed from Equation 19.

The effects of aging treatment on the mechanical properties and the quality indices of Al-Si casting alloys were examined and discussed in several studies.<sup>41, 48, 50-53, 57, 59, 61, 64</sup> Drouzy *et al.*<sup>41</sup> studied the effects of aging temperature and time on the tensile properties and the quality index of the sand-cast Al-7Si-Mg casting alloy, and observed that, in the underaged condition, the ultimate tensile strength increases while elongation decreases, as shown in Figure 2.19. For the range of over-aging conditions, it was observed that the ultimate tensile strength and elongation decreases with increasing aging time, as may be seen in Figure 2.19. With respect to the results shown for the same figure, it was observed

that, in the under-aging range, the quality of the alloys was observed to be independent of the aging conditions applied to the castings where the behavior of the aging curves are approximately parallel to the *iso-Q* lines.

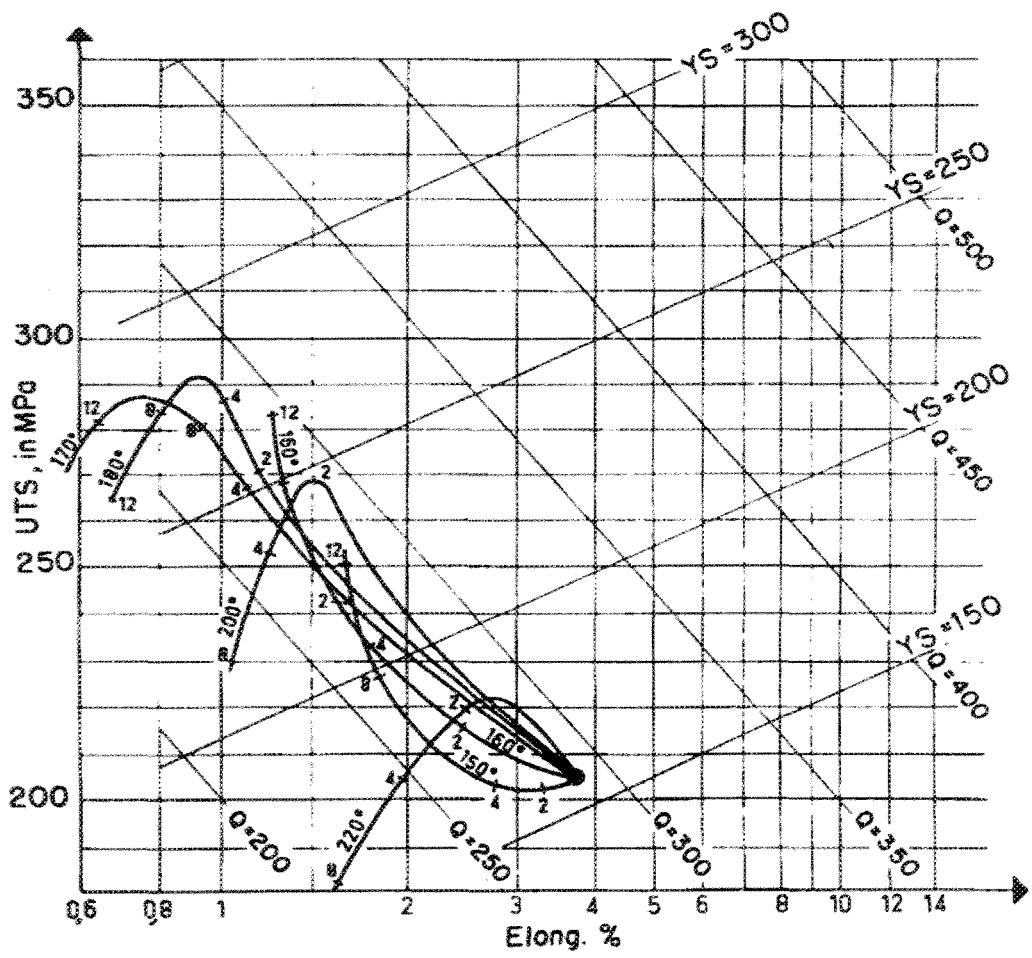


**Figure 2.19.** Effects of aging temperature and time on the tensile properties and quality index of the sand-cast 356 Al-7%Si-0.3%Mg alloy.<sup>41</sup>

The yield strength was observed to depend strongly on the aging conditions applied to the castings and on the presence of the hardening elements such as Mg. Drouzy *et al.*<sup>41</sup> observed that, within the range of aging conditions applied in practice, a 10°C rise in the aging temperature reduces the aging time by 50% to obtain the same level of tensile

properties. The variations in the yield strength of the 356 Al-7%Si-0.3%Mg and 357Al-7%Si-0.6%Mg alloys occurring with the aging temperature, aging time, and Mg-content are all shown in Figure 2.20. This figure represents a good correlation between the three variables of aging temperature, aging time, and Mg-content together with two mechanical properties, namely, yield strength and hardness. Figure 2.20 could be used to determine the suitable aging treatment for obtaining certain desired mechanical properties in the 356 and 357 alloys.

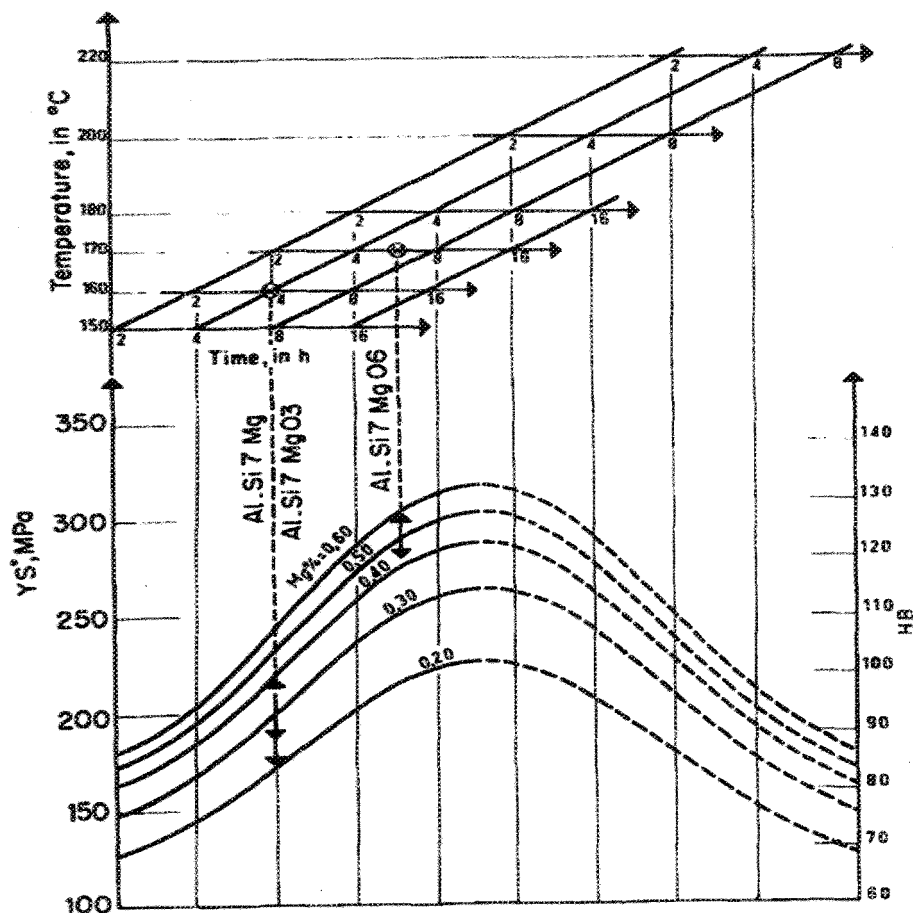


**Figure 2.20.** Effects of aging temperature and aging time as a function of Mg-content on the probable yield strength and hardness of sand cast 356 Al-7%Si-0.3%Mg and 357 Al-7%Si-0.6%Mg alloys, for each temperature, using only the portion of the curves corresponding to the graduated part of the time scale.<sup>41</sup>

## **CHAPTER 3**

# **METHODOLOGY AND EXPERIMENTAL TECHNIQUES**

## **CHAPTER 3**

### **3. METHODOLOGY AND EXPERIMENTAL TECHNIQUES**

#### **3.1. INTRODUCTION**

The subsections on methodology and experimental techniques were drawn up with a view to investigating the influence of a number of metallurgical parameters on the tensile properties and quality indices of 354-Al-9%Si-1.8%Cu-0.5%Mg and 359-Al-9%Si-0.5%Mg casting alloys. The variables investigated include iron (Fe) level; copper (Cu) content; strontium (Sr) level; magnesium (Mg) content; solidification rate; solution heat treatment temperature; solution heat treatment time; aging temperature; and aging time. For the purposes of accomplishing this objective, the methodology intended for the current study includes a number of different procedures. The experimental procedures applied to this research include melting and casting processes; heat treatment; tensile testing; and microstructural characterization. Each step of the experimental procedures will be elaborated upon subsequently.

#### **3.2. MELTING AND CASTING PROCESSES**

Alloy 356, in the form of ingots, was melted in 40-kg capacity silicon carbide crucibles; the alloying elements were then added to the molten metal in order to adjust the desired compositions of 354- and 359-type casting alloys. Silicon, copper, and magnesium were provided in the pure form, whereas iron and strontium were added in the form of Al-

25%Fe and Al-10%Sr master alloys, respectively. The alloys coded 1N and 10N represent the chemical composition of the unmodified 359- and 354-base alloys in the absence of any additions. Alloys coded 1S through 12S alloys were produced in order to study the influence of iron and copper on the tensile properties and quality indices of the Sr-modified alloys. Four levels of copper (0, 0.5, 1, and 1.8 wt%) and three percentages of iron (0.07, 0.2, and 0.35 wt%) were produced for the purposes of this study. The alloys coded 1SM through 6SM represent the 359 alloy containing six levels of magnesium (0.5, 0.6, 0.7, 0.8, 0.9, and 1 wt%) and were produced for the purpose of investigating the effects of Mg-content on the properties of this specific alloy.

The molten metal was degassed using pure argon injected into the melt by means of a rotary degassing impeller at a speed of 150 rpm/30 min. Five samples for chemical analysis were also taken simultaneously from each alloy during casting so as to make sure that the actual average chemical compositions were obtained. The chemical analysis was carried out using a Spectrolab Jr CCD Spark Analyzer shown in Figure 3.1; Table 3.1 thus shows the actual chemical compositions of the alloys produced.

After degassing and with the intention of casting tensile test bars, the molten metal was poured at  $735 \pm 5^\circ\text{C}$  into a permanent mold of the ASTM B-108 type which had been preheated to  $465^\circ\text{C}$ . Figure 3.2(a) shows a picture of the actual ASTM B-108 permanent mold used for casting, while Figure 3.2(b) is a schematic representation of the casting obtained from the mold where two test bars may be cast at the same time. Figure 3.2(b) also illustrates the dimensions of the tensile test specimens and their location within the permanent mold used. <sup>133</sup>

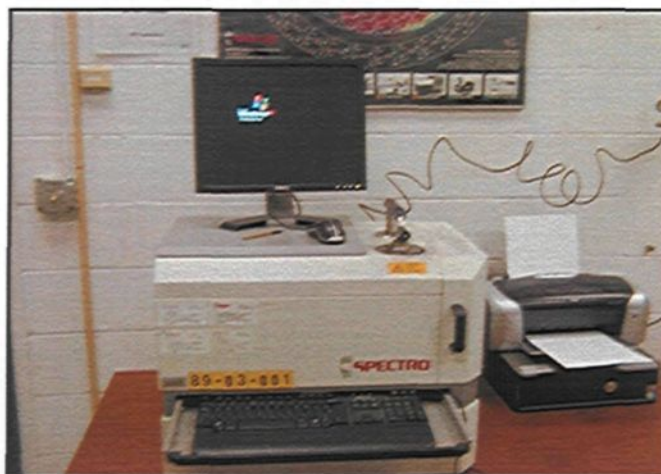


Figure 3.1. Spectrolab Jr CCD Spark Analyzer used in the current study.

Table 3.1. Actual chemical composition of the alloys investigated for the current study.

		Chemical Analysis, wt%												
		Si	Fe	Cu	Mg	Sr	Mn	Zn	Ti	B	Ga	V	Ni	Al
<b>Code of the Alloys Produced</b>	<b>1N</b>	8.530	0.080	0.101	0.458	0.000	0.001	0.002	0.007	0.000	0.009	0.011	0.004	Bal
	<b>10N</b>	8.650	0.082	1.780	0.486	0.000	0.001	0.001	0.007	0.001	0.009	0.009	0.003	Bal
	<b>1S</b>	8.721	0.077	0.012	0.478	0.010	0.001	0.001	0.007	0.001	0.009	0.007	0.003	Bal
	<b>2S</b>	8.757	0.217	0.011	0.496	0.011	0.001	0.001	0.007	0.001	0.009	0.008	0.003	Bal
	<b>3S</b>	8.707	0.379	0.010	0.465	0.010	0.001	0.001	0.007	0.001	0.009	0.007	0.003	Bal
	<b>4S</b>	9.170	0.087	0.446	0.491	0.011	0.000	0.001	0.007	0.001	0.009	0.008	0.003	Bal
	<b>5S</b>	8.984	0.225	0.451	0.494	0.011	0.001	0.001	0.007	0.002	0.009	0.008	0.003	Bal
	<b>6S</b>	8.779	0.392	0.496	0.494	0.010	0.002	0.001	0.007	0.002	0.009	0.008	0.003	Bal
	<b>7S</b>	9.142	0.094	0.913	0.498	0.011	0.000	0.001	0.008	0.001	0.009	0.008	0.004	Bal
	<b>8S</b>	8.957	0.224	0.919	0.506	0.012	0.001	0.001	0.008	0.002	0.009	0.008	0.003	Bal
	<b>9S</b>	8.850	0.386	0.920	0.490	0.011	0.002	0.002	0.007	0.001	0.009	0.008	0.003	Bal
	<b>10S</b>	9.080	0.095	1.953	0.506	0.012	0.000	0.001	0.007	0.001	0.009	0.009	0.004	Bal
	<b>11S</b>	9.058	0.234	1.796	0.506	0.012	0.001	0.001	0.007	0.001	0.009	0.008	0.004	Bal
	<b>12S</b>	8.954	0.398	1.753	0.495	0.011	0.002	0.001	0.008	0.001	0.009	0.008	0.003	Bal
	<b>1SM</b>	8.794	0.092	0.053	0.488	0.007	0.003	0.001	0.009	0.001	0.008	0.008	0.003	Bal
	<b>2SM</b>	8.885	0.095	0.056	0.603	0.007	0.004	0.001	0.010	0.001	0.008	0.008	0.003	Bal
	<b>3SM</b>	8.839	0.084	0.027	0.691	0.008	0.002	0.001	0.008	0.001	0.008	0.008	0.003	Bal
	<b>4SM</b>	8.953	0.087	0.028	0.818	0.007	0.002	0.001	0.008	0.001	0.008	0.008	0.003	Bal
<b>5SM</b>	8.935	0.102	0.015	0.914	0.007	0.001	0.001	0.007	0.001	0.007	0.008	0.003	Bal	
<b>6SM</b>	9.088	0.087	0.017	1.058	0.006	0.001	0.001	0.007	0.001	0.008	0.008	0.003	Bal	

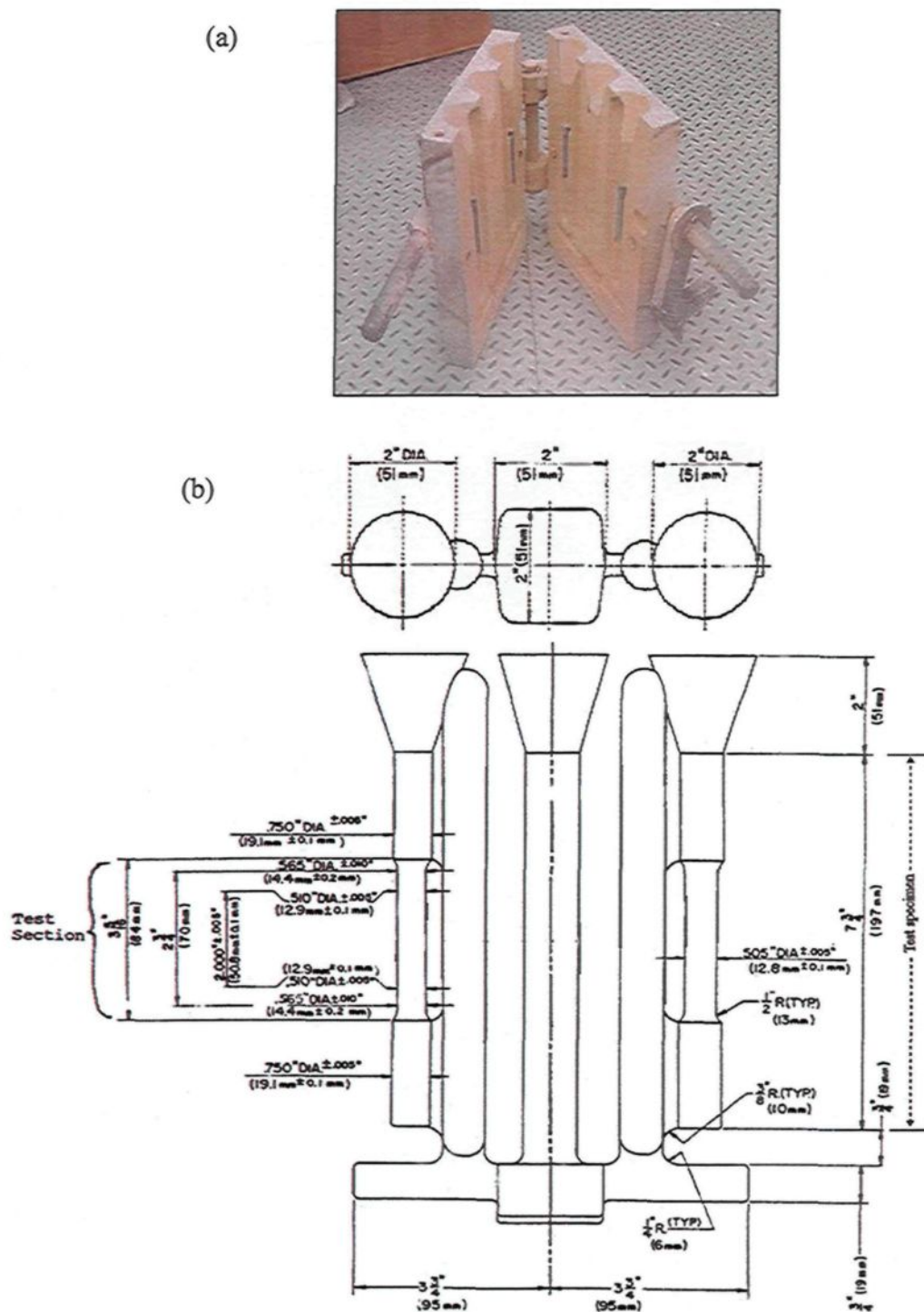
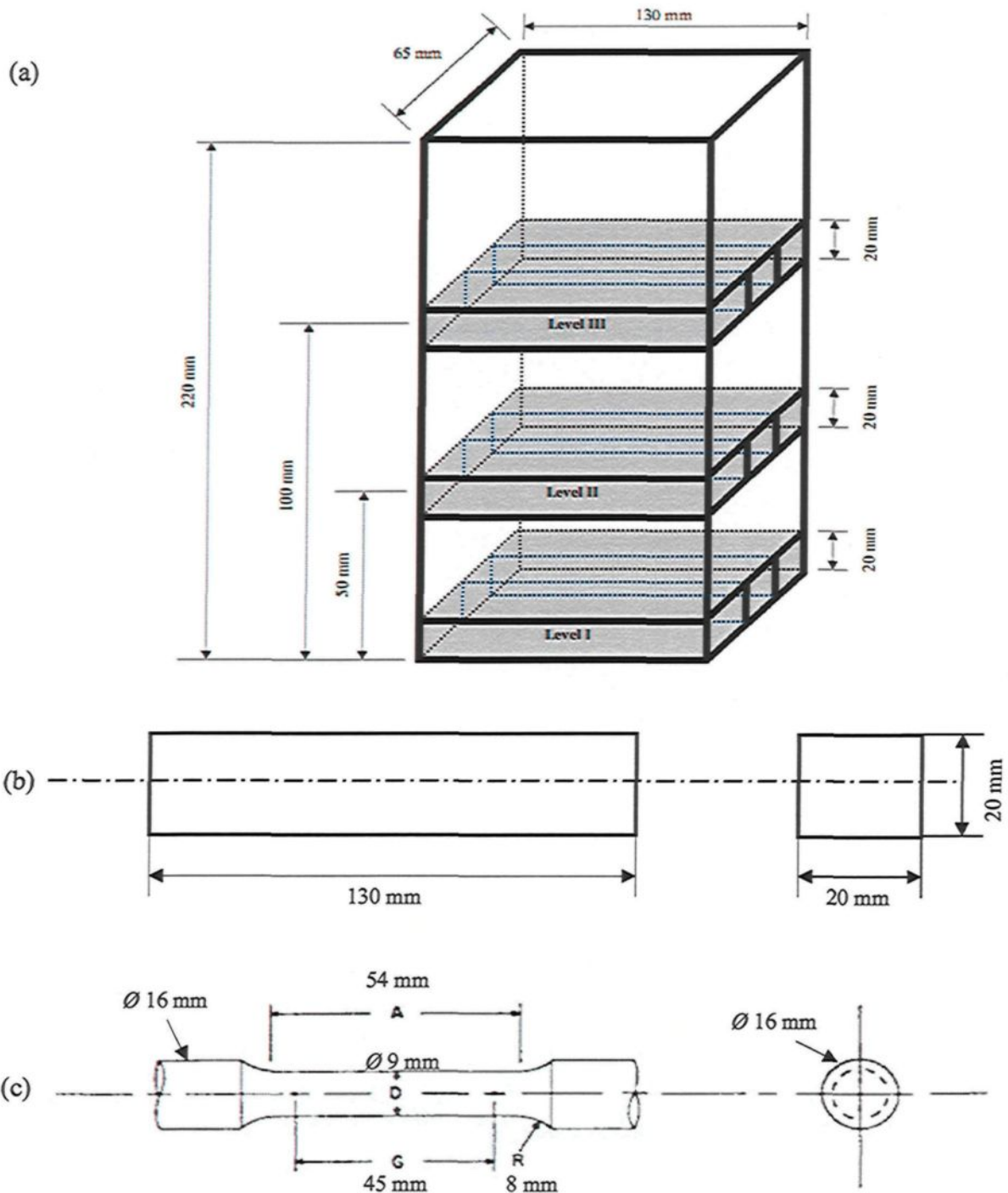


Figure 3.2. (a) ASTM B-108 permanent mold used for casting; and (b) schematic representation of the permanent mold casting used to prepare the tensile test specimens. <sup>133</sup>

A rectangular end-chill mold was used for casting a series of test bars made of the 1S and 10S alloys for the purpose of investigating the influence of solidification rate on the properties of the 359 (1S) and the 354 (10S) casting alloys. Refractory materials were used to construct the four walls of the mold. After assembling the end-chill mold, it was preheated to 250°C so as to dry it out by removing the moisture. The same melting procedures mentioned above for the ASTM B108 mold were applied to produce casting blocks using the end-chill mold.

The end-chill mold provides a range of cooling rates for the same casting based on the location of each part of the casting in relation to the base of the mold. The bottom portion of the casting has the highest cooling rate since it is attached to a copper base supplied with running water during the casting process. On the other hand, the upper portion of the casting has the lowest cooling rate. Three cooling rates were selected from the casting blocks produced, based on the distance from the bottom of the mold, as shown in Figure 3.3(a). The specimen blank corresponding to Level I provided samples with the highest solidification rate (SDAS  $\sim 30 \mu\text{m}$ ) while the Level III blank produced specimens with the lowest cooling rate (SDAS  $\sim 90 \mu\text{m}$ ). Each specimen blank provided three tensile test specimens. The specimen blanks were sectioned according to the dimensions shown in Figure 3.3(a). The dimensions of the blank used for machining each test specimen are shown in Figure 3.3(b); the centrelines of the tensile test bars machined from each blank passed through the selected levels, as shown in Figure 3.3(b,c). Figure 3.3(c) illustrates the dimensions of the test specimen which replies to the ASTM E8M-04 standards.<sup>134</sup>



**Figure 3.3.** A schematic representation of (a) the end-chill mold casting block used to prepare the tensile test specimens; (b) the blank used to machine the test specimen; and (c) the dimensions of test specimens prepared according to ASTM E8M-04 standards.<sup>134</sup>

### 3.3. HEAT TREATMENT

The heat treatment procedures were carried out in three treatment stages: *solution heat treatment, quenching, and aging*. The solutionizing procedures for the castings were carried out in a forced air furnace having  $\pm 2^\circ\text{C}$  as a temperature variation; these were followed by quenching in warm water at a temperature of  $60^\circ\text{C}$ , and finally the aging stage was completed by heating the castings in the same forced air furnace. Heat treatment procedures aim at investigating a number of variables relating to the tensile properties and the quality indices of the 354 and 359 casting alloys. The variables studied were:

*(i) The effects of solutionizing temperatures on the tensile properties and the quality indices of 354- and 359-type castings containing three levels of iron, i.e. 0.07%, 0.2%, and 0.35% Fe.* The solution heat treatment was carried out at ten different temperatures for the 354 alloys (10S, 11S and 12S) specifically  $490^\circ\text{C}$ ,  $495^\circ\text{C}$ ,  $500^\circ\text{C}$ ,  $505^\circ\text{C}$ ,  $510^\circ\text{C}$ ,  $515^\circ\text{C}$ ,  $520^\circ\text{C}$ ,  $525^\circ\text{C}$ ,  $530^\circ\text{C}$  and  $537^\circ\text{C}$ , while the solutionizing treatment for 359 alloys (1S, 2S and 3S) was carried out at  $490^\circ\text{C}$  and  $537^\circ\text{C}$ . All the solutionizing treatments mentioned were carried out for a fixed length of time of 12 hours followed by a pre-determined aging treatment at  $170^\circ\text{C}$  for 8 hours.

*(ii) The influence of solution heat treatment time on the tensile properties and the quality indices of modified and non-modified 354- and 359-type castings.* Alloys 10S and 1S represent the modified 354 and 359 alloys, respectively, whereas 10N and 1N represent the corresponding unmodified alloys. The solutionizing procedures for this stage were carried out for the alloys in the same forced air furnace as used above for six time-periods of 1 hour, 4 hours, 8 hours, 12 hours, 16 hours, and 24 hours each. All the solutionizing

treatments mentioned were carried out at a fixed solutionizing temperature of  $537 \pm 2^\circ\text{C}$  for the 359 alloys while for the 354 alloys a temperature of  $520^\circ\text{C} \pm 2^\circ\text{C}$  was applied. At this stage, the samples were solution heat-treated and then quenched in warm water at  $60^\circ\text{C}$ , after which the samples were subjected to tensile testing. A T4-temper was thus used during this stage to examine the effects of Sr-modification on the response of the castings to solutionizing treatment.

*(iii) The effects of aging temperatures and times on the tensile properties and quality indices of the 354 and 359 base alloys, i.e. 10N and 1N alloys, respectively.* These alloys were treated at various aging temperatures for a wide range of aging times, as listed in Table 3.2. The 354 alloy was solution heat-treated at  $520^\circ\text{C} \pm 2^\circ\text{C}$  for 12 hours for all the aging conditions studied, whereas the 359 alloy was solution heat-treated at  $537^\circ\text{C} \pm 2^\circ\text{C}$  for 12 hours for all the aging conditions studied. It should be noted that the solution and aging treatments were carried out in the same forced air furnace.

**Table 3.2.** Aging temperature and time as applied to the 1N and 10N alloys in this study.

Aging Temperature ( $^\circ\text{C}$ )	Aging Time (hours)
155	1, 2, 4, 6, 8, 10, 12, 16, 24, 32, 40, 48 and 72
170	1, 2, 4, 6, 8, 10, 12, 16, 24, 32, 40, 48 and 72
195	0.083, 0.17, 0.25, 0.50, 0.75, 1, 2, 4, 6, 8, 10, 12, 16, 24, 32, 40, 48 and 72
220	0.083, 0.17, 0.25, 0.50, 0.75, 1, 2, 4, 6, 8, 10, 12, 16, 24, 32, 40, 48 and 72
245	0.083, 0.17, 0.25, 0.50, 0.75, 1, 2, 4, 6, 8, 10, 12, 16, 24, 32, 40, 48 and 72

### 3.4. MECHANICAL TESTING

Tensile testing was carried out for the as-cast and the heat-treated test bars at room temperature using an MTS Servohydraulic mechanical testing machine working at a strain rate of  $1.0 \times 10^{-4}$ /s. The elongation of the test specimens was measured using a strain gauge extensometer attached to the specimen during the tension test. A data acquisition system was attached to the MTS machine to provide the results of the tensile test. Figure 3.4 shows the MTS Servohydraulic mechanical testing machine used in the current study. For each sample tested a stress-strain curve was obtained to illustrate the mechanical behavior of the specimen under the loads applied. The tensile test results obtained from testing a specific specimen present the data pertaining to elongation to fracture, yield strength at 0.2% offset strain and ultimate tensile strength. Ten tensile test bars for each composition were tested in the as-cast and the heat-treated conditions, while for the test specimens produced from the end-chill mold, six tensile test specimens were tested for each cooling rate of the 1S and 10S alloys. A large number of test bars (approximately 3000) were cast in order to obtain a reliable evaluation of the influence of metallurgical parameters on the tensile properties and the quality indices of the 354 and 359 casting alloys.



**Figure 3.4.** The MTS Servohydraulic mechanical testing machine used in the current study.

### **3.5. MICROSTRUCTURAL CHARACTERIZATION**

The characterization of the microstructure of the 354 and the 359 alloys aims at correlating the microstructural features of these alloys with their tensile properties as well as with their quality indices. Several techniques were used in this regard for the purpose of achieving a qualitative and quantitative analysis of the microstructural constituents and

features, these being eutectic silicon particles; secondary dendrite arm spacing; intermetallic phases; hardening precipitates; and fracture surface characteristics.

The characteristics of eutectic silicon particles were examined using a Clemex Vision PE4 optical microscope and image-analysis system, as shown in Figure 3.5. The samples were examined in such a way as to cover the entire sample surface in a regular and systematic manner. With regard to the 359 alloy, quantitative analysis of the eutectic silicon particles was carried out for (a) 1S alloy samples solution-treated for 12 hours at 490°C and 537°C, followed by quenching and then aging at 170°C for 8 hours, and (b) for 1N and 1S alloy samples solution heat-treated at 537°C for the six specified solution times, followed by quenching. For the 354 alloy, quantitative analysis of the eutectic silicon particles was carried out for (a) 10S alloy samples solution-treated for 12 hours at the ten designated solution temperatures, followed by quenching and then aging at 170°C for 8 hours, and (b) for 10N and 10S alloy samples solution heat-treated at 520°C for the six specified solution times, followed by quenching.

The samples used for characterizing eutectic silicon particles were prepared from the gauge length of the tensile-tested specimens where samples 10 mm high were sectioned 1 cm below the fracture surface. These samples were mounted and then subjected to grinding and polishing procedures to produce a mirror-like surface. The mounting of the samples in bakelite was carried out using a Struers LaboPress-3 machine, while the grinding and polishing procedures were carried out using a TegraForce-5 machine. The grinding procedures were applied using silicon carbide (SiC) papers in a sequence of 120 grit, 240 grit, 320 grit, 400 grit, 600 grit, 800 grit, and finally 1200 grit sizes; it should be

noted that the word “grit” is used to represent a measure of fineness for abrasive materials and that water was used as a lubricant in this stage.

Polishing was carried out using Struers diamond-suspension, which contains a diamond particle size of 6  $\mu\text{m}$ , as the first step of the polishing process followed by further polishing through the application of the same suspension containing a smaller diamond particle size of 3  $\mu\text{m}$ . The lubricant used for this polishing stage is a Struers DP-lubricant. The final stage of polishing was carried out using a Mastermet colloidal silica suspension,  $\text{SiO}_2$ , having a particle size of 0.6  $\mu\text{m}$ . Water was used as lubricant throughout the final polishing stage, after which the samples displayed a mirror-like surface and were ready for the microstructural examination.

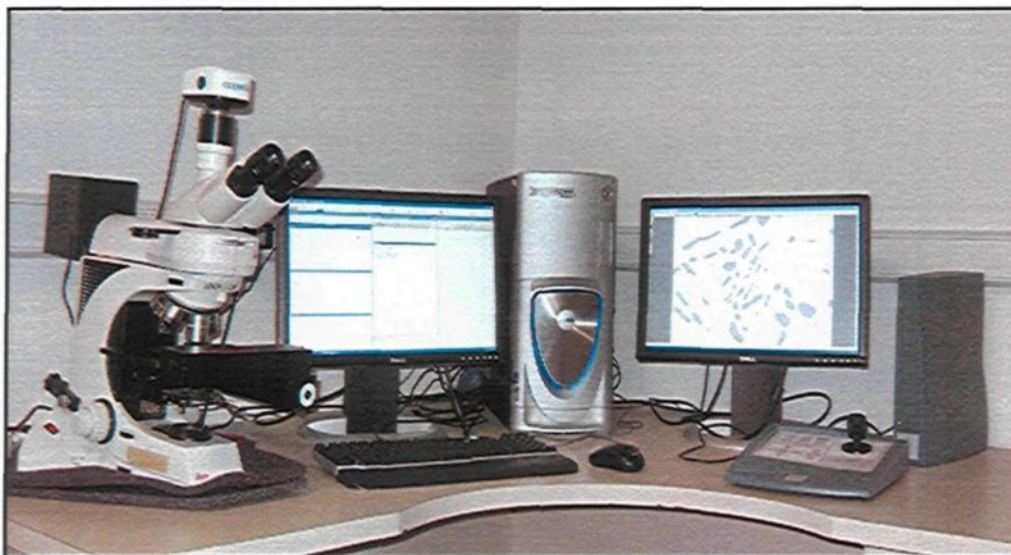


**Figure 3.5.** Clemex Vision PE4 image analysis system used for the present work.

Measurement of the secondary dendrite arm spacing (SDAS) was carried out for the 1S and 10S alloys which were cast using the end-chill mold. The SDAS was quantified for

the specimens obtained from the three levels of the casting blocks shown in Figure 3.3(a). The techniques used for measuring the SDAS involve using the same Clemex Vision PE4 optical microscope and image-analysis system. The line intercept method was used to calculate the average secondary dendrite arm spacing. Ten fields were examined for each sample, each field containing at least three lines which intercept the secondary dendrite arms. The samples were prepared for SDAS measurement using the same procedures applied for preparing the samples for eutectic silicon particle characterization.

The intermetallic phases were identified by means of an electron probe microanalyzer (EPMA) in conjunction with a wavelength dispersive spectrometer (WDS), using a JEOL JXA-8900L WD/ED Combined Microanalyzer operating at 20 kV and 30 nA with an electron beam size of  $\sim 2 \mu\text{m}$ . The electron probe microanalyzer system (EPMA) used in the current study is shown in Figure 3.6. The volume fraction of the intermetallic phases was quantified using a JEOL JXA-8900L model electron probe microanalyzer with a special built-in software based on phase brightness where the brightness of each phase is a function of its average atomic number. The atomic number of the phase measured must be greater than that of the aluminum base matrix (*i.e.* greater than 13). The quantification process is based on the elimination technique which calculates the volume fraction of each phase by subtracting the volume fraction of the brighter phases from the total volume fraction of the other phases present within the matrix. For each case, 15 fields were measured at 100X magnification.

The volume fraction of the intermetallic phases was quantified for alloys coded as 1S through 12S under three conditions, (i) as-cast, (ii) solutionized at 490°C, and (iii)

solutionized at 537°C for 359-type castings, *i.e.* the 1S through 9S alloys. For 354-type castings, *i.e.* 10S through 12S alloys, the intermetallic phases were quantified under as-cast, solutionized at 490°C and then again at 520°C. All the solutionizing treatments mentioned were carried out for a period of 12 hours each.

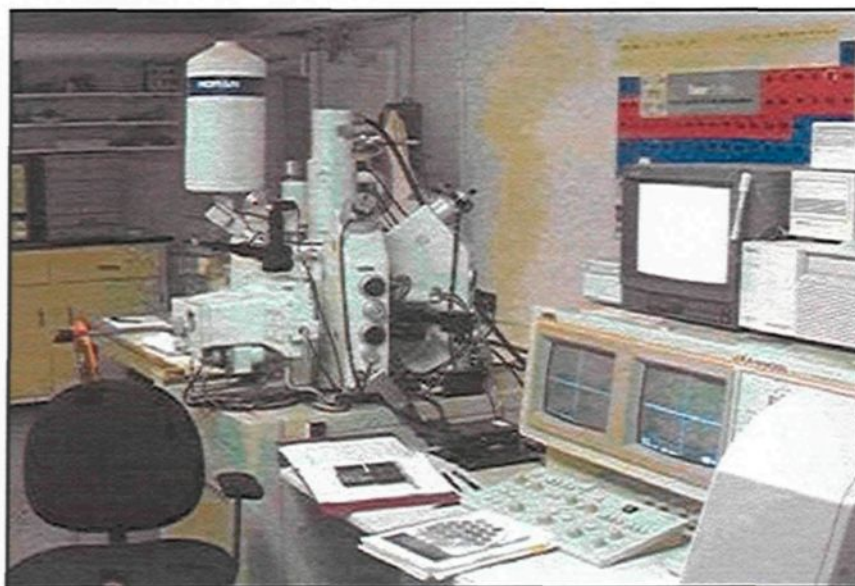


**Figure 3.6.** The electron probe microanalyzer (EPMA) system used in the current study.

The samples used for intermetallic phase identification were sectioned from castings prepared using a cylindrical graphite mold preheated to 600°C in order to obtain close-to-equilibrium solidification conditions. These samples were then mounted, ground, and polished using the same procedures as mentioned above.

Scanning electron microscopy (SEM) and field-emission scanning electron microscopy (FESEM) were used to examine the characteristics of the hardening precipitates under various heat treatment conditions for the 354 and 359 alloys. The purpose of applying these techniques of microscopic analysis is mainly to investigate the

distribution, size, and density of the hardening precipitates in the casting structure under the various aging temperatures and times involved. The SEM used in the current study is a JEOL 840A scanning electron microscope (SEM) attached to an EDAX Phoenix system designed for image acquisition and energy dispersive X-ray (EDX) analysis. The SEM was operated at a voltage of 15 kV, with a maximum filament current of 3 amperes. Figure 3.7 shows a photograph of the SEM used. The FESEM provides clear and less electrostatically distorted high resolution images even at low voltages; it produces images of 2.1 nm resolution at 1 kV and of 1.5 nm resolution at 15 kV. The FESEM used in this study is the Hitachi S-4700 FEGSEM shown in Figure 3.8.

The samples for precipitate characterization were prepared from the gauge length of the tensile-tested specimens. Samples 10 mm high were sectioned off 1 cm below the fracture surface. These samples were then subjected to grinding and polishing to produce a mirror-like surface by applying the same procedures used for preparing the samples for eutectic silicon particle characterization. Finally, these polished samples were further subjected to a chemical micro-etching process. The Keller etching reagent used for this study was the 0.5 mL HF (48%), *i.e.* a solution of 0.5 mL HF of a 48% concentration with the remaining 99.5 mL being water. This etchant was applied to the samples at room temperature for a length of time ranging from a few seconds to a few minutes based on the chemical composition of the alloys and the heat treatment procedures applied to them.

The fracture surface of selected samples was examined using the same JEOL 840A scanning electron microscope. Fracture surface analysis aims at investigating the nature of the fracture and identifying the main source of cracking and fracture in the alloy samples

examined. Samples for SEM examination were prepared from the tensile-tested specimens by sectioning them, this time, 1 cm immediately below the fracture surface, and mounting them carefully for subsequent fracture surface examination.



**Figure 3.7.** Scanning electron microscope system used in this work.



**Figure 3.8.** Field emission scanning electron microscopy used in the current study.

## **CHAPTER 4**

### **INFLUENCES OF ALLOY COMPOSITION, SOLIDIFICATION RATE, AND SOLUTIONIZING PARAMETERS**

## **CHAPTER 4**

### **4. INFLUENCES OF ALLOY COMPOSITION, SOLIDIFICATION RATE, AND SOLUTIONIZING PARAMETERS**

#### **4.1. INTRODUCTION**

The current chapter presents results and discussion concerning the influence of a number of metallurgical parameters on the tensile properties and quality indices of 354 and 359 casting alloys. The parameters studied are the effects of impurity elements such as iron; the influence of alloying elements such as copper and magnesium; the effects of solidification rate; the influence of solutionizing temperature; the effects of solution heat treatment time; and the influence of strontium on the response of the casting to solutionizing treatment. The tensile properties and the quality index of the castings will be correlated to their microstructural features and constituents under various conditions for the purposes of interpreting the results obtained. The microstructural characteristics of the castings will be presented in the next subsection.

#### **4.2. CHARACTERIZATION OF THE MICROSTRUCTURE**

The following subsections will discuss the characteristics of intermetallic phases, of eutectic silicon particles, and of secondary dendrite arm spacing (SDAS) under the specific conditions relative to 354 and 359 casting alloys.

#### 4.2.1. Characteristics of Intermetallic Phases

The characteristics of intermetallic phases observed in alloys 1S through 12S were examined using EPMA and WDS analysis for the as-cast and heat-treated conditions. The alloys produced for this purpose were cast using a graphite mold preheated to 600°C in order to obtain close-to-equilibrium solidification conditions. Alloys 1S through 9S were solution heat-treated at 490°C and at 537°C for a period of 12 hours each, followed by quenching in warm water at 60°C. These alloys, coded 1S through 9S, are 359-type castings containing varying levels of Fe and Cu additions. Similarly, EPMA and WDS analysis were also used to identify the intermetallic phases present in the 10S, 11S, and 12S alloys for samples corresponding to the as-cast conditions, as well as for the 490°C/12h and 520°C/12h solution heat-treated conditions. It should be noted that the alloys coded 10S through 12S represent the 354-type castings containing various levels of iron.

The intermetallic phases present in the alloys were of two types: either completely soluble or partially soluble. The  $\text{Al}_2\text{Cu}$  and  $\text{Mg}_2\text{Si}$  phases were the completely soluble ones as observed in the cast structure. The quantitative measurements, however, were carried out for the  $\text{Al}_2\text{Cu}$  phase only where the  $\text{Mg}_2\text{Si}$  phases appear darker than, or closer to, the degree of darkness in the backscattered images of the Al-matrix because of their smaller average atomic number. These phases dissolve during solutionizing treatment during which the principal elements Cu and Mg diffuse into the metal matrix and form a supersaturated solid solution after quenching. The volume fraction percentage of the  $\text{Al}_2\text{Cu}$  phase was observed to decrease with an increase in the solutionizing temperature, as illustrated in Figure 4.1(a) and listed in Table 4.1, although the incipient melting of such phases should

also be taken into consideration. The  $\text{Al}_2\text{Cu}$  phase dissolved completely after solutionizing of the castings at  $537^\circ\text{C}$  for alloys 1S through 9S and at  $520^\circ\text{C}$  for alloys 10S through 12S, as shown in Figure 4.1(a) and Table 4.1. The microstructure shown in Figures 4.2(c) and (d), and Figures 4.3(b) and (c) illustrate the disappearance of the  $\text{Al}_2\text{Cu}$  phase after solutionizing treatment.

The alloys coded 9S and 12S were selected to represent the characteristics of the intermetallic phases in the as-cast and heat-treated conditions. The microstructure of the alloy coded 9S reveals all the possible phases which may be formed in any one of the nine alloys coded 1S through 9S since it is similar in composition to the other alloys with a maximum level of copper and iron. Also, the microstructure of the alloy coded 12S reveals all the possible phases which may be formed in any one of the alloys coded 10S through 12S.

The volume fraction percentage of the partially soluble intermetallic phases was also observed to decrease with an increase in the solutionizing temperature, as illustrated in Figure 4.1(b) and Table 4.1. The principal partially soluble phases which formed in the 359 casting alloys, for example the 9S alloy in this case, were the iron-bearing  $\beta\text{-Al}_5\text{FeSi}$  and  $\pi\text{-Al}_8\text{Mg}_3\text{FeSi}_6$  compounds, as shown in Figure 4.2(a). The principal partially soluble phases in the 354 casting alloys, for instance the alloy coded 12S, are the  $\beta\text{-Al}_5\text{FeSi}$ ,  $\pi\text{-Al}_8\text{Mg}_3\text{FeSi}_6$ ,  $Q\text{-Al}_5\text{Mg}_8\text{Cu}_2\text{Si}_6$ , and  $\text{Al}_7\text{Cu}_2\text{Fe}$  compounds, as may be seen from Figures 4.3(a) and (b); the major phases observed in the as-cast structure, however, are  $\beta\text{-Al}_5\text{FeSi}$  and  $\pi\text{-Al}_8\text{Mg}_3\text{FeSi}_6$ , as shown in Figure 4.3(a). Increasing the iron content leads to an

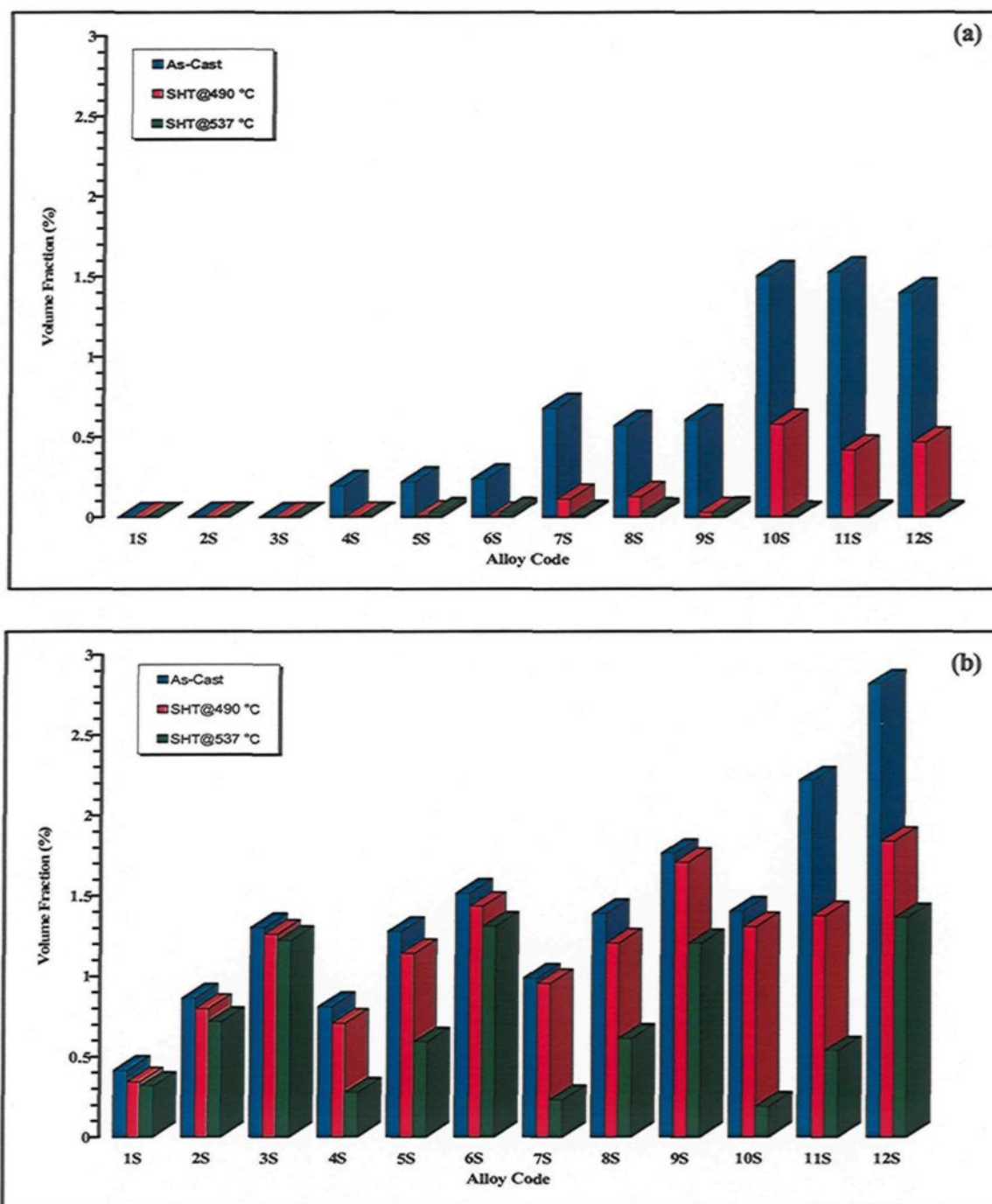


**Figure 4.1.** Volume fraction of intermetallic phases observed in the 354 and 359 alloys which were cast using a graphite mold preheated to 600°C: (a) soluble  $Al_2Cu$  phase, and (b) partially soluble Fe- and Cu-bearing phases. (It should be noted that the maximum solutionizing temperature applied to alloys coded 10S through 12S is 520°C.)

**Table 4.1.** Volume fractions of the intermetallic phases observed in 1S through 12S alloys, which were cast using a graphite mold preheated to 600°C, for the as-cast condition and two solutionizing temperatures.

Alloy Code	Volume Fraction of Intermetallic Phases											
	As-Cast				490°C				537°C			
	Completely Soluble		Partially Soluble		Completely Soluble		Partially Soluble		Completely Soluble		Partially Soluble	
	Av%	SD%	Av%	SD%	Av%	SD%	Av%	SD%	Av%	SD%	Av%	SD%
<b>1S</b>	0.00	0.00	0.42	0.34	0.00	0.00	0.35	0.18	0.00	0.00	0.32	0.10
<b>2S</b>	0.00	0.00	0.87	0.27	0.00	0.00	0.80	0.28	0.00	0.00	0.72	0.23
<b>3S</b>	0.00	0.00	1.31	0.30	0.00	0.00	1.26	0.20	0.00	0.00	1.23	0.18
<b>4S</b>	0.20	0.08	0.81	0.31	0.00	0.00	0.71	0.45	0.00	0.00	0.28	0.16
<b>5S</b>	0.23	0.06	1.28	0.40	0.01	0.03	1.15	0.45	0.03	0.05	0.59	0.19
<b>6S</b>	0.24	0.10	1.52	0.22	0.00	0.00	1.44	0.19	0.03	0.05	1.31	0.35
<b>7S</b>	0.68	0.17	0.99	0.34	0.11	0.18	0.96	0.90	0.01	0.04	0.23	0.06
<b>8S</b>	0.57	0.17	1.39	0.51	0.13	0.12	1.21	0.63	0.03	0.08	0.61	0.23
<b>9S</b>	0.61	0.25	1.77	0.59	0.03	0.05	1.71	0.38	0.04	0.05	1.21	0.30
<b>10S</b>	1.51	0.37	1.41	0.36	0.58	0.28	1.31	0.45	0.01	0.03	0.19	0.09
<b>11S</b>	1.53	0.59	2.22	0.54	0.42	0.19	1.38	0.48	0.01	0.04	0.54	0.23
<b>12S</b>	1.40	0.52	2.82	0.63	0.47	0.34	1.84	0.48	0.01	0.04	1.37	0.48

Av% and SD% refer to the average volume fraction percentage and standard deviation percentage of the intermetallic phases, respectively. It should be noted that 520°C is the maximum solutionizing temperature applied here to alloys coded 10S through 12S instead of 537°C.

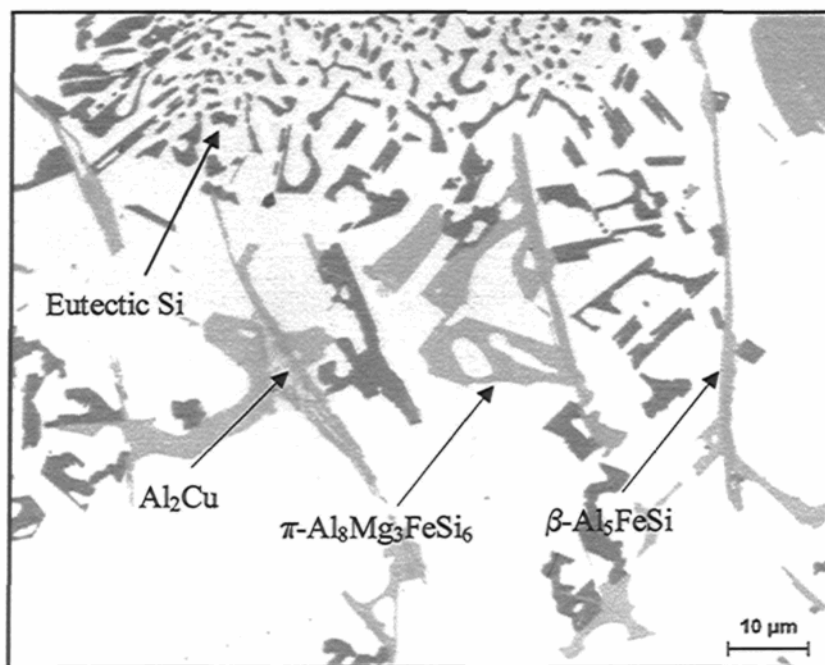
increase in the volume fraction of the partially soluble phases, as may be seen in Figure 4.1(b) and Table 4.1. Increasing the level of copper produces not only an increase in the volume fraction of the soluble phase through the formation of the  $Al_2Cu$  phase but also an increase in the volume fraction of the partially soluble phases, as may be seen in Figures 4.1(a) and (b) and is listed in Table 4.1. In the presence of copper, the increase in the volume fraction of the partially soluble phases is related to the formation of Cu-containing phases such as the  $Q-Al_5Mg_8Cu_2Si_6$  and  $Al_7Cu_2Fe$  phases which may be seen in Figure 4.3(b).

Solutionizing temperatures have been found to affect not only the volume fraction percentage of the completely soluble phases and partially soluble compounds but also the nature and the morphology of the iron-bearing phases, whether  $\pi$  or  $\beta$ . When applying solutionizing treatment, the  $\beta$ -phase platelets were observed to undergo changes in their morphology due to the dissolution, thinning, necking, and fragmentation of these platelets upon increasing the solutionizing temperature. These changes in the size and morphology of the Fe-bearing phases become apparent upon raising the solutionizing temperature of 359 alloys to 537°C, as shown in Figures 4.2(b) and (c). Similar observations were made upon raising the solutionizing temperature of the 354 alloys to 520°C, as shown in Figure 4.3(c). These morphological changes lead to a breakdown in the continuous nature of the platelets and ultimately result in the formation of small fragments of the  $\beta$ -phase. These changes in the morphology of the  $\beta$ -phase were also mentioned in several other studies.<sup>135, 136, 137</sup> The  $\pi$ -phase was observed to dissolve and/or transform into a cluster of very fine  $\beta$ -phase platelets, as may be seen in the optical micrograph shown in Figure 4.2(d). Similar observations regarding the transformation of the  $\pi$ -phase have been reported in a number of studies.<sup>89, 93, 138, 139</sup>

Figures 4.2(a) through (d) illustrate the various intermetallic phases arising in the structure of 359 alloys in the as-cast condition and after applying different solutionizing temperatures; it also illustrates the morphological changes occurring in the partially soluble intermetallic phases. Figure 4.2(a) shows the main phases in the as-cast structure of the 9S alloy as indicated by the arrows; Figure 4.2(b) illustrates the necking and the beginning of the  $\beta$ -phase fragmentation after applying a solutionizing treatment at 490°C, as indicated by

the arrows; Figure 4.2(c) shows the morphology of the  $\beta$ -phase after applying the solutionizing treatment at 537°C at which point small fragments of this phase are seen to form as a result of the fragmentation process; Figure 4.2(d) shows clusters of very fine platelets of the  $\beta$ -phase resulting from the transformation of the  $\pi$ -phase upon applying the solutionizing treatment to 359 alloys at 537°C.

Figure 4.3 shows the characteristics of the main intermetallic phases both for the 354 alloys in the as-cast condition and after applying solutionizing treatment at 520°C. Figures 4.3(a) and (b) illustrate the main phases in the cast structure of the 12S alloy; Figure 4.3(c) shows the changes in the size and morphology of the  $\beta$ -phase after applying solutionizing treatment to 354 alloys at 520°C.

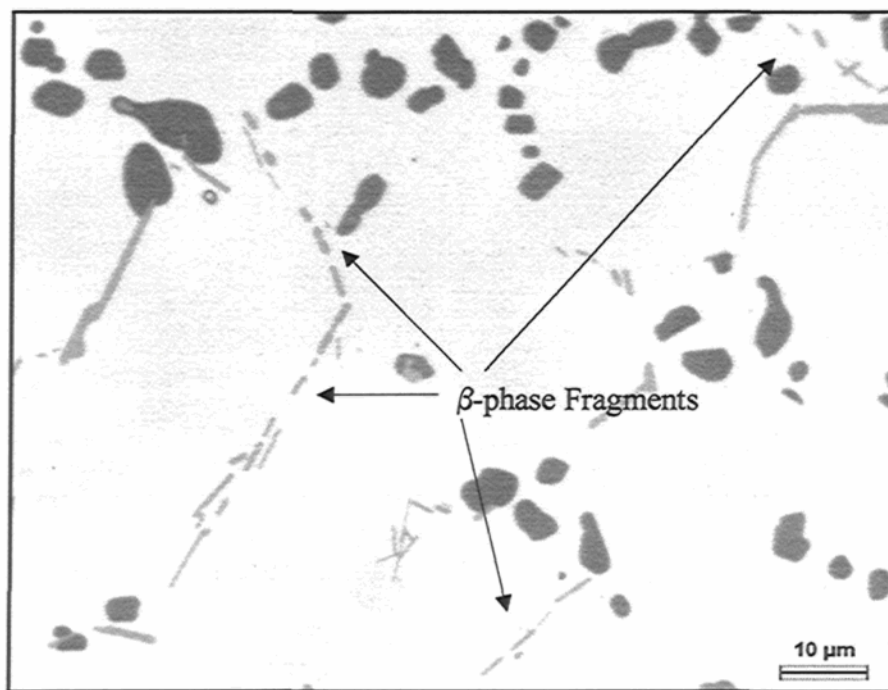


(a)

Figure 4.2

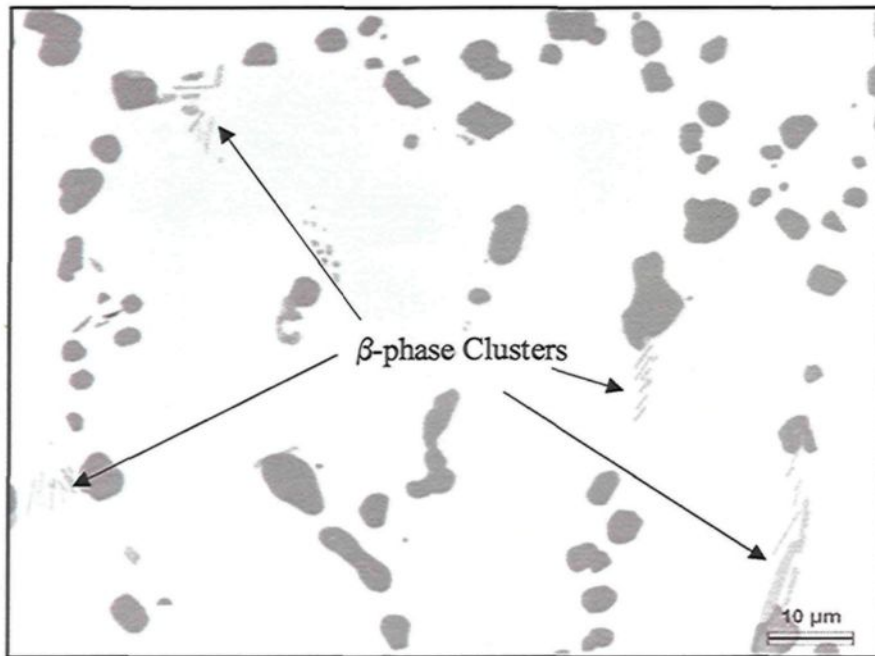


(b)



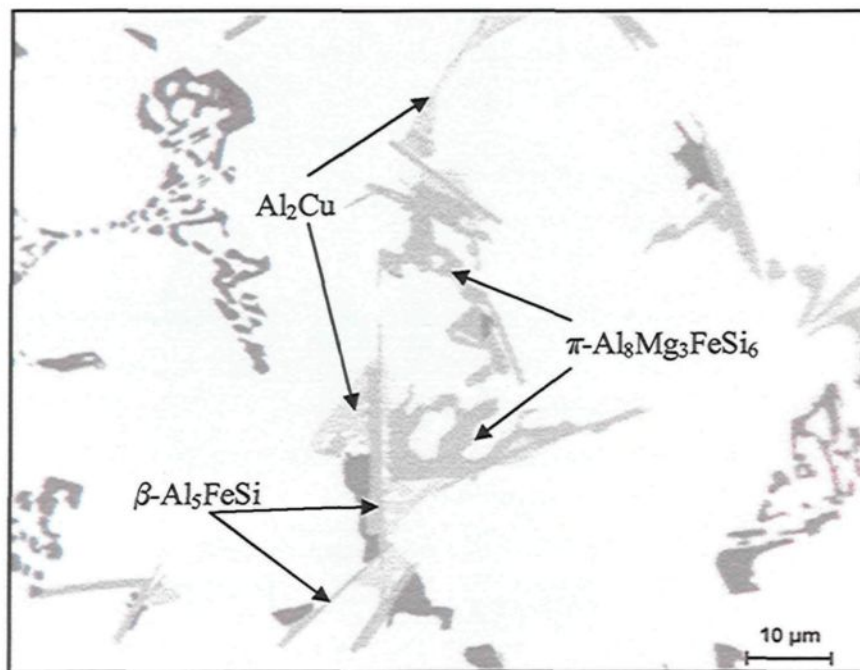
(c)

Figure 4.2



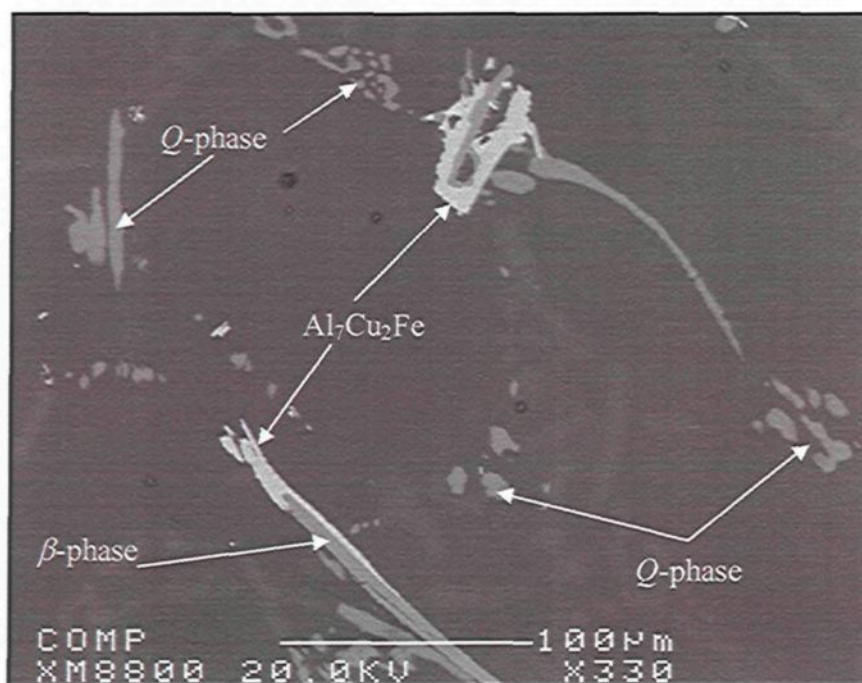
(d)

**Figure 4.2.** Morphology of the intermetallic phases observed in 9S alloy samples: (a) as-cast; (b) after solutionizing at 490°C; (c) and (d) after solutionizing at 537°C (samples were obtained from the gauge length of B108 test bars).

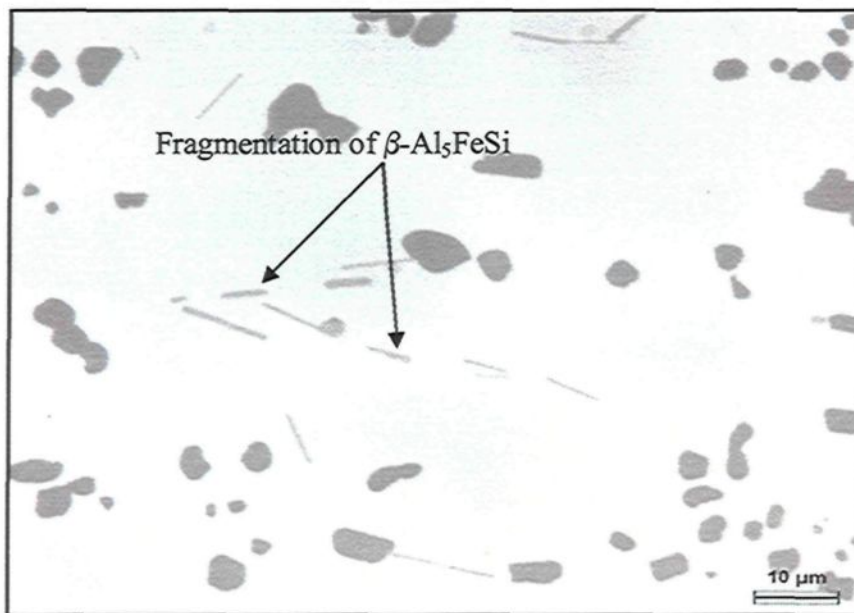


(a)

**Figure 4.3**



(b)



(c)

**Figure 4.3.** The intermetallic phases observed in 12S alloy samples: (a)  $\beta$ - $\text{Al}_5\text{FeSi}$  and  $\pi$ - $\text{Al}_8\text{Mg}_3\text{FeSi}_6$  phases in the as-cast condition; (b) backscattered image showing partially soluble phases remaining after solutionizing at  $520^\circ\text{C}$ ; (c) fragmentation of  $\beta$ - $\text{Al}_5\text{FeSi}$  phase after solutionizing at  $520^\circ\text{C}$  (samples were obtained from the gauge length of B108 test bars).

#### 4.2.2. Characteristics of Eutectic Silicon Particles

Quantitative analyses of eutectic silicon particles were carried out using an optical microscope/image-analysis system. Silicon particles were quantified for the 354- and the 359-type castings in the as-cast condition, and under heat-treated conditions. The alloys selected for this quantitative analysis were 1S, 1N, 10S, and 10N. Alloys coded 1S and 1N are Sr-modified and non-modified 359-type casting alloys, respectively, while alloys coded 10S and 10N are Sr-modified and non-modified 354-type casting alloys, respectively. Quantitative measurements of the eutectic silicon particles were carried out for the castings in the as-cast condition and the following solution heat treatment conditions:

- (i) solution heat treatment of alloy 1S at 490°C/12h, and 537°C/12h;
- (ii) solutionizing of 1S and 1N alloys for 1 h, 4 h, 8 h, 12 h, 16 h, and 24 h each at 537°C;
- (iii) solution heat treatment of the 10S alloy at 490°C, 495°C, 500°C, 505°C, 510°C, 515°C, 520°C and 525°C for 12 h each;
- (iv) solutionizing of 10S and 10N alloys for 1 h, 4 h, 8 h, 12 h, 16 h, and 24 h each at 520°C.

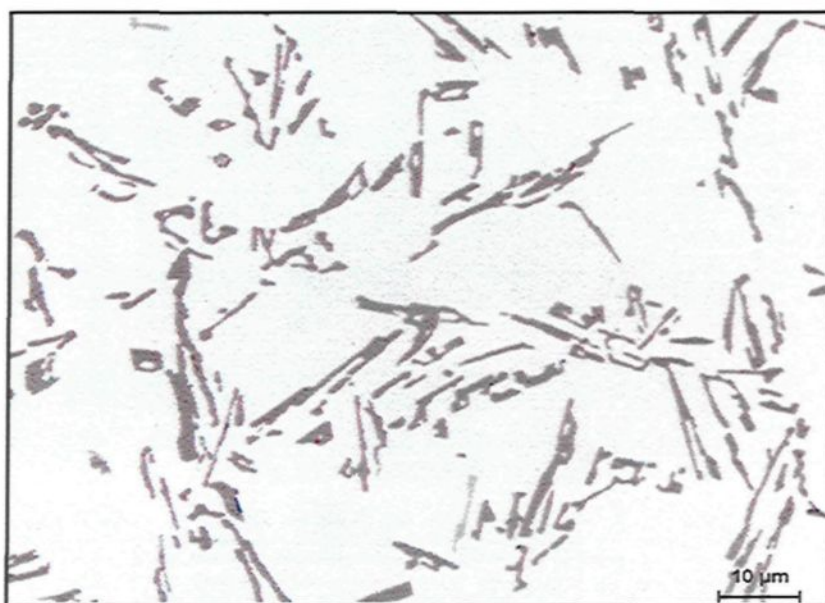
Solution heat treatment compared to the as-cast conditions results in transforming the morphology of eutectic silicon from acicular particles into fibrous ones.<sup>140, 141, 142</sup> Raising the solutionizing temperature and/or increasing the duration of solutionizing time also produce further improvements in the morphology of eutectic silicon particles. Particle area was seen to increase because of the coarsening brought about in these particles upon subjecting the castings to high solutionizing temperatures and/or to a longer solutionizing

time. On the other hand, the aspect ratio decreased because of the spheroidization of the same particles upon raising the solutionizing temperature and/or increasing the duration of the solutionizing time.

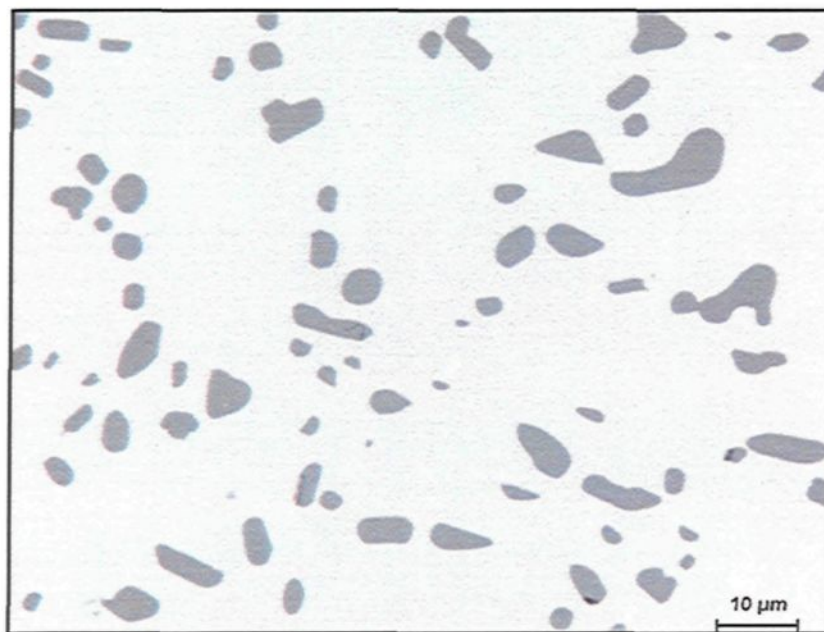
Figures 4.4(a) through (d) show examples of the morphology of eutectic silicon particles in non-modified and Sr-modified 359 casting alloys. The morphology of the Si particles in the as-cast condition of Sr-modified and non-modified 359 alloys are shown in Figures 4.4(a) and (c), respectively, while the change in the particle morphology of the same alloys after applying solutionizing treatments at 537°C for 24 h are shown in Figures 4.4(b) and (d). Similar observations were noted for the alloys 10N and 10S of the 354-type castings which were subjected to various solutionizing temperatures and times as mentioned. The morphology of the eutectic Si particles in the as-cast conditions of 10N and 10S alloys are shown in Figures 4.5(a) and (c). Figures 4.5(b) and (d) show examples of the morphology of the Si particles in non-modified and Sr-modified 354 alloys, respectively, after applying the solutionizing treatment at 520°C for 24 h.

Quantitative measurements of eutectic silicon particles under the solutionizing temperatures and times mentioned for 1S, 1N, 10S, and 10N alloys confirm these observations. The quantitative measurements of eutectic silicon particles, upon raising the solutionizing temperature of 359 and 354 alloys, are shown in Figures 4.6(a) and (b), respectively, where the area of the eutectic silicon particles increases with an increase in the solution heat treatment temperature, although the aspect ratio of these particles was observed to decrease. Increasing the duration of solution heat treatment time from 1 h to 24 h appears to produce advantageous changes in the size and morphology of the eutectic

silicon particles for both modified and non-modified 359 alloys, as shown in Figure 4.7(a), and for both modified and non-modified 354 alloys, as shown in Figure 4.7(b). The particle size increases while the aspect ratio decreases with an increase in solutionizing time.

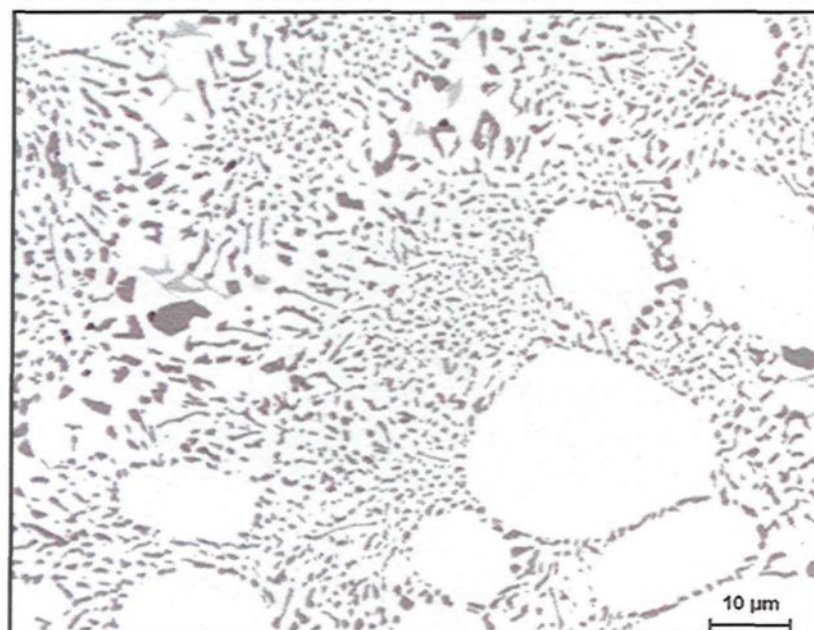


(a)

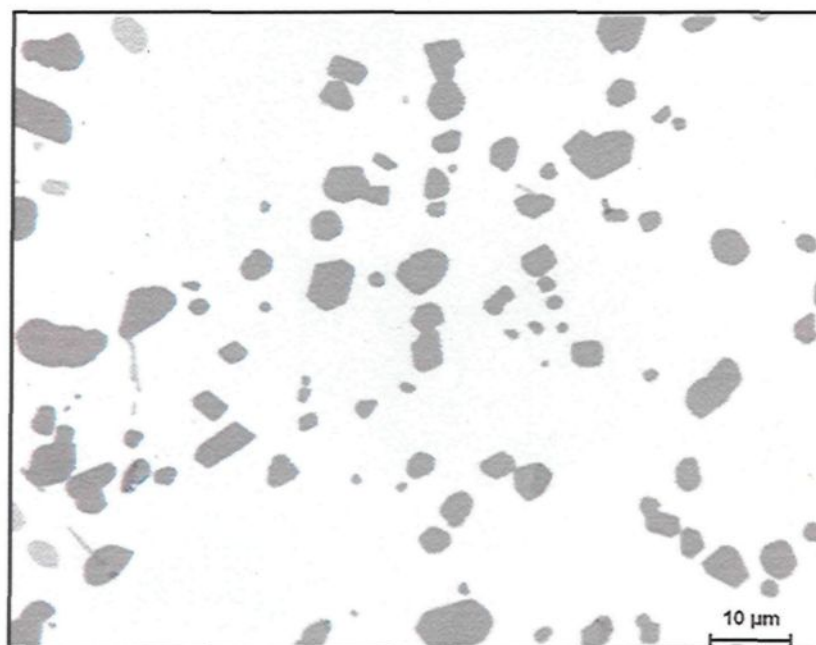


(b)

**Figure 4.4**

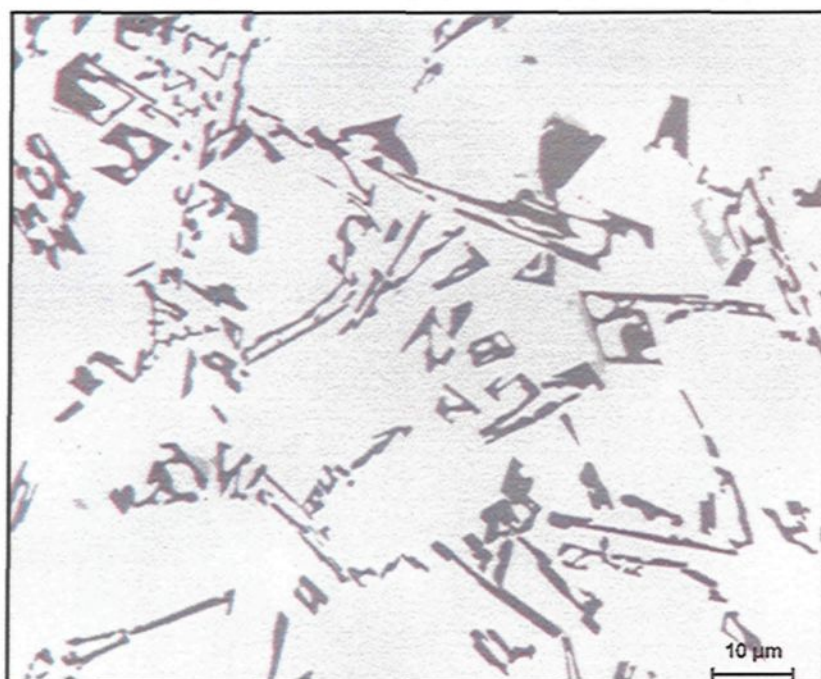


(c)

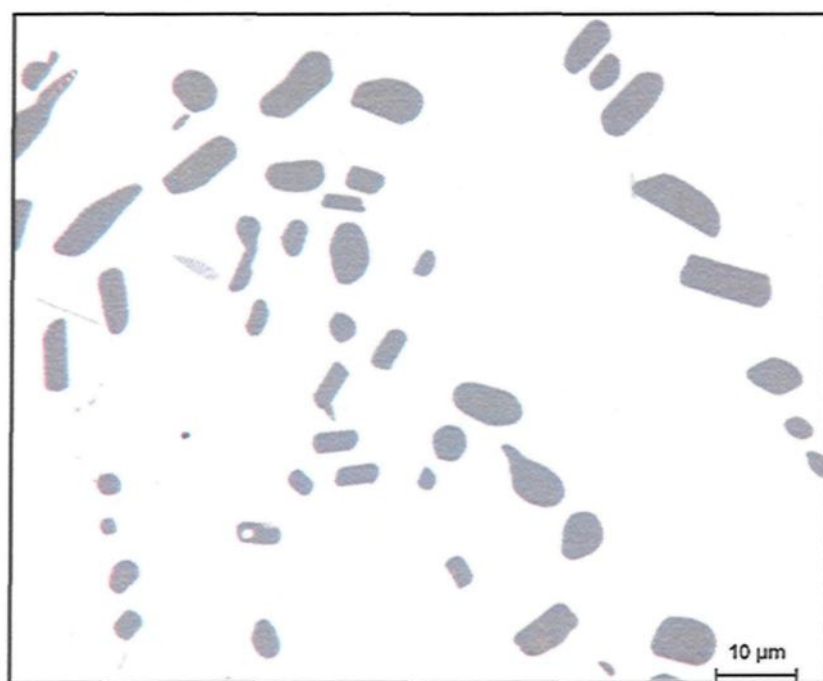


(d)

**Figure 4.4.** Morphology of eutectic silicon particles observed in non-modified and modified 359 casting alloys under the following conditions: (a) and (c) non-modified and modified alloys in the as-cast conditions, respectively; (b) and (d) non-modified and modified alloys after applying solutionizing treatment at 537°C for 24 h, respectively (samples were obtained from the gauge length of B108 test bars).

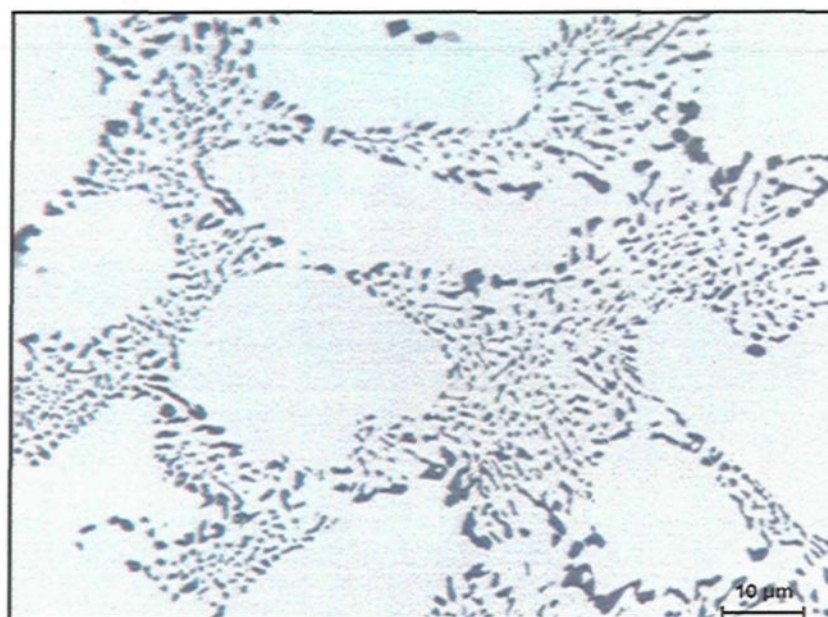


(a)



(b)

**Figure 4.5**



(c)



(d)

**Figure 4.5.** Morphology of eutectic silicon particles observed in non-modified and modified 354 casting alloys under the following conditions: (a) and (c) non-modified and modified alloys in the as-cast conditions, respectively; (b) and (d) non-modified and modified alloys after applying solutionizing treatment at 520°C for 24 h, respectively (samples were obtained from the gauge length of B108 test bars).

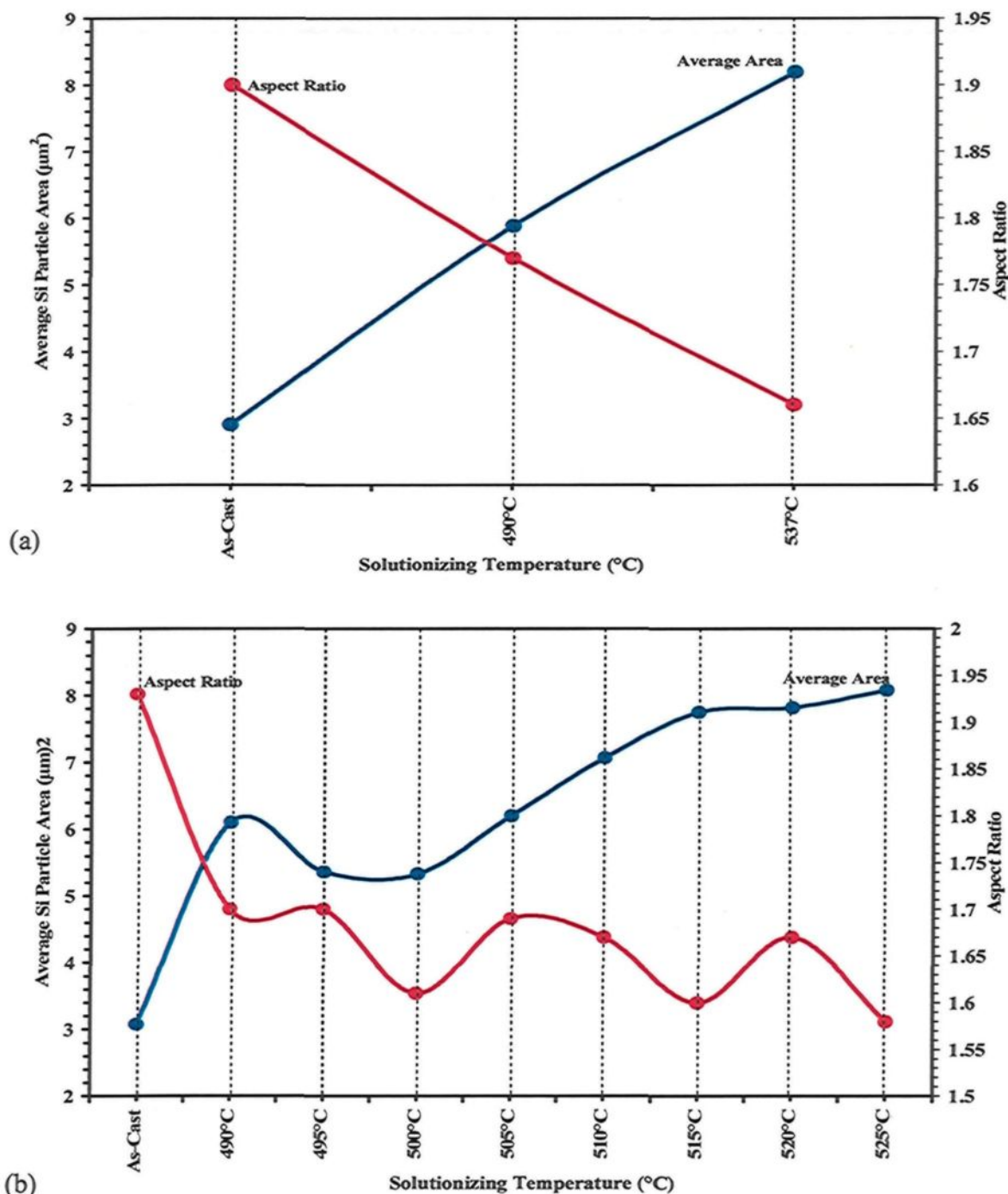


**Figure 4.6.** Characteristics of eutectic silicon particles, average area, and average aspect ratio, as functions of solutionizing temperature applied for 12 h to (a) alloy 1S from the 359-type castings; and (b) alloy 10S from the 354-type castings (samples were obtained from the gauge length of B108 test bars).

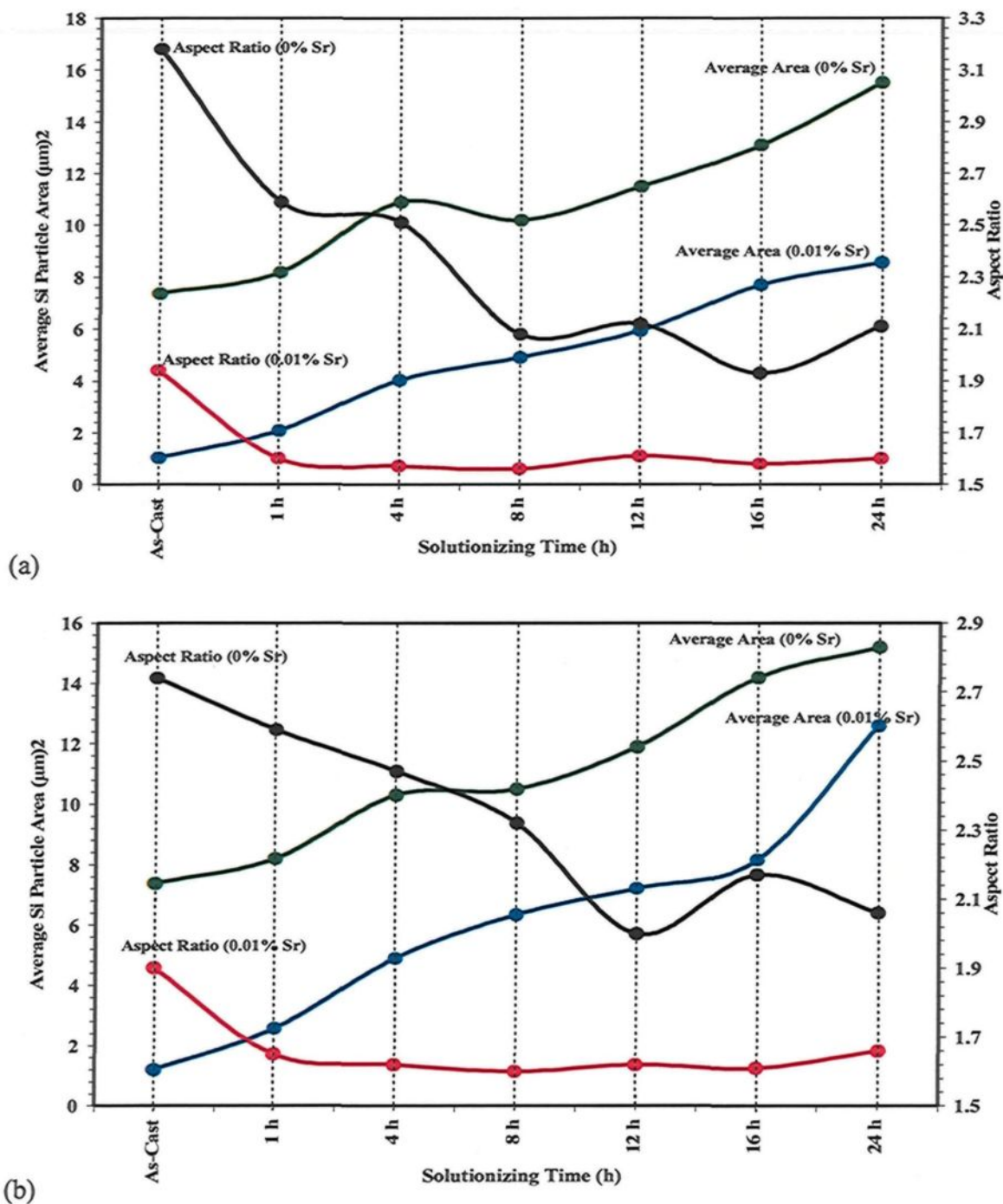


**Figure 4.7.** Characteristics of eutectic silicon particles, average area, and average aspect ratio, as functions of solutionizing time applied at 537°C to (a) alloys 1S and 1N from 359-type castings; and at 520°C to (b) alloys 10S and 10N from 354-type castings (samples were obtained from the gauge length of B108 test bars).

#### 4.2.3. Characteristics of Secondary Dendrite Arm Spacing (SDAS)

The measurement of secondary dendrite arm spacing (SDAS) was carried out for 1S and 10S alloys of 359- and 354-type castings, respectively, which were cast using an end-chill mold. The SDAS was quantified for the specimens obtained from the three levels of the casting block shown in Figure 3.3(a). The technique for measuring the SDAS is the same as the one applied for eutectic Si particles using a Clemex Vision PE4 optical microscope and image-analysis system.

Level I of the casting block provides the smallest SDAS related to the rapid cooling rate of the bottom portion of the casting block. The rapid solidification rate in the bottom portion of the casting is related to the copper base attached to the mold; this copper base is supplied with running water throughout the casting process. The presence of the copper base and the running water at the bottom of the end-chill mold produce a temperature gradient along the casting block resulting from the varied rate of heat extraction along the casting. Therefore, the fastest solidification rate, in other words the smallest SDAS, occurs at the bottom of the casting because of rapid heat extraction.

On the other hand, Level III of the casting block shown in Figure 3.3(a) displays the largest SDAS which is related to the slowest solidification rate associated with the slow heat extraction from the molten metal in this region of the casting. The SDAS measurements for 354 and 359 alloys which correspond to the three specified levels of the casting block are listed in Table 4.2. Figures 4.8(a) through (c) show the size of the  $\alpha$ -Al dendrites observed in the 359 casting alloys which is almost similar to that of the 354 alloys with a small noticeable increase in the SDAS of the 354 alloys, as listed in Table 4.2. The

size of the  $\alpha$ -Al dendrites in the 359 castings produced using the end-chill mold at Level I, Level II, and Level III are shown in Figures 4.8(a), (b), and (c), respectively.

**Table 4.2.** Average SDAS measured for the alloys coded 1S and 10S corresponding to 359 and 354 alloys, respectively (samples were obtained from the gauge length of E8M-04 test bars).

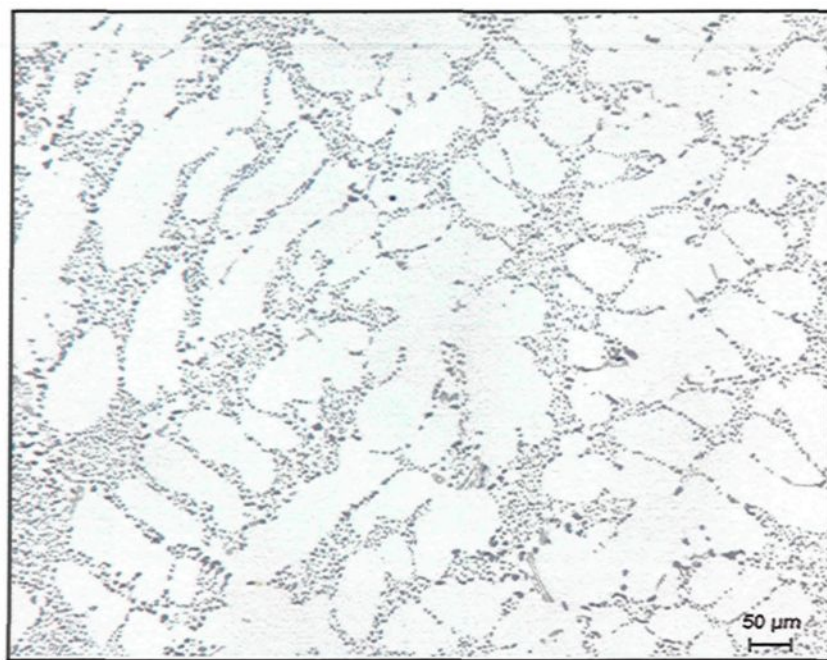
Alloy Code	SDAS ( $\mu\text{m}$ )	SD
1S-I	31.70	9.55
1S-II	51.10	15.40
1S-III	83.90	24.40
10S-I	32.60	6.91
10S-II	56.20	15.00
10S-III	90.60	24.20

Codes I, II, and III refer to Level I, Level II and Level III, respectively, in the casting block produced using an end-chill mold shown in Figure 3.3(a).

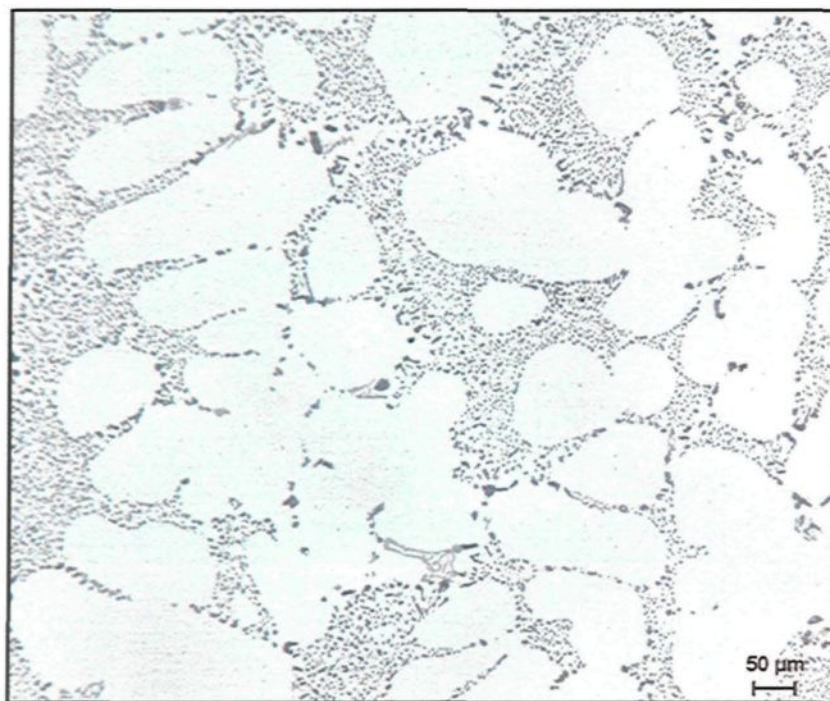


(a)

**Figure 4.8**



(b)



(c)

**Figure 4.8.** Optical micrographs showing the size of the  $\alpha$ -Al dendrites in the 359 alloys produced using an end-chill mold (a) Level I; (b) Level II; and (c) Level III (samples were obtained from the gauge length of the E8M-04 test bars).

#### 4.3. EVALUATION OF TENSILE PROPERTIES AND QUALITY INDEX

Two quality charts were selected for evaluating the influence of metallurgical parameters on the tensile properties and the quality indices of 354- and 359-type casting alloys. These charts are provided in Figure 2.3 and Figure 2.7. Equations 1 and 2 were used to generate *iso-Q* lines and *iso-yield strength* lines, respectively, in the quality chart shown in Figure 2.3. Equations 8 and 9 were used to generate *iso-flow* lines and *iso-q* lines, respectively, in the quality chart shown in Figure 2.7; the *Q*-values presented in this chart were determined by applying Equation 12.

The quality charts shown in Figure 2.3 and Figure 2.7 present all the tensile properties of the alloys, as discussed earlier in sections 2.4.1 and 2.4.3. Therefore, this particular type of plot represents a significant tool for the purposes of evaluating, selecting, and predicting the most appropriate metallurgical conditions to be applied to Al-Si casting alloys with a view to obtaining specific properties. Accordingly, all the pertinent results will be presented using these two types of charts, based on the tensile properties available for each point located in these charts. Generating these specific charts would provide a factual logic-based evaluation of the effects which various parameters may have on the tensile properties and quality indices of the castings under study. The results in each case were re-plotted in different formats such as scatterplots and contour plots to confirm the original analyses and interpretations made using the quality charts. The parameters discussed in the current chapter in relation to the tensile properties and quality indices of the 354 and 359 alloys include:

- (i) the effects of iron;

- (ii) the effects of copper;
- (iii) the effects of magnesium;
- (iv) the influence of solidification rate;
- (v) the influence of solution heat treatment temperature;
- (vi) the influence of solution heat treatment time; and
- (vii) the effects of strontium on the response of the castings to solutionizing treatment.

The influence of each parameter on the tensile properties and quality indices of the castings will be presented in the next subsections.

#### **4.3.1. Influence of Iron**

Iron has been observed to affect the strength, ductility, and quality of the 354- and 359-type castings in a detrimental way; thus, by increasing the iron level in these alloys, the strength is decreased, the ductility is reduced, and the quality is diminished. Figure 4.9 and Figure 4.10 show the quality charts which were generated to represent the effects of iron level and copper content on the properties of the 354 and 359 castings. Alloys coded 1S through 12S were produced for this purpose; three levels of Fe (0.07%, 0.2% and 0.35%) and four levels of Cu (0%, 0.5%, 1%, and 1.8%) were selected for the purposes of this study, the Fe-content and Cu-content were labeled on the curves. These compositions were investigated in relation to the as-cast condition and two solution heat treatment temperatures.

Alloys 1S through 9S, *i.e.* 359 alloys having various levels of Fe and Cu, were solutionized at 490°C/12h and 537°C/12h, while alloys 10S through 12S, *i.e.* 354 alloys

having three different Fe-levels, were solutionized at 490°C/12h and 520°C/12h. The solution heat-treated castings were subjected to aging treatment at 170°C for a duration of 8 hours. The selection of these solution heat treatment conditions, namely temperatures and times, will be discussed in detail in the section on solution heat treatment parameters.

With regard to the tensile properties and the quality indices of the castings in the as-cast condition and after applying the specified heat treatments, iron appears to have similar deleterious effects on the properties of the castings under study. The presence of this

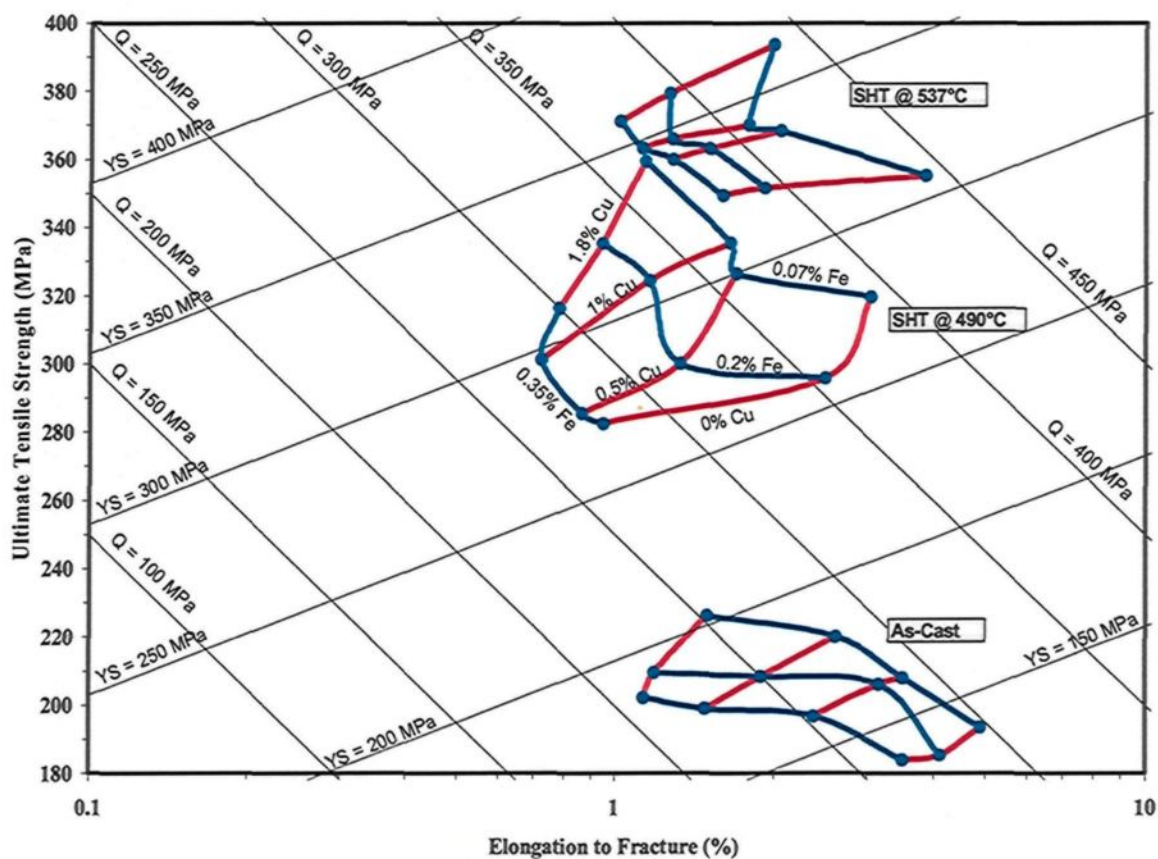


**Figure 4.9.** Quality chart generated using Equations 1 and 2 showing the influence of iron and copper on the tensile properties and the quality indices of 359- and 354-type B108 test bar castings under the specified conditions. It should be noted that the maximum solutionizing temperature applied to alloys coded 10S through 12S is 520°C.

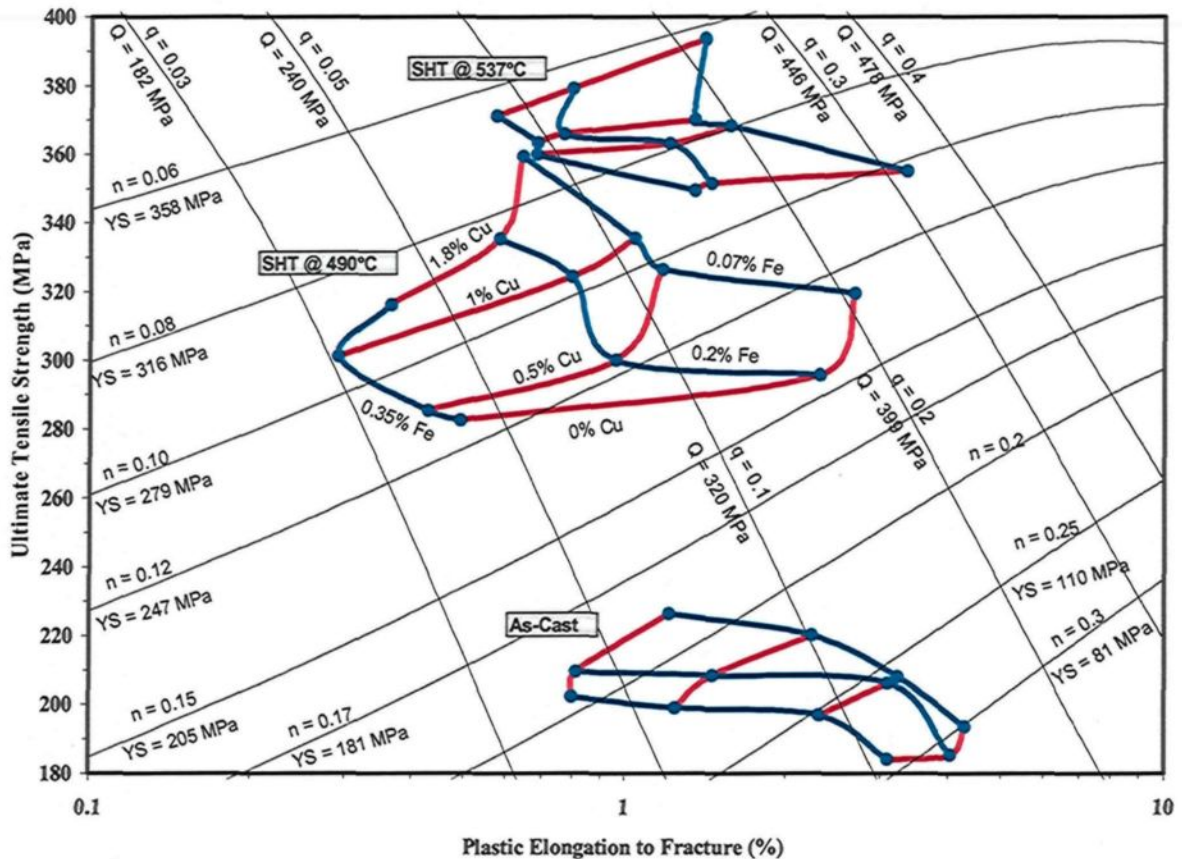


**Figure 4.10.** Quality chart generated using Equations 8 and 9 showing the influence of iron and copper on the tensile properties and the quality of the 359- and 354-type B108 test bar castings ( $K = 520$  MPa) under the specified conditions. It should be noted that the maximum solutionizing temperature applied to alloys coded 10S through 12S is  $520^{\circ}\text{C}$ .

element invariably has a deteriorating effect on the strength, ductility, and quality of the alloys in question. When increasing the Fe-level, the *iso-Fe* series shown in Figure 4.9 and Figure 4.10 are observed to shift virtually parallel to the *iso-Q* lines toward the lower left-hand side of the charts. From a design engineering point of view, this direction leads to the least useful location on the chart since all the desired properties are lowered. The yield strength, however, revealed no significant changes when increasing the Fe-level from

0.07% to 0.35%, as may be observed in Figure 4.9 and Figure 4.10 where each *iso-Cu* line, which represents three levels of iron, is roughly parallel to the *iso-yield strength* or *iso-flow* lines. Yield strength is independent of impurity elements such as Fe but it is strongly related to the hardening effects which result from the addition of hardening elements or from applying a suitable aging treatment.

In the current study,  $\beta$ -Al<sub>5</sub>FeSi and  $\pi$ -Al<sub>8</sub>Mg<sub>3</sub>FeSi<sub>6</sub> intermetallic phases are the main Fe-containing phases formed in these castings, as illustrated in Figure 4.2(a) and Figure 4.3(a). The size and morphology of the phases mentioned are the main source of the detrimental effect of iron on the tensile properties and quality index of the castings.<sup>67, 70, 71</sup> A number of studies<sup>143, 144, 145, 146, 147</sup> have revealed that the  $\beta$ -phase is the most deleterious Fe-bearing intermetallic because of its platelet-like shape, as shown in Figure 4.2(a) and Figures 4.3(a) and (b). This morphology produces high stress concentrations and constitutes a stress raiser at the edge of the platelets. The formation of stress raisers throughout the microstructure results in impaired mechanical properties and an impoverished quality of the castings. Furthermore, the  $\beta$ -phase acts as a barrier to molten metal feeding which leads to shrinkage porosity in the casting.<sup>148, 149, 150, 151</sup> Figure 4.11 shows an example of porosity formation due to the presence of the  $\beta$ -phase; such porosity in the cast structure reduces the mechanical properties and quality of the alloys.

Upon increasing the iron content there is a concomitant increase in the volume fraction percentage of the iron-bearing phases, as may be observed from Figure 4.1(b). As a result, the influence of these phases, specifically the  $\beta$ -phase, on the strength and the quality of the castings becomes increasingly detrimental, as may be distinguished from the quality

charts shown in Figure 4.9 and Figure 4.10. It will be clear from these charts that the alloys coded 3S, 6S, 9S and 12S continually produced the least useful strength, ductility, and quality values for all the conditions applied to the castings; such a fact may be attributable to the iron content since these alloys contain the maximum iron level of 0.35% each. On the other hand, the alloys coded 1S, 4S, 7S and 10S, in comparison with the other alloys under discussion, provide the best possible compromise between strength, ductility, and quality values under all conditions, as shown in Figure 4.9 and Figure 4.10; this fact may be related to the low iron-content of 0.07%.

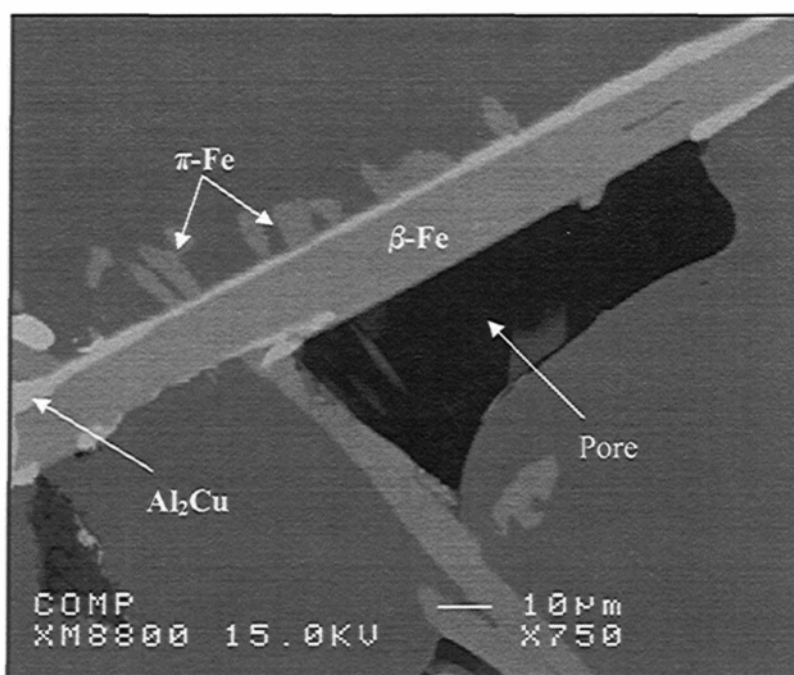


**Figure 4.11.** Porosity formation due to obstruction of liquid metal feeding by the  $\beta$ -Fe phase.

The application of a solutionizing treatment leads to significant improvement in the strength and quality of the same castings, even those containing high Fe-levels, as may be

seen in Figure 4.9 and Figure 4.10. Such improvement is most likely to be related to the changes which occur in the volume fraction percentage, in the size, and/or in the morphology of the Fe-containing phases after applying the specified solution heat treatments. These changes include the reduction in the volume fraction of the Fe-bearing phases, as shown in Figure 4.1(b); the dissolution, thinning, necking, and fragmentation of the  $\beta$ -phase, as may be seen in Figures 4.2(b) and (c), and in Figure 4.3(c); and also the dissolution and/or transformation of the  $\pi$ -phase into clusters of fine needles of the  $\beta$ -phase, as will be seen in Figure 4.2(d). According to these observations, the solutionizing treatment reduces the deleterious effects of iron through the beneficial changes occurring in the size and morphology of the Fe-phases upon applying a suitable solutionizing treatment. The effects of solutionizing treatments will be discussed in greater detail further on in the chapter.

The effects of Fe-content on the strength, ductility, and quality of aluminum castings were presented and discussed in a number of earlier studies<sup>41, 50, 72, 73</sup> in which these effects were also evaluated by using the quality charts. The results obtained in this current study are in entire agreement with those obtained in previous studies. Thus, reducing the iron levels in the 354- and 359-type castings may be considered an engineering objective and is to be recommended strongly for the purposes of developing greater strength and optimum quality values in these castings.

It will be observed in Figure 4.9 and Figure 4.10 that both illustrate similar behavior in the results obtained regarding the influence of the parameters under study on the tensile properties and the quality indices of the castings. Thus, there is no disagreement when

selecting a certain alloy from either of the two charts for a specific application since they both provide similar indications of quality and strength in the alloys investigated.

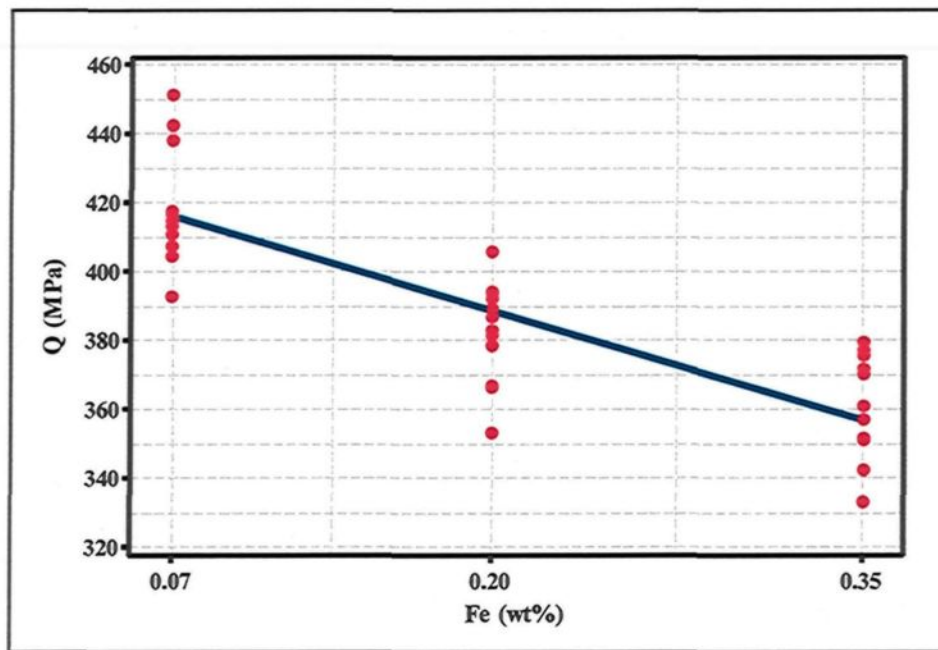
The yield strength of the castings which was calculated using Equation 2 and presented in the quality chart shown in Figure 4.9 provides high accuracy values with an error range of 1 to 7% for the heat-treated samples as opposed to the results obtained from the tensile testing machine. The calculated yield strength of the as-cast samples, on the other hand, suffers from a high error percentage of up to 45%, because Equations 1 and 2 were originally proposed for the heat-treated Al-Si casting alloys.<sup>41,42</sup> When comparing the actual yield strengths with the calculated yield strengths of the castings using Equation 8 as presented in Figure 4.10, it will be observed that the calculated yield strength of the alloys in the quality chart suffers in each case from a certain percentage of error depending on the deviation of the K-value from the average value; it should be noted that the chart shown in Figure 4.10 is plotted using a single K-value taken as an average for all the conditions presented therein. The error range in determining the yield strength, in this case, goes from 1 to 15%.

The error in both cases, however, will not affect the quality evaluation of the castings which is based on the actual values of the ultimate tensile strength and the real values of the elongation to fracture of these castings. The ultimate tensile strength is usually used for the specification and the quality control of the castings.<sup>46,47,152</sup> The ductility of the casting, which is expressed in elongation to fracture, is usually used as an indicator of casting quality because of its sensitivity to the presence of any impurity or defect in the cast structure.<sup>46,47,152</sup> Yield strength, on the other hand, does not represent the quality of the

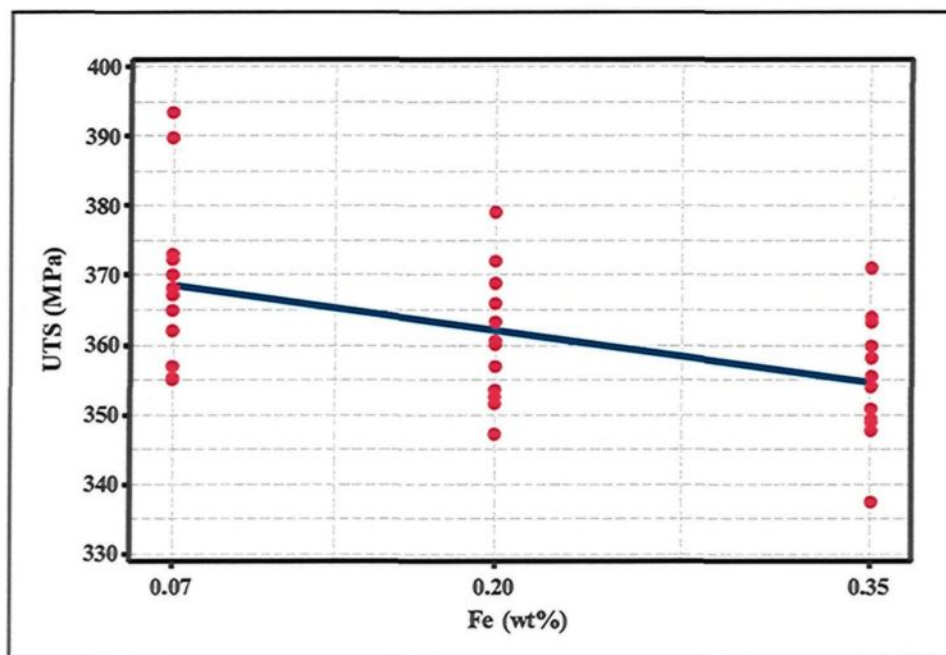
castings since it is a material property which is not affected by the level of defects or impurities present in the casting; it is a function of the moving dislocations through the casting structure and depends on the resistance exerted by the hardening precipitates against the moving dislocations.<sup>91, 153</sup> In general, these quality charts introduce a simple tool for recommending the appropriate processing conditions to obtain specified properties and hence to facilitate the selection of castings to meet these specifications.

The results provided in the quality charts in Figure 4.9 and Figure 4.10 were re-plotted using scatterplots, as shown in Figures 4.12(a) through (d). These plots correlate the effects of Fe-levels with the properties of the 359- and 354-type castings where the general trend resulting from the presence of iron under various conditions is shown. The properties of the castings shown are the quality index ( $Q$ ) calculated using Equation 1 and the tensile properties, namely, ultimate tensile strength ( $UTS$ ), yield strength ( $YS$ ), and elongation to fracture ( $E_f$ ).

Figures 4.12(a) through (d) show the scatterplots describing the correlation between the iron levels and the properties of the castings. Figure 4.12(a) illustrates the decreased quality index values ( $Q$ ) with increasing iron levels; Figure 4.12(b) shows the reduced ultimate tensile strength ( $UTS$ ) values upon increasing the iron content; Figure 4.12(c) indicates the slight changes occurring in the yield strength ( $YS$ ) with increasing iron content; and Figure 4.12(d) illustrates the negative effects of the high Fe-level on the ductility of the castings as represented by elongation to fracture,  $E_f$ . The scatterplots shown in Figures 4.12(a) through (d) are in a total agreement with the analysis and evaluation made using the quality charts shown in Figure 4.9 and Figure 4.10.

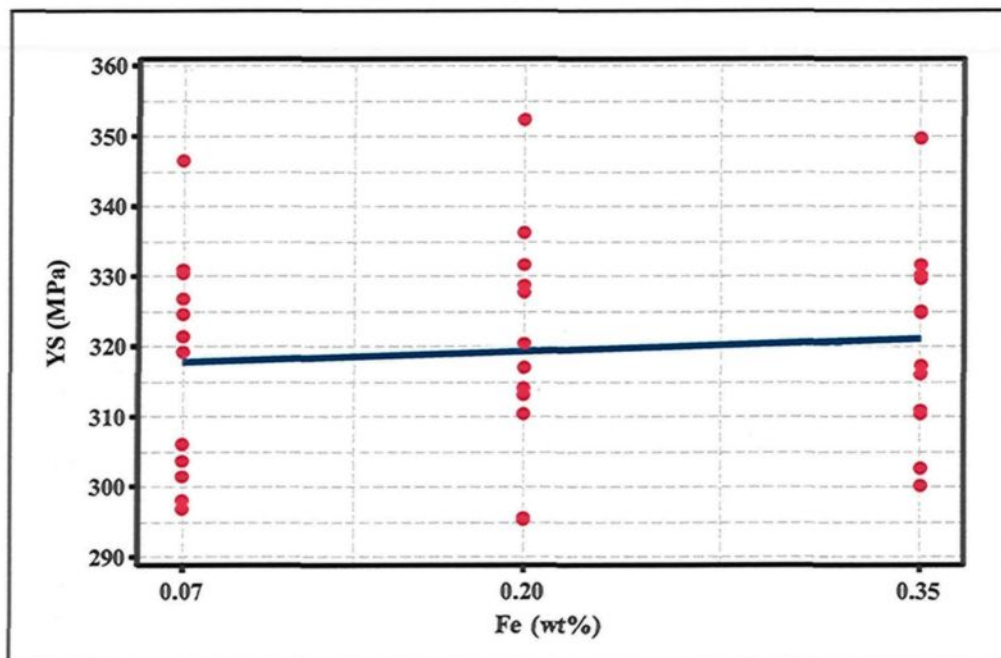


(a)

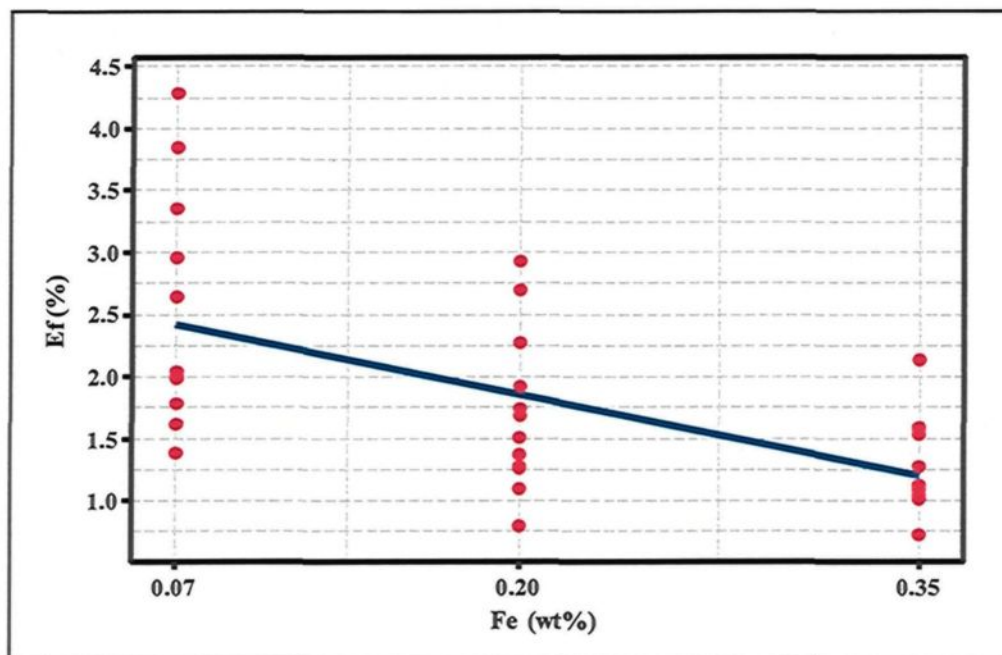


(b)

Figure 4.12



(c)



(d)

**Figure 4.12.** Scatterplots correlating iron content in 359- and 354-type castings with: (a) quality index values ( $Q$ ) calculated using Equation 1; (b) ultimate tensile strength ( $UTS$ ); (c) yield strength ( $YS$ ); and (d) elongation to fracture ( $E_f$ ).

### 4.3.2. Effects of Copper

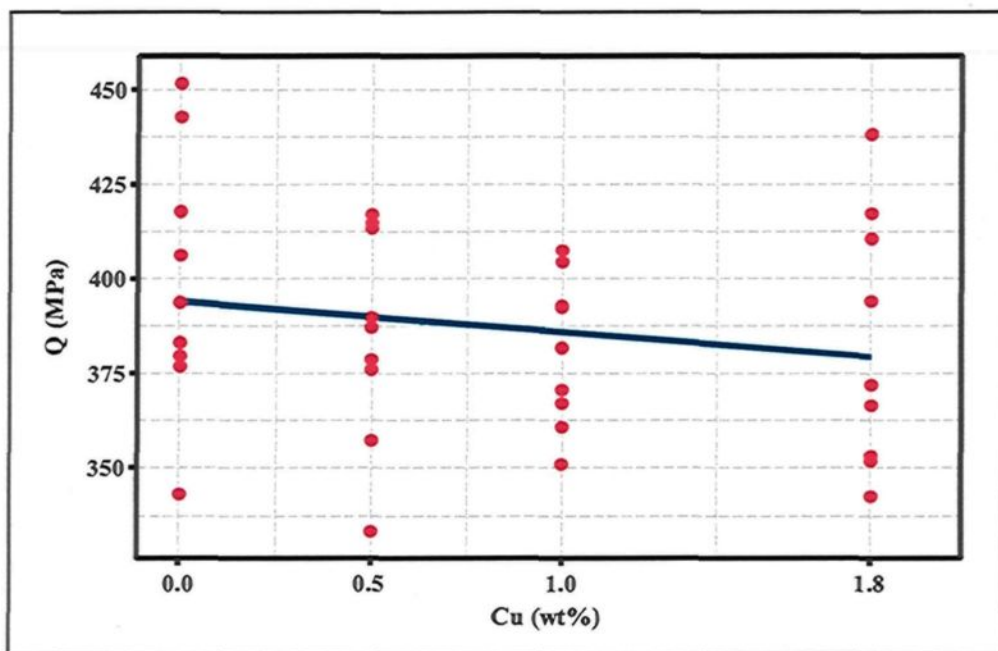
Additions of copper were made to 359 castings so as to further increase their strength. The 359 casting alloys contain 0%Cu while the 354 alloys contain 1.8% Cu. The current section will discuss the influence of copper additions (0%, 0.5%, 1%, and 1.8%) on the tensile properties and quality indices of 359 Al-9%Si-0.5%Mg castings. By increasing the copper content, it is possible to improve the strength of the alloys, although this will result in a reduction in ductility.<sup>6, 75, 76</sup> The beneficial outcome of the addition of copper may be further optimized by applying adequate heat treatment procedures.<sup>4, 154, 155</sup>

The strengthening effect obtained by adding copper to an Al-9%Si-0.5%Mg alloy is based on the formation of Cu- and Cu-Mg-containing precipitates such as  $\theta$  ( $\text{Al}_2\text{Cu}$ ),  $S$  ( $\text{Al}_2\text{CuMg}$ ),  $\sigma$  ( $\text{Al}_5\text{Cu}_6\text{Mg}_2$ ), and  $Q$  ( $\text{Al}_5\text{Cu}_2\text{Mg}_8\text{Si}_6$ ).<sup>104, 154, 156, 157, 158</sup> The strengthening effect may be further optimized by applying the adequate heat treatment procedures, as shown in Figure 4.9 and Figure 4.10; such an intervention which involves applying the suitable heat treatment to castings containing the same copper content ultimately leads to significant improvements in the strength and quality of these castings. The influence of solution heat treatment will be elaborated upon in later subsections of this chapter, while the effects of aging treatment will be discussed in detail in the next chapter.

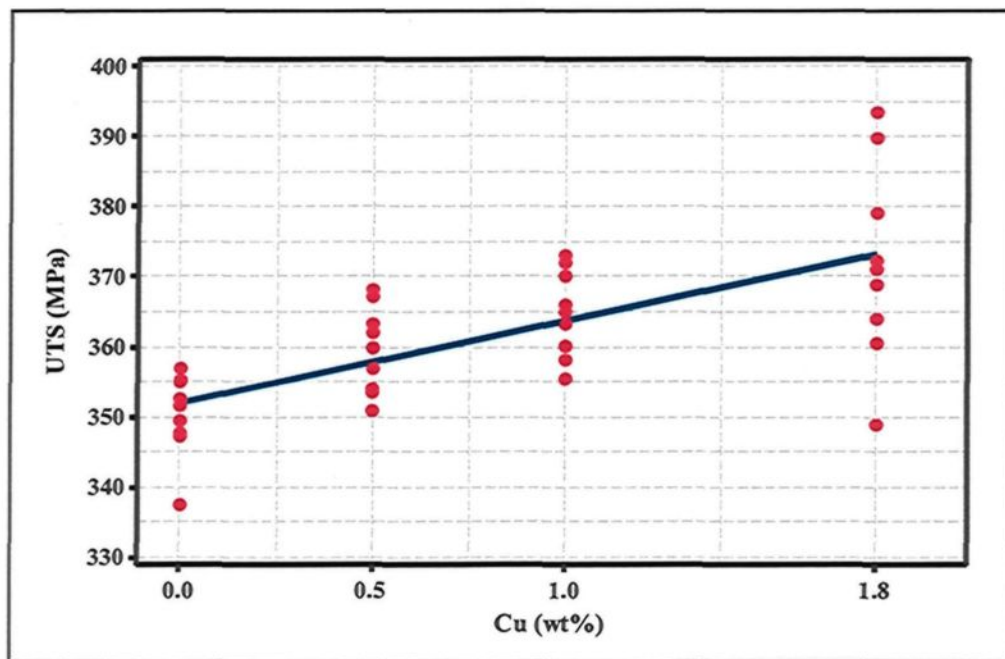
The copper levels mentioned above are labeled on the curves shown in Figure 4.9 and Figure 4.10; from these charts, it will be evident that upon increasing the copper content, the *iso-Cu* series shifts toward the upper left-hand side of the chart, virtually parallel to the *iso-yield strength* or the *iso-flow* lines. This behavior leads to greater yield strength and ultimate tensile strength values upon the addition of copper. The improvement

in alloy strength, however, is usually accompanied by a lessening in ductility. The quality of these castings will be affected according to the net amount by which the strength is increased and the ductility is lessened; it should be noted, however, that the influence of copper on the strength values is much more significant than its effect on the quality of the castings. Alloys 10S, 11S, and 12S (*i.e.* the 354 alloys) which contain the highest levels of copper content, provide the maximum strength under various heat treatment conditions applied to the castings, as shown in Figure 4.9 and Figure 4.10. It was observed that the strength of the 359 alloys may be improved by increasing the copper content to 0.5% and 1%, as shown in the same quality charts. On the other hand, alloys 1S, 2S, and 3S containing no copper additions provide the minimum strength values under all the heat treatment conditions applied to the castings, as will be seen in Figure 4.9 and Figure 4.10.

The results shown in the quality charts in Figure 4.9 and Figure 4.10 were re-plotted using the scatterplots shown in Figures 4.13(a) through (d). These plots describe the correlation between the copper content and the properties of the castings. Figure 4.13(a) illustrates the slight reduction in the quality index values with increasing copper content caused by the lessening in ductility. Figure 4.13(b) shows the improved tensile strength values with increasing copper levels. Figure 4.13(c) reveals the significant increase to be observed in the yield strength upon increasing the copper content. Figure 4.13(d) illustrates the reduction occurring in the ductility of the castings as a result of increasing the copper content. The behavior of the results presented using the scatterplots shown in Figures 4.13(a) through (d) is an accurate match for the evaluation made using the quality charts shown in Figure 4.9 and Figure 4.10.

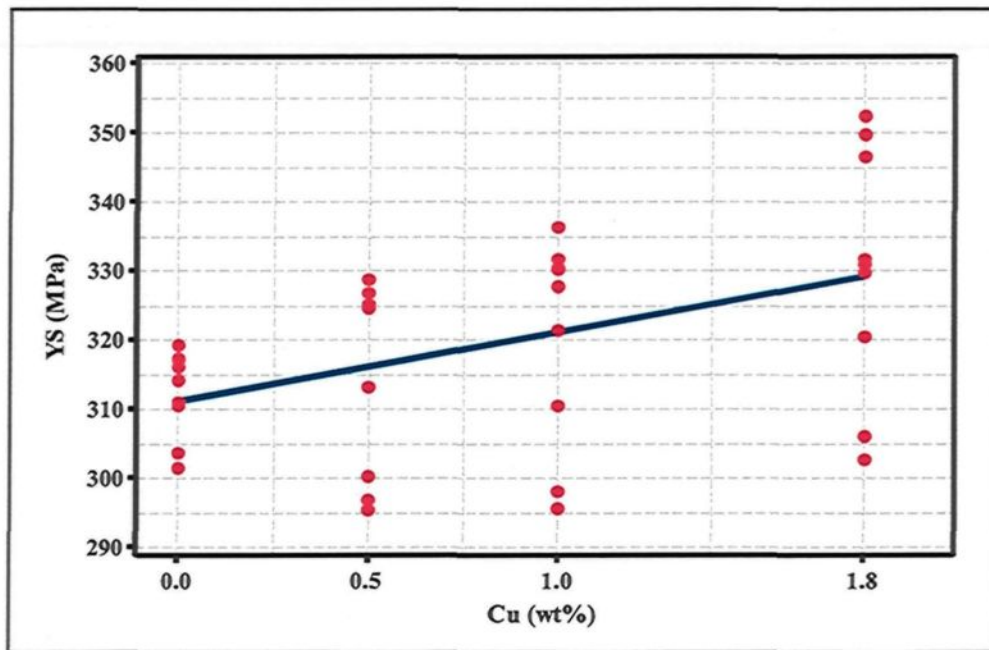


(a)

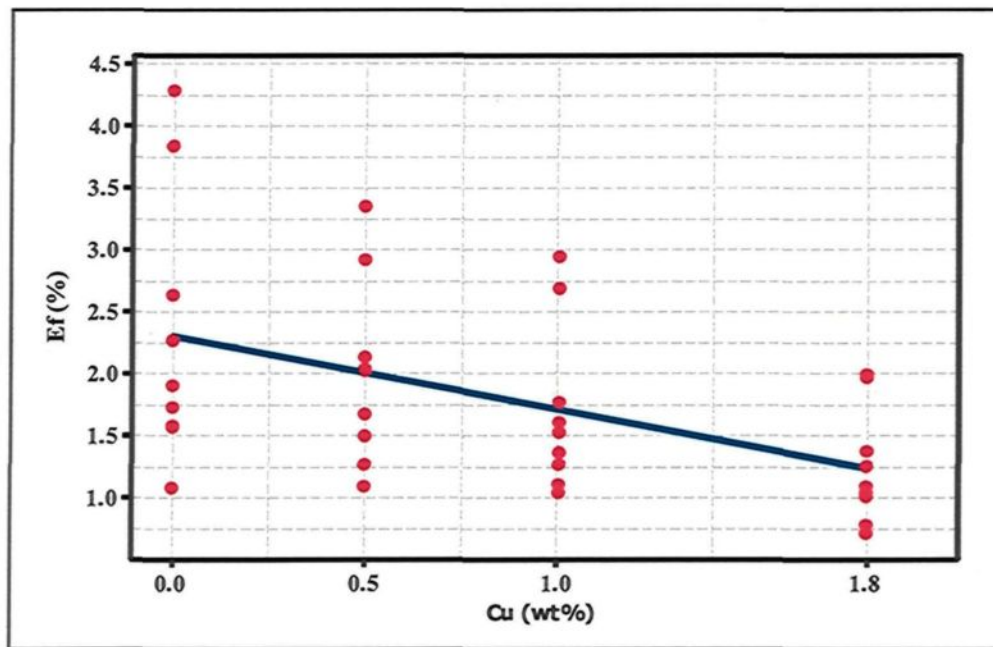


(b)

Figure 4.13



(c)



(d)

**Figure 4.13.** Scatterplots correlating copper content in Al-9%Si-0.5%Mg casting alloys with: (a) quality index values ( $Q$ ) calculated using Equation 1; (b) ultimate tensile strength ( $UTS$ ); (c) yield strength ( $YS$ ); and (d) elongation to fracture ( $E_f$ ).

### 4.3.3. Influence of Magnesium

The current section will discuss the effects of magnesium levels on the tensile properties and the quality index of the 359 casting alloys. Magnesium is added to Al-Si castings to increase their hardness and strength, although these improvements occur at the expense of ductility.<sup>5, 7, 159, 160</sup> The Mg-content of the 359 castings, *i.e.* 0.5%, was increased to five different levels including 0.6%, 0.7%, 0.8%, 0.9%, and 1% for the purposes of obtaining further improvement in the strength of these castings. The alloys coded 1SM, 2SM, 3SM, 4SM, 5SM, and 6SM have Mg-levels of 0.5%, 0.6%, 0.7%, 0.8%, 0.9%, and 1%, respectively. These castings were subjected to fixed heat treatment steps including solution heat treatment at 537°C for 12 hours followed by aging treatment at 170°C for 8 hours.

The increase in the Mg-content from 0.5% to 0.6% leads to an improvement in the strength of the castings and to a slight decrease in ductility, but without any noticeable lessening of quality, as may be seen from the quality charts shown in Figure 4.14 and Figure 4.15. These observations relate to the fact that the amount by which the strength of the alloy is increased compensates for the amount by which the ductility is decreased.

Further additions of Mg beyond 0.6%, *i.e.* in the range of 0.7% – 1%, result in a further slight increase in the alloy strength with a large reduction in quality index values from 458 MPa for the 2SM alloy to 410 MPa for the 6SM alloy, as may be seen in the same quality charts shown in Figure 4.14. The large reduction in alloy quality was brought about by the decrease in alloy ductility, as will also be clear from the same quality charts. The improved strength of the castings obtained by increasing the Mg-level is directly related to

the precipitation of  $Mg_2Si$  phases. Higher Mg-content will produce a higher density of these hardening phases.

The higher Mg-content, on the other hand, will also bring about the precipitation of a large volume fraction of the  $\pi-Al_8Mg_3FeSi_6$  phase which ultimately has a deleterious effect on both the strength and the ductility of the castings and consequently on their quality.<sup>7, 161, 162, 163</sup> The formation of the  $\pi-Al_8Mg_3FeSi_6$  phase negatively affects the strength of the castings since it reduces the magnesium in the supersaturated solid solution and therefore leads to a decrease in the density of  $Mg_2Si$  precipitates which tend to form after aging treatment.<sup>164</sup> This latter case may explain the reason for the slight increase in the strength values upon adding Mg in the range of 0.7% - 1%. The  $\pi$ -phase also has a deleterious effect on the ductility of the castings due to its brittle nature since it acts as a preferred crack initiation site where the fracture is triggered.

In the case where the Mg-level is 0.5%, after solutionizing treatment at 537°C, the  $\pi$ -phase was observed to dissolve or transform into a cluster of very fine  $\beta$ -phase platelets, as may be seen in Figure 4.2(d). In the case where the Mg-level is high at 1% and after applying the same solutionizing treatment, large particles of the  $\pi$ -phase remained undissolved in the matrix, as may be seen in the optical micrograph shown in Figure 4.16(a). These remaining  $\pi$ -phases are considered to be responsible for the deterioration in the tensile properties and quality indices of these castings, in particular, their ductility. These phases act as preferred crack initiation sites and accelerate the fracture of the samples because of their brittle nature, as may be seen in Figures 4.16(b) and (c). These figures show the longitudinal sections which were taken beneath the fracture surface of 6SM

(1%Mg) samples, illustrating that the cracks start at the arrowed  $\pi$ -phases. On the other hand, Figure 4.16(d) also shows a section taken beneath the fracture surface of the 5SM (0.5%Mg) alloy; the higher quality of this alloy is related to the dissolution or transformation of the  $\pi$ -phase, where no more  $\pi$ -phase appears to exist either in the matrix or beneath the fracture surface, as may be seen in Figure 4.2(d) and Figure 4.16(d), respectively. The fracture, in this case, occurs mainly as a result of the cracking of silicon particles which are the harder constituent of the matrix.

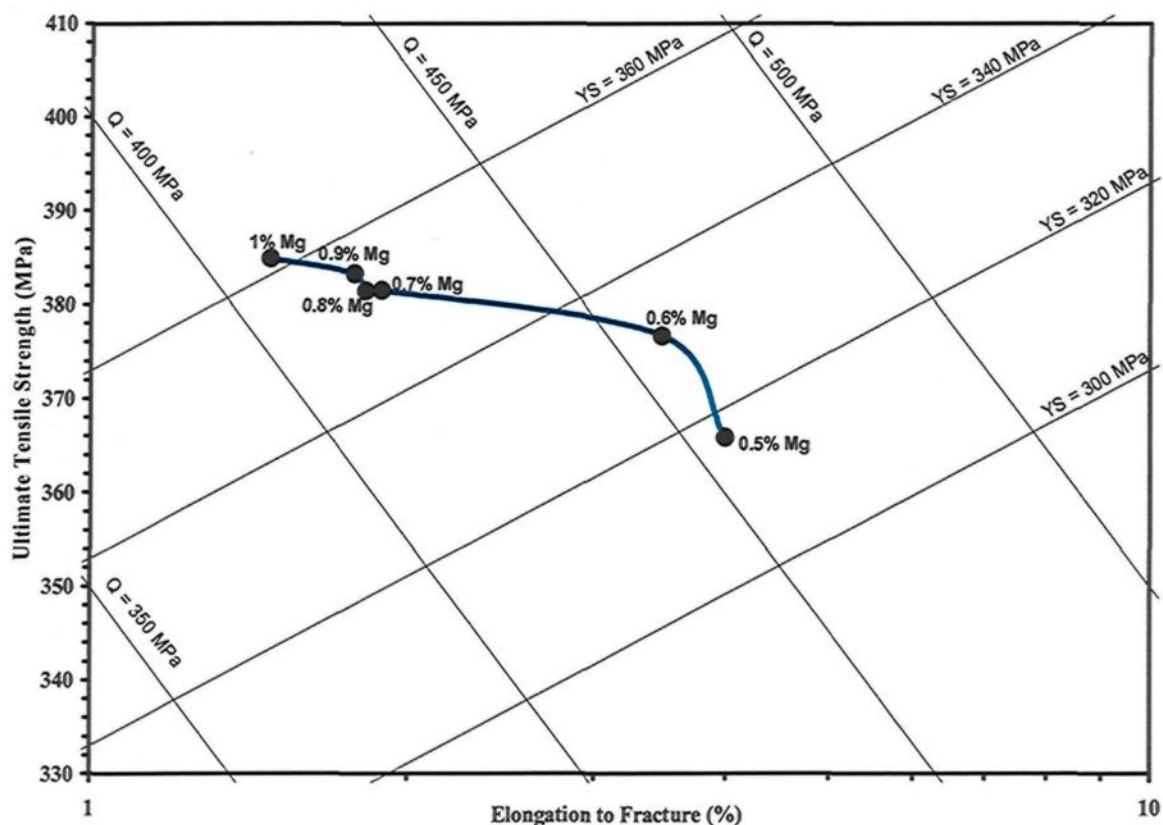


**Figure 4.14.** Quality chart generated using Equations 1 and 2 illustrating the influence of magnesium content on the tensile properties and the quality of the 359-type B108 test bar castings containing 0.07%Fe. (These castings were subjected to solutionizing treatment at 537°C for 12 hours followed by aging treatment at 170°C for 8 hours.)

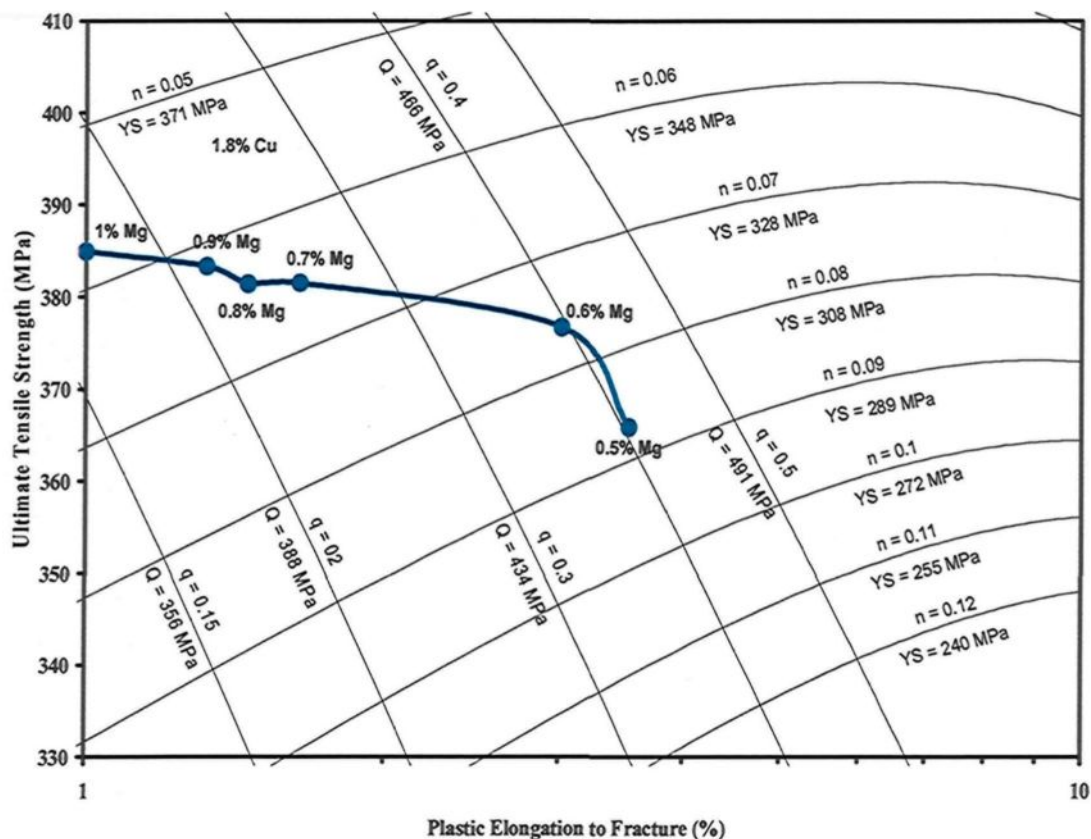
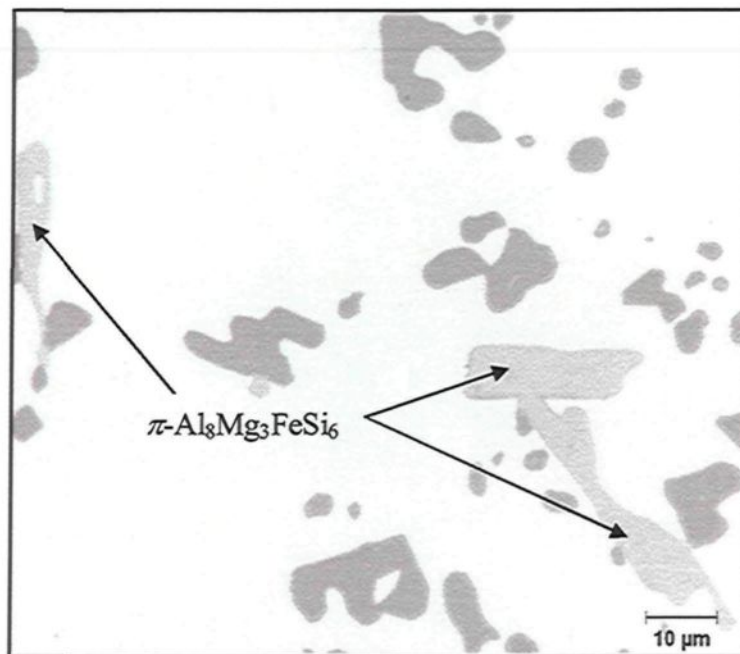
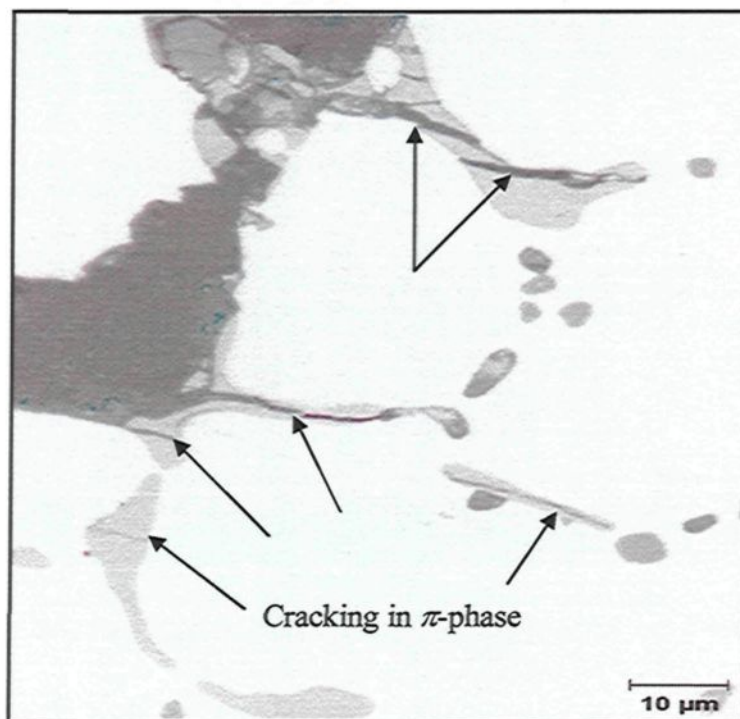


**Figure 4.15.** Quality chart generated using Equations 8 and 9 illustrating the influence of magnesium content on the tensile properties and the quality of the 359-type B108 test bar castings containing 0.07%Fe ( $K = 507$  MPa). (These castings were subjected to solutionizing treatment at  $537^{\circ}\text{C}$  for 12 hours followed by aging treatment at  $170^{\circ}\text{C}$  for 8 hours.)

According to the results obtained and presented in Figure 4.14 and Figure 4.15, 0.6% Mg is the maximum recommended level of magnesium for addition to 359 castings. This specific content of magnesium provides the best possible compromise between strength, ductility, and the quality index for these castings.

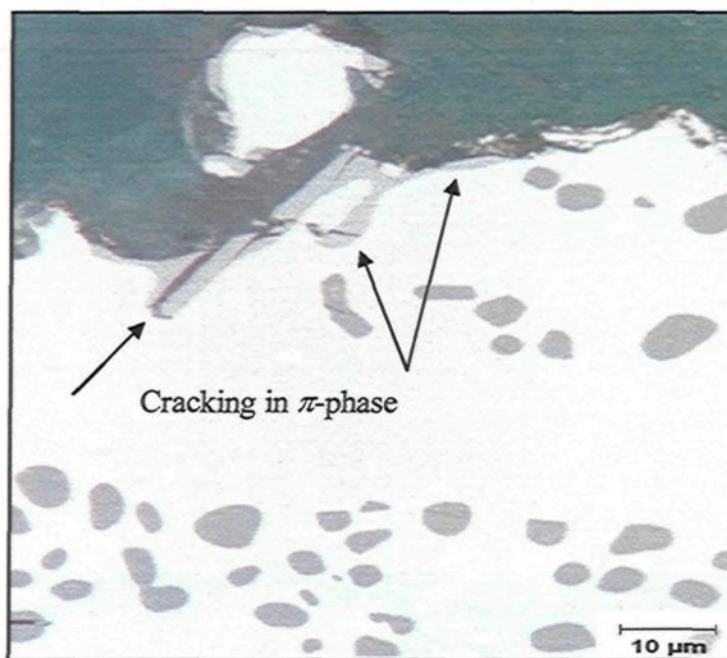


(a)

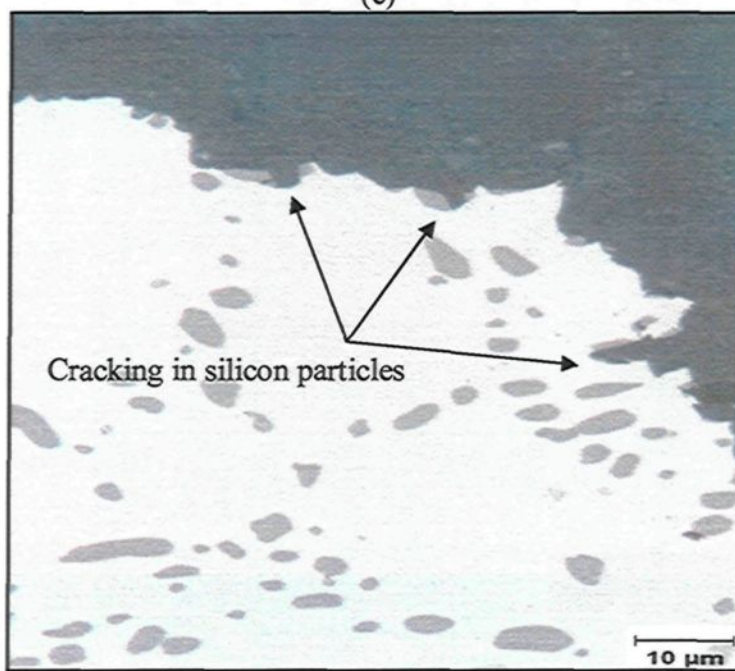


(b)

Figure 4.16



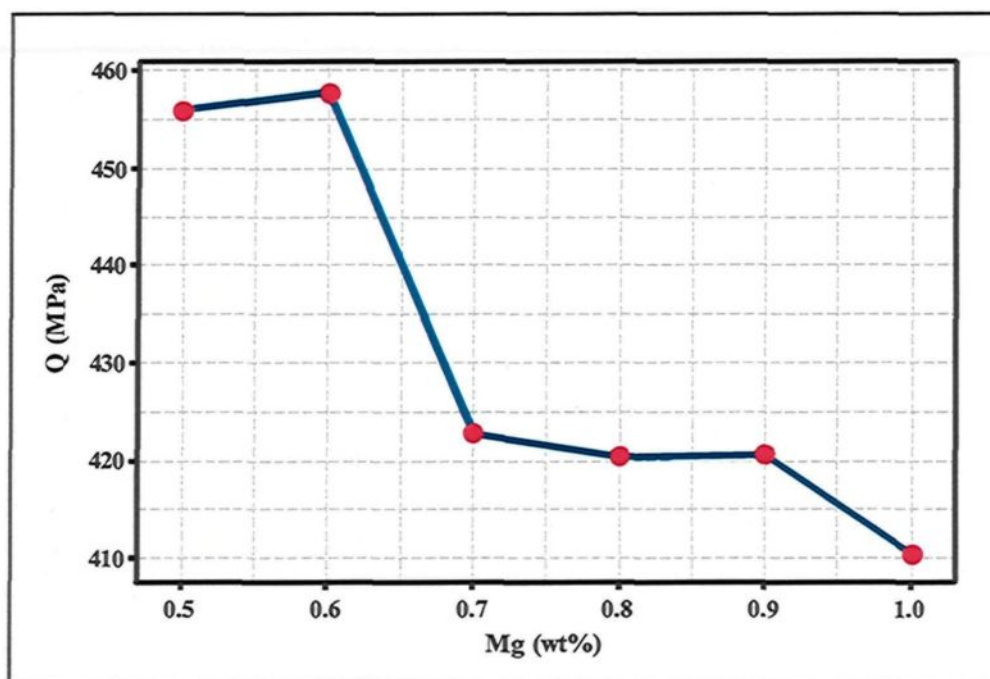
(c)



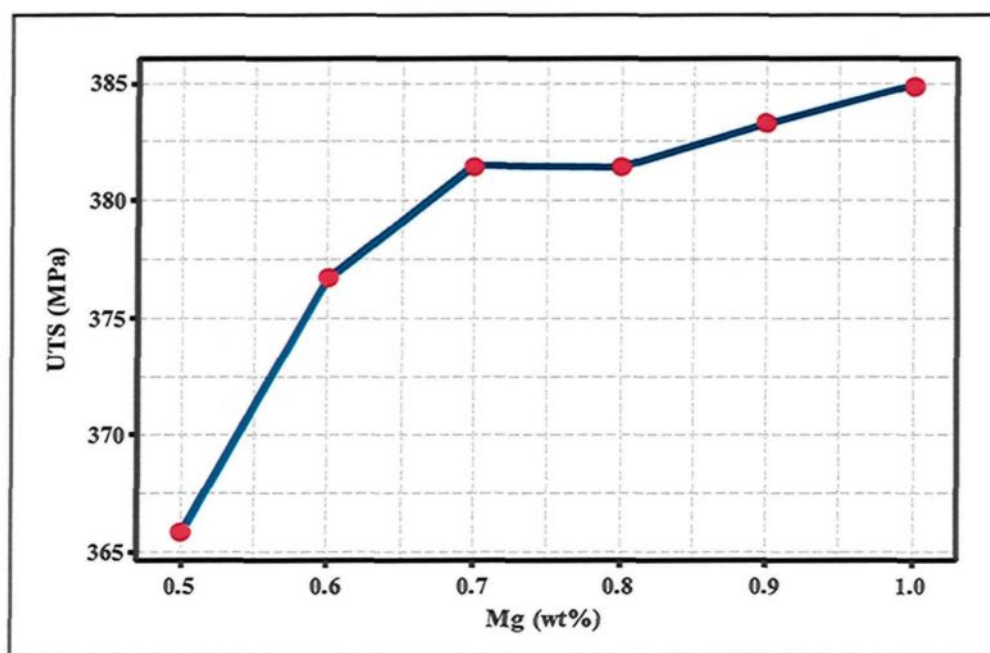
(d)

**Figure 4.16.** Optical micrographs showing (a)  $\pi$ -phases remaining in the 6SM alloy (1%Mg) after applying solutionizing treatment at 537°C for 12 h followed by aging treatment at 170°C for 8 h; (b) and (c) longitudinal sections beneath the fracture surface of 6SM alloy; (d) longitudinal section beneath the fracture surface of 1SM alloy (samples were obtained from the gauge length of B108 test bars).

The quality charts shown in Figure 4.14 and Figure 4.15 reveal similar behavior concerning the effects of Mg-level on the tensile properties and the quality index values of 359 casting alloys. Using any one of these two charts will lead to the same interpretation of the results and to the same evaluation of the properties of the alloys. The results shown in the quality charts in Figure 4.14 and Figure 4.15 were re-plotted using matrix plots, as shown in Figures 4.17(a) through (d). These plots represent the correlation between the levels of magnesium and the properties of the castings. Figure 4.17(a) illustrates the decrease in the quality index values with increasing Mg-levels beyond 0.6%. Figure 4.17(b) shows the increased tensile strength values occurring with an increase in magnesium content. Figure 4.17(c) shows the increase in the yield strength with an increasing Mg-content. Figure 4.17(d) illustrates the reduction occurring in the ductility of the castings as a result of increasing the Mg-content. The results obtained using the matrix plots shown in Figures 4.17(a) through (d) are a satisfactory match for the evaluations made using the quality charts in Figure 4.14 and Figure 4.15.

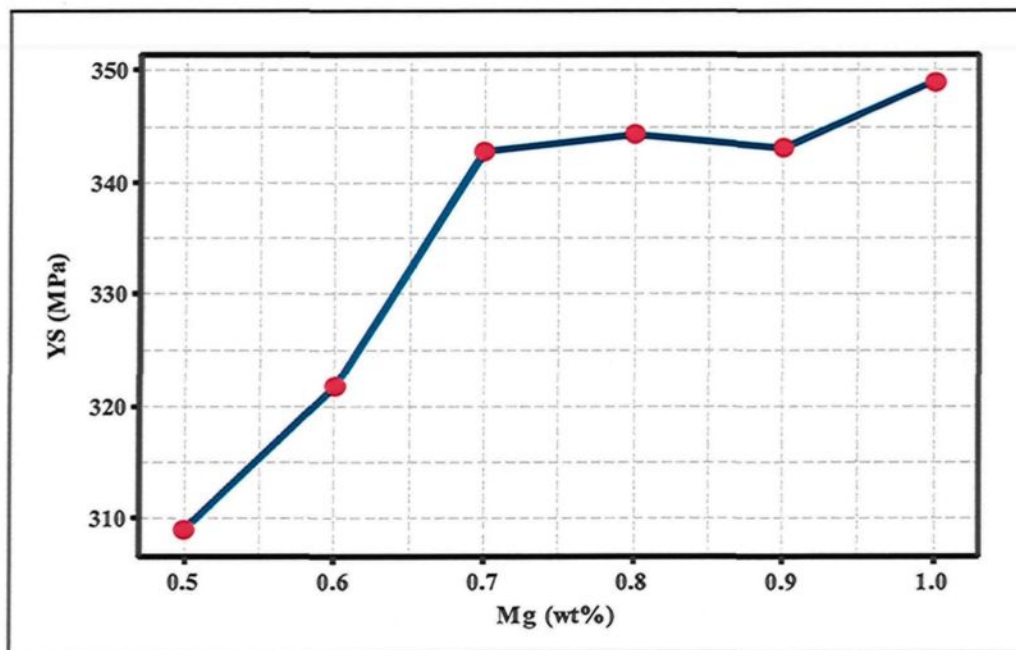


(a)

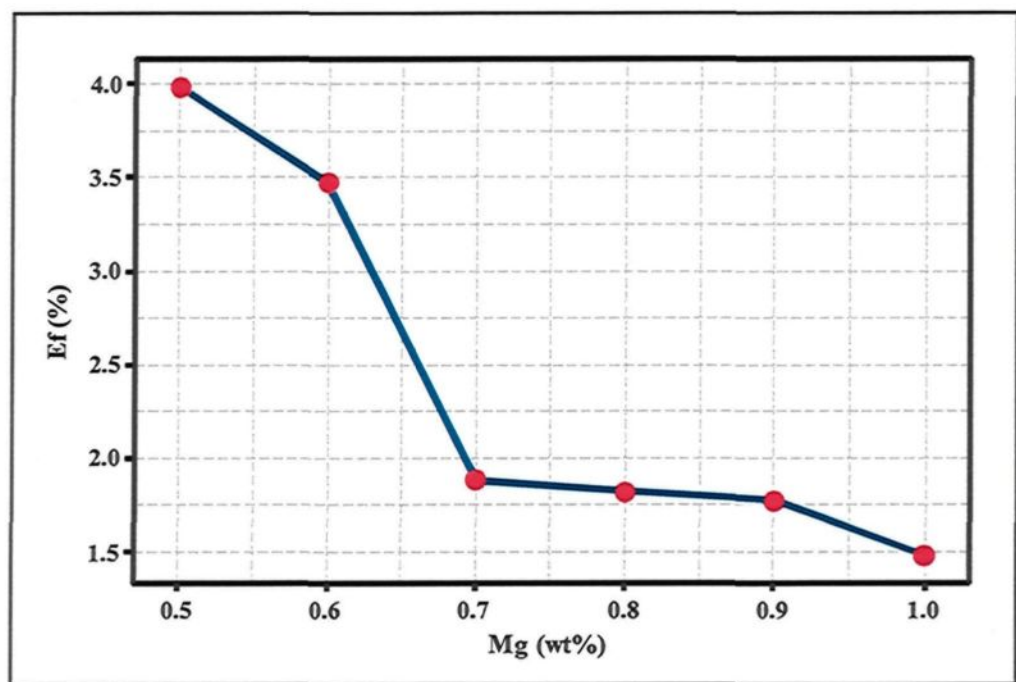


(b)

Figure 4.17



(c)



(d)

**Figure 4.17.** Scatterplots correlating Mg-content in 359-type B108 test bar castings containing 0.07%Fe with: (a) quality index values ( $Q$ ) calculated using Equation 1; (b) ultimate tensile strength (UTS); (c) yield strength (YS); and (d) elongation to fracture ( $E_f$ ).

#### 4.3.4. Effects of Solidification Rate

The current section presents results and discussion pertaining to the influence of solidification rate on the tensile properties and the quality indices of 354 and 359 casting alloys. Alloys coded 1S and 10S, corresponding to the 359 and 354 alloys, were cast using an end-chill mold for the purpose of providing different cooling rates at various portions of the castings, as mentioned earlier in section 4.2.3.

The quality charts shown in Figure 4.18 and Figure 4.19 present the tensile properties and the quality index values of the 354 and 359 alloys displaying various cooling rates. These charts indicate that increasing the solidification rate leads to an improvement in the tensile properties and the quality index values of both 354 and 359 castings. Level I of the casting block provides the best possible compromise between the tensile properties and the quality index values of both these castings, as shown in Figure 4.18 and Figure 4.19.

Level III of the casting, on the other hand, provides the least satisfactory tensile properties and quality index values for the same alloys, as shown in Figure 4.18 and Figure 4.19. These figures show that increasing the cooling rate of the castings results in shifting their tensile properties and quality indices towards the upper right-hand corner of the chart which is the optimum location from the point of view of the designer engineer. On the other hand, decreasing the cooling rate results in shifting the same properties towards the bottom left-hand corner of the chart which is the least satisfactory location. The bottom portion of the casting, *i.e.* Level I, reveals the maximum solidification rate, as indicated by the smallest SDAS listed in Table 4.2 and shown in Figure 4.8(a), while the upper portion of

the casting, *i.e.* Level III, reveals the minimum cooling rate, as indicated by the largest SDAS listed in Table 4.2 and shown in Figure 4.8(c).

The enhanced tensile properties and quality indices of the castings at Level I are related to a number of microstructural features which accompany the rapid cooling rate. These include the refinement of the grain size and the SDAS;<sup>91, 165</sup> the modification of eutectic silicon particles;<sup>166, 167, 168</sup> the reduced size and level of porosity;<sup>169, 170, 171</sup> and the reduced size and level of the intermetallic phases.<sup>172, 173, 174, 175, 176</sup>

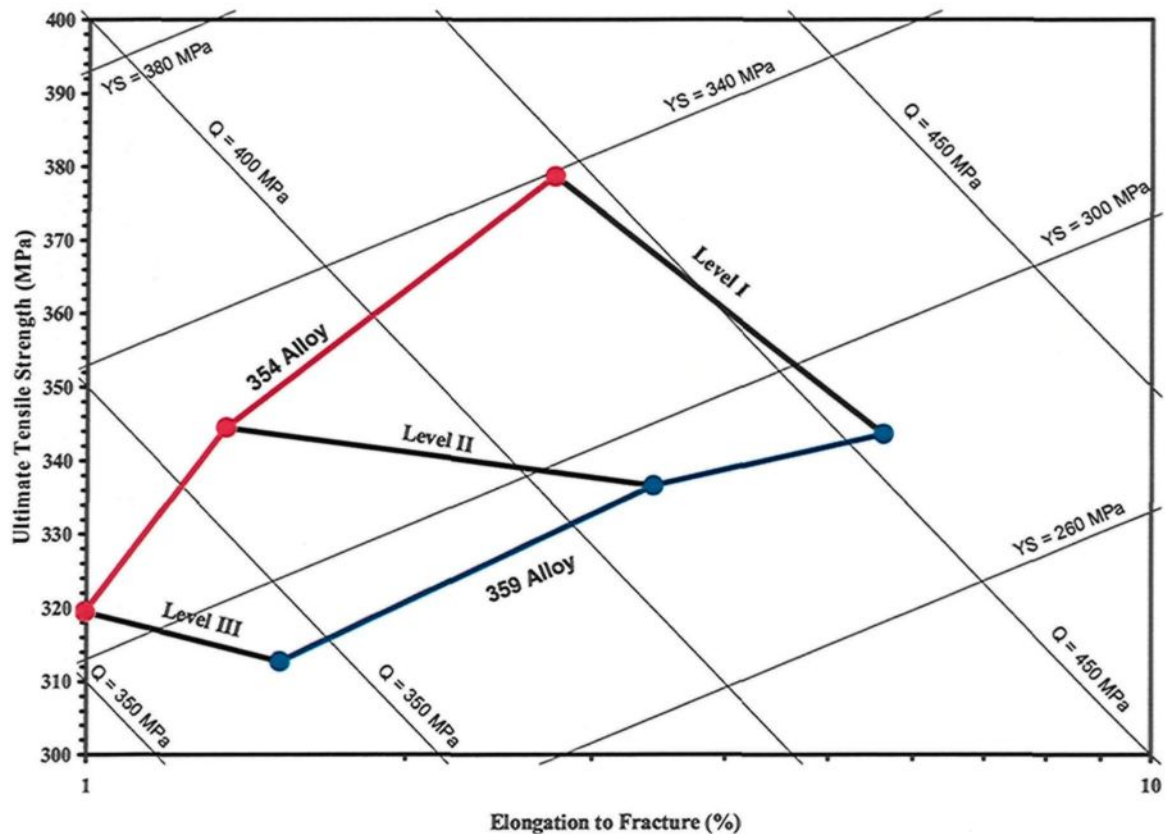


**Figure 4.18.** Quality chart generated using Equations 1 and 2 showing the influence of solidification rate on the tensile properties and the quality indices of the 1S-359 and 10S-354-type E8M-04 test bar castings containing 0.07%Fe. The 359 and 354 castings were subjected to solutionizing treatment at 537°C and 520°C, respectively, for 12 h followed by aging treatment at 170°C for 8h.

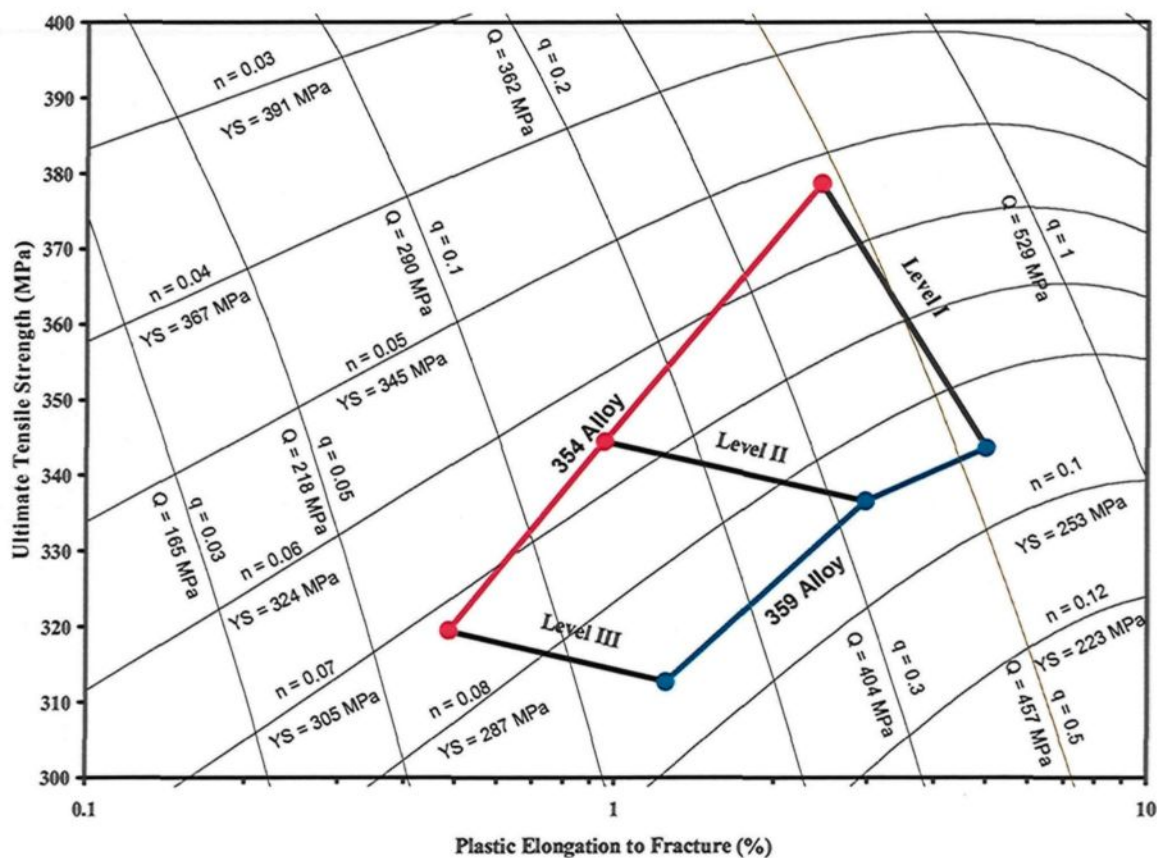


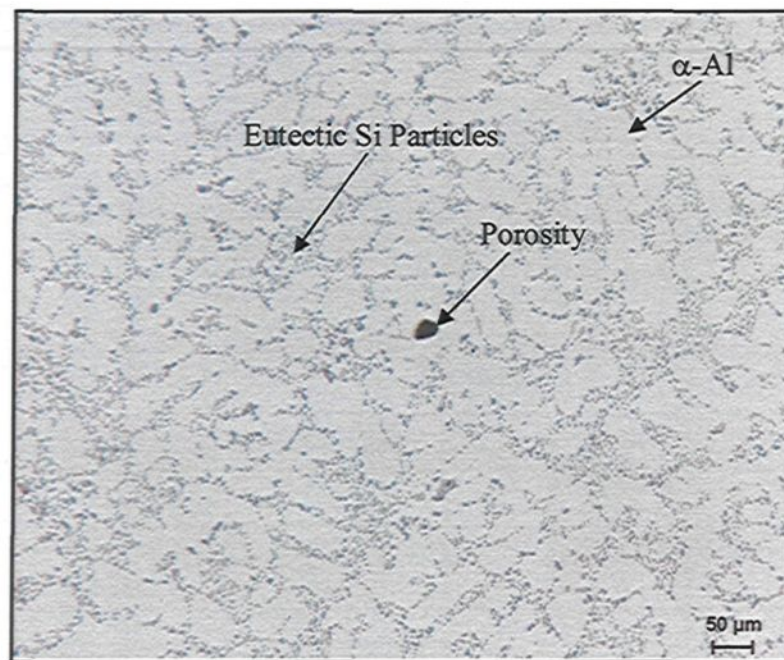
**Figure 4.19.** Quality chart generated using Equations 8 and 9 showing the influence of solidification rate on the tensile properties and the quality indices of the 1S-359 and 10S-354-type E8M-04 test bar castings containing 0.07%Fe ( $K = 472$  MPa). The 359 and 354 castings were subjected to solutionizing treatment at 537°C and 520°C, respectively, for 12 h followed by aging treatment at 170°C for 8 h.

Figures 4.20(a) and (b) show the microstructural characteristics of the 1S-359 castings containing 0.07%Fe at various solidification rates; it should be noted that the microstructural features will be presented here only for the 359 alloys to avoid repetition, although similar behavior is to be expected for the 354 castings as well. At Level I, the microstructure seems sound with small SDAS, fine eutectic silicon particles, and small sized shrinkage pores, as shown in Figure 4.20(a); at Level III, on the other hand, a coarser

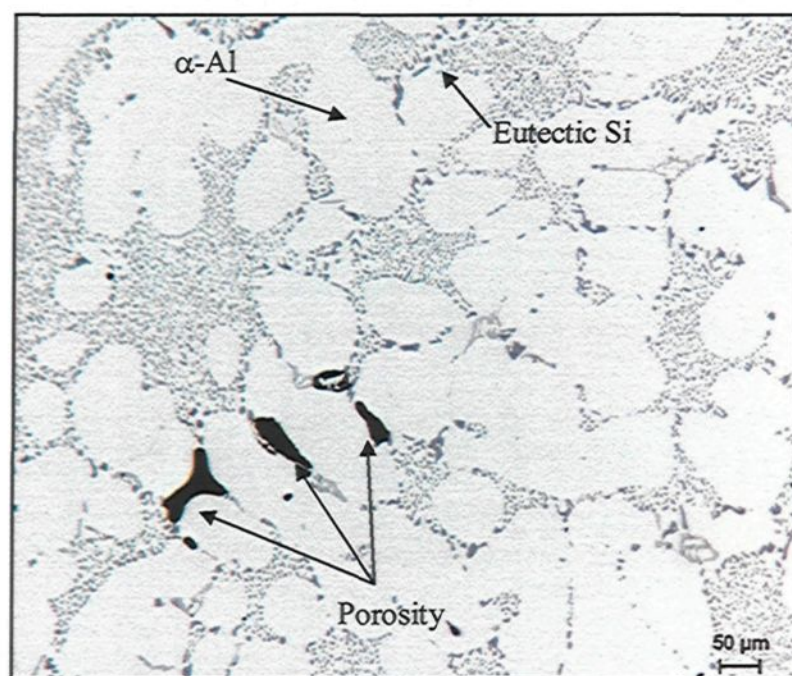
microstructure may be seen with larger SDAS, coarser eutectic silicon particles, and a larger size and level of shrinkage porosity, as shown in Figure 4.20(b).

The backscattered images shown in Figure 4.21 provide examples of the size of the platelet-like  $\beta$ -Al<sub>5</sub>FeSi phase at the fracture surface of the 1S-359 alloy samples containing 0.07%Fe cast at both rapid and slow cooling rates. Figure 4.21(a) shows small fragments of the  $\beta$ -Al<sub>5</sub>FeSi phase when casting the 359 alloy at rapid solidification rates, *i.e.* at Level I, while Figure 4.21(c) shows the large platelet-like  $\beta$ -Al<sub>5</sub>FeSi phase formed when casting the same alloy at a slow cooling rate, *i.e.* at Level III. Figures 4.21(b) and (d) illustrate the EDX spectra corresponding to the  $\beta$ -phases observed in Figures 4.21(a) and (c), respectively.

The reduction in the tensile properties and the quality index values of the castings accompanying the slower solidification rates are related to the changes occurring in the microstructural features and constituents of these castings. The microstructural aspects include larger SDAS, coarser eutectic silicon particles, larger sizes and levels of porosity, and larger amounts and sizes of the Fe-containing phases. According to the results presented in the quality charts shown in Figure 4.18 and Figure 4.19, a rapid cooling rate is recommended for the purposes of enhancing the tensile properties and the quality indices of the 354 and the 359 castings. With respect to the influence of solidification rates on the tensile properties and the quality index of these same casting alloys, the results obtained in the current study are in full agreement with a number of other studies applied to Al-Si castings.<sup>42, 50, 72-74</sup>



(a)

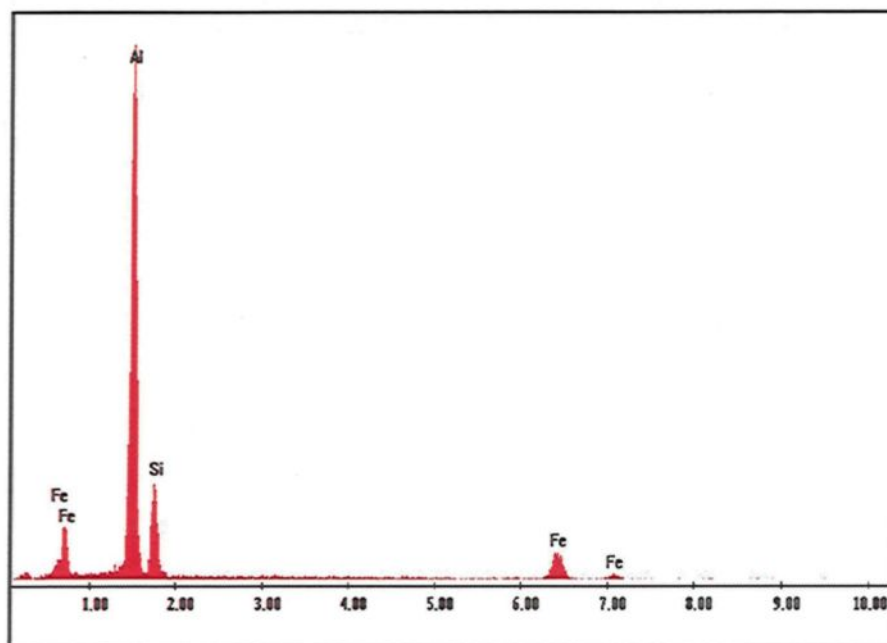


(b)

**Figure 4.20.** Optical micrographs illustrating the microstructural features in the 359 castings produced using an end-chill mold at (a) Level I; and (b) Level III (samples were obtained from the gauge length of E8M-04 test bars).

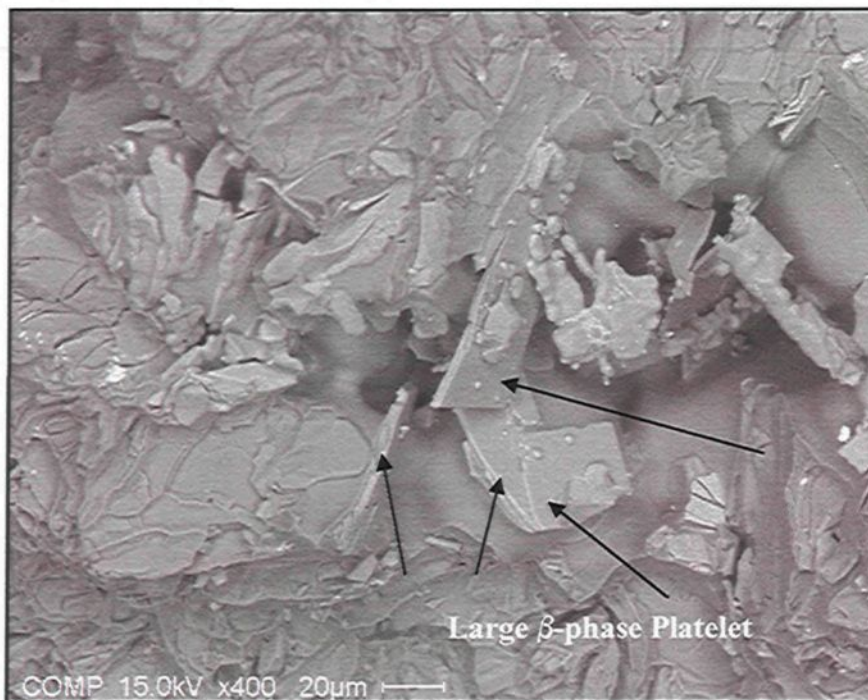


(a)

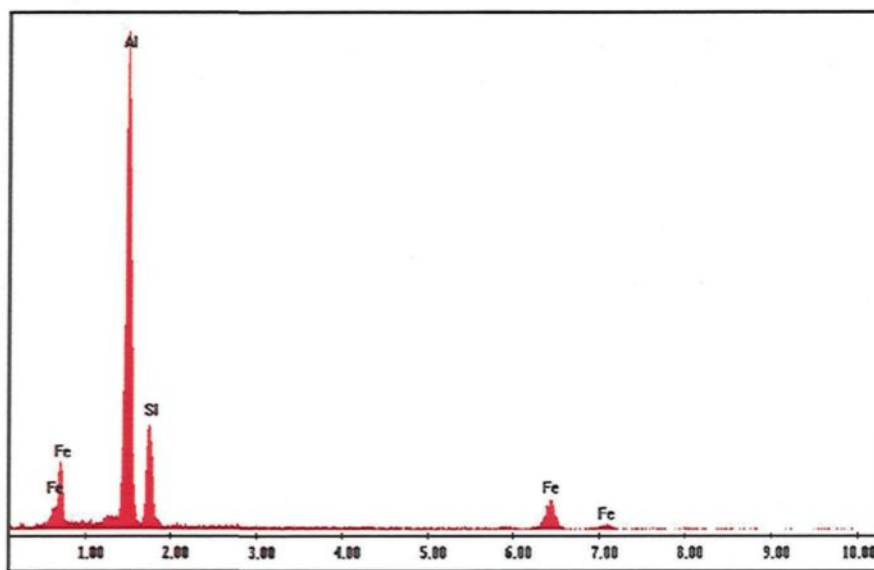


(b)

Figure 4.21



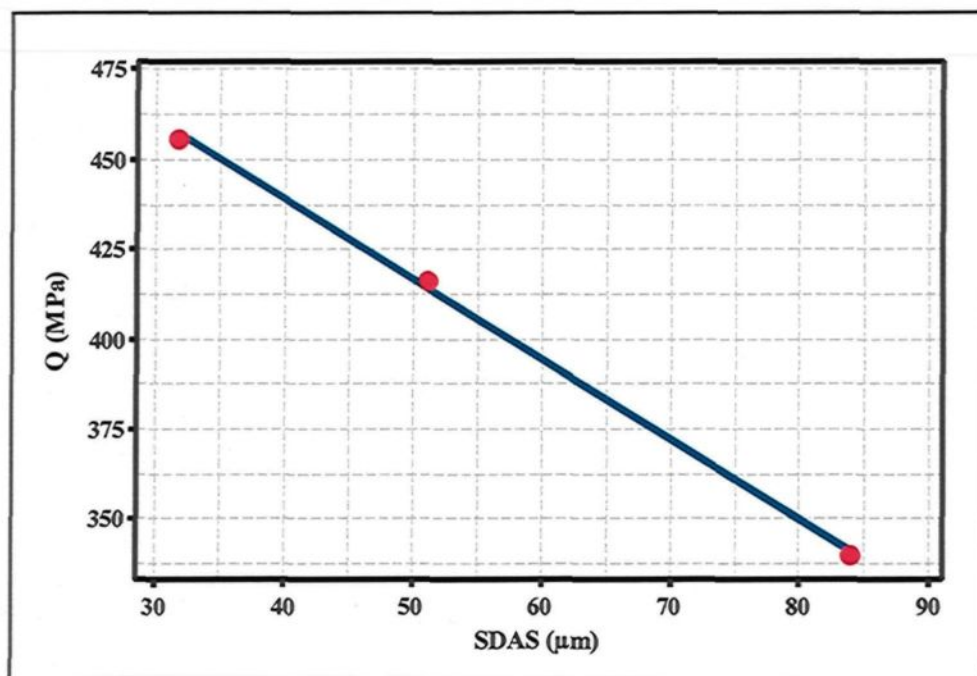
(c)



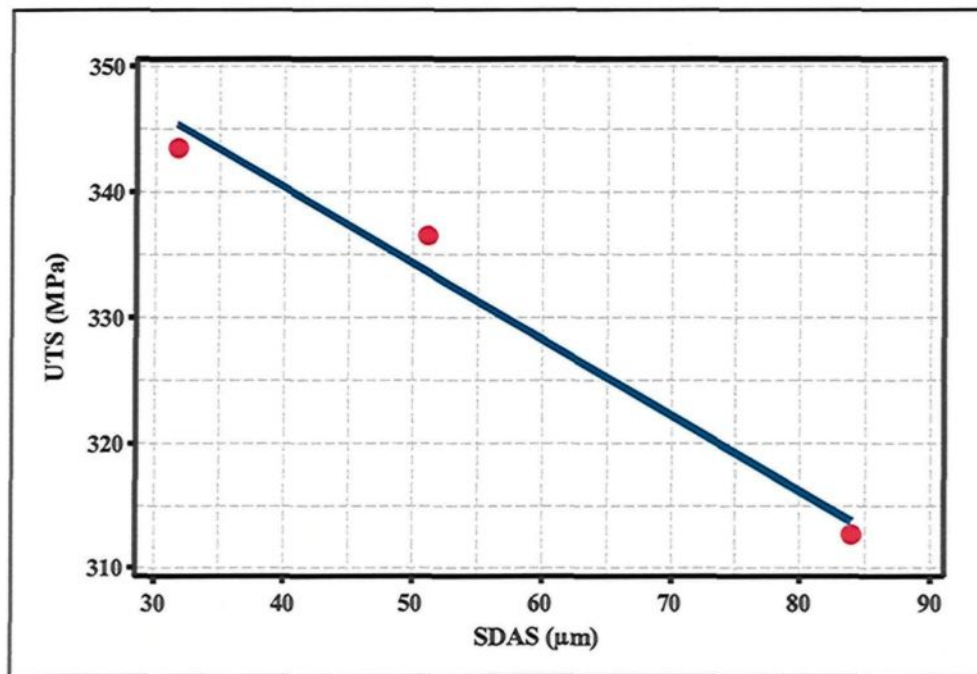
(d)

**Figure 4.21.** (a) and (c) are backscattered images showing the size of the  $\beta$ - $\text{Al}_5\text{FeSi}$  phase observed at the fracture surface (arrowed) of 1S-359 alloy samples containing 0.07%Fe and obtained from Levels I and III, respectively; (b) and (c) are the EDX spectra corresponding to the phases in the images shown in (a) and (c), respectively (the fractographs were obtained from the fracture surface of the E8M-04 test bars).

As observed earlier, the two models of the quality charts used to evaluate the results obtained have provided the same interpretation of behavior regarding the influence of solidification rates on the properties of the 354 and the 359 castings, as shown in Figure 4.18 and Figure 4.19. The results shown in these quality charts were re-plotted using scatterplots and presented in Figures 4.22(a) through (d). These scatterplots describe the correlation between the solidification rates indicated by the SDAS and the properties of castings. Figure 4.22(a) illustrates the decrease in the quality index values which occurs upon decreasing the solidification rates. Figure 4.22(b) shows the decreased tensile strength values which occur upon increasing the SDAS, *i.e.* decreasing the cooling rate. Figure 4.22(c) illustrates the decrease in the yield strength which occurs upon decreasing the solidification rate, *i.e.* upon increasing the SDAS. Figure 4.22(d) illustrates the reduction occurring in the ductility of the castings as a result of increasing the SDAS. The behavior of the results presented using the scatterplots shown in Figures 4.22(a) through (d) is in full agreement with the evaluation made using the quality charts shown in Figure 4.18 and Figure 4.19.

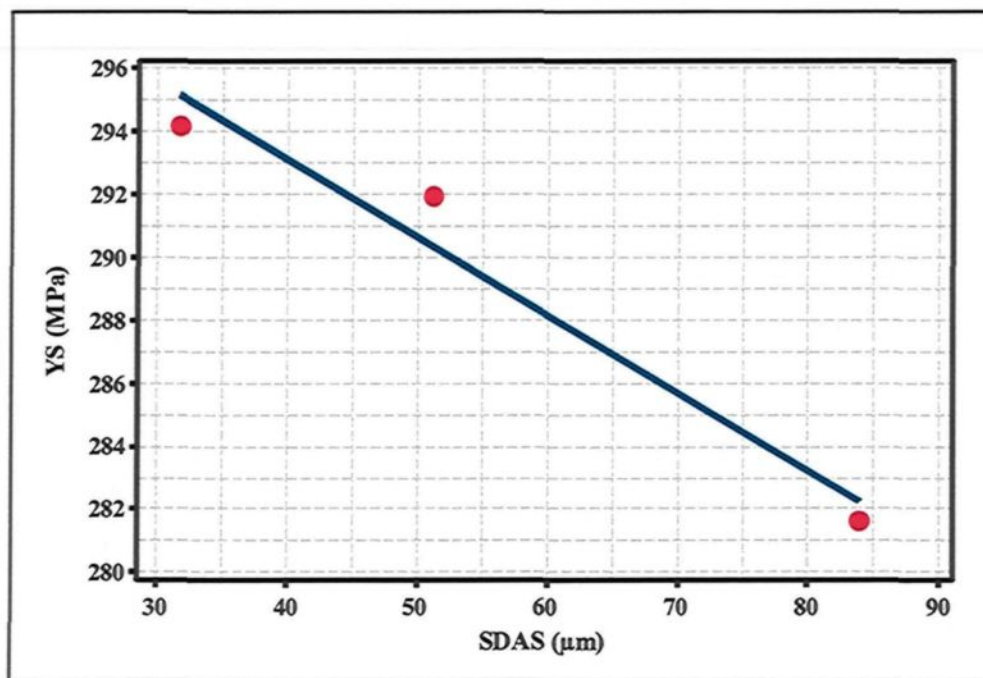


(a)

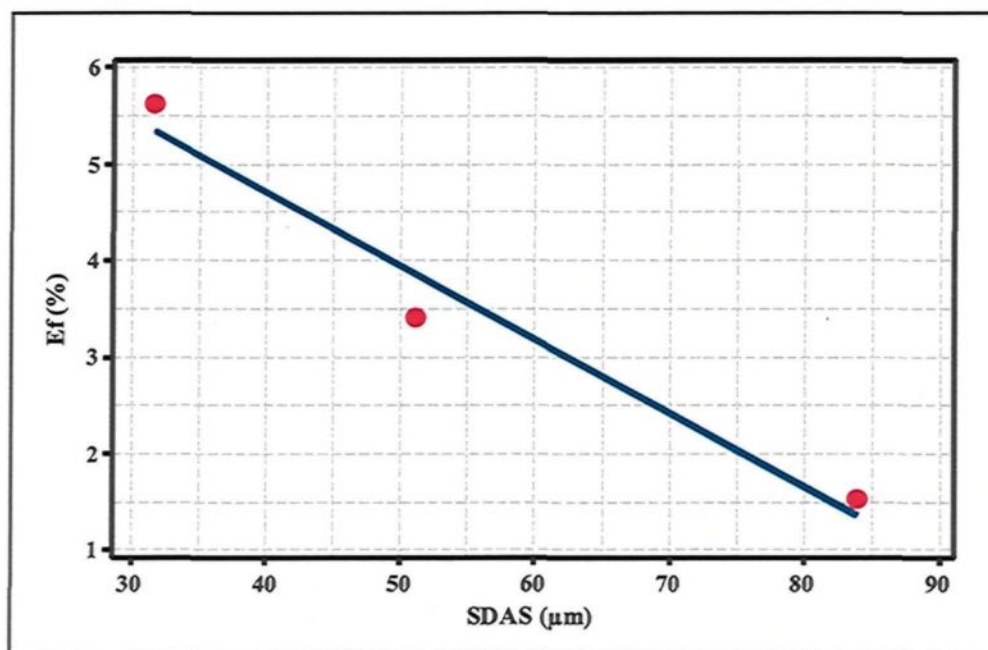


(b)

Figure 4.22



(c)



(d)

**Figure 4.22.** Scatterplots correlating solidification rate in terms of SDAS in 359 castings with: (a) quality index values ( $Q$ ) calculated using Equation 1; (b) ultimate tensile strength ( $UTS$ ); (c) yield strength ( $YS$ ); and (d) elongation to fracture ( $E_f$ ).

#### **4.3.5. Influence of Solution Heat Treatment Parameters**

One of the main objectives of this study is to select the appropriate solution heat treatment parameters for 354 and 359 castings in order to improve the tensile properties and quality indices. The parameters investigated are: (i) the solutionizing temperature for 354 and 359 alloys containing different levels of iron, and (ii) the solutionizing time for modified and non-modified 354 and 359 alloys. The results of these heat treatment procedures will be presented and discussed in the following subsections.

##### **4.3.5.1. Influence of Solutionizing Temperature**

The appropriate solutionizing temperatures for the 354 and 359 casting alloys were selected through an extensive investigation of the effects of solution heat treatment temperature on the tensile properties and the quality indices of these castings. This study includes: (i) an investigation of 359 alloy samples containing three levels of iron and three levels of copper content, *i.e.* alloys coded 1S through 9S, in relation to two solutionizing temperatures of 490°C and 537°C for a fixed time period of 12 h, as presented in Figure 4.9 and Figure 4.10; and (ii) an investigation of 354 alloy samples with three levels of iron content, *i.e.* alloys coded 10S, 11S and 12S, in relation to ten solutionizing temperatures of 490°C, 495°C, 500°C, 505°C, 510°C, 515°C, 520°C, 525°C, 530°C, and 537°C for a fixed time period of 12 h, as presented in Figure 4.23 and Figure 4.24. It should be noted that the solutionizing temperature of 354 alloys is a critical selection process because of the high copper content (1.8%Cu) of these castings making it necessary for applying ten trials to be carried out, in this case, to select the most appropriate solutionizing temperature. All the

solutionizing conditions mentioned in (i) and (ii) were followed by a fixed aging treatment at 170°C for 8 h.

With regard to the 359 alloys, increasing the solutionizing temperature in the selected range, *i.e.* 490°C - 537°C, produces significant improvements in the strength and quality of the castings containing various levels of iron and copper, *i.e.* in the alloys coded 1S through 9S, shown by the quality charts in Figure 4.9 and Figure 4.10.

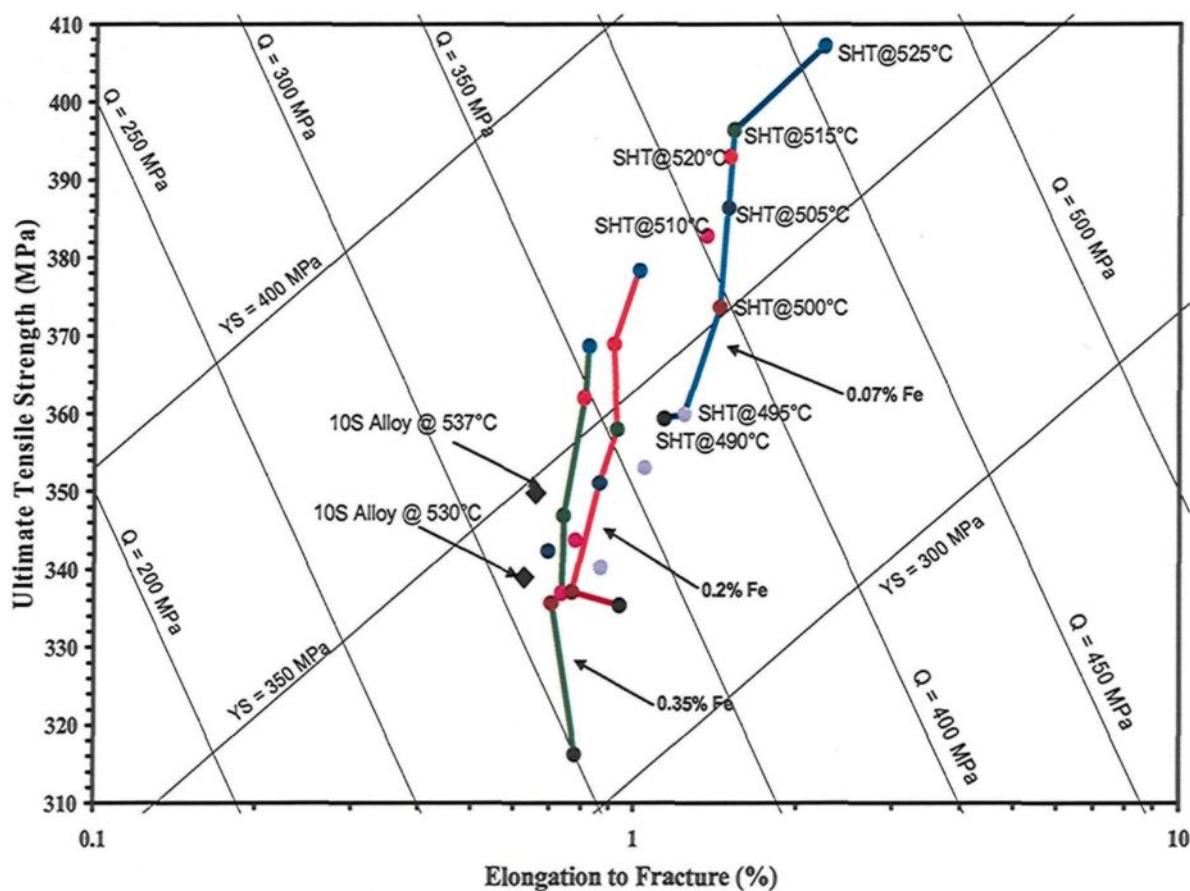


**Figure 4.23.** Quality chart generated using Equations 1 and 2 showing the influence of solutionizing temperatures on the properties of 354-type B108 test bar castings containing three levels of iron. All samples were solutionized for 12 h followed by aging treatment at 170°C for 8 h. The two additional points represent the 10S alloy solutionized at 530°C and 537°C for 12 h each followed by the same aging treatment.

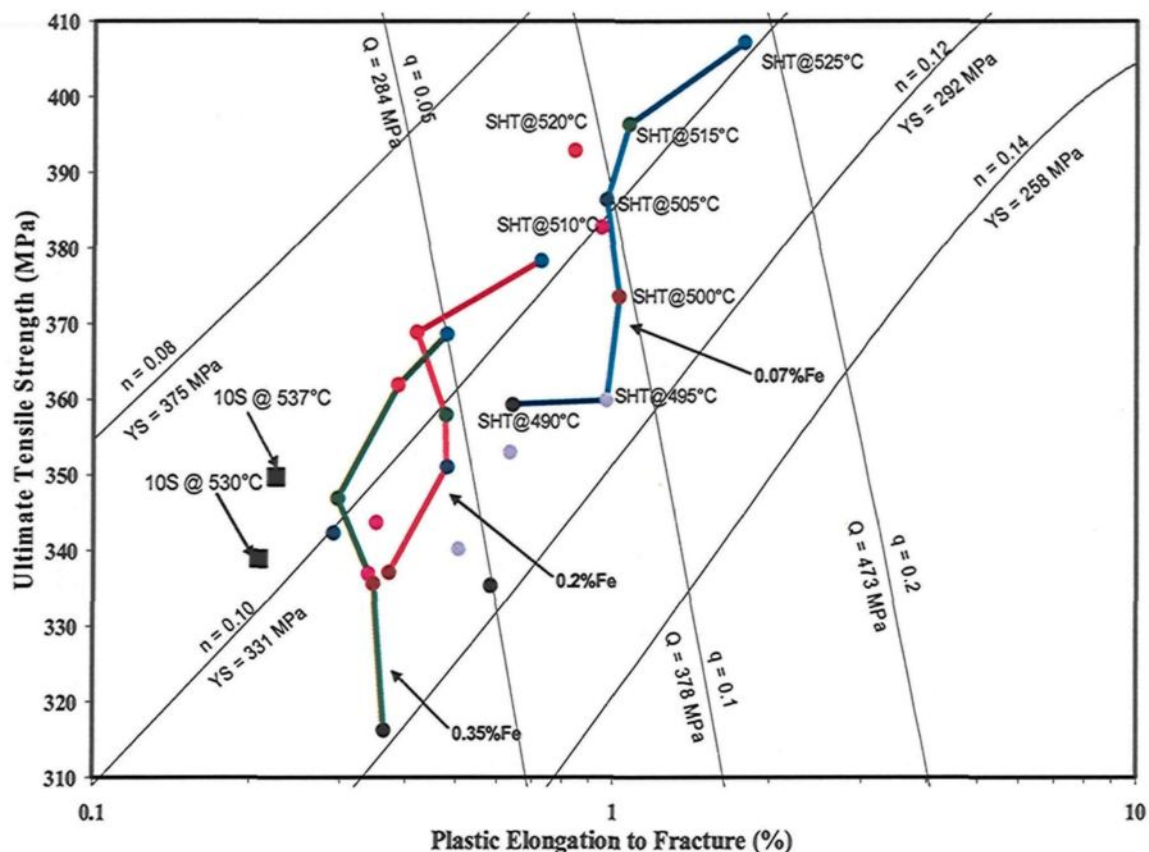


**Figure 4.24.** Quality chart generated using Equations 8 and 9 showing the influence of solutionizing temperatures on the properties of 354-type B108 test bar castings containing three levels of iron ( $K = 617 \text{ MPa}$ ). All samples were solutionized for 12 h followed by aging treatment at  $170^\circ\text{C}$  for 8 h. The two additional points represent the 10S alloy solutionized at  $530^\circ\text{C}$  and  $537^\circ\text{C}$  for 12 h each followed by the same aging treatment.

On the other hand, increasing the solutionizing temperature of the 354 castings to a particular limit will enhance the strength and the quality of the castings significantly. Figure 4.23 and Figure 4.24 show the quality charts generated to evaluate the tensile properties and the quality indices of the 354 alloys containing three levels of iron, *i.e.* the 10S, 11S, and 12S alloys. These figures show that raising the solutionizing temperature from  $490^\circ\text{C}$  to the specific temperature of  $525^\circ\text{C}$  results in a noticeable increase in the

strength and the quality indices of castings containing the three Fe-levels. Increasing solution heat treatment temperatures to 530°C and 537°C results in a sharp reduction in the tensile properties and quality indices of the castings, as shown in the same quality charts. The reasons for the reduction in the strength and the quality of the castings upon increasing the solution temperature to above 525°C will be explained further on in this subsection.

The significant enhancements which occur in the strength and quality of the 354 and 359 alloys upon increasing the solutionizing temperature to 525°C and 537°C, respectively, may be related to the following advantages brought about in the cast structure.

Increasing the solution heat treatment temperature to within the specified limits for the 354 and 359 alloys results in the homogenization of the microstructure, since higher temperatures provide a greater driving force for the segregated atoms to diffuse through the metal matrix producing a homogeneous structure.<sup>177, 178, 179</sup>

Raising the solutionizing temperature for the 354 and 359 alloys to 525°C and 537°C, respectively, produces considerable changes in the size and morphology of eutectic silicon particles, as may be observed in Figures 4.6(a) and (b). These figures show that the size of the eutectic silicon particles had increased whereas the aspect ratio had decreased upon raising the solutionizing temperature to the specified limits for the 354 and 359 alloys. The changes which occur in the size and morphology of eutectic silicon particles improve the strength of the alloys and enhance their ductility and therefore improve their quality. The mechanism of thermal modification of the eutectic silicon particles includes their necking, fragmentation, spheroidization, and coarsening.<sup>87, 88, 140, 141, 180</sup>

Solutionizing treatment at 525°C and 537°C applied to 354 and 359 castings, respectively, provides an opportunity for the complete dissolution of the undissolved  $\text{Al}_2\text{Cu}$  and  $\text{Mg}_2\text{Si}$  soluble phases which form during the solidification process so as to obtain the maximum amount of the hardening elements, Cu and Mg, in the solid solution. This step supports the subsequent aging treatment through a successful precipitation process.<sup>97, 136, 181</sup> The strengthening elements will precipitate out of the supersaturated solid solution during the aging process in the form of hardening phases, which tends to increase the strength of the castings. Figure 4.1(a) and Table 4.1 show the volume fraction percentage of the  $\text{Al}_2\text{Cu}$  phase which dissolved completely after solution heat treatment at the specified temperatures. For instance, the backscattered images shown in Figure 4.25(a) illustrate the  $\text{Al}_2\text{Cu}$  phases in the as-cast structure of the 10S-354 alloy which was cast using a graphite mold preheated to 600°C, while Figure 4.25(b) reveals the complete dissolution of these phases after applying a solutionizing treatment at 520°C for 12 h.

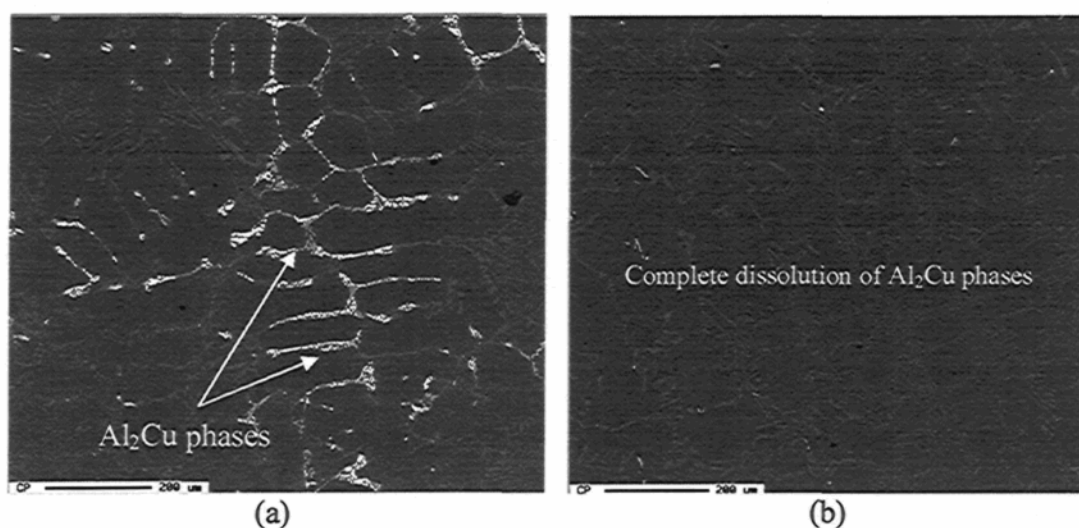


**Figure 4.25.** Backscattered images showing the matrix of the 10S-354 alloy in (a) the as-cast condition containing a large volume fraction of  $\text{Al}_2\text{Cu}$  phases; and (b) where, after applying solutionizing treatment at 520°C for 12 h, a complete dissolution of the same phases may be observed.

Solution heat treatments at 525°C and 537°C applied to 354 and 359 castings, respectively, neutralize the detrimental consequences of the partially soluble phases. These iron-containing intermetallic phases, and most specifically the  $\beta$ - and  $\pi$ -phases are noticeably affected, since significant changes are produced in the volume fraction, size, and morphology of these phases. Table 4.1 and Figure 4.1(b) show that the maximum reduction in the volume fraction of the partially soluble phases prevails at 520°C and 537°C when applied to 354 and 359 castings, respectively. Thinning, necking, and fragmentation of the  $\beta$ -phase will occur upon raising the solutionizing temperatures applied to 359 castings, as shown in Figures 4.2(b) and (c). Similar observations were made concerning the 354 castings, as shown in Figure 4.3(c). These changes in the size and morphology of the  $\beta$ -phase lead to a breakdown in the continuous nature of these particles and to the formation of small fragments of the  $\beta$ -phase, as shown in Figure 4.2(c) and Figure 4.3(c). Raising the solutionizing temperature also affects the  $\pi$ -phase where this specific phase was seen to dissolve and/or transform into a cluster of very fine  $\beta$ -phase platelets, as is shown in the optical micrograph provided in Figure 4.2(d).

The reasons previously mentioned explain why solutionizing temperatures of 525°C and 537°C produce the best possible strength and optimum quality index values in the 354 and 359 casting alloys, respectively. An increase in the iron content is always deleterious to the strength and quality of the castings in all of the conditions investigated, although solutionizing treatment has produced promising improvements in those qualities and strengths which contain the same iron-level, as may be observed in the quality charts shown in Figure 4.9, Figure 4.10, Figure 4.23, and Figure 4.24. Such enhancements are directly

related to the effects of this particular solutionizing treatment on the volume fraction percentage, size, and morphology of the iron-bearing compounds, as discussed earlier. These observations indicate that the proper solutionizing treatment has the potential for partially neutralizing the deleterious consequences of iron.

The influence of copper on the strength of the 359 castings was reinforced after the solutionizing treatment was applied at 537°C with a considerable increase in the quality indices of the castings, as shown in Figure 4.9 and Figure 4.10. As discussed earlier in this chapter, this effect is related to the influence of the solutionizing process on the dissolution of the  $Al_2Cu$  phase. In addition, the solutionizing treatment was followed by the application of an aging treatment at 170°C for 8 h which would lead to the precipitation of hardening phases in the metal matrix. It may be concluded, from the preceding, that applying the proper heat treatment results in reinforcing the effects which copper is known to have on the strength of the castings.

As discussed earlier, both models of the quality charts, as shown in Figure 4.23 and Figure 4.24, represent similar behavior resulting from the dual effects of solutionizing temperature and iron-content on the properties of the 354 casting alloys. The same results were re-plotted using a different format, as shown in Figures 4.26(a) through (c); these figures show the relevant results in the form of contour plots correlating the dual effects, indicated in these plots as ST (°C) and Fe (wt%), with the properties of the 354 castings, namely, the quality index value ( $Q$ ), the ultimate tensile strength ( $UTS$ ), and the yield strength ( $YS$ ).

The contour plots confirm that the best quality and the highest strength values for 354 alloys may be attained when minimizing the iron-levels and increasing the solutionizing temperature to within the specified limits at 525°C. The results presented using the contour plots shown in Figures 4.26(a) through (c) display the same behavior as that observed during the evaluation made by the quality charts shown in Figure 4.23 and Figure 4.24. This matching of behaviors supports using the quality charts in the interpretation and evaluation of the tensile properties of these castings.

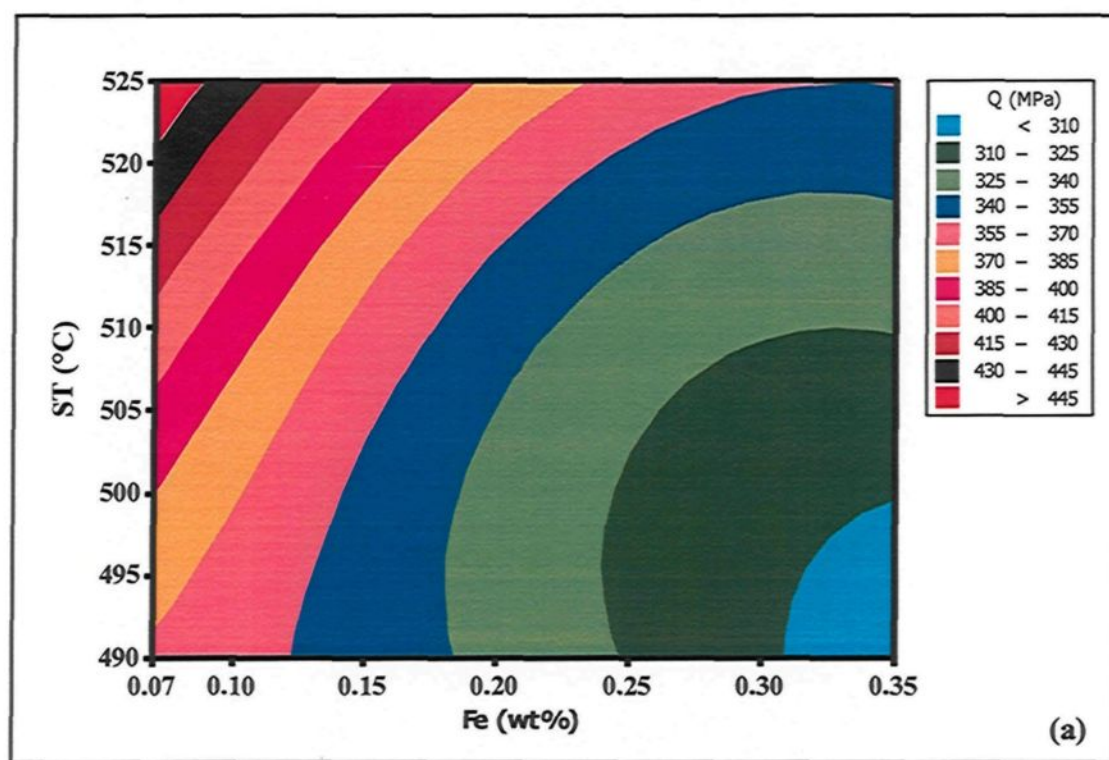
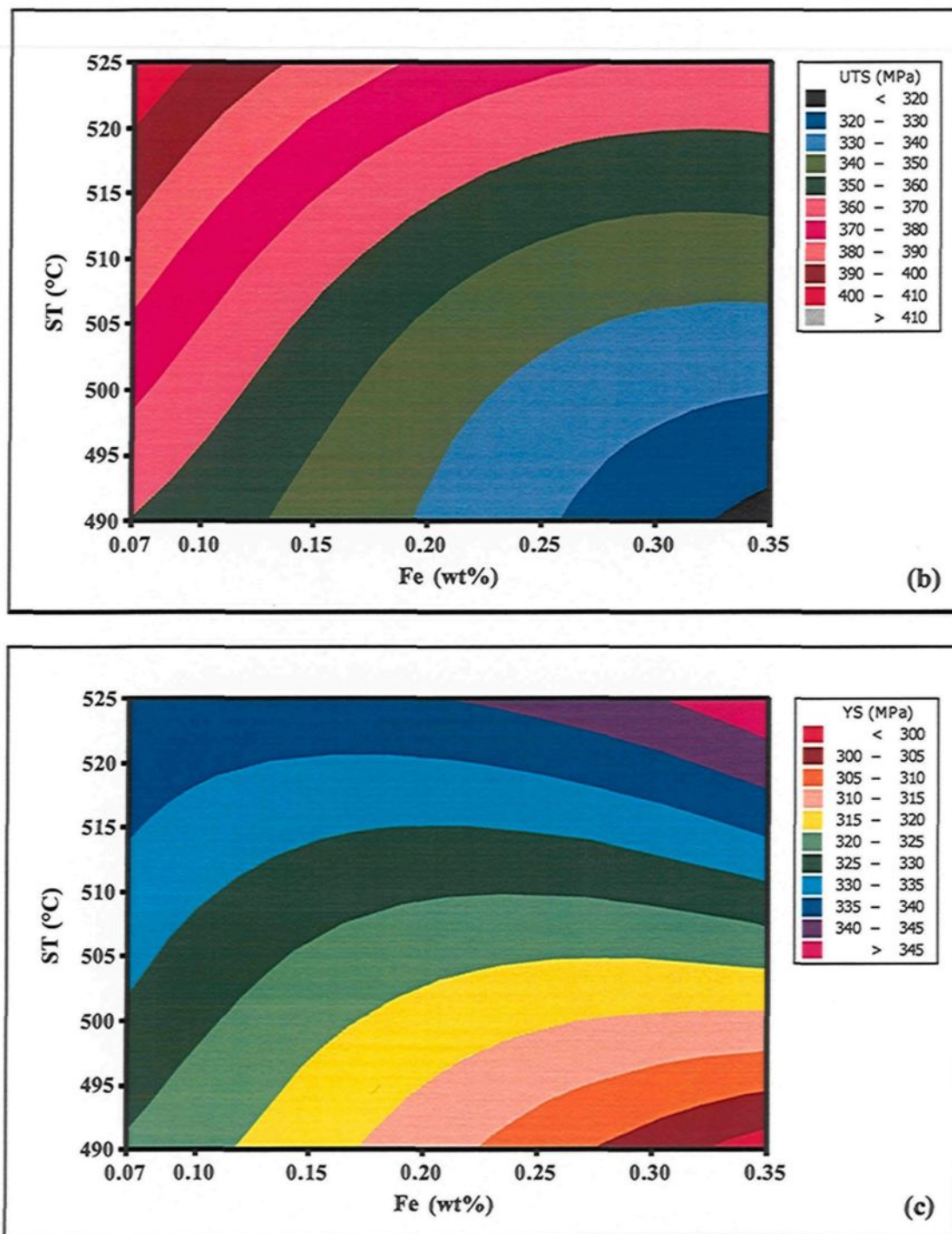


Figure 4.26



**Figure 4.26.** Contour plots correlating the dual effects of solutionizing temperature (ST) and Fe-levels in 354 castings: (a) with quality index values ( $Q$ ) calculated using Equation 1; (b) with ultimate tensile strength (UTS); and (c) with yield strength (YS).

The deleterious effects caused by the increase in the solutionizing temperature of 354 castings to 530°C and 537°C (as shown in Figure 4.23 and Figure 4.24) are directly related to partial or complete melting of the ternary eutectic structure  $\alpha$  (Al)-Si-Al<sub>2</sub>Cu, also known as incipient melting. This phenomenon occurs when the solutionizing temperature applied to the castings exceeds the melting temperature of the eutectic phases; in this case, the phases in question melt and form shrinkage porosity upon quenching.<sup>98, 101-103</sup>

Figures 4.27(a) through (c) show the cast structure of the 10S alloy upon solutionizing at 525°C, 530°C, and 537°C. The cast structure appears sound when solutionizing the samples at 525°C, as shown in Figure 4.27(a); however, increasing the solution heat treatment temperature to 530°C results in a partial melting of the ternary eutectic structure  $\alpha$  (Al)-Si-Al<sub>2</sub>Cu, as shown in Figure 4.27(b); a further increase in the solutionizing temperature to 537°C results in a complete melting of the eutectic phases, as may be seen in Figure 4.27(c). Therefore, a large amount of shrinkage porosity in the cast structure is observed to form upon solutionizing the 10S alloys at 530°C and 537°C, as may be seen in Figures 4.27(b) and (c), respectively.

The fracture surfaces of the 10S alloy samples solutionized at 525°C and 537°C are shown in Figures 4.28(a) and (b) from which it is clear that solutionizing at 525°C results in a normal fracture surface which consists mainly of dimples, as may be seen in Figure 4.28(a). On the other hand, Figure 4.28(b) shows the fracture surface of the same alloy solutionized at 537°C where it may be seen that a smooth fracture surface is obtained due, in this case, to the rapid fracture of the sample during tensile testing. The fracture surface of the samples solutionized at 537°C consists mainly of a massive aluminum area embedded

with polygonal silicon particles which grew in the liquid state as a result of the incipient melting. The formation of porosity and the transformation of the morphology of the Si-particles into polygonal shapes, having sharp edges and sharp corners, are the main factors responsible for the rapid fracture and the reduced properties of the 354 castings occurring as a result of raising the solutionizing temperature to 530°C and 537°C. An example of the polygonal silicon particles appearing on the fracture surface is shown in Figure 4.28(c).

Based on the foregoing results, it is clear that the suitable solutionizing temperature for 359 casting alloys is 537°C providing the best possible compromise between strength, ductility, and quality values, as shown in the quality charts presented in Figure 4.9 and Figure 4.10. The most efficacious and appropriate solution heat treatment temperature for the 354 casting alloys is 525°C at which temperature the best possible compromise between tensile properties and quality indices may be obtained, as shown in the quality charts provided in Figure 4.23 and Figure 4.24. To remain on the safe side, however, a solutionizing temperature of 520°C is recommended for solutionizing the 354 alloys so as to make sure that these castings are protected from any possibility of incipient melting.

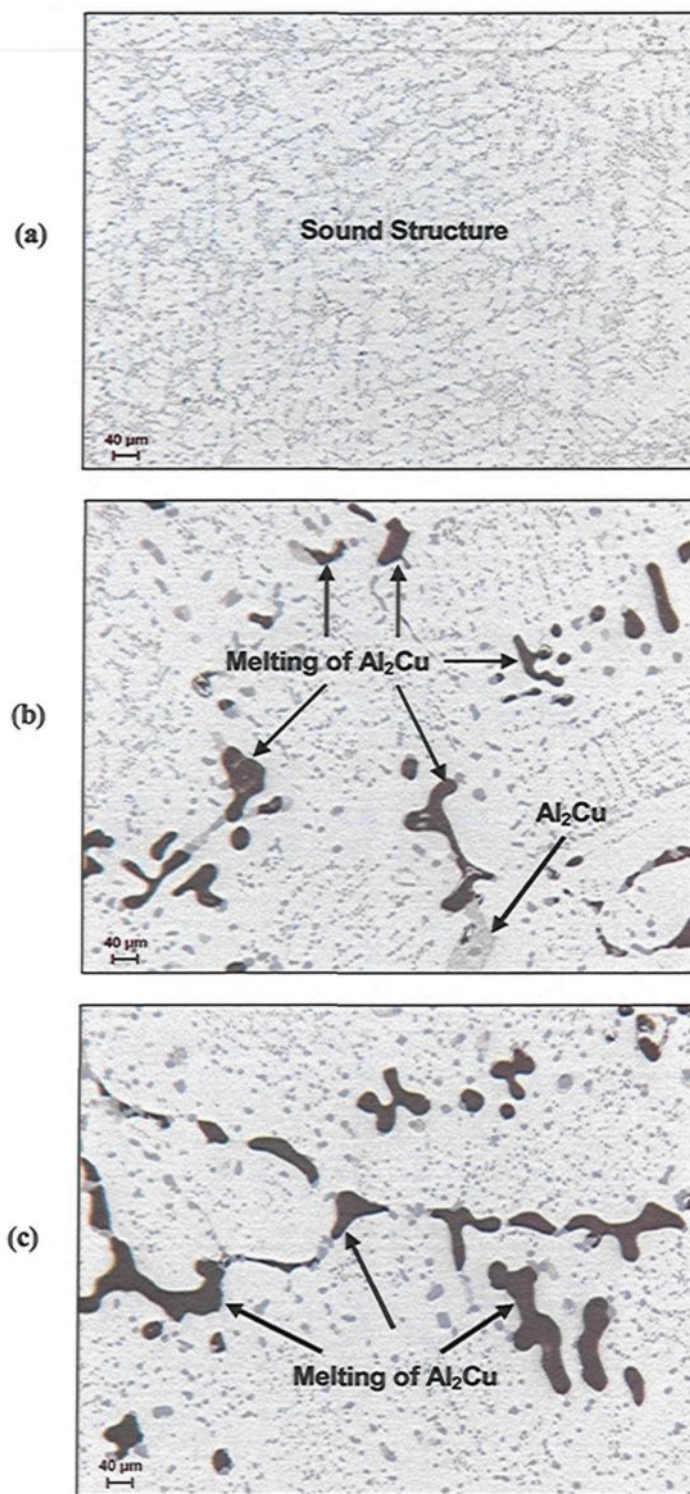


**Figure 4.27.** Microstructure of 354 castings subjected to solutionizing temperatures of (a) 525°C; (b) 530°C; and (c) 537°C for 12 h each (samples were obtained from the gauge length of B108 test bars).

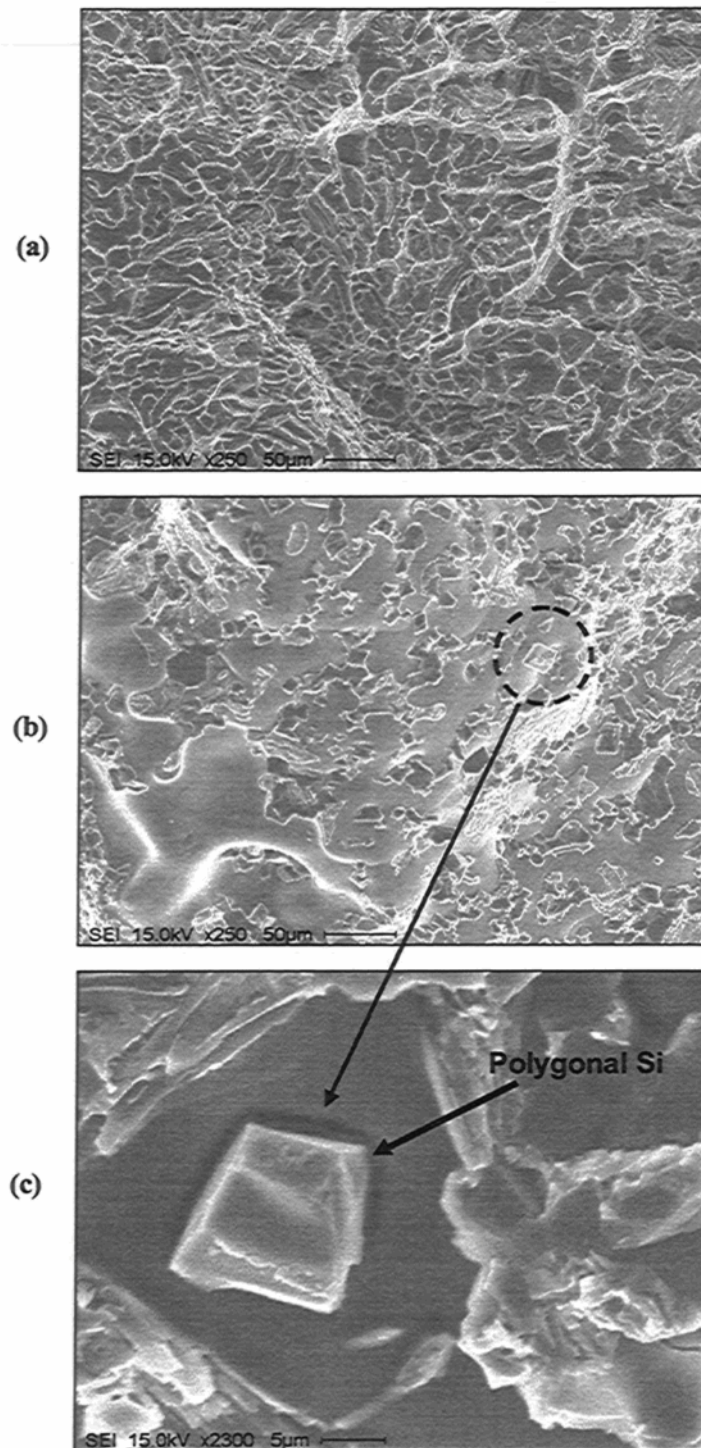


**Figure 4.28.** SEM images of the fracture surface of 354 alloy samples (a) solutionized at 525°C; (b) solutionized at 537°C; and (c) a high magnification image of the circled area in (b) showing enhanced detail of the polygonal Si particles (fractographs were obtained from the fracture surface of B108 test bars).

#### 4.3.5.2. Influence of Solution Heat Treatment Time

This subsection will discuss the influence of solution heat treatment time on the tensile properties and the quality index values of modified and non-modified 354 and 359 casting alloys. The alloys coded 10S and 10N are the modified and the non-modified 354 castings, respectively, while, alloys coded 1S and 1N are the modified and the non-modified 359 castings, respectively. The solution heat treatment procedures carried out on these alloys were for six time durations, namely, 1 h, 4 h, 8 h, 12 h, 16 h, and 24 h each at 520°C for 354 castings and at 537°C for 359 castings, all followed by quenching in warm water at 60°C after which the samples were forwarded for tensile testing. This stage was completed by applying a T4-temper to examine the effects of Sr-modification on the response of 354 and 359 castings to solution heat treatment.

The prolonged solution heat treatment time is observed to increase the strength and the quality index values of both modified and non-modified alloys significantly, either for 354 or for 359 casting alloys, as shown in Figure 4.29. The improvements occurring in the strength and quality of the modified and non-modified 354 and 359 casting alloys when increasing solutionizing times is related to the changes in the microstructural features, as explained earlier in the case of increasing the solutionizing temperature. These microstructural changes include the homogenization of the cast structure; the changes in the volume fraction percentage, size, and morphology of the intermetallic phases; and the changes in the size and morphology of eutectic Si particles. As outlined in section 4.2.2, increasing the duration of solutionizing time up to 24 h was seen to produce advantageous changes in the size and morphology of the eutectic Si particles for both modified and non-

modified 359 castings; this will be clear from the optical micrographs shown in Figures 4.4(a) through (d) as well as in Figures 4.5(a) through (d) for the 354 alloys. The size of the Si particles increases whereas their aspect ratio decreases upon increasing the solution heat treatment time for both modified and non-modified 354 and 359 alloys, as may be observed in the qualitative analysis presented in Figure 4.7.

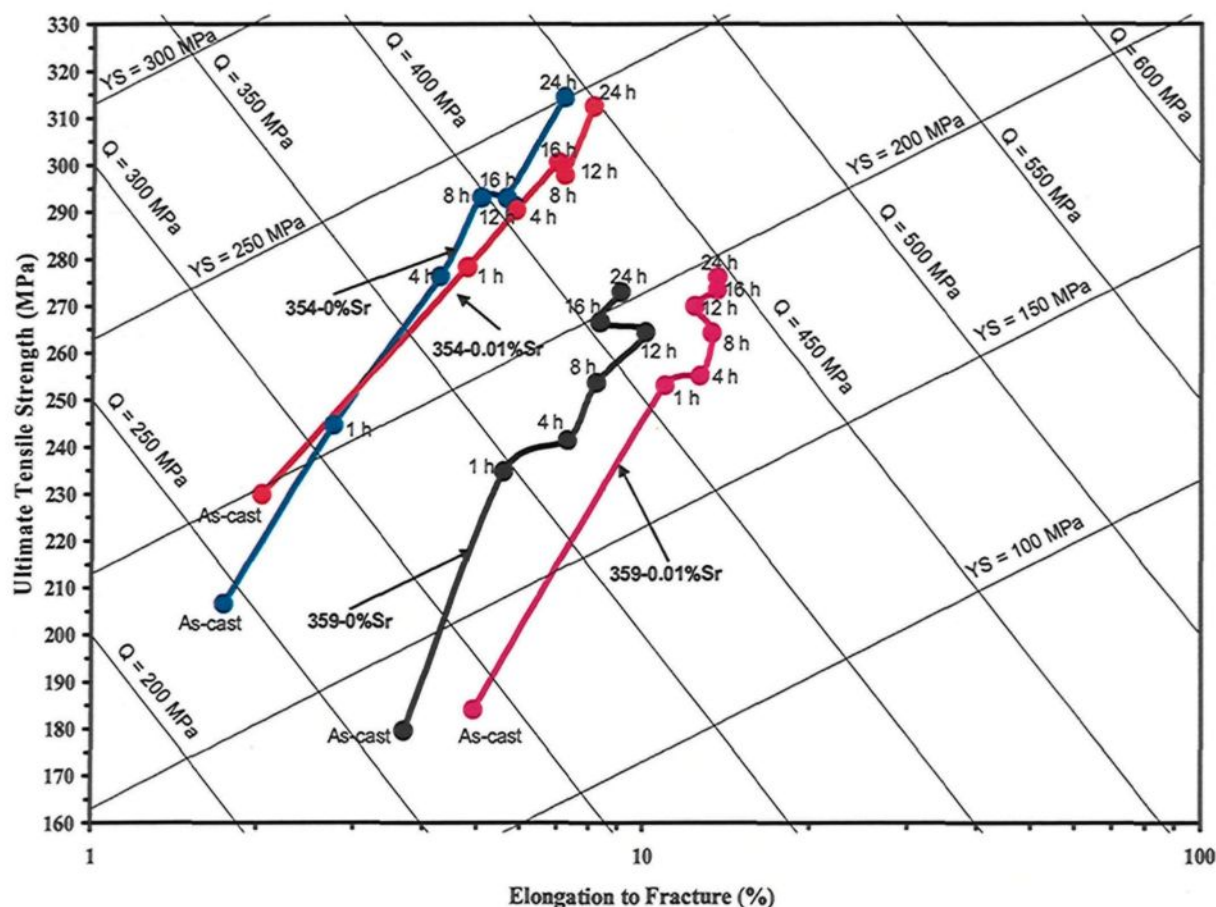


**Figure 4.29.** Quality chart generated using Equations 1 and 2 illustrating the influence of solution heat treatment times and Sr-modification on the tensile properties and quality index of 354- and 359-type B108 test bars castings. The 354 samples were solutionized at 520°C for the specified time durations, while the 359 samples were solutionized at 537°C for the same time periods.

The results concerning the effects of solution time on the properties of the 1N and 10N castings were re-plotted in a different format using the matrix plots shown in Figure 4.30 and Figure 4.31 for the 1N-359 and 10N-354 alloys, respectively. These matrix plots correlate the solutionizing time with the quality index value ( $Q$ ) and the tensile properties of these castings. The relevant properties provided in these figures are the ultimate tensile strength ( $UTS$ ), the yield strength ( $YS$ ), and the elongation to fracture ( $E_f$ ). Figure 4.30 and Figure 4.31 show that prolonged solution heat treatment time results in an increase in the values of all the tensile properties and the quality indices of the 354 and 359 alloys, thereby confirming the evaluation made using the quality chart shown in Figure 4.29.

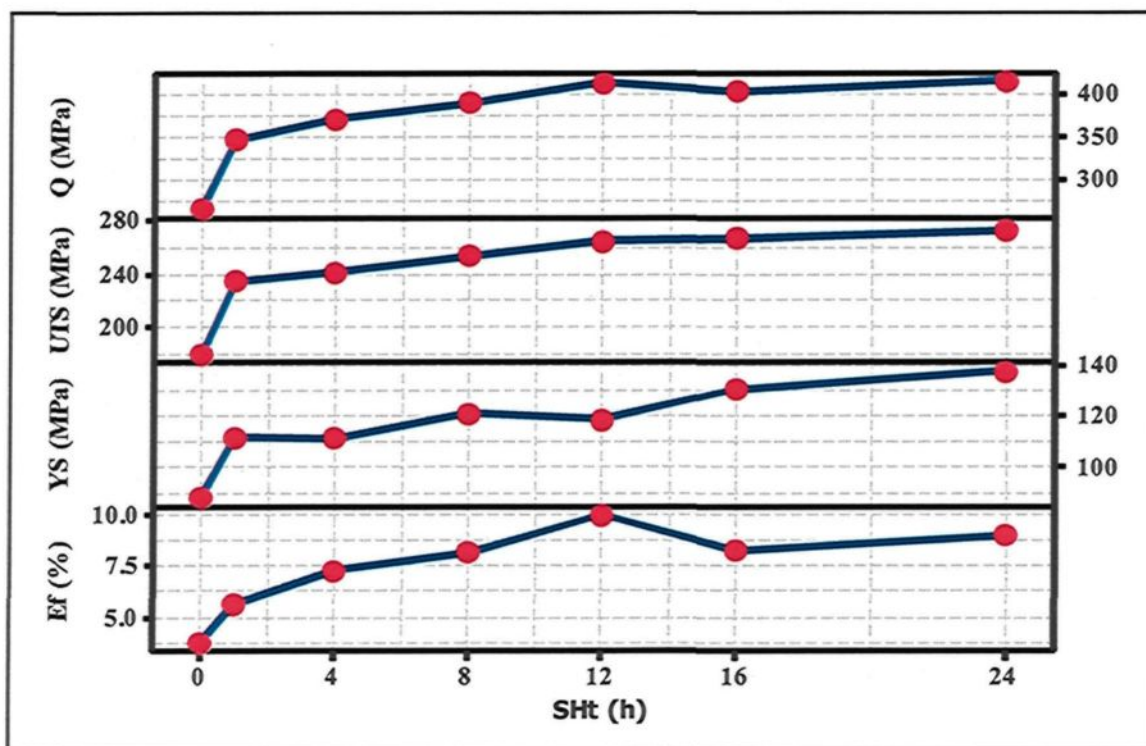


**Figure 4.30.** Tensile properties (ultimate tensile strength,  $UTS$ ; yield strength,  $YS$ ; and elongation to fracture,  $E_f$ ) and quality index ( $Q$ ) correlated to the solution heat treatment times (Sht) of the 1N-359 alloys.

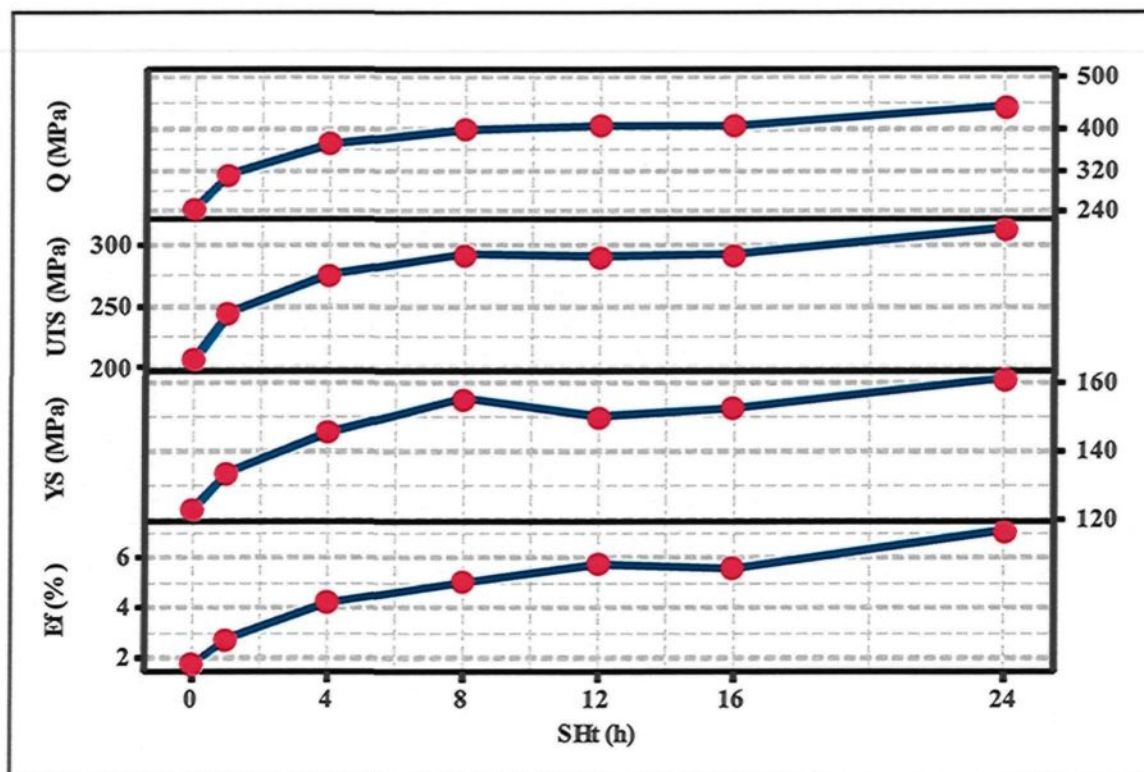


**Figure 4.31.** Tensile properties (ultimate tensile strength, *UTS*; yield strength, *YS*; and elongation to fracture, *E<sub>f</sub>*) and quality index (*Q*) correlated to the solution heat treatment times (SHt) of the 10N-354 alloys.

The addition of strontium to 354 and 359 castings, *i.e.* the 10S and 1S alloys, respectively, has been observed to affect the response of these castings to solution heat treatment. The principal action of strontium in this particular case is revealed in its effect on the length of time required to attain certain mechanical properties and quality index values in the alloys under study since most of the solutionizing time is spent in modifying eutectic silicon particles.<sup>8, 87</sup> For instance, the tensile properties and quality index values of the unmodified 354 and 359 alloys which have been solutionized for 8 hours may be obtained after solutionizing for only 4 hours in the case of modification through Sr addition, as will be seen in Figure 4.29.

According to the results obtained and shown in Figure 4.29, it will be seen that approximately the same level of tensile properties and quality index values in 354 and 359 castings may be obtained with or without Sr-modification; in the case of unmodified samples, however, the solutionizing time required will be longer in order to obtain the same level of tensile properties and quality index values than for the modified samples. The effects of Sr-modification in the current case are technologically significant from the economic point of view because of the need to reduce the required time for solutionizing treatments. The influence of Sr-modification on reducing solution heat treatment times was also remarked upon in number of studies.<sup>87, 88, 140, 182</sup>

The effects of Sr-modification on the response of the castings to solution heat treatment tend to decrease when the solutionizing time increases, as will be clear from Figure 4.32. This figure illustrates that increasing the solutionizing time results in a continuous narrowing of the gap between the quality index values of the modified and unmodified 354 castings; it should be noted that the 359 castings are expected to display similar behavior to that of the 354 alloys. Figure 4.29 and Figure 4.32 illustrate the fact that both the modified and unmodified 354 alloys produce approximately the same quality index values and the same tensile property values after undergoing solution treatment for 24 h. Strontium modification is more effective for shorter time durations although this advantage diminishes with increasing solutionizing times where, beyond 24 h of solutionizing treatment, the Sr-modification no longer has any effect. The reduced efficacy of Sr with prolonged solutionizing time is related to the fact that the eutectic Si particles

have already been modified thermally by the solutionizing treatment, as may be seen in the optical micrographs shown in Figures 4.5(a) and (b).

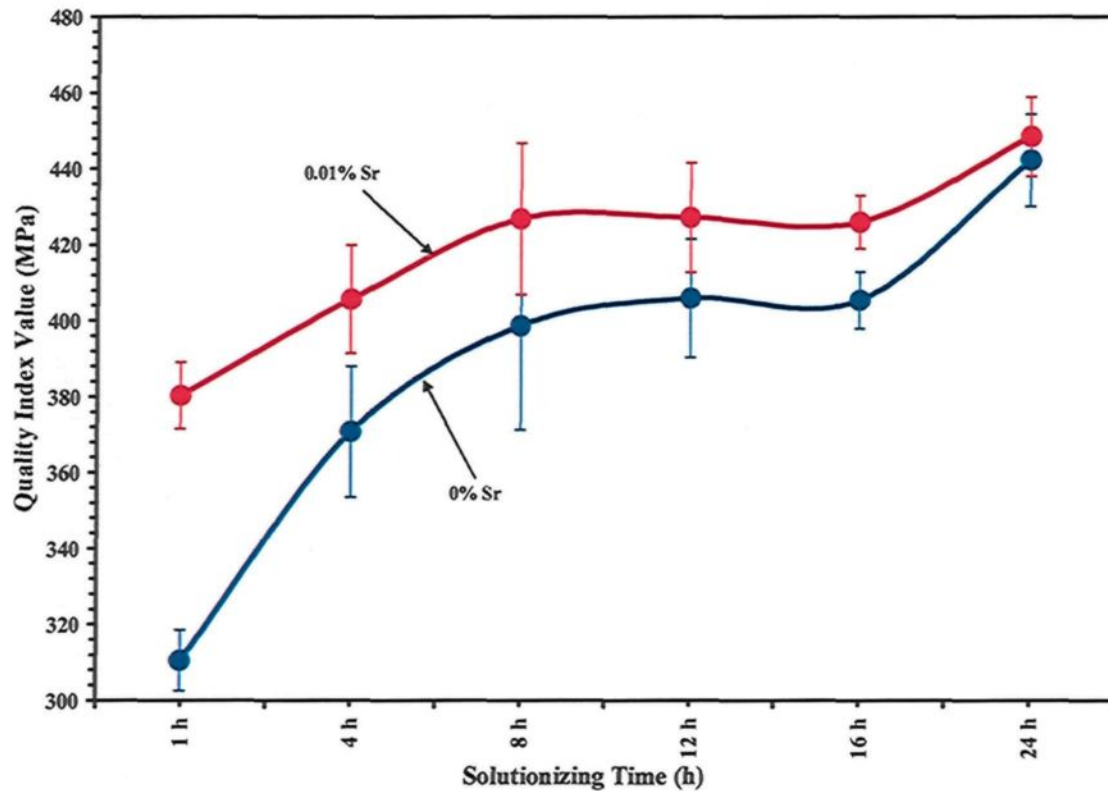


**Figure 4.32.** Quality index values shown as a function of solutionizing time and Sr-modification of the 354 alloys.

From the results obtained in the previous sections for the solutionizing time of 354 and 359 castings, a time duration of 24 h provides the best possible compromise between the tensile properties and quality index values of these castings, as will be observed in Figure 4.29 through Figure 4.31, although a 12 h period should be recommended so as to improve the economic relevance of solutionizing treatments. Based on the results obtained in the current study, solution heat treatment for 12 h causes no observably significant

change in either the tensile properties or in the quality index values of modified and unmodified samples, as seen in Figure 4.29.

It should be noted that the above results were presented using the quality chart generated using Equations 1 and 2 shown in Figure 4.29. It will have been noted from the earlier sections that this quality chart and the one generated using Equations 8 and 9 describe similar behavior as to the effects of various metallurgical conditions on the properties of the 354 and 359 castings. Therefore, there is complete agreement between the evaluations made using any one of these two charts so that the results may be presented using only the quality chart based on Equations 1 and 2.

Applying the quality chart which is generated using Equations 8 and 9 is a time-consuming process since several procedures must be carried out in order to generate this particular type of plot. Such procedures include the following: (i) changing the engineering stress and engineering strain obtained from the tensile testing machine into true stress and true strain for all the samples tested; (ii) calculating the  $n$  and  $K$  values for the samples; and (iii) calculating the plastic elongation to fracture for each sample tested; where Equations 8 and 9 were derived from Equation 4, the latter equation applies only to the plastic strain.

One other problem associated with the quality charts generated using Equations 8 and 9 is the  $K$ -value. Each chart is generated using a single  $K$ -value which is the average of the  $K$ -values for all the points representing the conditions under investigation and presented in the same chart. This means that if the number of points in the same chart change, the  $K$ -value would also change and consequently the *iso-flow* lines and the *iso-q* lines would shift, either positively or negatively, according to the new average  $K$ -value; in addition to this,

the calculated  $n$ - and  $YS$ -values labeled on the *iso-flow* lines and the calculated  $q$ - and  $Q$ -values labeled on the *iso-q* lines would also be altered for the same points mentioned according to the new average  $K$ -value.

The quality chart based on Equations 1 and 2, on the other hand, is generated simply without any further requirement. According to this preceding discussion, using the simple quality chart based on Equations 1 and 2 is to be recommended. In the next chapter, the results will be presented using only the quality chart generated by Equations 1 and 2.

**CHAPTER 5**  
**INFLUENCE OF AGING PARAMETERS**

## CHAPTER 5

### 5. INFLUENCE OF AGING PARAMETERS

#### 5.1. INTRODUCTION

Aging treatment follows upon the solution treatment and quenching processes where the castings are subjected to a specified temperature for a certain length of time. The excess solute atoms in the supersaturated solid solution of  $\alpha$ -Al ultimately precipitate after a certain time duration depending on the temperature applied to the castings during this treatment. Solute atoms diffuse from the supersaturated structure towards such high energy sites as the grain and the phase boundaries.<sup>40</sup> The vacant sites in the lattice structure, produced from solutionizing and quenching treatments, are a significant condition for the diffusion of the excess solute atoms through the metal matrix. Accordingly, these vacancies have a strong influence on the kinetics of the precipitation of the second phase particles.<sup>183</sup>

The redistribution of the solute atoms in the early stages of aging treatment results in the formation of coherent Guinier-Preston (GP) zones accompanied by an improvement in the strength of the alloy. A further increase in the time duration of the aging treatment results in forming coherent and semi-coherent transition phases at the GP zone sites, by means of which a further increase in the strength of the casting may be attained up to a maximum level at peak-aging. Any further aging beyond the peak-strength results in over-

aging in which equilibrium and coarser phases form and lead to a reduction in the strength of the casting.

The present chapter discusses the influence of the age-hardening parameters, namely temperature and time, on the tensile properties and the quality index values of 354 and 359 casting alloys. The alloys selected for this purpose are the 354 and 359 base alloys, or 10N and 1N alloys, respectively. Five aging temperatures were applied to each alloy for a wide range of aging times, as listed in Table 3.2. These aging temperatures are 155°C, 170°C, 195°C, 220°C, and 245°C. The time duration applied for the two lower temperatures, 155°C and 170°C, ranged between 1 hour and 72 hours, while for the remaining three higher temperatures, the time duration ranged between 5 minutes (0.083 h) and 72 hours. In the latter case, it is expected that the peak-strength will be reached rapidly upon aging at high temperatures so that the time durations applied in this case start from 5 minutes, as listed in Table 3.2. The 354 alloy was solution heat-treated at 520°C for 12 hours for all the subsequent aging conditions studied, whereas the 359 alloy was solution heat-treated at 537°C for 12 hours for all the relevant aging conditions. The aging behavior of the 354 alloy will be introduced and discussed in the next subsection.

## **5.2. AGING BEHAVIOR OF 354 CASTING ALLOYS**

The present subsection will discuss the influence of aging temperatures and times on the tensile properties and quality index values of the 354-base alloy, or 10N alloy; the aging parameters applied to the 354 castings are shown in Table 3.2. The chemical composition of 354 casting alloys contains three hardening elements, namely, copper, magnesium, and silicon. The application of an aging treatment to these alloys causes an

entire range of precipitates to form according to the temperature and time applied. The precipitation hardening of this particular alloy system is a complicated process because of the variety of phases which are expected to precipitate during the aging cycle. These precipitates may include Mg-Si, Al-Cu, Al-Cu-Mg, and the Al-Cu-Mg-Si-containing phases.

Age-hardening treatment of Al-Si-Cu-Mg alloys, *i.e.* 354 alloys, results in the precipitation of the quaternary  $Q$ -phase and its precursors, which play an essential role in the strengthening of this specific alloy system.<sup>184, 185, 186, 187</sup> The  $Q$ -phase has been identified previously in several studies; the exact composition of this particular phase, however, is not always the same. Several formulas were suggested for the  $Q$ -phase including  $\text{Al}_5\text{Cu}_2\text{Mg}_8\text{Si}_6$ ,  $\text{Al}_4\text{CuMg}_5\text{Si}_4$ ,  $\text{Al}_4\text{Cu}_2\text{Mg}_8\text{Si}_7$  and  $\text{Al}_3\text{Cu}_2\text{Mg}_9\text{Si}_7$ .<sup>126, 128</sup>

The  $Q$ -phase is the stable form resulting from the phase transformation of two different meta-stable precursors, namely  $QP$  and  $QC$ .<sup>127, 129</sup> A further transition phase was reported to precipitate during the aging treatment of Al-Si-Cu-Mg alloys. This metastable phase was designated as  $Q'$  and it has a lathlike morphology and the same hexagonal structure as the stable  $Q$ -phase.<sup>126, 127, 129</sup> The precipitation sequence of the  $Q$ -phase during aging treatment starts by forming the  $QP$ ;  $QC$ ;  $Q'$  phases; and, lastly, the stable  $Q$  ( $\text{Al}_5\text{Cu}_2\text{Mg}_8\text{Si}_6$ ) phase.<sup>126, 127, 129</sup> In addition to the precipitation of the  $Q$ -phases, several others, such as  $\theta$ - $\text{Al}_2\text{Cu}$ ,  $\beta$ - $\text{Mg}_2\text{Si}$ ,  $S$ - $\text{Al}_2\text{CuMg}$ ,  $\sigma$ - $\text{Al}_5\text{Cu}_6\text{Mg}_2$  and their precursors, are also expected to precipitate during age-hardening treatment of 354-Al-Si-Cu-Mg alloys.<sup>104, 127,</sup>

Figure 5.1 shows the effects of aging temperature and time on the tensile properties of 354-type castings, namely, ultimate tensile strength (*UTS*), yield strength (*YS*), and percentage elongation to fracture (*E<sub>f</sub>*). This diagram shows that aging at 155°C results in a continuous increase in strength with an increase in the aging time of up to 72 hours at which point the maximum strength is obtained; the peak-aging, however, is expected to be attained upon extending the aging time beyond 72 hours. There is a possibility that this peak-strength may be reached after a shorter aging time with increasing aging temperatures; this is clear from Figure 5.1 in which the aging times required to reach the peak-strength are 40 hours, 8 hours, 1 hour, and 15 minutes, when applying aging temperatures of 170°C, 195°C, 220°C, and 245°C, respectively. It should be noted that the yield strength curves shown in Figure 5.1 are used to determine the peak-aging time for each temperature. Aging treatment under the abovementioned four temperatures results in a continuous increase in the strength of the casting accompanied by a reduction in ductility up to peak-aging. Any further increase in aging time after reaching the peak-strength for each temperature leads to over-aging conditions where the strength of the castings starts to diminish and the ductility to increase, as will be seen in Figure 5.1.

The results shown in Figure 5.1 were re-plotted using quality charts, as shown in Figures 5.2(a) and (b). Figure 5.2(a) shows the aging curves obtained from applying all aging temperatures and times to the 354 alloy. Figure 5.2(b) illustrates the aging curves for three temperatures only, 155°C, 170°C, and 245°C to show a simplified version of the same quality chart presented in Figure 5.2(a).

Aging behavior at 155°C for up to 72 h is quasi-parallel to the *iso-Q* lines, as will be observed in the quality chart shown in Figures 5.2(a) and (b). This behavior illustrates that aging time up to peak-strength does not affect the quality index values of the 354 castings. Such an observation is related to the fact that increasing the aging time up to 72 h results in a continuous increase in the strength of the casting at the expense of its ductility, although the increase compensates for the reduction in ductility in accordance with Equation 1. Thus, the net effect of this aging treatment ultimately leads to non-significant changes in the quality index values.

The aging behavior observed when applying aging temperature at 155°C is related to the precipitation of the Cu- and Mg-containing phases in the metal matrix. The features of these precipitates vary according to the aging time applied to the castings. The increased strength observed in the early stages of aging is related to the redistribution of the excess solute atoms which thus form clusters of the coherent metastable rod-shaped *QP* phase.<sup>126, 127, 129</sup> As mentioned earlier, in the Al-Si-Cu-Mg quaternary system, such precipitates as the Guinier-Preston (GP) zones are expected to form in the early stages of this aging treatment, they are precursors of the equilibrium  $\theta$ -Al<sub>2</sub>Cu and  $\beta$ -Mg<sub>2</sub>Si precipitates. In addition, other Cu- and Mg-containing precipitates such as the coherent rodlike Guinier-Preston-Bagaryatsky (GPB) zones may also form as precursors of the stable *S*-Al<sub>2</sub>CuMg phase.

A further increase in the aging time at 155°C results in the dissolution of the zones mentioned and the formation of coherent transition phases at the same sites. The *Q'*-phase is coherent with the matrix and it contributes to increasing the hardening level of these alloys.<sup>126, 186, 188</sup> In addition to the lathlike *Q'* phase, the other coherent phases which are

expected to form at this stage are the needlelike  $\beta''$ ,<sup>116, 117, 118, 119</sup> the platelike  $\theta''$ <sup>113, 115, 120</sup> and the lathlike  $S''$ <sup>113, 120</sup> phases. The formation of these coherent precipitates is the main source of strengthening in the 354 casting alloys and leads to an increase in strength to a maximum level at 72 h which, in this case, is considered to be the peak-aging time. The over-aging conditions were not reached when applying aging treatment at 155°C for up to 72 h upon which the maximum strength level was observed and was attributed to the formation of the coherent  $Q'$ ,  $\beta''$ ,  $\theta''$  and  $S''$  phases. It should be noted that peak-strength may also be attained in the presence of both coherent and semi-coherent precipitates. The semi-coherent precipitates which may be present in the peak-aging conditions are the needlelike  $\beta'$ , the plate-shaped  $\theta'$ , and the lathlike  $S'$  phases.

With regard to the aging behavior of the 354 alloy at 170°C, Figures 5.2(a) and (b) show that increasing the aging time up to 40 h results in an increase in the alloy strength with a decrease in its ductility. The aging behavior displays a quasi-linear relationship with a negative slope between the elongation to fracture and the strength of the alloy up to peak-aging which occurs at 40 h. The aging curve when applying 170°C for up to 40 h is virtually parallel to the *iso-Q* lines; this trend implies that applying such a specific aging temperature for up to 40 h does not affect the quality index values of the casting. A further increase in the aging time at 170°C results in a decrease in the alloy strength and its quality as a result of the over-aging conditions.

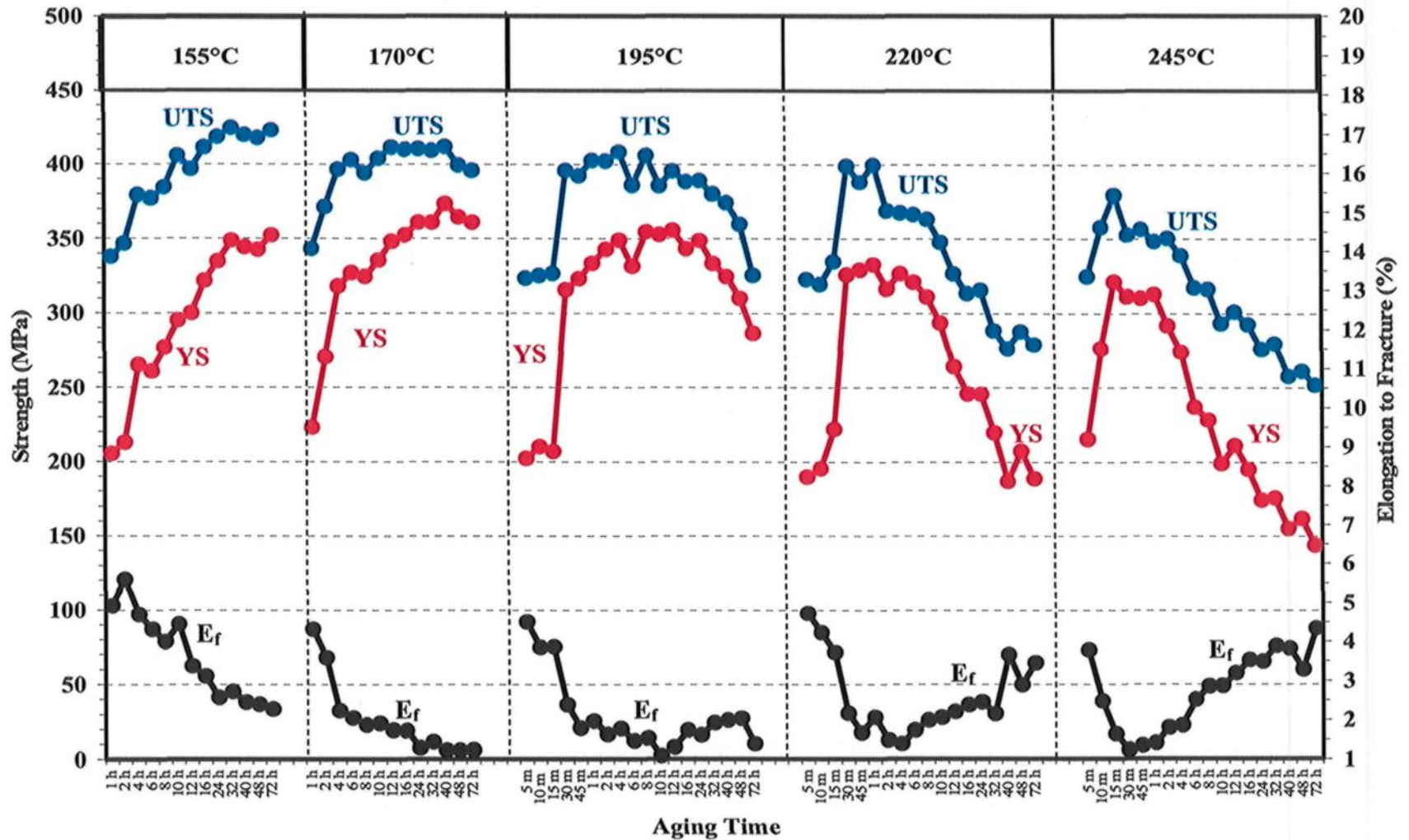
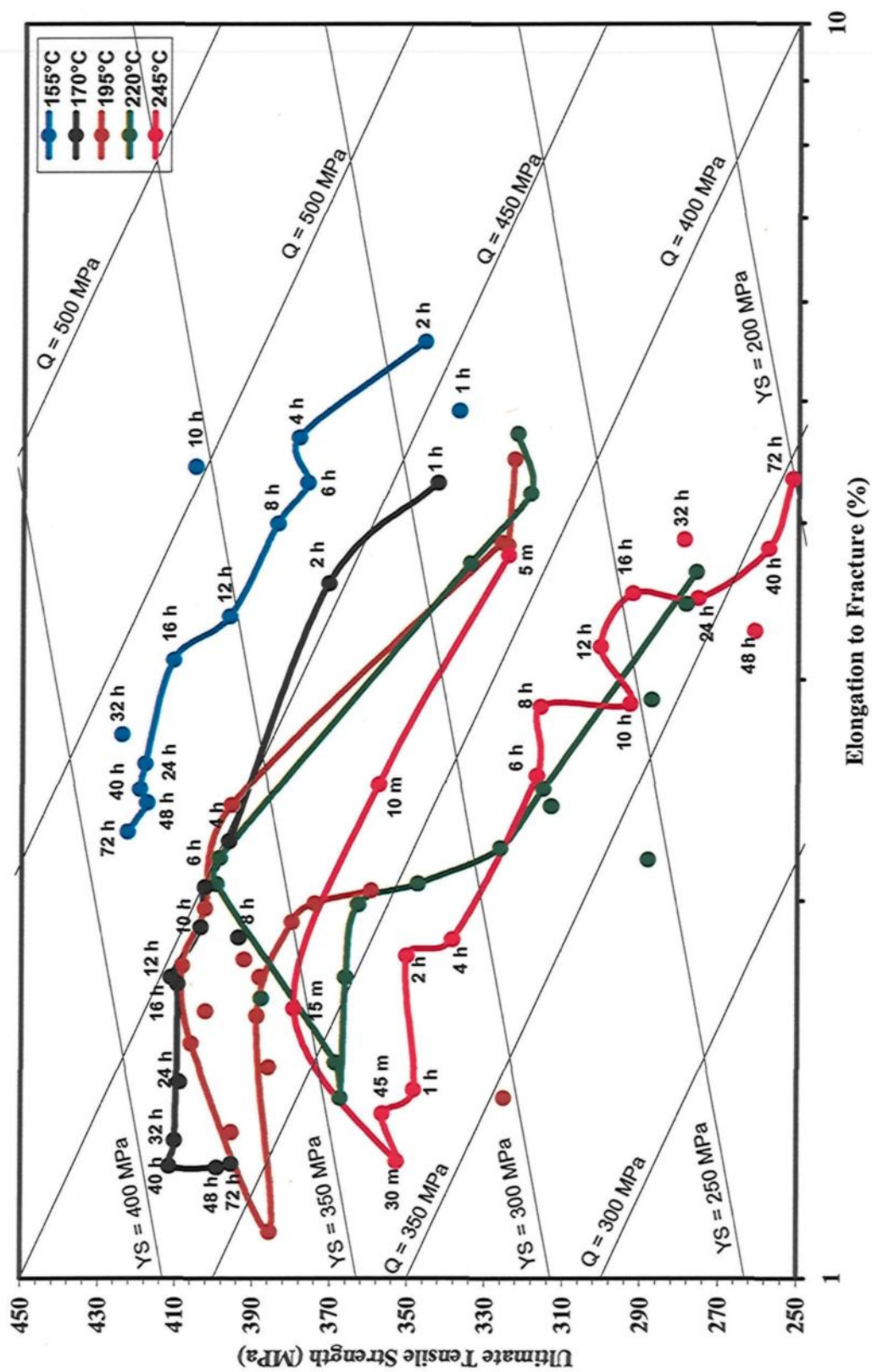
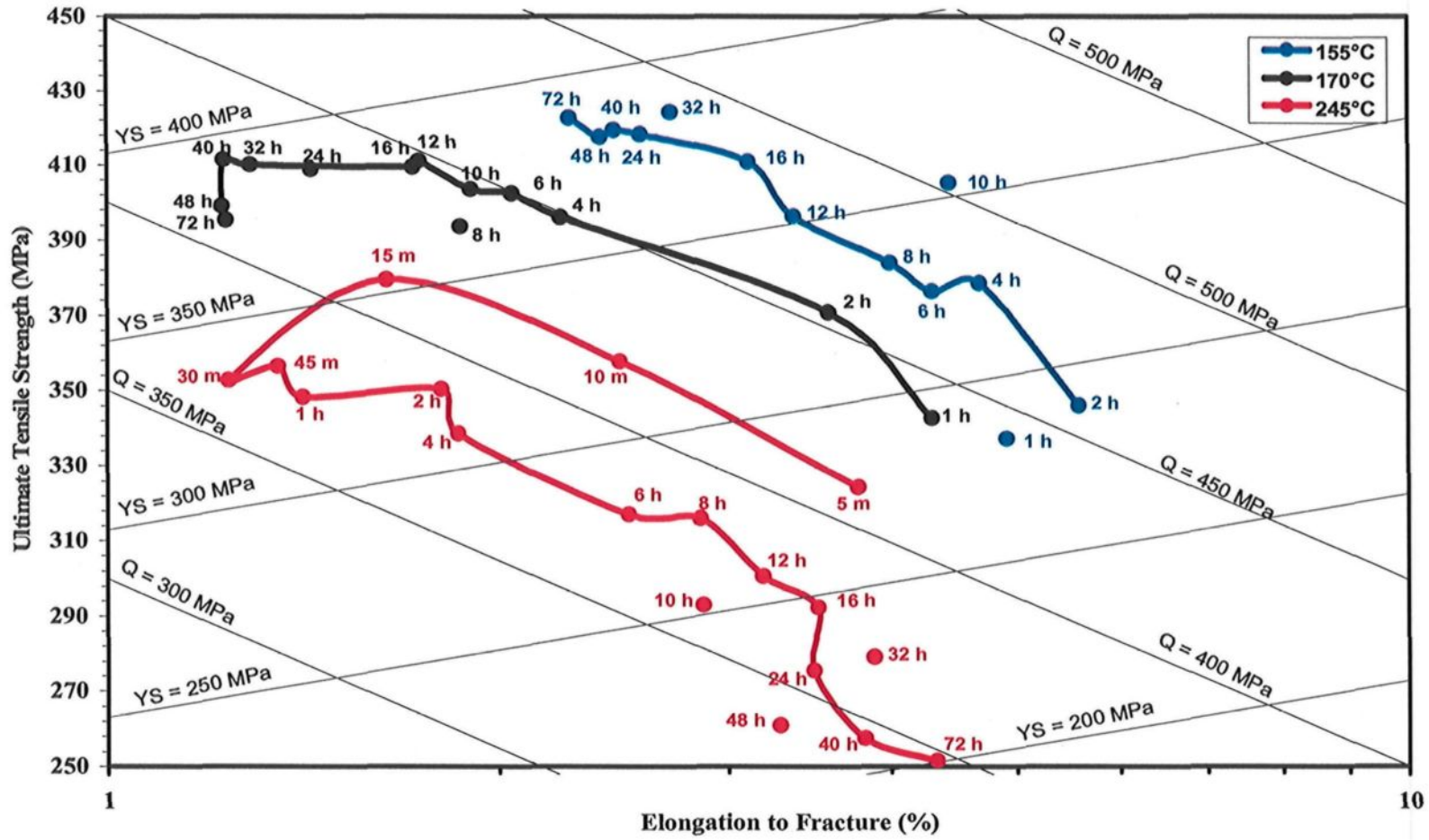


Figure 5.1. The tensile properties of the 354 alloy (10N) under various aging temperatures and aging times. (Note: "m" and "h" on the X-axis indicate minutes and hours, respectively.)



(a)  
Figure 5.2



(b)

Figure 5.2. Quality chart generated using Equations 1 and 2 illustrating (a) the strength and quality of the 354 alloy under all aging temperatures and times applied; and (b) a simplified chart of (a) showing the strength and quality of the 354 alloy under the three specified aging temperatures.

The increased strength when applying aging treatment at 170°C for up to 40 h, as was described earlier in the case of applying aging treatment at 155°C, is related to the precipitation of the GP and GPB zones followed by the formation of coherent and semi-coherent precipitates. These precipitation sequences result in an increase in the strength of the castings up to the point of attaining the maximum level of strength at peak-aging, which occurs at 40 h. At 170°C, aging time beyond 40 h, a decrease in the strength and quality index values of the 354 castings is observed, as may be seen in Figure 5.2(b), attributed to the loss of coherency strain surrounding the precipitates. The disappearance of the coherency strain accompanies the formation of the incoherent equilibrium precipitates such as the plate-shaped  $\beta$ , the platelike  $\theta$ , the rodlike  $S$ , and the rod-shaped  $Q$  phases. The formation of these equilibrium phases results in a reduction in the strength and quality index values of the alloys, as may be seen in Figure 5.2.

Increasing the aging temperature to 195°C, 220°C, and 245°C results in reducing the required time to reach peak-aging which was observed at 8 hours, 1 hour, and 15 minutes, respectively, as shown in Figure 5.1 and Figure 5.2(a). The aging curves in the case of aging at these high temperatures display curvilinear forms, as shown in Figure 5.2(a). This specific form of the aging curves is a result of the over-aging conditions which occur upon increasing the aging time for durations longer than the specified peak-aging times with respect to each temperature. Only one example for the aging behavior at high temperatures will be discussed here since the aging behavior at these three high temperatures is approximately similar and follows the same concepts. The example to be

discussed is the aging behavior of the 354 alloy subjected to the aging temperature of 245°C for time durations in the range of 5 minutes to 72 hours.

Applying an aging temperature of 245°C results in a rapid increase in alloy strength where the aging time required to reach peak strength is only 15 minutes. This rapid aging treatment is related to the high rate of atomic diffusion accompanying high aging temperatures and the direct precipitation of the coherent and semi-coherent phases which are the main causative source of peak-strength. This aging temperature of 245°C is expected to be higher than the solvus temperatures for the precipitates and zones which usually form during the early stages of aging; consequently, the time spent in the precipitation and dissolution of these precipitates at lower aging temperatures will be saved when increasing the aging temperature to 245°C. The peak-strength observed at 15 minutes is related to the formation of the same coherent and semi-coherent precipitates as described in the case of applying aging treatment to 354 alloys at 155°C and 170°C.

Increasing the aging time from 5 minutes to 15 minutes at 245°C leads to a linear relationship between the strength of the 354 alloy and the elongation to fracture, as shown in Figure 5.2(b). The portion of the aging curve up to peak-aging is parallel to the *iso-Q* lines; as indicated earlier, this implies that in this range of aging time the quality index values of the alloy do not display any significant changes. A further increase in the aging time to 30 minutes results in a decrease in the alloy strength and quality, as shown in Figure 5.2(b). Any further increase in the aging time results in a further decrease in the alloy strength, an increase in the ductility, and a non-significant change in the quality, as seen in Figure 5.2(b); the increased ductility has compensated for the decreased strength in

Equation 1, thus, the overall quality does not display any significant change within this range of time. Such a decrease in strength and increase in the ductility of the alloy is related to the softening which occurs as a result of the over-aging conditions at which the equilibrium precipitates form, leading to the loss of the coherency strain between the precipitates and the matrix. In addition, the over-aging conditions result in the continuous growth of the large precipitates at the expense of the smaller ones, ultimately leading to coarser precipitates with less density in the metal matrix having large inter-particle spacing. All the changes mentioned which accompany the over-aging condition contribute to a decrease in the strength of the castings, as will be discussed in subsequent paragraphs.

For the castings under study, Figure 5.2 shows that aging behavior at 245°C produces lower levels of strength and quality index values than do the same properties when obtained at lower aging temperatures. Regarding the strength and quality of the castings at the peak-aging conditions of 155°C and 245°C for 72 hours and 15 minutes, respectively, it will be observed that the tensile strength, yield strength, and quality index values are reduced by 10%, 9%, and 13%, respectively, when applying a high aging temperature of 245°C. The peak-aging time, however, is reduced by 99.9% taking into account the fact that 72 h is considered to be the peak aging time at 155°C. Aging at higher temperatures, however, introduces a technologically useful strategy in that by applying a rapid aging treatment to this particular alloy system, it becomes possible to contribute a significant economical factor in the form of a noticeable reduction in the aging time required to reach peak-strength. This time reduction in relation to industrial applications has several benefits including lower energy consumption, longer lifetime for the heating

furnaces, greater productivity, lower labour costs, and a number of other analogous advantages.

The results concerning the aging treatment of the 354 alloys at 155°C and 245°C for the specified aging times were re-plotted in the form of matrix plots, as shown in Figure 5.3. These plots illustrate the effects of the two aging temperatures 155°C and 245°C on the strength and quality index values of the 354 castings. As may be seen, increasing the aging temperature results in a decrease in the quality index values ( $Q$ ); a lowering of the ultimate tensile strength ( $UTS$ ); and a reduction in the yield strength ( $YS$ ). The negative slopes in Figure 5.3 indicate that increasing the aging temperature has a negative influence on the overall strength and quality levels of the castings. These observations are in keeping with the evaluation made using the quality charts shown in Figure 5.2.

The size and density of the precipitates formed at specific aging temperatures are shown in Figures 5.4(b) through (e). Figure 5.4(a) is an optical micrograph illustrating the dendrite region from which the SEM images shown in Figures 5.4(b) through (e) were taken; Figure 5.4(b) is an SEM image of the dendrite region of the 354 alloy in the as-cast condition, where no precipitates were formed before applying any heat treatment; Figure 5.4(c) is an SEM image showing the size and density of the hardening precipitates which were formed after aging at 155°C for 72 hours; Figure 5.4(d) is an SEM image illustrating the characteristics of the hardening precipitates which were formed after aging at 195°C for 72 hours; Figure 5.4(e) is an SEM image showing the size and density of the hardening precipitates which were formed after aging at 245°C for 72 hours; and Figure 5.4(f) shows an EDX spectrum corresponding to the phases observed.

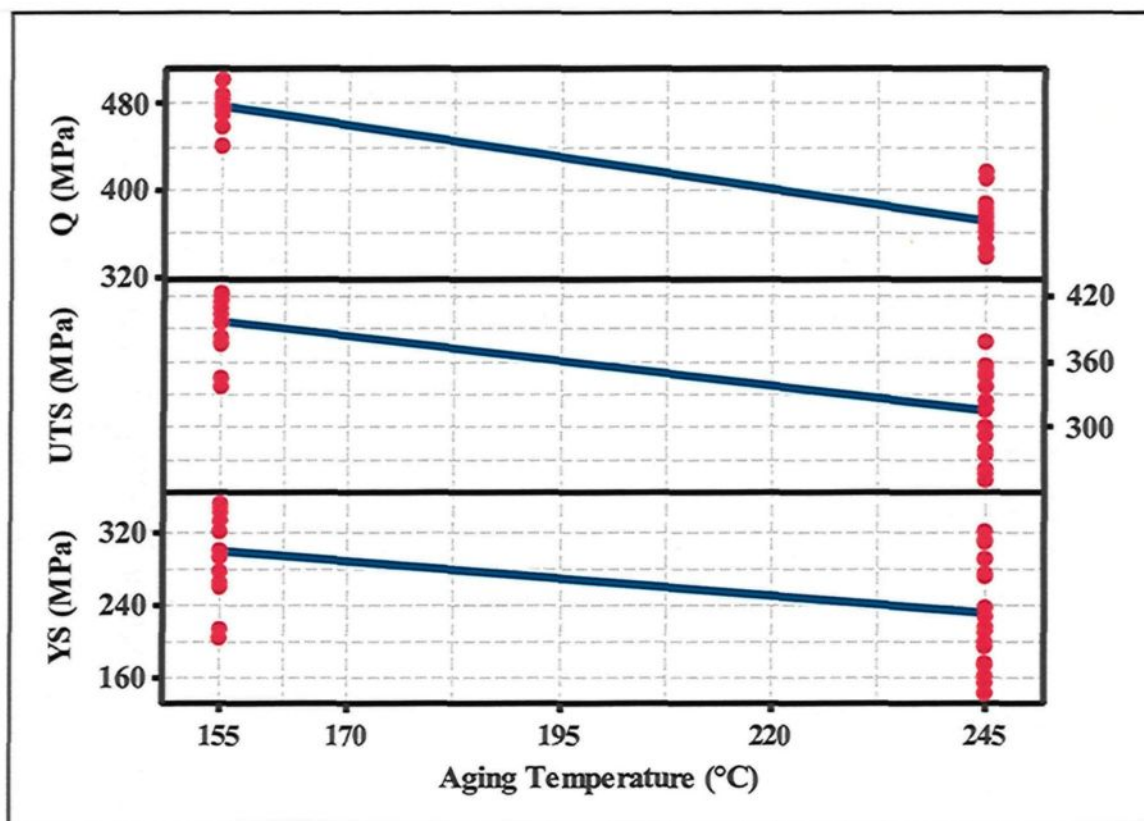


**Figure 5.3.** Matrix plots correlating the quality index ( $Q$ ), ultimate tensile strength ( $UTS$ ) and yield strength ( $YS$ ) with aging temperature for 354 (10N) alloy aged at 155°C and 245°C.

The size and density of the hardening precipitates under the effect of prolonged aging times at a specific temperature of 245°C are shown in Figures 5.5(a) through (c). Figure 5.5(a) is an SEM image showing the matrix at a magnification of 20000x in the as-cast condition where no precipitates were formed in the metal matrix before applying the heat treatment; Figure 5.5(b) is an SEM image illustrating the size and density of the precipitates when applying aging treatment at 245°C for 1 h; Figure 5.5(c) is an SEM image showing the coarsening which occurs in the precipitates at the expense of their

density upon applying aging treatment at the same temperature for 72 h; and Figure 5.5(d) shows an EDX spectrum corresponding to the phases observed.

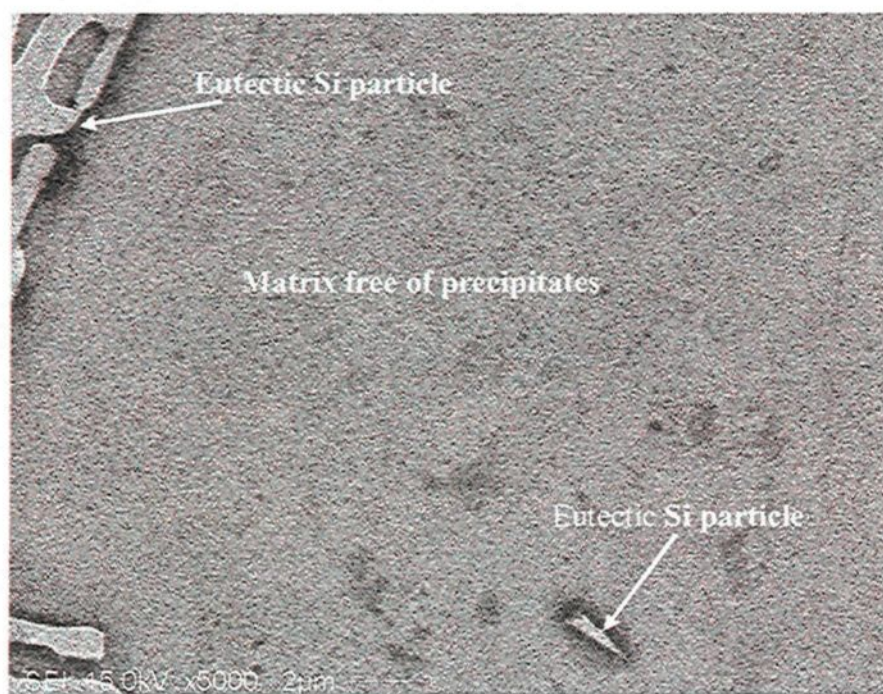
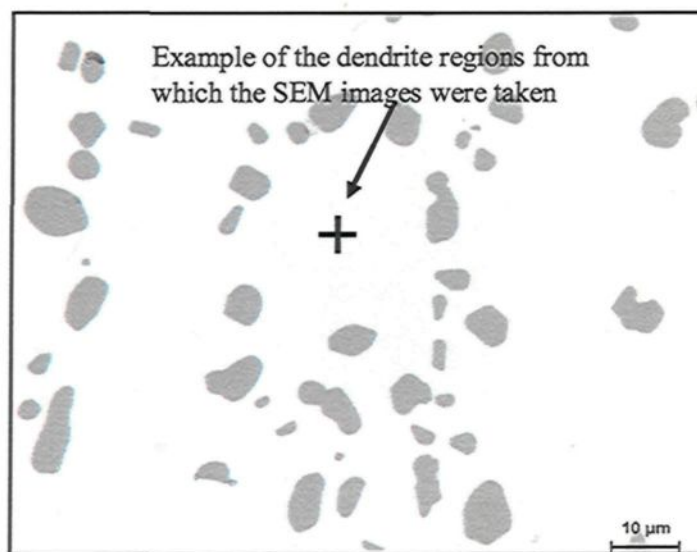


**Figure 5.4**

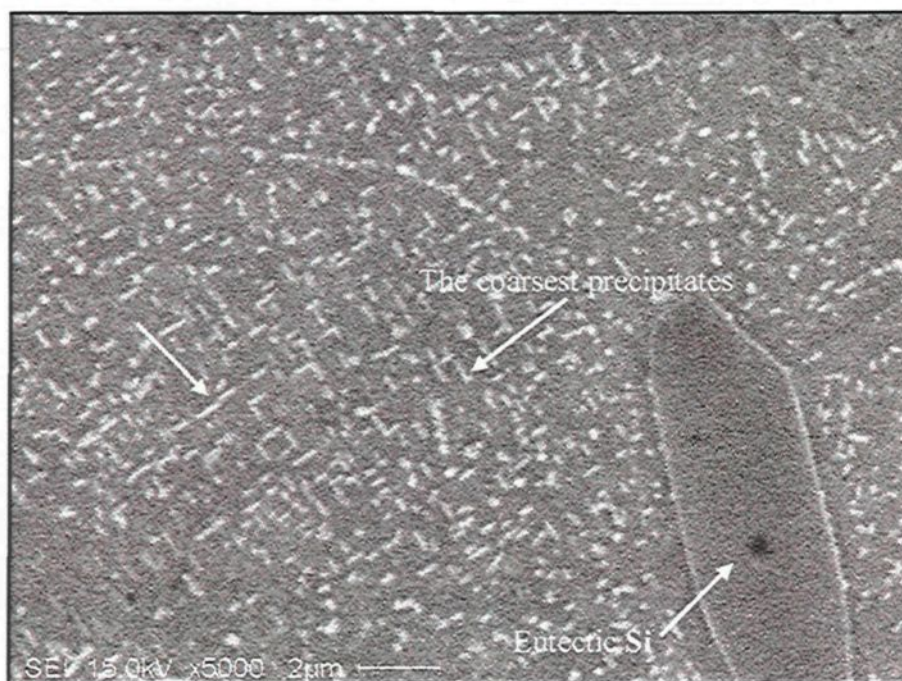


(c)

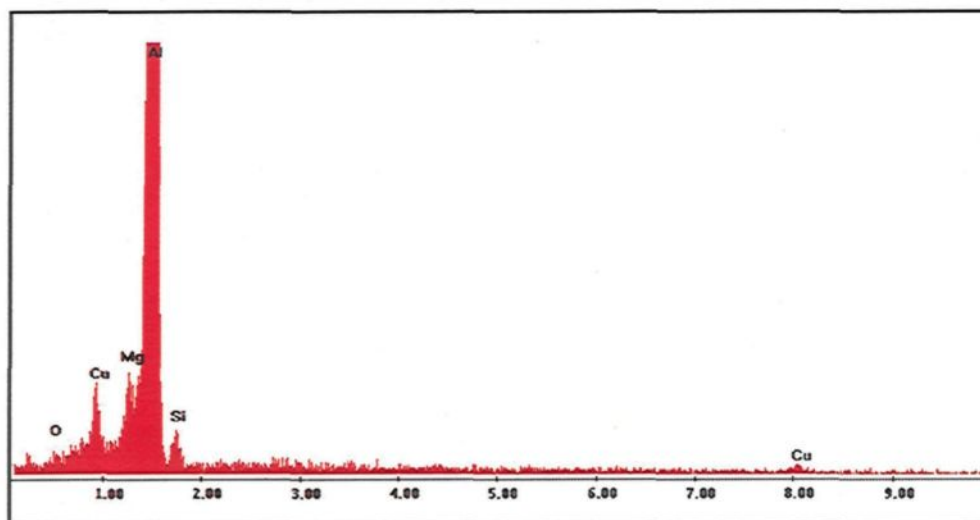


(d)

**Figure 5.4**



(e)

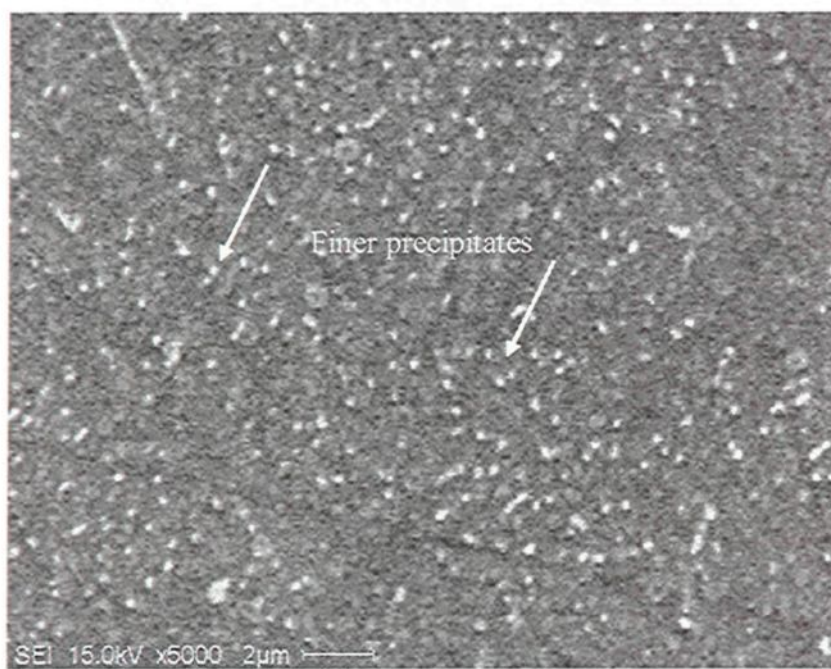


(f)

**Figure 5.4.** Size and density of precipitates formed at various aging temperatures in 10N-354 alloy: (a) optical micrographs showing the dendrite regions from which the SEM images were taken; (b) SEM image, as-cast condition; (c) SEM image after aging at 155°C for 72 h; (d) SEM image after aging at 195°C for 72 h; (e) SEM image after aging at 245°C for 72 h; and (f) EDX spectrum corresponding to the precipitates observed (samples were obtained from the gauge length of B108 test bars).



(a)

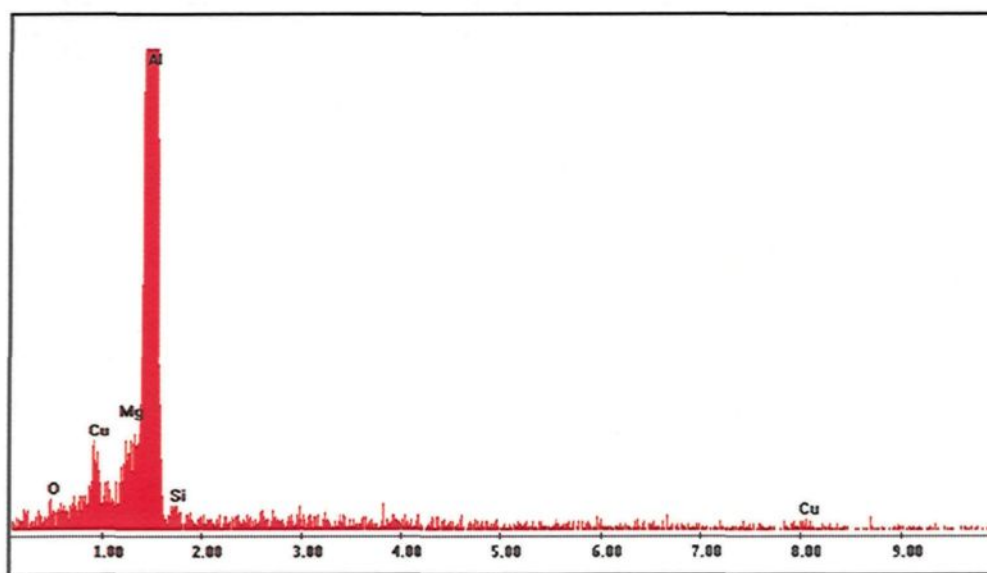


(b)

**Figure 5.5**



(c)



(d)

**Figure 5.5.** SEM images taken from dendrite regions showing the effects of aging time on the size and density of the precipitates in 10N-354 alloy corresponding to: (a) as-cast condition, 20000x; (b) after aging at 245°C for 1 h; (c) after aging at 245°C for 72 h; and (d) EDX spectrum corresponding to the precipitates observed (samples were obtained from the gauge length of B108 test bars).

Figures 5.4(c) through (e) illustrate that applying aging treatment for 72 h at a lower temperature of 155°C results in the precipitation of finer and denser precipitates in the metal matrix, as may be seen in Figure 5.4(c). Increasing the aging temperature to 195°C for the same aging time results in a coarsening of the precipitates and a reduction of their density in the matrix, as observed in Figure 5.4(d). A further increase in the aging temperature to 245°C for the same time duration of 72 h leads to a continuous increase in the size of the precipitates and a further reduction in their density in the metal matrix. Similar observations were made regarding the influence of longer aging times at a specific temperature, as may be seen in Figures 5.5(b) and (c). Aging treatment at 245°C for 1 h results in the formation of finer and denser precipitates, as may be noted in Figure 5.5(b), whereas increasing the aging time to 72 h at the same temperature results in a coarsening of these precipitates at the expense of their density, as shown in Figure 5.5(c).

The coarsening of the precipitates together with the reduction in their density upon raising the aging temperature and/or extending the aging time are in conformity with the Ostwald ripening concept.<sup>40, 132, 183, 188, 189</sup> This concept hypothesizes that the large precipitates are thermodynamically favorable to growing at the expense of atoms from the smaller precipitates which are thermodynamically unstable and will ultimately dissolve completely. These changes are favorable from the thermodynamic point of view where the system tends to lower its energy through the formation of coarse stable incoherent precipitates with lower interfacial energy. The growth of the large precipitates results in the formation of fewer coarse precipitates displaying a wide inter-particle spacing. The

coarsening which occurs in the size of the precipitates is the main reason for the reduced strength and subsequently for the diminished quality which was observed when raising the aging temperature applied to the 354 castings.

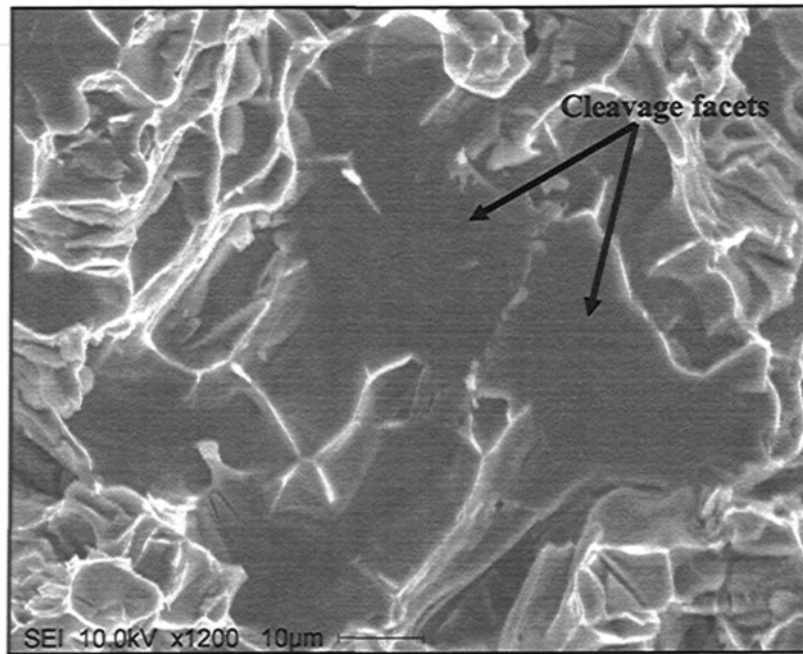
In a similar manner, the same concepts are applied to explain the reduced strength and quality index values of the alloy when increasing the aging time beyond peak-aging, as observed in Figure 5.2. The coarsening of the precipitates and the reduced density at higher aging temperatures or longer aging times, as shown in Figure 5.4(e) and Figure 5.5(c), respectively, widen the inter-particle spacing and facilitate the dislocation motion through the metal matrix.

According to the Orowan relationship, as provided in Equation 19, inter-particle spacing plays a principle role in determining the overall strength of the castings as a result of resisting the dislocation motion by means of the phases precipitated.<sup>131, 132</sup> Larger inter-particle spacing results in a decrease in the resistance to dislocation motion thereby facilitating the occurrence of Orowan looping. The increased deformability of the matrix via the easy dislocation motions leads to reduced strength and subsequently diminished quality index values in the castings. On the other hand, the precipitates at lower aging temperatures or shorter aging times are finer in size with greater density in the matrix, as may be seen in Figure 5.4(c) and Figure 5.5(b), respectively; these precipitates therefore have small inter-particle spacing. In this latter case, the precipitates provide strong resistance to dislocation motion and the occurrence of Orowan looping becomes difficult leading to a hardening of the materials and an increase in the overall strength leading to an increase in the quality index values of the castings, as shown in Figure 5.2.

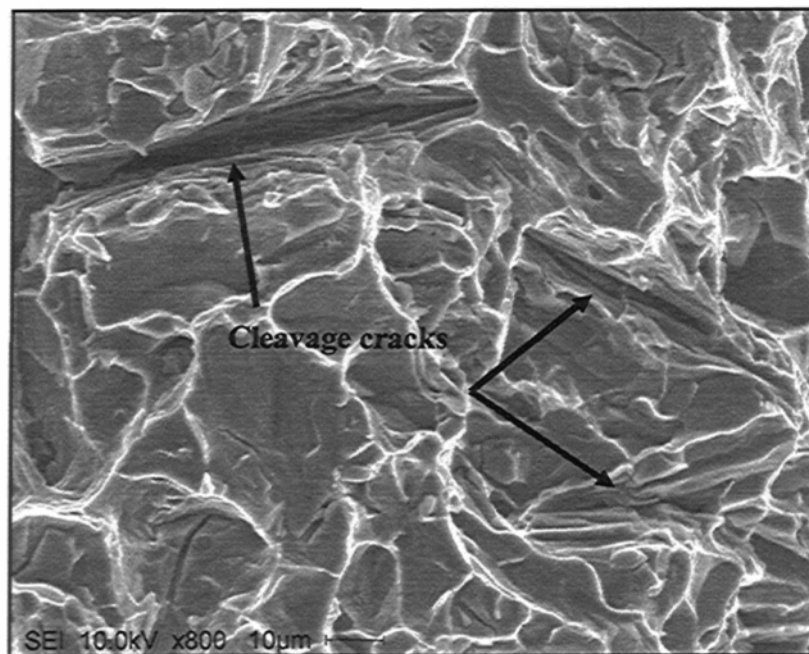
The EDXs presented in Figure 5.4(f) and Figure 5.5(d) show the composition of the phases precipitated during the aging treatment of the 354 alloy; each EDX shows that the precipitates contain Cu, Mg, and Si in addition to Al. The compositions shown are most probably those of the  $Q$ - $\text{Al}_5\text{Cu}_2\text{Mg}_8\text{Si}_6$  phase, although other phases such as  $\theta$ - $\text{Al}_2\text{Cu}$ ,  $\beta$ - $\text{Mg}_2\text{Si}$ , and  $S$ - $\text{Al}_2\text{CuMg}$  may coexist in the matrix. It was not possible, however, for all these precipitates to be identified precisely using the EDX in conjunction with SEM techniques because of the small size of these phases. It should be noted here that the main objective for using SEM techniques was to provide an overview of the size and density of the precipitates under various aging temperatures and times as applied to the castings.

The fracture surface analysis was carried out using SEM for selected samples where specimens of the 354 alloys aged at 155°C and 245°C for 72 hours each were chosen for this analysis. In the case of aging treatment at a low temperature of 155°C, a mixed fracture mode with brittle/ductile features was observed. The analysis of the fracture surface reveals such characteristics of brittle fracture as cleavage facets and cleavage cracks which are shown in Figures 5.6(a) and (b), respectively. The cleavage facets or the flat facets shown in Figure 5.6(a) are characteristics of local crystallographic orientation occurring along crystallographic planes within one specific grain.<sup>32, 46</sup> The existence of the multiple cleavage cracks shown in Figure 5.6(b) is another indication of the fracture of a hard matrix. These brittle features at the fracture surface are indications of the hardening effects which occur upon applying a low aging temperature of 155°C as a result of the formation of fine dense precipitates with smaller inter-particle spacing.

On the other hand, when applying aging treatment at 245°C for 72 h, a ductile fracture mode may be observed; this involves the necking of the specimen at a certain stress when subjected to tension testing. Several micro-voids form at the neck region; then with continuous tension these micro-voids grow, elongate, and coalesce leading ultimately to the rupture of the specimen.<sup>32, 46</sup> This ductile fracture is characterized by deep shear dimples at the fracture surface, as shown in Figures 5.6(c) and (d). These dimples are oval-like or cup-like depressions at the fracture surface and are elongated in the direction of the applied load.<sup>32, 46</sup> This fracture mode, observed upon aging at 245°C, is related to the softening effect happening to the 354 alloy as a result of the coarsening of the large precipitates at the expense of the smaller ones. This coarsening effect produces small numbers of coarse precipitates widely dispersed from each other in the metal matrix. The dislocation motion occurs much more easily when meeting with such coarse precipitates, thereby resulting in a deformable soft material. This fracture-surface analysis corroborates the results presented earlier concerning the influence of aging temperature on the strength of the castings.

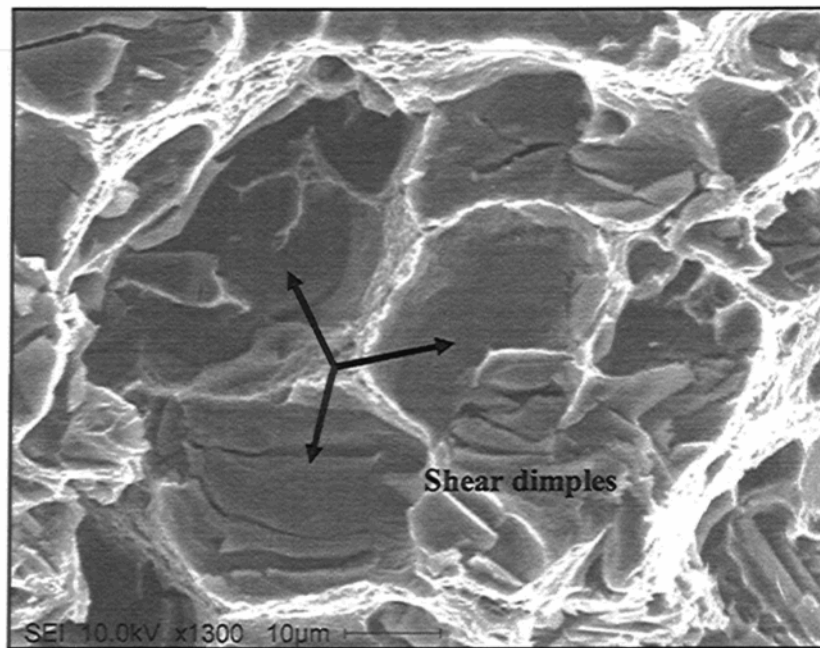


(a)

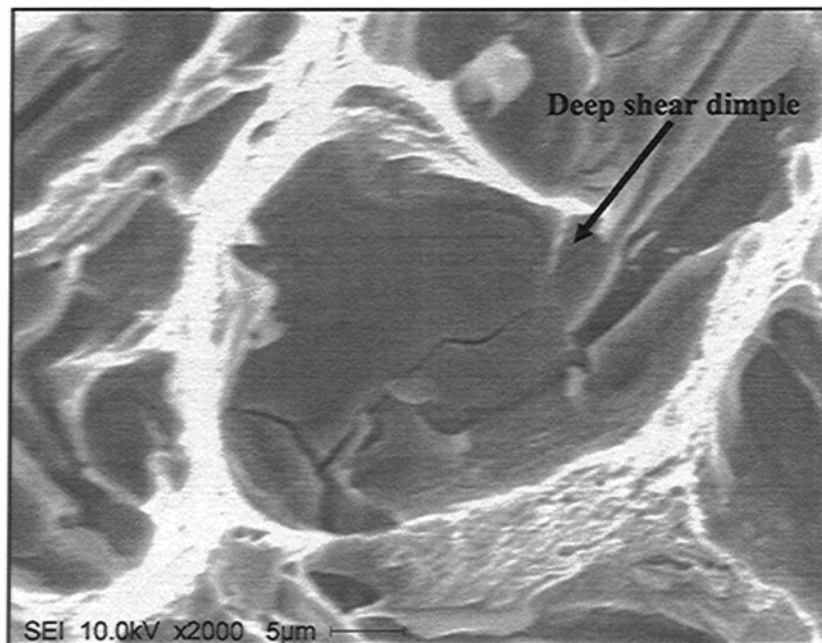


(b)

Figure 5.6



(c)



(d)

**Figure 5.6.** SEM images of the fracture surface of the 354 alloy, or 10N casting; (a) and (b) cleavage facets and cleavage cracks which are characteristic of the mixed fracture mode observed upon aging at 155°C for 72 h; (c) and (d) deep shear dimples which are features of the ductile fracture mode observed upon aging at 245°C for 72 h (fractographs were obtained from the fracture surface of B108 test bars).

### 5.3. AGING BEHAVIOR OF 359 CASTING ALLOYS

The current subsection will discuss the effects of aging temperatures and times on the tensile properties and quality index values of the 359-base alloy, or 1N alloy. The aging temperatures and times applied to the 1N alloy are shown in Table 3.2. The composition of the 359-Al-Si-Mg alloys contains two efficacious hardening elements, namely, magnesium and silicon. The objective of applying aging treatment to these castings is to precipitate the excess Mg and Si out of the supersaturated solid solution in the form of hardening phases containing Mg and Si. According to the temperature and time applied to the 359 castings, the decomposition of the supersaturated solid solution may involve the formation of independent clusters of Si and Mg followed by co-clusters of both Si and Mg; coherent needlelike GP zones; coherent needle-shaped  $\beta''$ ; coherent rod-shaped  $\beta'$ ; and, lastly, the incoherent plate-shaped  $\beta$ -Mg<sub>2</sub>Si phase. The preceding precipitation sequence is the one most frequently accepted upon applying aging treatment to an Al-Si-Mg alloy.<sup>109, 110, 111, 112</sup>

The effects of aging temperatures and times on the tensile properties of 359 alloys are shown in Figure 5.7. The tensile properties presented in this figure are ultimate tensile strength (*UTS*), yield strength (*YS*), and percentage elongation to fracture (*E<sub>f</sub>*). This plotted graph shows that aging at 155°C results in an increase in the strength of the 359 alloy with a concomitant increase in the aging time up to peak-aging which was observed at 32 hours. This increase is accompanied by a reduction in ductility up to peak-aging. Any further increase in the aging time to beyond 32 hours at 155°C results in over-aging conditions where the strength starts diminishing and the ductility starts to increase, as will be seen in Figure 5.7.

As in the case of the 354 alloy, when aging the 359 alloy there is a possibility for peak-aging to be attained in a shorter aging time as the aging temperature increases. Figure 5.7 illustrates that the aging times required to reach the peak-strength are 32 hours, 24 hours, 1 hour, 30 minutes, and 10 minutes when applying aging temperatures of 155°C, 170°C, 195°C, 220°C, and 245°C, respectively. The peak-aging times were determined using the yield strength curves shown in Figure 5.7. Aging treatment at 170°C, 195°C, 220°C, and 245°C results in an increase in the strength of the casting up to peak-aging at the expense of the ductility of the alloys. Over-aging takes place after reaching the peak-strength at the specified aging times for each temperature where the strength of the castings begins diminishing and the ductility starts increasing, as illustrated in Figure 5.7.

The results shown in Figure 5.7 were re-plotted using quality charts, as shown in Figures 5.8(a) and (b). Figure 5.8(a) shows the aging curves obtained from applying all aging temperatures and times to 359 alloys, while Figure 5.8(b) illustrates the aging curves for only three temperatures, namely, 155°C, 170°C, and 245°C, chosen to present a simplified version of the same quality chart shown in Figure 5.8(a).

Applying aging treatment to the 359 Al-Si-Mg alloy at 155°C for up to 32 h results in a continuous increase in the alloy strength at the expense of ductility; it also leads to non-significant variations in its quality index values, as may be seen in the quality charts shown in Figures 5.8(a) and (b). The same quality charts illustrate that a further increase in the aging time beyond 32 hours results in reducing the strength and the quality index values of the castings.

The aging behavior of the 359 casting observed when applying the aging temperature at 155°C is related to the precipitation of the various precursors of the Mg<sub>2</sub>Si phase in the metal matrix according to the aging time applied. The early increase in the strength of the alloy is related to the formation of individual clusters of Mg and Si, as well as to co-clusters of the same hardening elements, and to the GP zones. The peak-strength obtained at 32 hours is related to the formation of the coherent  $\beta''$  precipitate which is considered to be the main causative source of strength in the Al-Si-Mg alloys. In this regard, several studies<sup>190, 191, 192, 193</sup> reported that  $\beta''$  precipitate acts as the main source of strength in Al-Mg-Si alloys where the peak hardness of these alloys is related directly to the precipitation of this particular phase. The coherent metastable  $\beta'$  precipitate may coexist with the  $\beta''$  phase at peak-aging conditions; its contribution to peak-strength, however, is less than that of the  $\beta''$  phase.<sup>193</sup>

The decrease in the strength of the 359 alloy which accompanies the over-aging conditions is related to the loss of the coherency strain surrounding the precipitates through the formation of incoherent stable  $\beta$ -Mg<sub>2</sub>Si phases. In addition to the loss of coherency, the longer aging time results in the coarsening of the large precipitates at the expense of the small ones. This coarsening effect produces a lower density of the widely dispersed coarse precipitates. As discussed in the previous subsection, these changes in the features of the precipitates reduce the resistance to the dislocation motion through the metal matrix and lead to a deformable soft matrix.

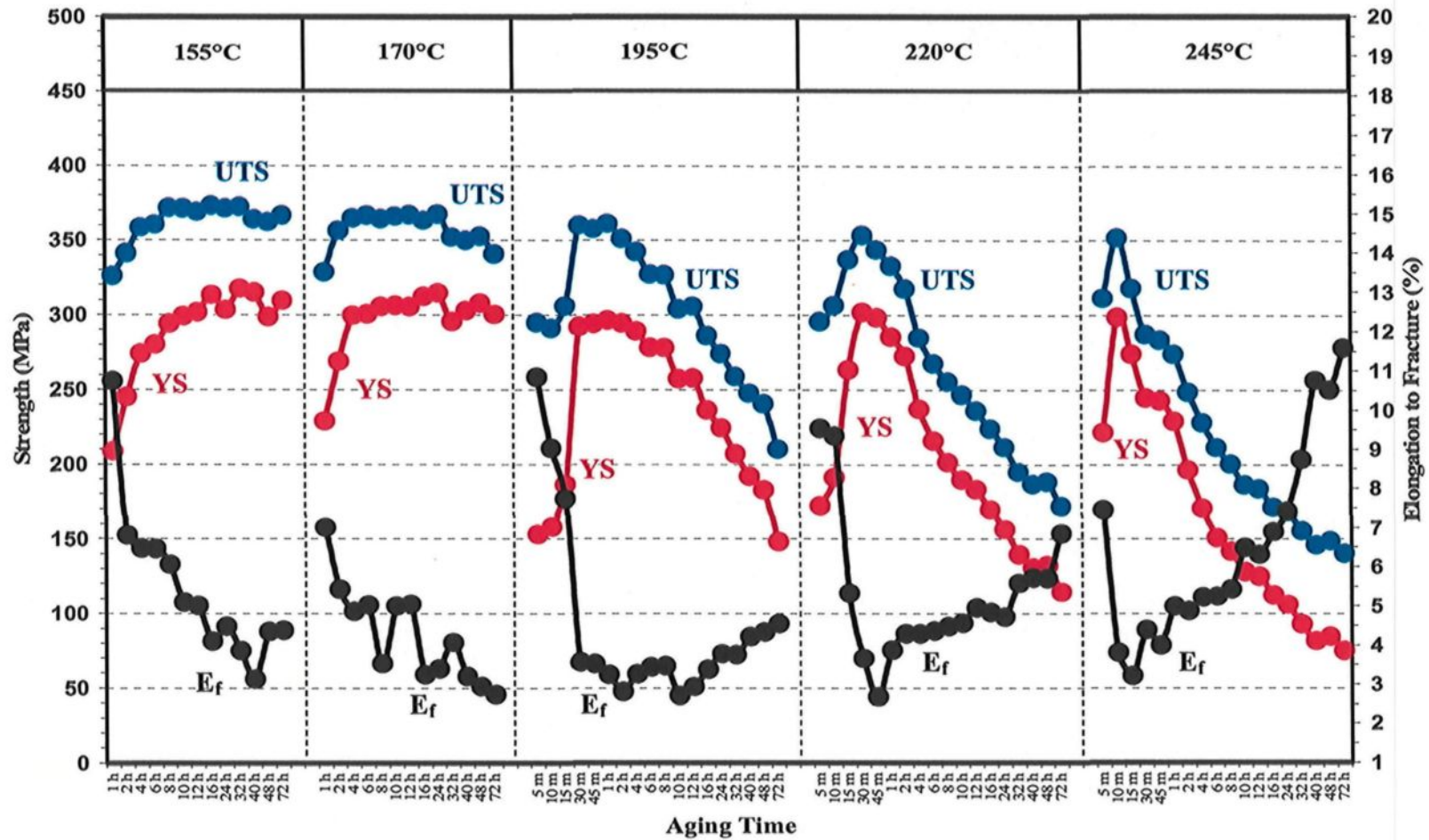
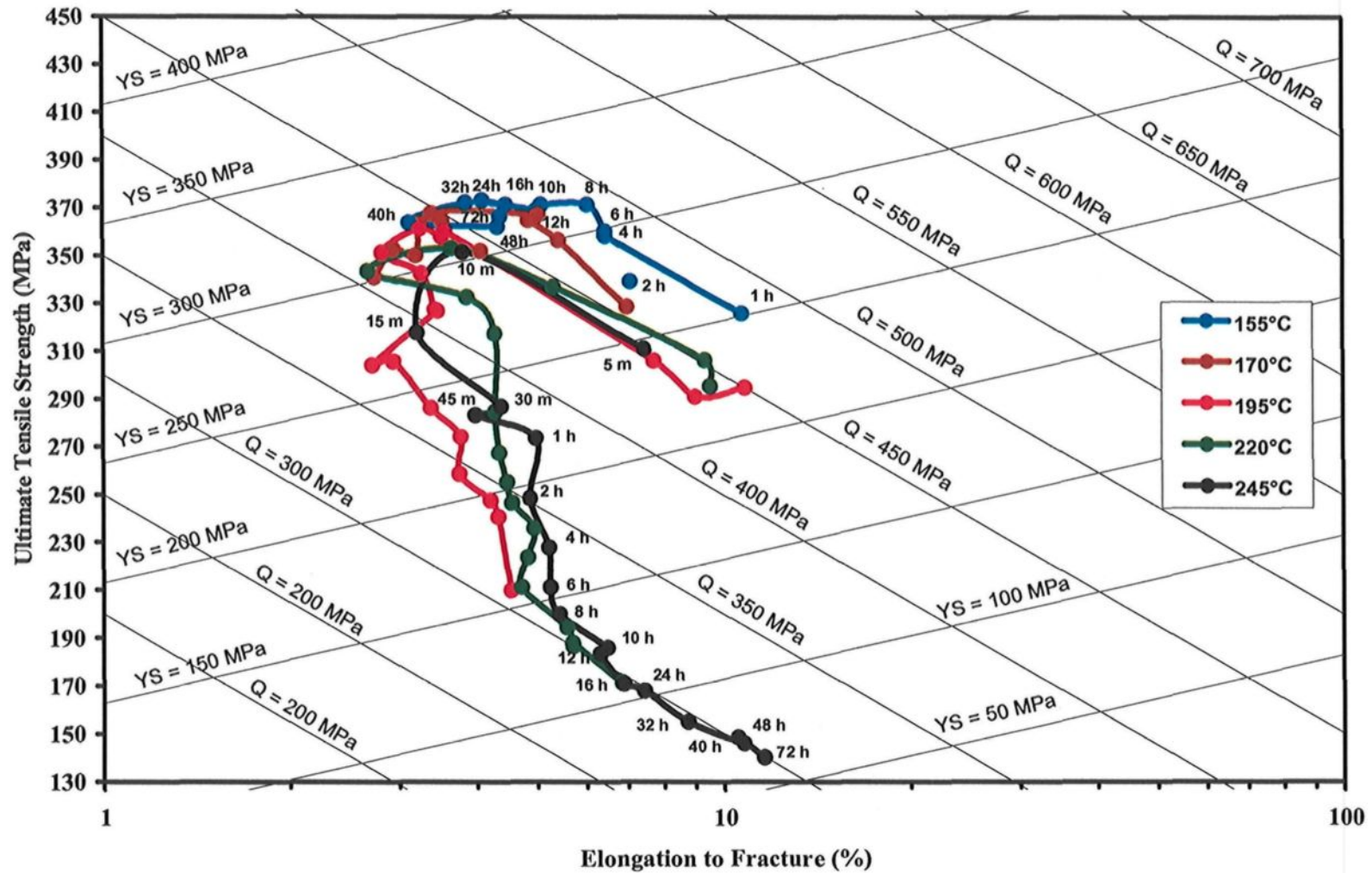
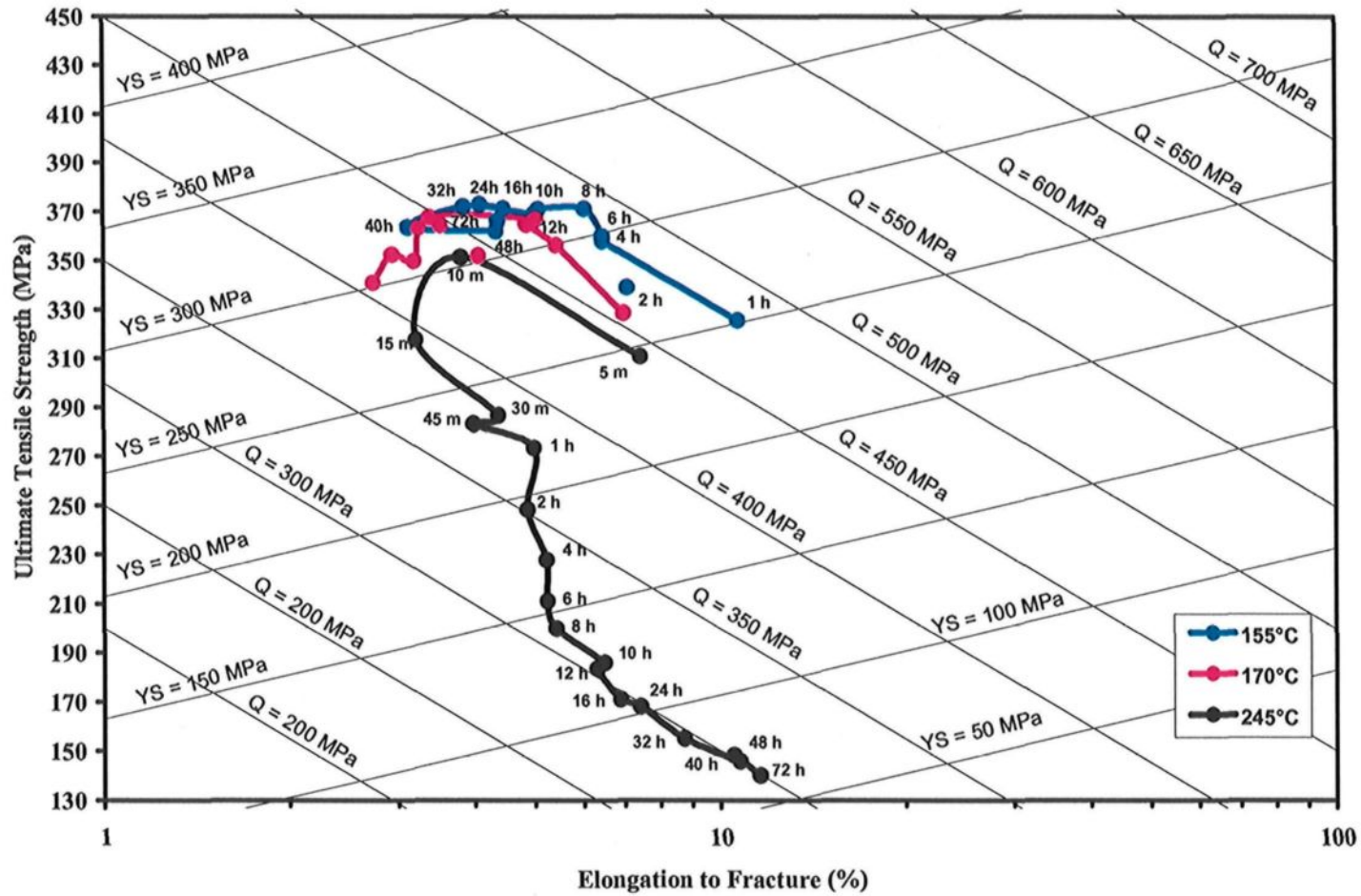


Figure 5.7. The tensile properties of the 359 alloy (1N) under various aging temperatures and aging times. (Note: “m” and “h” on the X-axis indicate minutes and hours, respectively.)



(a)  
Figure 5.8



(b)

Figure 5.8. Quality chart generated using Equations 1 and 2 illustrating (a) the strength and quality of the 359 alloy under all aging temperatures and times applied; and (b) a simplified chart of (a) showing the strength and quality of the 359 alloy under the three specified aging temperatures.

With respect to the aging at high temperatures of 170°C, 195°C, 220°C, and 245°C, it will be observed in Figure 5.8(a) that the aging curves under these temperatures display similar curvilinear behavior. The alloy strength increases up to peak-aging with a decrease in its ductility and without any significant change in the alloy quality index. Beyond peak-aging, the strength and the quality index values of the 359 alloy decrease with all further increases in aging time at each temperature. The increase in the aging temperatures provides a high rate of atomic diffusion and, in so doing, accelerates the precipitation process thus reaching peak-strength faster than when applying aging at lower temperatures. For example, upon applying aging treatment at 245°C to the 359 castings, the peak-strength was observed to be attained after only 10 minutes as compared to 32 hours when applying 155°C. The increase in the aging temperature provides a rapid aging treatment with several economical benefits.

Figure 5.8(b) shows that increasing the aging temperature from 155°C to 245°C results in shifting the aging curve of the 359 casting towards the bottom left-hand corner of the quality chart. The shift occurring in the aging curve indicates that lower levels of strength and quality index for the same 359 alloy were obtained when increasing the aging temperature. For instance, the ultimate tensile strength, yield strength, and quality index values obtained for peak-aging at 155°C are 372 MPa, 317 MPa, and 460 MPa, respectively, while the values for the same properties obtained upon increasing the aging temperature to 245°C at peak-aging are 352 MPa, 298 MPa, and 439 MPa, respectively. The effects of increasing aging temperature are clearer when comparing these properties in the 359 alloys aged at 155°C and 245°C for the same time duration of 72 hours. The

ultimate tensile strength, the yield strength, and the quality index values obtained when aging the 1N alloy at 155°C for 72 h are 366 MPa, 309 MPa, and 462 MPa, respectively, while the values for the same properties obtained upon increasing the aging temperature to 245°C for the same time duration of 72 h are 140 MPa, 75 MPa, and 300 MPa, respectively.

As was explained earlier in the case of the 354 alloys, the noticeable reduction in the strength and quality index values of the 359 alloys, upon increasing the aging temperature, is related to the formation of coarser precipitates with lesser density in the matrix displaying large inter-particle spacing, as illustrated in the schematic representation shown in Figure 5.9. These changes facilitate dislocation motion and result in softening effects, thereby reducing the strength and the quality index values of the castings under investigation.

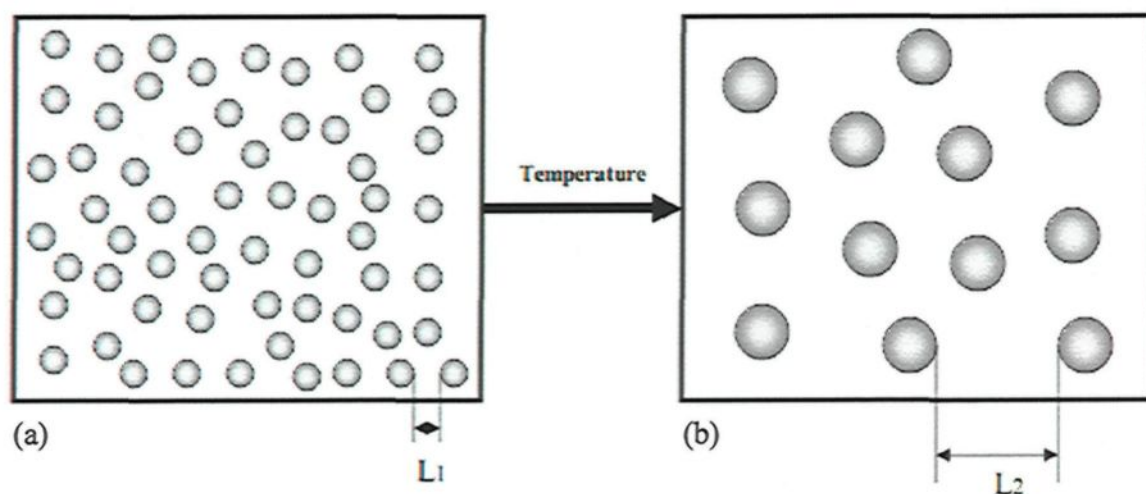
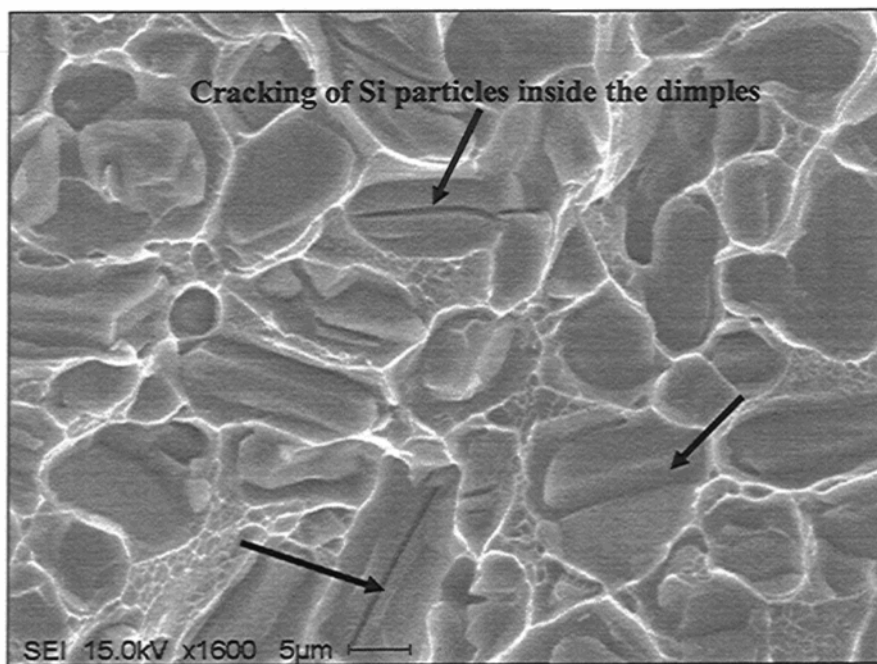
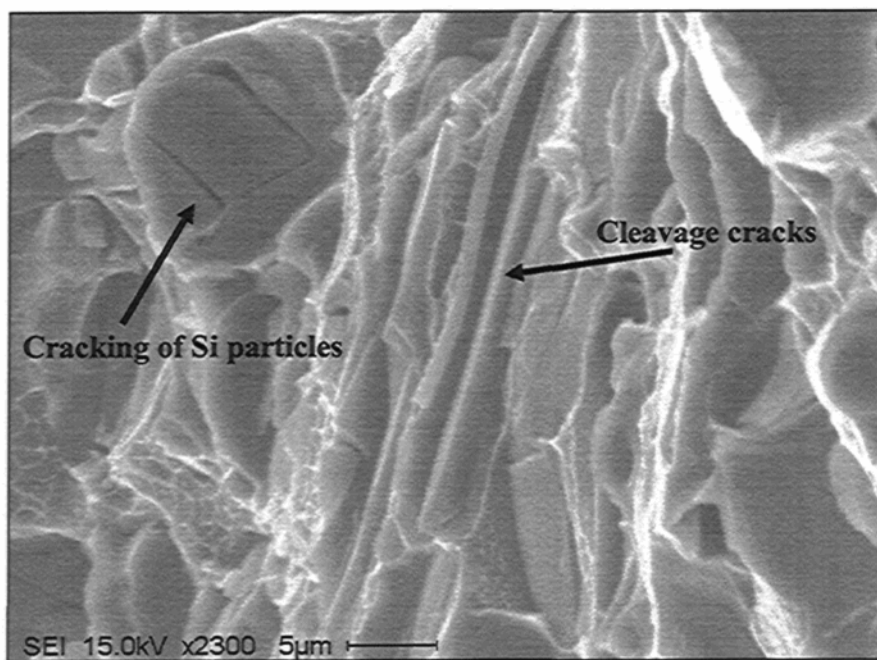


**Figure 5.9.** Schematic representation showing the influence of increasing aging temperature on the size, density, and inter-particle spacing of the hardening precipitates: (a) at a low aging temperature, and (b) at a high aging temperature. (L1 and L2 indicate the inter-particle spacing in each case.)

The softening effects which occur upon increasing the aging temperature may be substantiated by the fracture-surface analysis presented in Figures 5.10(a) through (c). These figures show the SEM images of the fracture surface of selected samples of the 359 alloys. Figures 5.10(a) and (b) show the SEM images of the fracture surface of 1N alloys aged at 155°C for 72 h; a mixed fracture mode may be observed in this case illustrating brittle/ductile features. The cleavage cracking of Si particles inside the dimples will be seen in Figure 5.10(a) which shows the occurrence of the fracture, known as cellular fracture, in a two-phase region.<sup>32</sup> In this latter type of fracture, two different phases coexist and each one has its own mode of fracture. The phases in this specific case are the hard Si particles and the ductile  $\alpha$ -Al-matrix. The hard silicon particles were observed to fracture in a brittle manner through several cleavage cracks, as may be seen in Figure 5.10(a), whereas the  $\alpha$ -Al-matrix displays a ductile fracture mode within the formation of the oval-shaped dimples. Cleavage cracks are also shown in Figure 5.10(b) indicating the brittle features observed at the fracture surface of the samples which were subjected to aging at a lower treatment temperature of 155°C for 72 h. On the other hand, the fracture surface of the 1N alloy aged at 245°C for 72 h shows a ductile fracture mode characterized by deep shear dimples. This type of dimple is a characteristic feature of the rupture of a soft matrix, as shown in Figure 5.10(c).

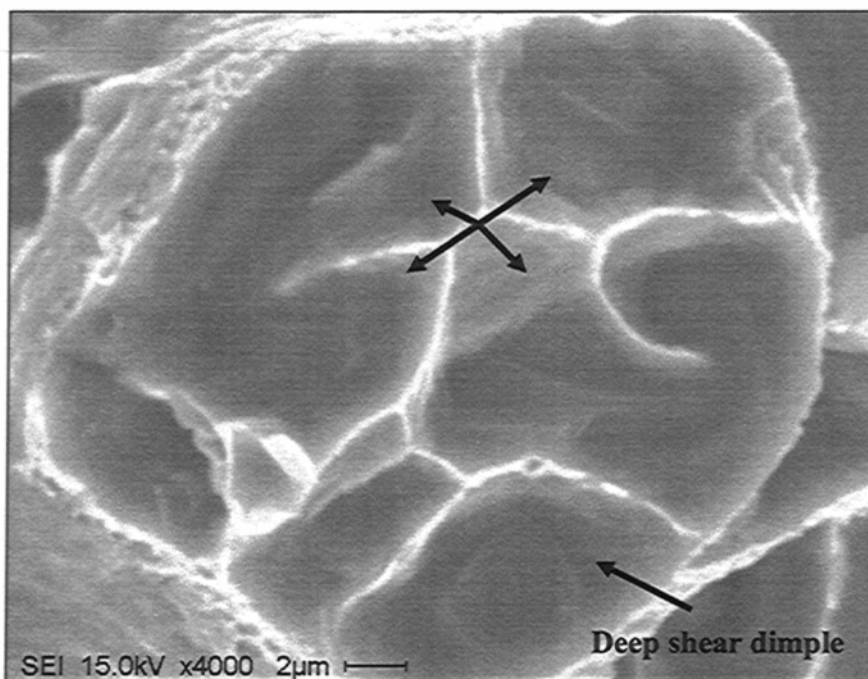


(a)



(b)

Figure 5.10



(c)

**Figure 5.10.** SEM images of the fracture surface of the 359 alloy or 1N casting (a) and (b) cleavage cracking which characterizes the mixed fracture mode observed upon aging at 155°C for 72 h; and (c) deep shear dimples which are features of the ductile fracture mode observed upon aging at 245°C for 72 h (fractographs were obtained from the fracture surface of B108 test bars).

The matrix plots shown in Figure 5.11 likewise correlate the properties of the 359 alloys with the same two aging temperatures of 155°C and 245°C. The points presented at each aging temperature in these plots represent the various aging times used at that temperature. These plots also show that increasing the aging temperatures from 155°C to 245°C decreases the properties of the 359 alloy, *i.e.*, the ultimate tensile strength (*UTS*); the yield strength (*YS*); and the quality index values (*Q*). As before, the matrix plots confirm the observations made from the quality charts presented in Figure 5.8.

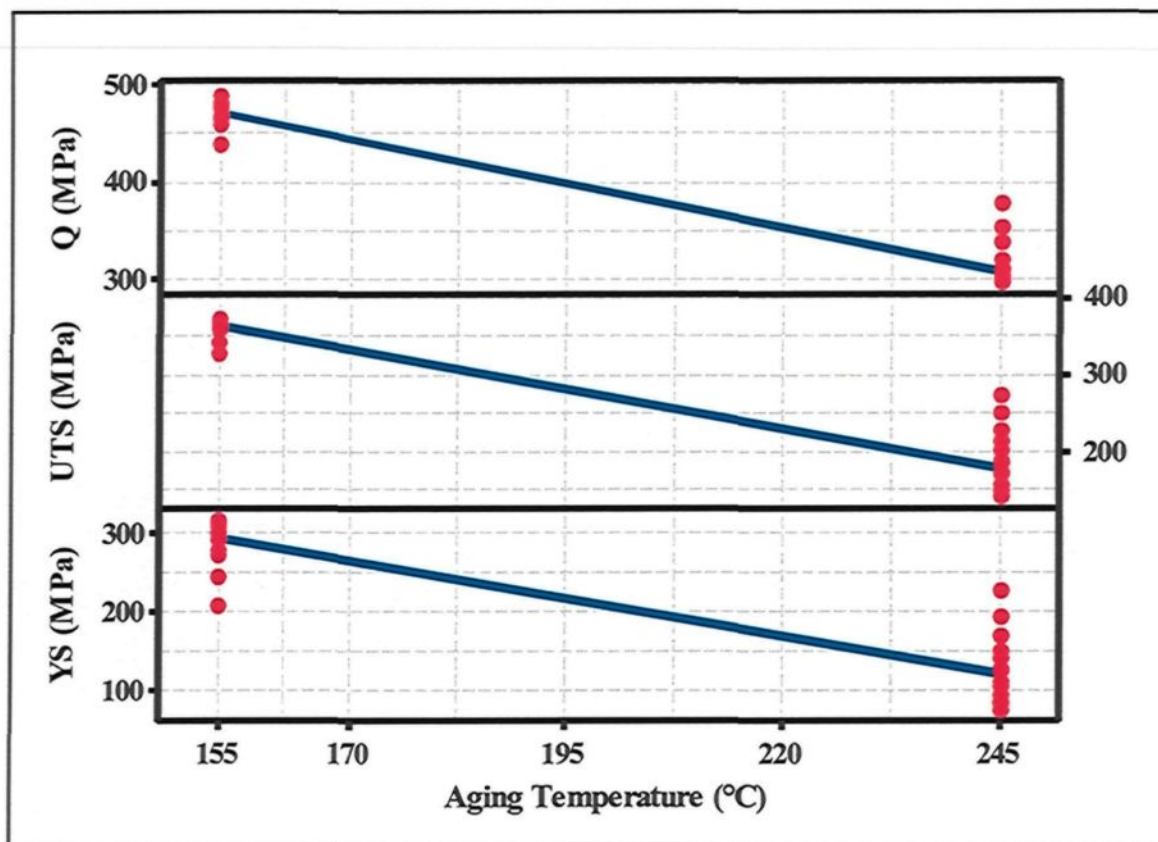


**Figure 5.11.** Matrix plots correlating the quality index ( $Q$ ), ultimate tensile strength ( $UTS$ ) and yield strength ( $YS$ ) with aging temperature for 359 (1N) alloy aged at 155°C and 245°C.

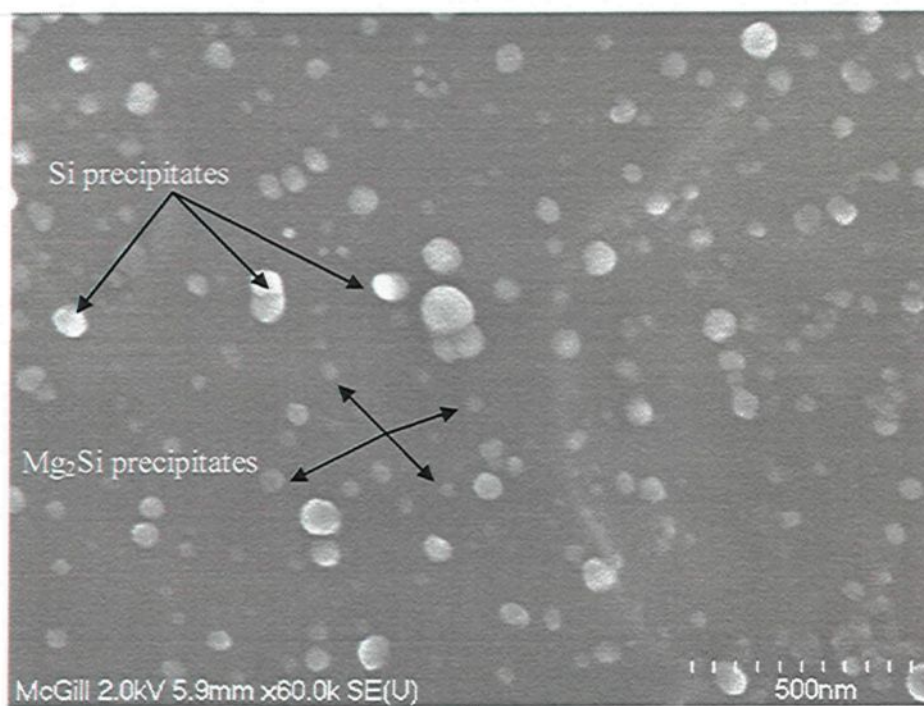
The SEM techniques which were used to characterize the precipitates in the case of the 354 alloys were not sufficient for a clear characterization of the precipitates formed after applying aging treatment to 359 alloys. This insufficiency may be related to the smaller size and the grey color of the  $\beta$ -Mg<sub>2</sub>Si phase and its precursors which are the main phases observed to precipitate during aging treatment of the 359 alloys.

The FESEM technique was used to identify the precipitates observed in the 359 alloy which was subjected to aging treatments. The FESEM, as compared to the SEM, provides clear high-resolution images even at low voltages; it also produces images of 1.5

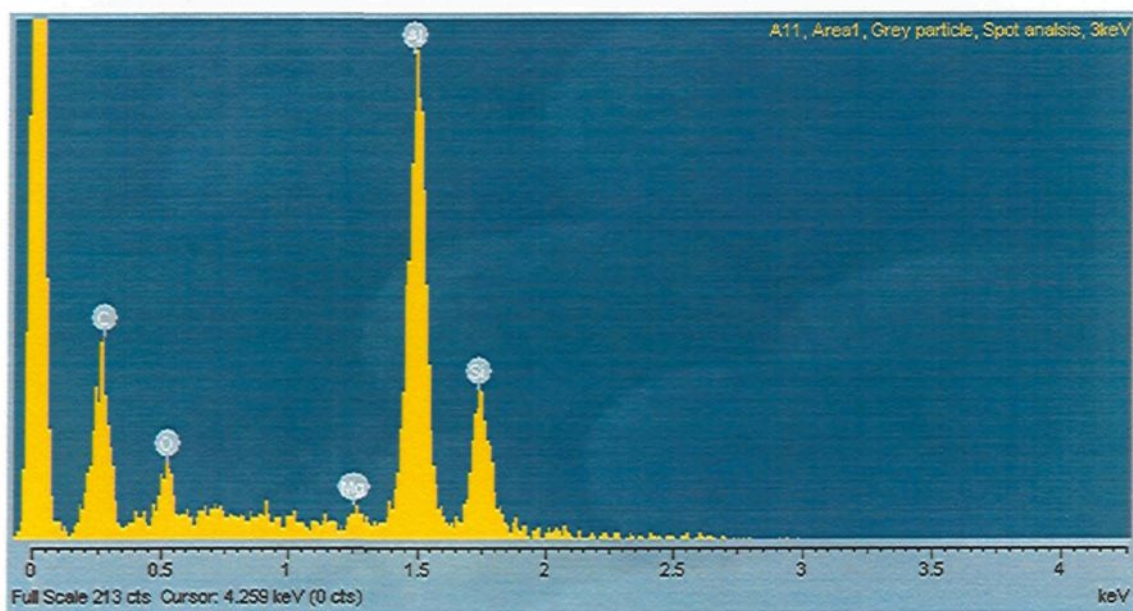
nm resolution at 15 kV and of 2.1 nm resolution at 1 kV. In addition, it provides high resolution and good contrast even at very high magnifications. The maximum magnification obtainable using SEM techniques is 30,000x, while that obtained when using the FESEM technique is 500,000x.

Figure 5.12 shows the main precipitates observed in the 359-Al-Si-Mg alloy after applying aging treatment at 220°C for 72 h, as an example. Figure 5.12(a) illustrates an SEM image taken from the dendrite region at a magnification of 60,000x. From this figure it will be noticed that two types of precipitate coexist in the metal matrix, visible as both gray and bright particles. The EDX analysis illustrates the fact that the gray particles are Mg-Si-containing precipitates which indicate the presence of  $\beta$ -Mg<sub>2</sub>Si phases; this analysis is presented through the EDX spectrum shown in Figure 5.12(b). The EDX spectrum shown in Figure 5.12(c) corresponds to the bright particles in the SEM image shown in Figure 5.12(a); from this spectrum it may be concluded that the bright particles are silicon precipitates. The precipitation of silicon in the Al-Si-Mg alloys was also reported in number of studies where it was observed that silicon precipitates form during the aging cycle in the final stage of the phase transformation process.<sup>111, 112, 116, 192, 194</sup>

Based on the analysis made using the FESEM, it may be concluded that the strengthening of the 359 alloys during aging treatment results from the precipitation of the  $\beta$ -Mg<sub>2</sub>Si phase with its precursors as well as that of Si particles. The effects of aging temperatures and times on the size and density of the Mg<sub>2</sub>Si and Si precipitates in the 359 alloy are expected to develop along the same lines as those observed in the case of the 354 alloy.

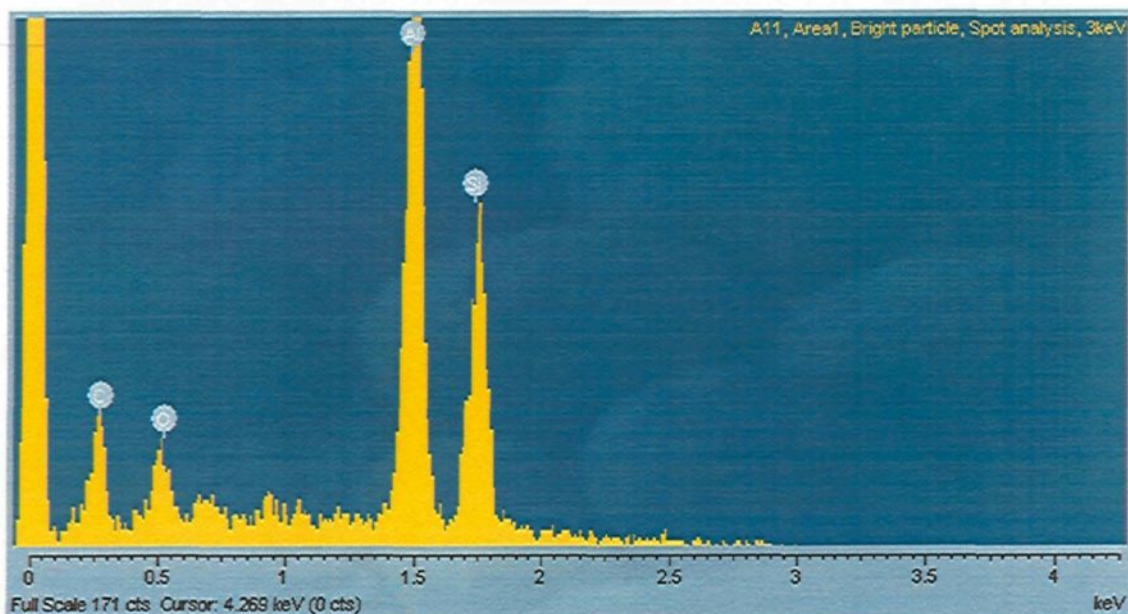


(a)



(b)

Figure 5.12



(c)

**Figure 5.12.** FESEM analysis of the precipitates observed in the 359 or 1N alloy (a) SEM image taken from the dendrite region of the 1N alloy aged at 220°C for 72 h; (b) EDX spectrum corresponding to the gray particles in the SEM image; (c) EDX spectrum corresponding to the bright precipitates in the SEM image (samples were obtained from the gauge length of B108 test bars).

#### 5.4. COMPARISON BETWEEN AGING BEHAVIOR OF 354 AND 359 ALLOYS

The aging conditions listed in Table 3.2 were applied for both the 354 and the 359 casting alloys, *i.e.* 10N and 1N, respectively. Figure 5.13 through Figure 5.17 show a comparison between the aging behaviors of both alloys at each temperature for the specified time range. The quality chart shown in Figure 5.13 illustrates the strength and the quality indices for the 354 alloy, as compared to those of the 359 alloy when subjected to the same aging treatment at 155°C for time durations in the range of 1 h to 72 h. Figure 5.14 shows a comparison between the properties of the alloys subjected to an aging temperature of 170°C for 1 h to 72 h. Figure 5.15 illustrates the aging behavior of the 354

casting, as compared to that of the 359 casting subjected to the same aging temperature of 195°C for the same time durations ranging from 5 minutes to 72 hours. The quality chart shown in Figure 5.16 presents a comparison between the aging behaviors of both alloys aged at 220°C for time durations in the range of 5 minutes to 72 hours. Figure 5.17 is a comparison between the properties of the alloys aged at 245°C for time periods ranging between 5 minutes and 72 hours.

The quality charts shown in Figure 5.13 through Figure 5.17 reveal that, in comparison to the aging curves for the 359 alloys, those for the 354 alloys shift toward the upper left-hand side of the quality charts at all aging temperatures, and keep quasi-parallel to the same *iso-Q* line. This behavior implies that the 354 alloys display high strength levels compared to the 359 alloys under all aging conditions studied. These strength levels, however, are obtained at the expense of the ductility, as revealed in the same quality charts. Accordingly, the 354 castings will display only slight variations in the quality index values when compared to those of the 359 castings subjected to the same aging conditions, as may be seen from Figure 5.13 and Figure 5.17. These observations match the results presented in subsection 4.3.2 which investigated the effects of copper on the strength and the quality index values of the alloys under investigation. The addition of 1.8%Cu to the 359-Al-9%Si-0.5%Mg produces the 354 alloys. The Cu-content of the 354 alloys is the main source of the increased strength and the decreased ductility of these castings when compared to the same properties in the 359 alloys after being subjected to the same aging treatments. As mentioned earlier, the increased strength compensates for the decreased ductility so that the

net effect of increasing copper from 0% (359) to 1.8% (354) on the quality index values is non-significant.

The 359 alloys are observed to attain peak-strength faster than the 354 alloys at all the aging temperatures applied to both castings. The aging times required to reach peak-strength for 359 alloys is 32 hours, 24 hours, 1 hours, 30 minutes, and 10 minutes, when applying aging temperatures of 155°C, 170°C, 195°C, 220°C, and 245°C, respectively. On the other hand, the aging times required to reach peak-aging in the case of 354 alloys is 72 hours, 40 hours, 8 hours, 1 hour, and 15 minutes, when applying the same aging temperatures of 155°C, 170°C, 195°C, 220°C, and 245°C, respectively. Rapidly attaining peak-strength in the case of 359 alloys may be related to the simple precipitation process from the ternary Al-Si-Mg system, as compared to the complex precipitation process from the quaternary Al-Si-Mg-Cu system. Precipitation-hardening in the 359 alloys involves the precipitation of  $Mg_2Si$  and silicon phases, as explained in subsection 4.3, while the precipitation sequence in the case of 354 alloys is more complicated because it involves the formation of several hardening phases and their precursors during the aging treatment such as  $Q-Al_5Cu_2Mg_8Si_6$ ,  $\theta-Al_2Cu$ ,  $\beta-Mg_2Si$ , and  $S-Al_2CuMg$ , as discussed in subsection 4.2.

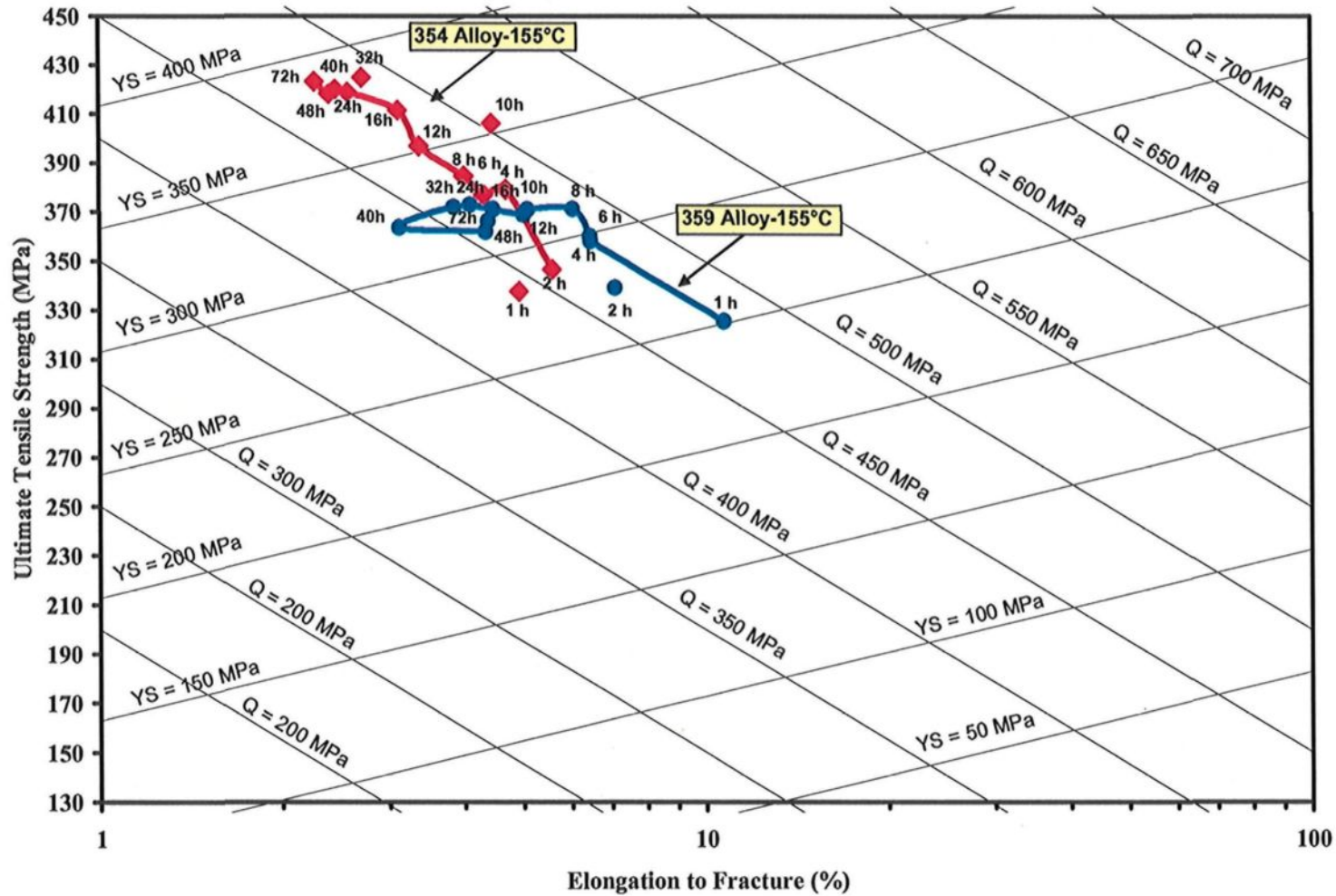


**Figure 5.13.** Quality chart generated using Equations 1 and 2 to compare the strength and quality of the 354 and 359 alloys or 10N and 1N castings, respectively, aged at 155°C for time durations of 1 hour - 72 hours, as labeled on the curves.

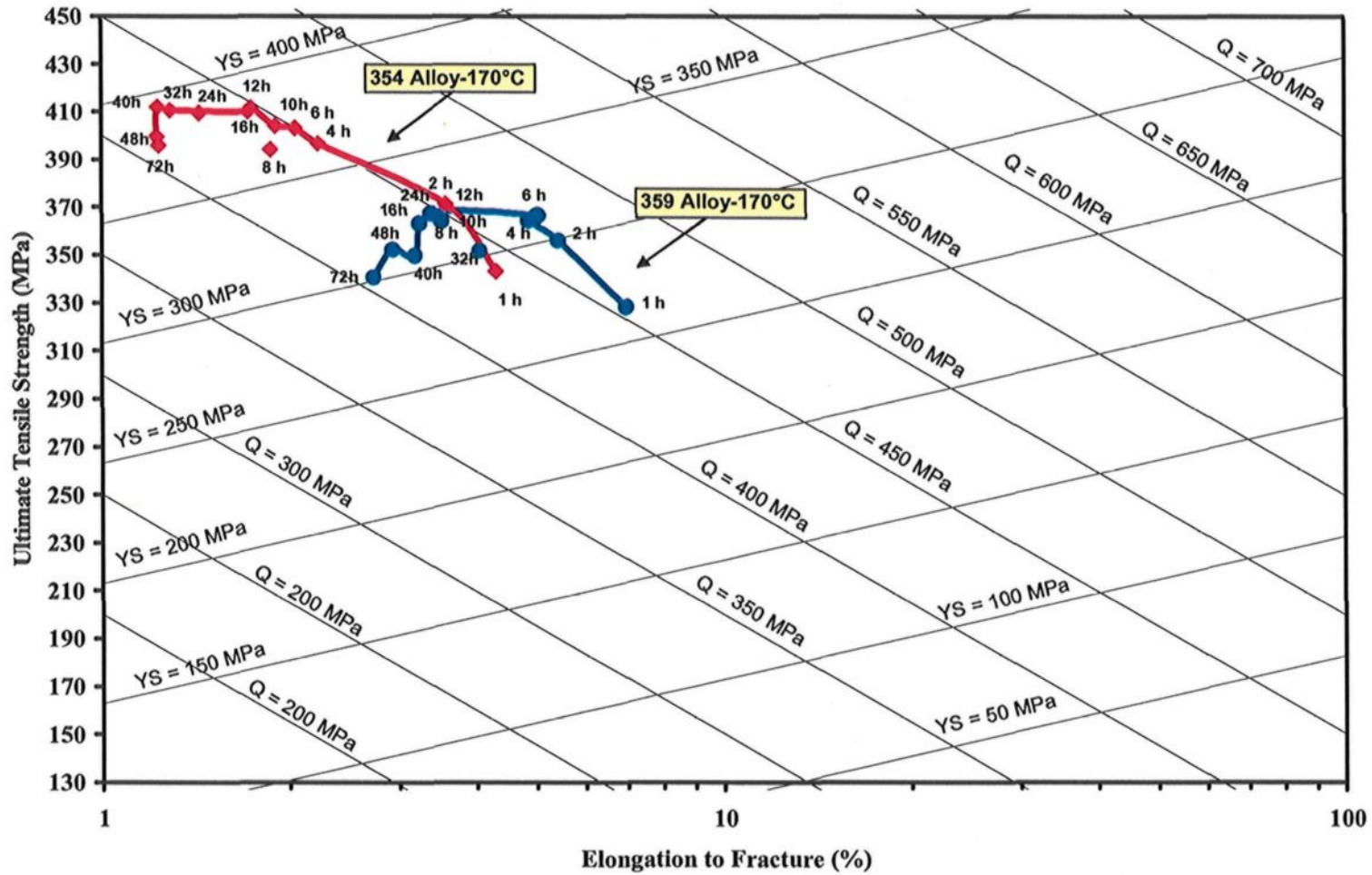


Figure 5.14. Quality chart generated using Equations 1 and 2 to compare the strength and quality of the 354 and 359 alloys or 10N and 1N castings, respectively, aged at 170°C for time durations of 1 hour - 72 hours, as labeled on the curves.

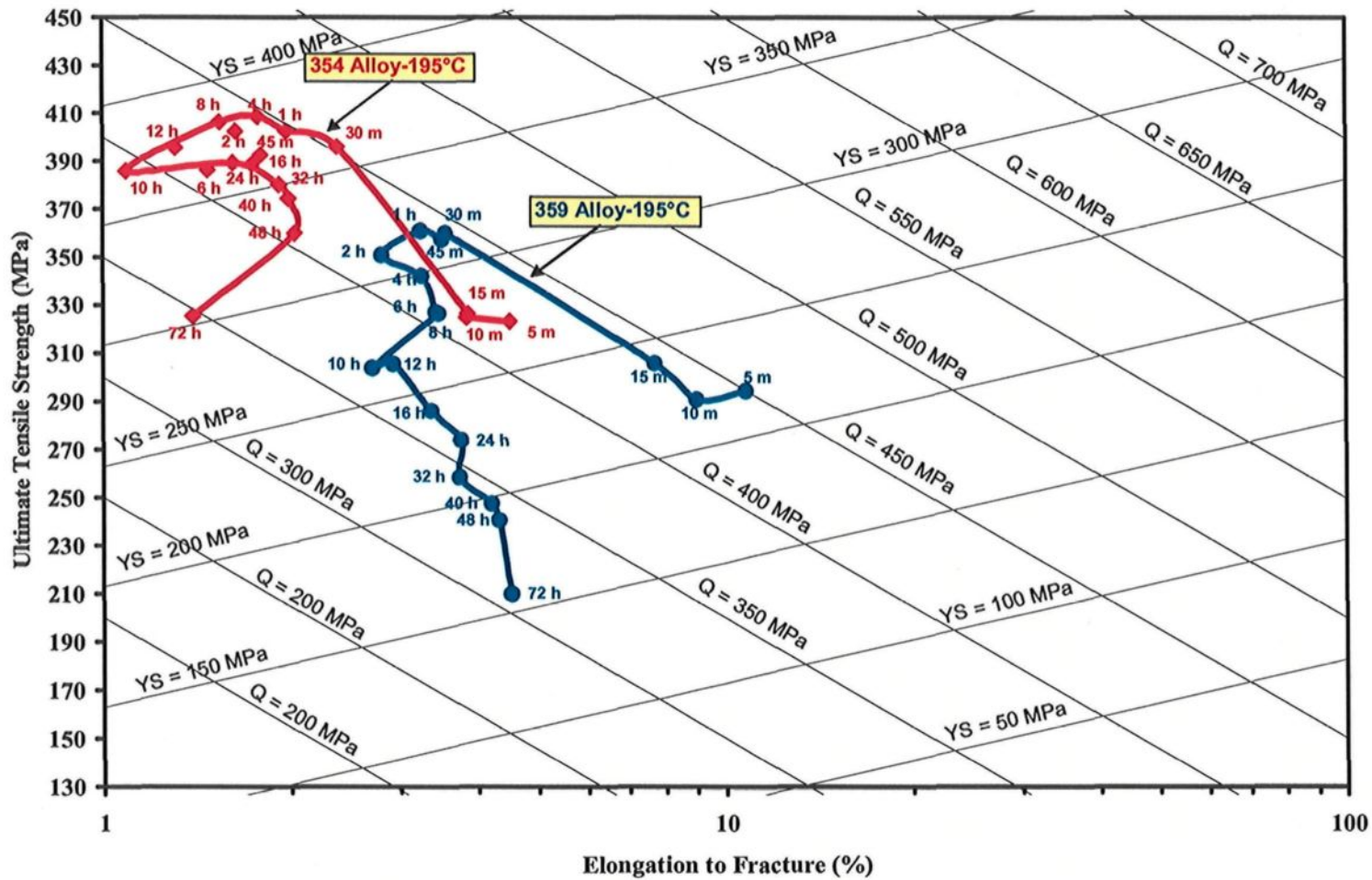
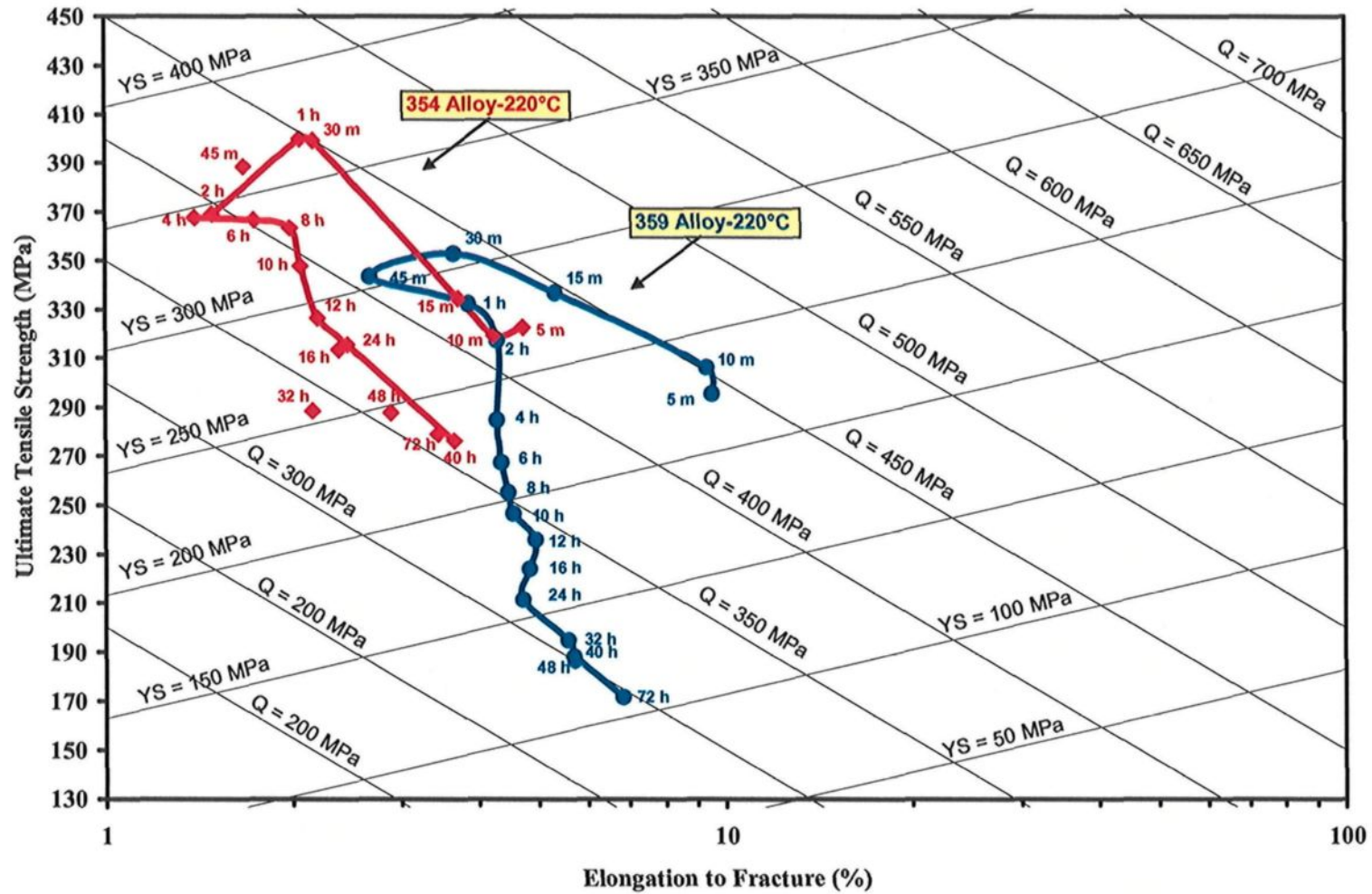


Figure 5.15. Quality chart generated using Equations 1 and 2 to compare the strength and quality of the 354 and 359 alloys or 10N and 1N castings, respectively, aged at 195°C for time durations of 5 minutes - 72 hours, as labeled on the curves.



**Figure 5.16.** Quality chart generated using Equations 1 and 2 to compare the strength and quality of the 354 and 359 alloys or 10N and 1N castings, respectively, aged at 220°C for time durations of 5 minutes - 72 hours, as labeled on the curves.

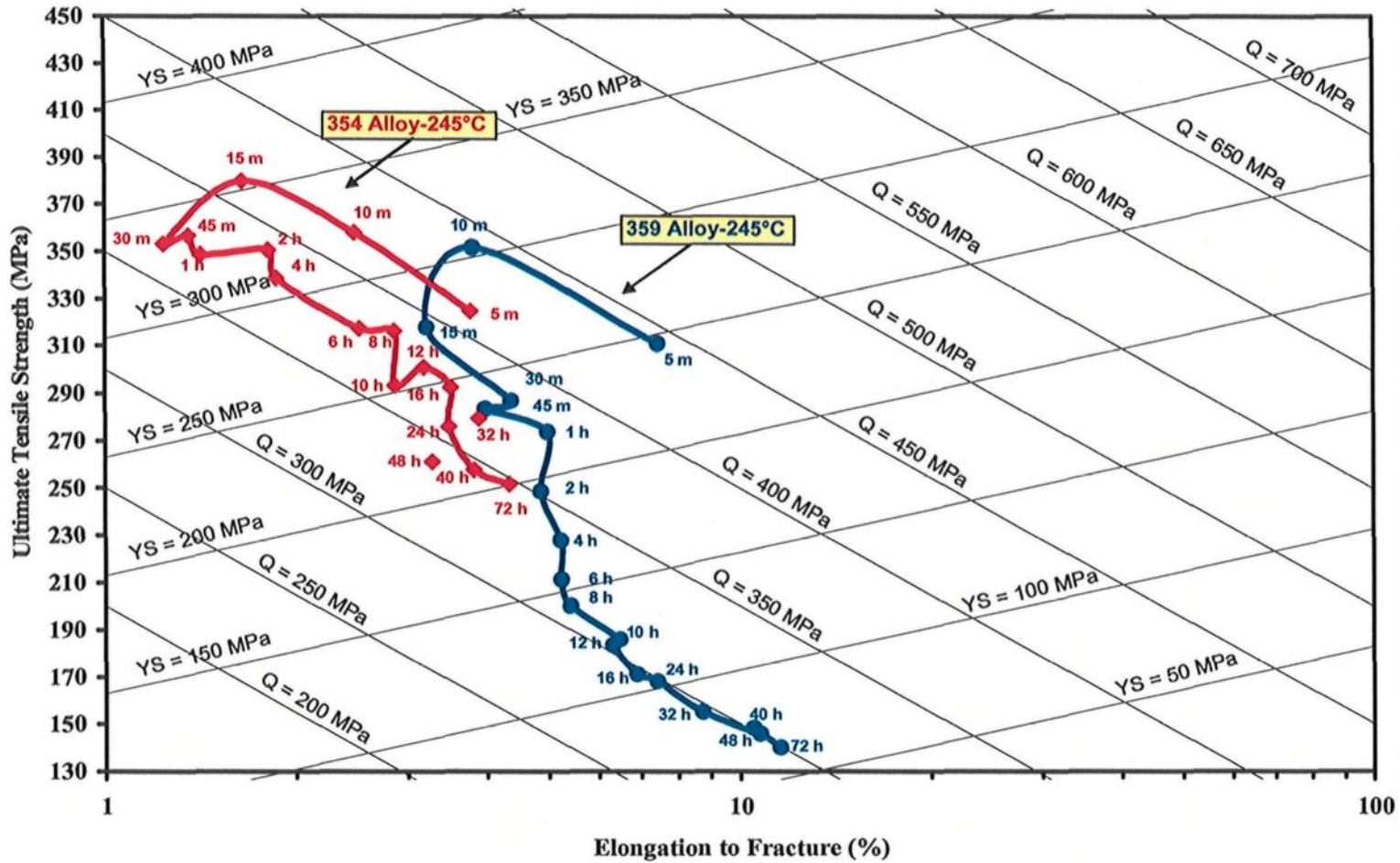


Figure 5.17. Quality chart generated using Equations 1 and 2 to compare the strength and quality of the 354 and 359 alloys or 10N and 1N castings, respectively, aged at 245°C for time durations of 5 minutes - 72 hours, as labeled on the curves.

## **CHAPTER 6**

### **CONCLUSIONS AND RECOMMENDATIONS**

## CHAPTER 6

### 6. CONCLUSIONS AND RECOMMENDATIONS

The current study was carried out with a view to investigating the influence of a number of metallurgical parameters on the tensile properties and quality indices of two high strength Al-9%Si casting alloys, namely, 354-Al-9%Si-1.8%Cu-0.5%Mg and 359-Al-9%Si-0.5%Mg. The variables investigated include iron level; copper content; magnesium level; strontium content; solidification rate; solution heat treatment temperatures; solution heat treatment times; aging temperatures; and aging times. Quality charts were used as an evaluation tool for selecting the optimum conditions to be applied in practice in order to develop high strength and optimum quality in 354 and 359 castings. From the analysis of the results obtained, the following may be concluded:

1. The addition of iron has deleterious effects on both the strength and the quality of the 354- and the 359-type castings. Such effects are related to the size and morphology of the iron-containing phases, specifically,  $\beta$ -Al<sub>5</sub>FeSi and  $\pi$ -Al<sub>8</sub>Mg<sub>3</sub>FeSi<sub>6</sub> formed in these alloys.
2. Minimum iron-content is always recommended in the production of the 354 and 359 casting alloys. With regard to the castings which contain high iron-levels, appropriate solution heat treatment procedures may partially neutralize the deleterious effects of the iron-bearing phases.

3. The addition of copper to 359-type alloys plays a significant role in improving the strength of these alloys; this improvement occurs, however, at the expense of ductility and therefore has only a slight effect on the quality index of these castings.
4. The addition of up to 0.6% Mg to 359-type alloys has a significant influence on their strength without affecting their quality. Magnesium levels above 0.6% result in a slight increase in the alloy strength with a noticeable reduction in the ductility and quality index value. This reduction is attributed to the formation of a large volume fraction of  $\pi$ -Al<sub>3</sub>Mg<sub>3</sub>FeSi<sub>6</sub> phase, the particles of which have a propensity for crack initiation, thus accelerating the fracture of the sample.
5. When adding the hardening elements Cu and Mg to 359 alloy, the quality index of the alloy castings will be affected in accordance with the net amount by which the strength is increased and the ductility is reduced.
6. A rapid solidification rate enhances the tensile properties and quality indices of both 354- and the 359-type casting alloys. Such enhanced properties and indices are related to a number of microstructural features which accompany the high solidification rate, including refinement of the SDAS; modification of eutectic silicon particles; reduced size and levels of porosity; and reduced size and volume fractions of the intermetallic phases.
7. An increase in the solutionizing temperature further improves the strength and quality of the castings. In accordance with these findings, a maximum safe solutionizing temperature of 520°C and 537°C is recommended for heat treating 354- and 359-type castings, respectively, to produce superior strength and optimum quality.

8. Solutionizing treatment at these temperatures is observed to bring about a number of improvements in the microstructure by which the strength and the quality are greatly enhanced. The solutionizing treatment was observed to accomplish the following: (i) to produce a partial neutralization of the deleterious effects of iron by improving the size and morphology of the Fe-containing phases; (ii) to maximize the copper concentration in solid solution through the complete dissolution of the  $\text{Al}_2\text{Cu}$  phase; the same process is also expected to occur for Mg through complete dissolution of the  $\text{Mg}_2\text{Si}$  phase; and (iii) to produce significant changes in the eutectic silicon particle characteristics, particularly a reduction in the aspect ratio.
9. Solutionizing treatment applied to 354 alloys is considered to be a critical process because of the low melting point of the  $\text{Al}_2\text{Cu}$  phases present in the alloy. Increasing the solutionizing temperature to over  $525^\circ\text{C}$  results in a sharp reduction in the tensile properties and quality index values of these alloys due to the incipient melting of the ternary eutectic structure  $\alpha$  (Al)-Si- $\text{Al}_2\text{Cu}$  and the formation of high levels of shrinkage porosity after quenching.
10. As a consequence of the incipient melting, the silicon particle morphology is observed to change to polygonal type during the liquid state of the ternary eutectic structure  $\alpha$  (Al)-Si- $\text{Al}_2\text{Cu}$ , which may also contribute to the degradation in properties of the 354 alloys at solution temperatures above  $525^\circ\text{C}$ .
11. An increase in the solution heat treatment time further enhances the tensile properties and the quality index values of the 354 and the 359 alloys. Twelve hours was the time judged most suitable for optimum solution heat treatment of these alloys.

12. The solution heat treatment time required to attain specific tensile properties and quality index values in the unmodified 354 and 359 alloys may be shortened by modifying these alloys with strontium.
13. The effects of Sr-addition on the response of the 354 and 359 alloys to solutionizing treatment diminish upon increasing the solution heat treatment time as, after a certain length of time, both modified and unmodified alloys display almost the same properties for the subsequent solutionizing time.
14. Aging treatment of 354- and 359-type castings produces a wide range of tensile properties and quality index values based on the aging temperatures and times applied to these castings. Depending on the required tensile properties, suitable aging conditions may be recommended based on the best possible compromise between strength, quality, and the aging time involved in the process.
15. Aging at a low temperature of 155°C was observed to produce the greatest strength and optimum quality in both 354- and 359-type castings compared to aging at higher temperatures.
16. The peak-strength observed for 354 and 359 alloys may be attained after shorter aging times on condition that the aging temperature is increased. The aging times required for reaching peak-strength in 354 alloys are 72 hours, 40 hours, 8 hours, 1 hour, and 15 minutes at aging temperatures of 155°C, 170°C, 195°C, 220°C, and 245°C, respectively.
17. The 359 alloys reach peak-strength more rapidly than the 354 alloys at all the aging temperatures studied. The aging times required for reaching peak-strength in 359

alloys are 32 hours, 24 hours, 1 hour, 30 minutes, and 10 minutes, at aging temperatures of 155°C, 170°C, 195°C, 220°C, and 245°C, respectively.

18. Aging treatment at higher temperatures is accompanied by a reduction in the tensile properties and quality index values of the castings; however, it also introduces the possibility of a significant economical strategy for minimizing the time and the cost of this same treatment.
19. Aging treatment at a lower temperature of 155°C produces fine and dense precipitates having a smaller inter-particle spacing, while at higher aging temperatures, such as 245°C, the precipitates are coarser in size, less dense, and more widely dispersed.
20. The 354 alloys display higher strength levels when compared to the 359 alloys for all aging treatments applied to the two alloys. This high strength, however, is obtained at the expense of ductility, creating slight changes in the quality index values.
21. The quality charts developed in the course of the current research facilitate the interpretation and evaluation of the tensile properties of 354 and 359 alloys. Such charts provide a logical evaluation tool, from the metallurgical point of view, for an accurate predication of the influence of the various metallurgical parameters studied on these alloys.
22. Based on the quality charts developed, it is possible to make a rigorous selection as to the most suitable metallurgical parameters to be applied to the 354 and 359 alloys

so as to obtain the best possible cost-effective compromise between alloy strength and quality.

23. The generation of quality charts using Equations 1 and 2 is simpler than generating them using Equations 8 and 9, as the latter case entails a very time-consuming process. There exists, however, a complete concordance between the evaluations made using either one of these two routes.

## RECOMMENDATIONS FOR FUTURE WORK

The premium strength and superior quality of the 354- and 359-type castings demonstrated in the current study indicate that they contain much promise for successful engineering applications in the automotive, defence, and aerospace industries. According to the results obtained in this study, the following points may be explored for the purposes of providing a complete and well-established background for these two alloys.

1. Studying the influences of metallurgical parameters on the other mechanical properties of these alloys, namely, the hardness, impact, and fatigue properties. To date, there has been little research work carried out towards this end, in spite of the fact that these alloys are very promising for industrial applications and are expected to replace the two most common commercial Al-Si casting alloys namely, 319 and 356.
2. Investigating the effects of adding other alloying elements such as Ag, Zn, Ti, Zr, and Ni, as well as rare earth metals, which may contribute to a further increase in the strength of these alloys.
3. Investigating the effects of mold design on the mechanical properties and quality indices of these castings.
4. Determining the characteristics of the hardening precipitates formed during the various aging treatments applied to these alloys, using TEM techniques, to understand their effect on the alloy properties.

## REFERENCES

## REFERENCES

---

1. R.C. Lemon and C.R. Howle, "Premium Strength Aluminum Casting Alloys 354 and 359," *AFS Transactions*, Vol. 70, 1963, pp 465-470.
2. C.H. Cáceres, I.L. Svensson and J.A. Taylor, "Strength-Ductility Behaviour of Al-Si-Cu-Mg Casting Alloys in T6 Temper," *International Journal of Cast Metals Research*, Vol. 15, 2003, pp 531-543.
3. C.H. Cáceres and J.A. Taylor, "Enhanced Ductility in Al-Si-Cu-Mg Casting Alloys with High Si Content," *Metallurgical and Materials Transactions B*, Vol. 37(6), 2006, pp. 897-903.
4. Y.J. Li, S. Brusethaug and A. Olsen, "Influence of Cu on the Mechanical Properties and Precipitation Behavior of AlSi7Mg0.5 Alloy during Aging Treatment," *Scripta Materialia*, Vol. 54, 2006, pp. 99-103.
5. M. A. Moustafa, F.H. Samuel, H.W. Doty and S. Valtierra, "Effect of Mg and Cu Additions on the Microstructural Characteristics and Tensile Properties of Sr-Modified Al-Si Eutectic Alloys," *International Journal of Cast Metals Research*, Vol. 14, 2002, pp. 235-253.
6. A.L. Dons, G. Heiberg, J. Voje, J.S. Maeland, J.O. Løland and A. Prestmo, "On the Effect of Additions of Cu and Mg on the Ductility of Al-Si Foundry Alloys Cast with a Cooling Rate of Approximately 3 K/s," *Materials Science and Engineering A*, Vol. 413-414, 2005, pp. 561-566.
7. Q.G. Wang and C.H. Cáceres, "Mg Effects on the Eutectic Structure and Tensile Properties of Al-Si-Mg Alloys," *Materials Science Forum*, Vol. 242, 1997, pp. 159-164.
8. G.K. Sigworth, "The Modification of Al-Si Casting Alloys: Important Practical and Theoretical Aspects," *International Journal of Metalcasting*, Vol. 2 (2), 2008, pp. 19-40.
9. S. Hegde and K.N. Prabhu, "Modification of Eutectic Silicon in Al-Si Alloys," *Journal of Materials Science*, Vol. 43, 2008, pp. 3009-3027.
10. F. Paray and J.E. Gruzleski, "Factors to Consider in Modification," *AFS Transactions*, Vol. 102, 1994, pp. 833-842.
11. J.A. Taylor, "The Effect of Iron in Al-Si Casting Alloys," *Proceeding of the 35th Australian Foundry Institute National Conference*, Adelaide, Australia, 31 Oct - 3 Nov 2004, pp. 148-157.

- 
12. L. Lu and A.K. Dahle, "Iron-Rich Intermetallic Phases and Their Role in Casting Defect Formation in Hypoeutectic Al-Si Alloys," *Metallurgical and Materials Transactions A*, Vol. 36A, 2005, pp. 819-835.
  13. C.S. Cole and A.M. Sherman, "Lightweight Materials for Automotive Applications," *Materials Characterization*, Vol. 35 (1), 1995, pp. 3-9.
  14. W.S. Miller, L. Zhuang, J. Bottema, A.J. Wittebrood, P. De Smet, A. Haszler and A. Vieregge, "Recent Development in Aluminum Alloys for the Automotive Industry," *Materials Science and Engineering A*, Vol. 280, 2000, pp. 37-49.
  15. F. Palazzo, "The Future of Aluminum in the Automotive Industry," *Aluminio*, Vol. 46 (9), 1977, pp. 323-334.
  16. G.L. Armstrong, "Alloy Selections for Automotive Aluminum Castings," *Society of Automotive Engineers (SAE)*, Technical Paper # 780249, 1978.
  17. A.T. Spada, "In Search of Light-Weight Components: Automotive's Cast Aluminum Conversion," *Engineered Casting Solutions*, Vol. 4 (2), 2002, pp. 28-31.
  18. J-P. Immarigeon, R.T. Holt, A.K. Koul, L. Zhao, W. Wallace and J.C. Beddoes, "Lightweight Materials for Aircraft Applications," *Materials Characterization*, Vol. 35 (1), 1995, pp. 41-67.
  19. I.N. Fridlyander, "Aluminum Alloys in Aircraft in the Periods of 1970-2000 and 2001-2015," *Metal Science and Heat Treatment*, Vol. 43 (1-2), 2001, pp. 6-10.
  20. I.N. Fridlyander, V.G. Sister, O.E. Grushko, V.V. Berstenev, L.M. Sheveleva and L.A. Ivanova, "Aluminum Alloys: Promising Materials in the Automotive Industry," *Metal Science and Heat Treatment*, Vol. 44 (9-10), 2002, pp. 365-370.
  21. [http://www.alcoa.com/car\\_truck/en/pdf/Ducker\\_Webinar\\_Presentation\\_Final.pdf](http://www.alcoa.com/car_truck/en/pdf/Ducker_Webinar_Presentation_Final.pdf)
  22. <http://www.autoaluminum.org/downloads/DuckerInternationalFinalReport2009II.pdf>
  23. J.R. Davis, *Aluminum and Aluminum Alloys*, ASM Specialty Handbook, ASM International, Materials Park, OH, U.S.A., 1993.
  24. J.G. Kaufman and E.L. Rooy, *Aluminum Alloy Castings: Properties, Processing, and Applications*, ASM International, Materials Park, Ohio, U.S.A., 2004.

- 
25. J.E. Hatch, *Aluminum: Properties and Physical Metallurgy*, American Society for Metals, Metals Park, OH, U.S.A., 1984.
  26. *ASM Handbook Vol. 2, "Properties and Selection: Nonferrous Alloys and Special-Purpose Materials,"* ASM International, Materials Information Society, U.S.A., 1990.
  27. J.E. Gruzleski and B.M. Closset, *The Treatment of Liquid Aluminum-Silicon Alloys*, American Foundrymen's Society, Inc., Des Plaines, IL, U.S.A., 1990.
  28. L. Heusler and W. Schneider, "Influence of Alloying Elements on the Thermal Analysis Results of Al-Si Cast Alloys," *Journal of Light Metals*, Vol. 2, 2002, pp. 17-26.
  29. L. Lu, K. Nogita and A.K. Dahle, "Combining Sr and Na Additions in Hypoeutectic Al-Si Foundry Alloys," *Materials Science and Engineering A*, Vol. 399, 2005, pp. 244-253.
  30. L. Lu, and A.K. Dahle, "Effects of Combined Additions of Sr and AlTiB Grain Refiners in Hypoeutectic Al-Si Foundry Alloys," *Materials Science and Engineering A*, Vol. 435-436, 2006, pp. 288-296.
  31. L. Bäckerud, G. Chai and J. Tamminen, *Solidification Characteristics of Aluminum Alloys, Vol. 2 Foundry Alloys*, AFS/Skanaluminium, Des Plaines, IL, U.S.A., 1990.
  32. M. Warmuzek, *Aluminum-Silicon Casting Alloys: Atlas of Microfractographs*, ASM International, Materials Park, OH, U.S.A., 2004.
  33. J. Asesio-Lozano and B. Suarez-Peña, "Effect of the Addition of Refiners and/or Modifiers on the Microstructure of Die Cast Al-12Si Alloys," *Scripta Materialia*, Vol. 54, 2006, pp. 943-947.
  34. J.L. Jorstad, "Hypereutectic Al-Si Casting Alloys: 25 Years, What's Next," *AFS Transactions*, Vol. 104, 1996, pp. 669-671.
  35. J. Li, M. Elmadagli, V.Y. Gertsman, J. Lo and A.T. Alpas, "FIB and TEM Characterization of Subsurfaces of an Al-Si Alloy (A390) Subjected to Sliding Wear," *Materials Science and Engineering A*, Vol. 421, 2006, pp. 317-327.
  36. M. Zuo, X. Liu and Q. Sun, "Effects of Processing Parameters on the Refinement of Primary Si in A390 Alloys with A New Al-Si-P Master Alloy," *Journal of Materials Science*, Vol. 44, 2009, pp. 1952-1958.

- 
37. V.C. Srivastava, R.K. Mandal and S.N. Ojha, "Evolution of Microstructure in Spray Formed Al-18%Si Alloy," *Materials Science and Engineering A*, Vol. 383, 2004, pp. 14-20.
  38. A.-S. Lee, "A Study on the Economics of Hypereutectic Aluminum-Silicon (Al-Si) Alloy Machining," *International Journal of Advanced Manufacturing Technology*, Vol. 16, 2000, pp. 700-708.
  39. J.G. Kaufman, *Properties of Aluminum Alloys: Tensile, Creep, and Fatigue Data at High and Low Temperatures*, ASM International, Materials Park, OH, U.S.A., 1999.
  40. J.L. Jorstad, W.M. Rasmussen and D.L. Zalenskas, *Aluminum Casting Technology*, Second Edition, The American Foundrymen's Society, Inc., Des Plaines, IL, U.S.A., 1993.
  41. M. Drouzy, S. Jacob and M. Richard, "Interpretation of Tensile Results by Means of Quality Index and Probable Yield Strength," *AFS International Cast Metals Journal*, Vol. 5, 1980, pp. 43-50.
  42. S. Jacob, "Quality Index in Predicting of Properties of Aluminum Castings-A Review," *AFS Transactions*, Vol. 108, 2000, pp. 811-818.
  43. T. Din, A.K.M.B. Rashid and J. Campbell, "High Strength Aerospace Casting Alloys: Quality Factor Assessment," *Materials Science and Technology*, Vol. 12, 1996, pp. 269-273.
  44. C.H. Cáceres, "A Rationale for the Quality Index of Al-Si-Mg Casting Alloys," *International Journal of Cast Metals Research*, Vol. 10, 1998, pp. 293-299.
  45. C.H. Cáceres, "A Phenomenological Approach to the Quality Index of Al-Si-Mg Casting Alloys," *International Journal of Cast Metals Research*, Vol. 12, 2000, pp. 367-375.
  46. G.E. Dieter, *Mechanical Metallurgy: Third Edition*, McGraw-Hill, New York, 1986.
  47. J.R. Davis, *Tensile Testing: Second Edition*, ASM International, Materials Park, OH, U.S.A., 2004.
  48. C.H. Cáceres, "Microstructure Design and Heat Treatment Selection for Casting Alloys Using the Quality Index," *Journal of Materials Engineering and Performance*, Vol. 9 (2), 2000, pp. 215-221.

- 
49. C.H. Cáceres, "Particle Cracking Damage and Quality Index of Al-Si-Mg Casting Alloys," *AFS Transactions*, Vol. 108, 2000, pp. 709-712.
  50. C.H. Cáceres and J. Barresi, "Selection of Temper and Mg Content to Optimize the Quality Index of Al-7Si-Mg Casting Alloys," *International Journal of Cast Metals Research*, Vol. 12, 2000, pp. 377-384.
  51. C.H. Cáceres, J.H. Sokolowski and P. Gallo, "Effect of Aging and Mg Content on the Quality Index of Two Model Al-Cu-Si-Mg Alloys," *Materials Science and Engineering A*, Vol. 271, 1999, pp. 53-61.
  52. C.H. Cáceres, M. Makhlof, D. Apelian and L. Wang, "Quality Index Chart for Different Alloys and Temperatures: A Case Study on Aluminum Die-Casting Alloys," *Journal of Light Metals*, Vol. 1, 2001, pp. 51-59.
  53. C.H. Cáceres, T. Din, A.K.M.B. Rashid and J. Campbell, "Effect of Aging on Quality Index of an Al-Cu Casting Alloy," *Materials Science and Technology*, Vol. 15 (6), 1999, pp. 711-716.
  54. C.H. Cáceres, L. Wang, D. Apelian and M. Makhlof "Alloy Selection for Die Castings Using the Quality Index," *AFS Transactions*, Vol. 107, 1999, pp. 239-247.
  55. C.H. Cáceres, I.L. Svensson and J.A. Taylor, "Microstructural Factors and the Mechanical Performance of Al-Si-Mg and Al-Si-Cu-Mg Casting Alloys," *Proceedings of the 2<sup>nd</sup> International Aluminum Casting Technology Symposium*, ASM International, Columbus, OH, U.S.A., 7-9 October, 2002, pp. 427-434.
  56. N.D. Alexopoulos and S.G. Pantelakis, "A New Quality Index for Characterizing Aluminum Cast Alloys with Regard to Aircraft Structure Design Requirements," *Metallurgical and Materials Transactions A*, Vol. 35A, 2004, pp. 301-308.
  57. N.D. Alexopoulos and S.G. Pantelakis, "Quality Assessment of Artificially Aged A357 Aluminum Alloy Cast Ingots by Introducing Approximate Expressions of the Quality Index  $Q_D$ ," *Metallurgical and Materials Transactions A*, Vol. 35A, 2004, pp. 3079-3089.
  58. N.D. Alexopoulos and S.G. Pantelakis "Evaluation of the Effects of Variations in Chemical Composition on the Quality of Al-Si-Mg, Al-Cu, and Al-Zn-Mg Cast Aluminum Alloys," *Journal of Materials Engineering and Performance*, Vol. 12 (2), 2003, pp. 196-205.

- 
59. N.D. Alexopoulos and S.G. Pantelakis, "Quality Evaluation of A357 Cast Aluminum Alloy Specimens Subjected to Different Artificial Aging Treatment," *Materials and Design*, Vol. 25, 2004, pp. 419-430.
  60. N.D. Alexopoulos, "Definition of Quality in Cast Aluminum Alloys and Its Characterization with Appropriate Indices," *Journal of Materials Engineering and Performance*, Vol. 15 (1), 2006, pp. 59-66.
  61. N.D. Alexopoulos, "Generation of Quality Maps to Support Material Selection by Exploiting the Quality Indices Concept of Cast Aluminum Alloys," *Materials and Design*, Vol. 28, 2007, pp. 534-543.
  62. M. Tiryakioğlu, J.T. Staley and J. Campbell, "Evaluating Structural Integrity of Cast Al-7%Si-Mg Alloys Via Work Hardening Characteristics: II. A New Quality Index," *Materials Science and Engineering A*, Vol. 368, 2004, pp. 231-238.
  63. H.R. Ammar, C. Moreau, A.M. Samuel, F.H. Samuel and H.W. Doty "Influences of Alloying Elements, Solution Treatment Time and Quenching Media on Quality Indices of 413-Type Al-Si Casting Alloys," *Materials Science and Engineering A*, Vol. 489 (1-2), 2008, pp. 426-438.
  64. H.R. Ammar, C. Moreau, A.M. Samuel, F.H. Samuel and H.W. Doty, "Effects of Aging Parameters on the Quality of 413-Type Commercial Alloys," *Materials & Design*, Vol. 30 (4), 2009, pp. 1014-1025.
  65. H.R. Ammar, F.H. Samuel, A.M. Samuel, G.K. Sigworth and J.C. Lin, "Developing Superior Strength and Optimum Quality in Al-9%Si-0.5%Mg Casting Alloys for Structural Applications," *AFS Transactions*, Vol. 117, 2009, pp. 149-168.
  66. H.R. Ammar, F.H. Samuel, A.M. Samuel, G.K. Sigworth and J.C. Lin, "Appropriate Heat Treatment Procedures for Improving Strength and Quality in 354-Type Casting Alloys," *AFS Transactions*, Vol. 118, 2010, in Press.
  67. T.O. Mbuya, B.O. Odera and S.P. Ng'ang'a, "Influence of Iron on Castability and Properties of Aluminum Silicon Alloys: Literature Review," *International Journal of Cast Metals Research*, Vol. 16 (5), 2003, pp. 451-465.
  68. L.F. Mondolfo, "*Aluminium Alloys: Structure and Properties*," Butterworths, London, 1976.
  69. L. Wang, M. Makhlof and D. Apelian, "Aluminum Die Casting Alloys: Alloy Composition, Microstructure, and Properties - Performance Relationships," *International Materials Reviews*, Vol. 40 (6), 1995, pp. 221-238.

- 
70. P.N. Crepeau, "Effect of Iron in Al-Si Casting Alloys: A Critical Review," *AFS Transactions*, Vol. 103, 1995, pp. 361-366.
  71. A. Couture, "Iron in Aluminum Casting Alloys - A Literature Survey," *AFS International Cast Metals Journal*, Vol. 6, 1981, pp. 9-17.
  72. G.K. Sigworth, "Controlling Tensile Strength in Aluminum Castings," Special Communication, 2006.
  73. G.K. Sigworth and C.H. Cáceres, "Quality Issues in Aluminum Net Shape Castings," *AFS Transactions*, Vol. 112, 2004, pp. 1-15.
  74. G.K. Sigworth, "Aluminum Casting Alloys," Special Communication, 2008.
  75. Y-H. Cho, Y-R. Im, S-W. Kwon, and H-C. Lee, "The Effect of Alloying Elements on the Microstructure and Mechanical Properties of Al-12Si Cast Alloys," *Materials Science Forum*, Vol. 426-432, 2003, pp. 339-344.
  76. M. Zeren, "Effect of Copper and Silicon Content on Mechanical Properties in Al-Cu-Si-Mg Alloys," *Journal of Materials Processing Technology*, Vol. 169, 2005, pp. 292-298.
  77. S.G. Shabestari and F. Shahri, "Influences of Modification, Solidification Conditions and Heat Treatment on the Microstructure and Mechanical Properties of A356 Aluminum Alloy," *Journal of Materials Science*, Vol. 39, 2004, pp. 2023-2032.
  78. M.M. Haque, "Effects of Strontium on the Structure and Properties of Aluminum-Silicon Alloys," *Journal of Materials Processing Technology*, Vol. 55, 1995, pp. 193-198.
  79. H. Liao, Y. Sun and G. Sun, "Correlation between Mechanical Properties and Amount of Dendritic  $\alpha$ -Al Phase in As-Cast Near-Eutectic Al-11.6% Si Alloys Modified with Strontium," *Materials Science and Engineering A*, Vol. 335, 2002, pp. 62-66.
  80. Suárez-Peña and J. Asesio-Lozano, "Microstructure and Mechanical Property Developments in Al-12Si Gravity Die Castings after Ti and/or Sr Additions," *Materials Characterization*, Vol. 57, 2006, pp. 218-226.

- 
81. R.W. Smith, "Modification of Aluminum Silicon Alloys," *Proceedings of the Conference on Solidification of Metals*, Iron and Steel Institute, Brighton, London, U.K., 1967, pp. 224-236.
  82. S-Z Lu and A. Hellawell, "The Mechanism of Silicon Modification in Aluminum-Silicon Alloys: Impurity Induced Twinning," *Metallurgical Transactions A*, Vol. 18A, 1987, pp. 1721-1733.
  83. S-Z Lu and A. Hellawell, "Modification and Refinement of Cast Al-Si Alloys," *Light Metals*, 1995, pp. 989-993.
  84. J.E. Gruzleski, "The Art and Science of Modification: 25 Years of Progress," *AFS Transactions*, Vol. 100, 1992, pp. 673-683.
  85. G. Chai and L. Bäckerud, "Factors Affecting Modification of Al-Si Alloys by Adding Sr-Containing Master Alloys," *AFS Transactions*, Vol. 100, 1992, pp. 847-854.
  86. P.B. Crosley and L.F. Mondolfo, "The Modification of Aluminum Silicon Alloys," *Modern Casting*, Vol. 49, 1966, pp. 89-100.
  87. H.J. Li, S. Shivkumar, X.J. Luo and D. Apelian, "Influence of Modification on the Solution Heat-Treatment Response of Cast Al-Si-Mg Alloys," *Cast Metals*, Vol. 1 (4), 1989, pp. 227-234.
  88. S. Shivkumar, S. Ricci, Jr., B. Steenhoff, D. Apelian and G. Sigworth, "An Experimental Study to Optimize the Heat Treatment of A356 Alloy," *AFS Transactions*, Vol. 97, 1989, pp. 791-810.
  89. B. Closset and J.E. Gruzleski, "Structure and Properties of Hypoeutectic Al-Si-Mg Alloys Modified with Pure Strontium," *Metallurgical Transactions A*, Vol. 13A, 1982, pp. 945-951.
  90. R. DasGupta, C.G. Brown and S. Marek, "Analysis of Overmodified 356 Aluminum Alloys," *AFS Transactions*, Vol. 96, 1988, pp. 297-310.
  91. J.M. Boileau, J.W. Zindel and J.E. Allison, "The Effect of Solidification Time on the Mechanical Properties in a Cast A356-T6 Aluminum Alloy," *SAE Transactions*, Vol. 106 (5), 1997, pp. 63-74.
  92. K.J. Oswalt and M.S. Misra, "Dendrite Arm Spacing (DAS): A Nondestructive Test to Evaluate Tensile Properties of Premium Quality Aluminum Alloy (Al-Si-Mg) Castings," *AFS Transactions*, Vol. 88, 1980, pp. 845-862.

- 
93. J.A. Taylor, D.H. StJohn and M.J. Couper, "Solution Treatment Effects in Al-Si-Mg Casting Alloys: Part II: Solid Solution Chemistry," *Aluminum Transactions*, Vol. 4-5, 2001, pp. 111-124.
  94. S. Shivkumar, S. Ricci, Jr. and D. Apelian, "Influence of Solution Parameters and Simplified Supersaturation Treatments on Tensile Properties of A356 Alloy," *AFS Transactions*, Vol. 98, 1990, pp. 913-992.
  95. D. Emadi, L.V. Whiting, M. Sahoo, J.H. Sokolowski, P. Burke and M. Hart, "Optimal Heat Treatment of A356.2 Alloy," *Proceedings of the 132<sup>th</sup> TMS Annual Conference, Light Metals 2003*, The Mineral, Metals & Materials Society, San Diego, CA, USA, 2003, pp. 983-989.
  96. S. Shivkumar, S. Ricci, Jr., C. Keller and D. Apelian, "Effect of Solution Treatment Parameters on Tensile Properties of Cast Aluminum Alloys," *Journal of Heat Treating*, Vol. 8 (1), 1990, pp. 63-70.
  97. P-S. Wang, S-L. Lee, J-C. Lin and M-T. Jahn, "Effects of Solution Temperatures on Mechanical Properties of 319.0 Aluminum Casting Alloys Containing Trace Beryllium," *Journal of Materials Research*, Vol. 15 (9), 2000, pp. 2027-2035.
  98. A.M. Samuel, J. Gauthier and F.H. Samuel, "Microstructural Aspects of the Dissolution and Melting of Al<sub>2</sub>Cu Phase in Al-Si Alloys during Solution Heat Treatment," *Metallurgical and Materials Transactions A*, Vol. 27A, 1996, pp. 1785-1798.
  99. R. Li, "Solution Heat Treatment of 354 and 355 Cast Alloys," *AFS Transactions*, Vol. 104, 1996, pp. 777-783.
  100. R-X. Li, R-D. Li, Y-H. Zhao and C-X. Li, "Effect of Heat Treatment on Eutectic Silicon Morphology and Mechanical Property of Al-Si-Cu-Mg Cast Alloys," *Transactions of Nonferrous Metals Society of China*, Vol. 14 (3), 2004, pp. 496-500.
  101. F.H. Samuel, "Incipient Melting of Al<sub>5</sub>Mg<sub>8</sub>Si<sub>6</sub>Cu<sub>2</sub> and Al<sub>2</sub>Cu Intermetallics in Unmodified and Strontium-Modified Al-Si-Cu-Mg (319) Alloys during Solution Heat Treatment," *Journal of Materials Science*, Vol. 33, 1998, pp. 2283-2297.
  102. H.J. Sokolowski, X-C. Sun, G. Byczynski, D.O. Northwood, D.E. Penrod, R. Thomas and A. Esseltine, "The Removal of Copper-Phase Segregation and the Subsequent Improvement in Mechanical Properties of Cast 319 Aluminum Alloys

- 
- by a Two-Stage Solution Heat Treatment," *Journal of Materials Processing Technology*, Vol. 53, 1995, pp. 385-392.
103. O. Reiso, H-G. Øverlie and N. Ryum, "Dissolution and Melting of Secondary Al<sub>2</sub>Cu Phase Particles in an AlCu Alloy," *Metallurgical and Materials Transactions A*, Vol. 12A, 1990, pp. 1689-1695.
  104. R.N. Lumley, R.G. Odonnell, D.R. Gunasegaram and M. Givord, "Heat Treatment of High-Pressure Die Castings," *Metallurgical and Materials Transactions A*, Vol. 38A, 2007, pp. 2564-2574.
  105. R.N. Lumley, R.G. Odonnell, D.R. Gunasegaram and M. Givord, "Blister Free Heat Treatment of High Pressure Die-Casting Alloys," *Materials Science Forum*, Vol. 519-521, 2006, pp. 351-358.
  106. D. Apelian, S. Shivkumar and G. Sigworth, "Fundamental Aspects of Heat Treatment of Cast Al-Si-Mg Alloys," *AFS Transactions*, Vol. 97, 1989, pp. 727-742.
  107. D.L. Zhang and L. Zheng, "The Quench Sensitivity of Cast Al-7 Wt Pct Si-0.4 Wt Pct Mg Alloy," *Metallurgical and Materials Transactions A*, Vol. 27A, 1996, pp. 3983-3991.
  108. G.E. Byczynski, W. Kierkus, D.O. Northwood, D. Penrod, J.H. Sokolowski, W.A. Esseltine, J. Oswald and R. Thomas, "The Effect of Quench Rate on Mechanical Properties of 319 Aluminum Alloy Castings," *Materials Science Forum*, Vol. 217-222, 1996, pp. 783-788.
  109. J. Man, L. Jing and S.G. Jie, "The Effects of Copper Additions on the Microstructure and Thermal Stability of an Al-Mg-Si Alloy," *Journal of Alloys and Compounds*, Vol. 437, 2007, pp. 146-150.
  110. M. Murayama, K. Hono, M. Saga and M. Kikuchi, "Atom Probe Studies on the Early Stages of Precipitation in Al-Mg-Si Alloys," *Materials Science and Engineering A*, Vol. 250, 1998, pp. 127-132.
  111. L. Zhen, W.D. Fei, S.B. Kang and H.W. Kim, "Precipitation Behaviour of Al-Mg-Si Alloys with High Silicon Content," *Journal of Materials Science*, Vol. 32, 1997, pp. 1895-1902.
  112. W.F. Miao and D.E. Laughlin, "Precipitation Hardening in Aluminum Alloy 6022," *Scripta Materialia*, Vol. 40 (7), 1999, pp. 873-878.

- 
113. D.G. Eskin, "Decomposition of Supersaturated Solid Solutions in Al-Cu-Mg-Si Alloys," *Journal of Materials Science*, Vol. 38, 2003, pp. 279-290.
  114. S.K. Son, M. Takeda, M. Mitome, Y. Bando and T. Endo, "Precipitation Behaviour of an Al-Cu Alloy during Isothermal Aging at Low Temperatures," *Materials Letters*, Vol. 75, 2005, pp. 629-632.
  115. S.P. Ringer and K. Hono, "Microstructural Evolution and Age Hardening in Aluminum Alloys: Atom Probe Field-Ion Microscopy and Transmission Electron Microscopy Studies," *Materials Characterization*, Vol. 44, 2000, pp. 101-131.
  116. S.J. Andersen, C.D. Marioara, R. Vissers, A. Frøseth and H.W. Zandbergen, "The Structural Relation Between Precipitates in Al-Mg-Si Alloys, the Al-Matrix and Diamond Silicon, With Emphasis on the Trigonal Phase U1-MgAl<sub>2</sub>Si<sub>2</sub>," *Materials Science and Engineering A*, Vol. 444, 2007, pp. 157-169.
  117. C.D. Marioara, S.J. Andersen, J. Jansen and H.W. Zandbergen, "Atomic Model for GP-Zones in A 6082 Al-Mg-Si System," *Acta Materialia*, Vol. 49, 2001, pp. 321-328.
  118. R. Vissers, M.A. Van Huis, J. Jansen, H.W. Zandbergen, C.D. Marioara and S.J. Andersen, "The Crystal Structure of the  $\beta'$  Phase in Al-Mg-Si Alloys," *Acta Materialia*, Vol. 55, 2007, pp. 3815-3823.
  119. S.J. Andersen, C.D. Marioara, A. Frøseth, R. Vissers and H.W. Zandbergen, "Crystal Structure of the Orthorhombic U2-Al<sub>4</sub>Mg<sub>4</sub>Si<sub>4</sub> Precipitate in the Al-Mg-Si Alloy System and Its Relation to the  $\beta'$  and  $\beta$ " Phases," *Materials Science and Engineering A*, Vol. 390, 2005, pp. 127-138.
  120. G.E. Totten and D.S. Mackenzie, "*Handbook of Aluminum, Vol. 1: Physical Metallurgy and Processes*," Marcel Dekker, NY, U.S.A., 2003.
  121. S.C. Wang, M.J. Starink and N. Gao, "Precipitation Hardening in Al-Cu-Mg Alloys Revisited," *Scripta Materialia*, Vol. 54, 2006, pp. 287-291.
  122. P. Ratchev, B. Verlinden, P. De Smet and P. Van Houtte, "Effect of Cooling Rate and Predeformation on the Precipitation Hardening of an Al-4.2wt.%Mg-0.6wt.%Cu Alloy," *Scripta Materialia*, Vol. 38 (8), 1998, pp. 1195-1201.
  123. A. Charai, T. Walther, C. Alfonso, A.-M. Zahra and C.Y. Zahra, "Coexistence of Clusters, GPB Zones, S"-, S'- and S-Phases in an Al-0.9%Cu-1.7%Mg Alloy," *Acta Materialia*, Vol. 48, 2000, pp. 2751-2764.

- 
124. P. Ratchev, B. Verlinden, P. De Smet and P. Van Houtte, "Precipitation Hardening of an Al-4.2wt.%Mg-0.6wt.%Cu Alloy," *Acta Materialia*, Vol. 46 (10), 1998, pp. 3523-3533.
  125. S.P. Ringer, B.T. Sofyan, K.S. Prasad and G.C. Quan, "Precipitation Reactions in Al-4.0Cu-0.3Mg (wt.%) Alloy," *Acta Materialia*, Vol. 56, 2008, pp. 2147-2160.
  126. D.J. Chakrabarti and D.E. Laughlin, "Phase Relations and Precipitation in Al-Mg-Si Alloys with Cu Additions," *Progress in Materials Science*, Vol. 49, 2004, pp. 389-410.
  127. C. Cayron and P.A. Buffat, "Transmission Electron Microscopy Study of the  $\beta'$  Phase (Al-Mg-Si Alloys) and QC Phase (Al-Cu-Mg-Si Alloys): Ordering Mechanism and Crystallographic Structure," *Acta Materialia*, Vol. 48, 2000, pp. 2639-2653.
  128. C. Wolverton, "Crystal Structure and Stability of Complex Precipitate Phases in Al-Cu-Mg-(Si) and Al-Zn-Mg Alloys," *Acta Materialia*, Vol. 49, 2001, pp. 3129-3142.
  129. C. Cayron, L. Sagalowicz, O. Beffort and P.A. Buffat, "Structural Phase Transition in Al-Cu-Mg-Si Alloys by Transmission Electron Microscopy Study on an Al-4wt%Cu-1wt%Mg-Ag Alloy Reinforced by SiC Particles," *Philosophical Magazine A*, Vol. 79 (11), 1999, pp. 2833-2851.
  130. I.J. Polmear, "Role of Age Hardening in Modern Aluminum Alloys," *Proceedings of the Third International Conference on Aluminum Alloys: ICAA3*, The Norwegian Institute of Technology, Trondheim, Norway, 1992, pp. 371-384.
  131. T. Gladman, "Precipitation Hardening in Metals," *Materials Science and Technology*, Vol. 15 (1), 1999, pp. 30-36.
  132. R.E. Smallman and A.H.W. Ngan, *Physical Metallurgy and Advanced Materials*, Seventh Edition, Elsevier Ltd, Jordan Hill, Oxford, U.K., 2007.
  133. *Annual Book of ASTM Standards, Section 2: Nonferrous Metal Products, Aluminum and Magnesium Alloys*, Vol. 02.02, 2004, B108-03a.
  134. *Annual Book of ASTM Standards, Section 3: Metals Test Methods and Analytical Procedures, Metal-Mechanical Testing; Elevated and Low-Temperature Tests; Metallography*, Vol. 03.01, 2004, E8M-04.

135. L.A. Narayanan, F.H. Samuel and J.E. Gruzleski, "Dissolution of Iron Intermetallics in Al-Si Alloys through Nonequilibrium Heat Treatment," *Metallurgical and Materials Transactions A*, Vol. 26A, 1995, pp. 2161-2174.
136. E. Tillová and M. Panušková, "Effect of Solution Treatment on Intermetallic Phases Morphology in AlSi9Cu3 Cast Alloy," *Metallurgija*, Vol. 47 (3), 2008, pp. 207-210.
137. J.A. Taylor, D.H. StJohn, J. Barresi and M.J. Couper, "Influence of Mg Content on the Microstructure and Solid Solution Chemistry of Al-7%Si-Mg Casting Alloys During Solution Treatment," *Materials Science Forum*, Vol. 331-337, 2000, pp. 277-282.
138. Q.G. Wang and C.J. Davidson, "Solidification and Precipitation Behaviour of Al-Si-Mg Casting Alloys," *Journal of Materials Science*, Vol. 36, 2001, pp. 739-750.
139. G. Gustafsson, T. Thorvaldsson and G.L. Dunlop, "The Influence of Fe and Cr on the Microstructure of Cast Al-Si-Mg Alloys," *Metallurgical Transactions A*, Vol. 17A, 1986, pp. 45-52.
140. S. Shivkumar, "The Interactive Effects of Sr Modification and Heat Treatment on the Mechanical Properties of Cast Aluminum Alloys," *17th ASM Heat Treating Society Conference Proceedings Including the 1st International Induction Heat Treating Symposium*, Vol. 15-18, 1998, pp. 265-269.
141. D.L. Zhang, L.H. Zheng and D.H. StJohn, "Effect of a Short Solution Treatment Time on Microstructure and Mechanical Properties of Modified Al-7wt.%Si-0.3wt.%Mg Alloy," *Journal of Light Metals*, Vol. 2, 2002, pp. 27-36.
142. W.R. Osório, L.R. Garcia, P.R. Goulart and A. Garcia, "Effects of Eutectic Modification and T4 Heat Treatment on Mechanical Properties and Corrosion Resistance of an Al-9wt%Si Casting Alloy," *Materials Chemistry and Physics*, Vol. 106, 2007, pp. 343-349.
143. S. Murali, K.S. Raman and K.S.S. Murthy, "The Formation of  $\beta$ -FeSiAl<sub>5</sub> and Be-Fe Phases in Al-7Si-0.3Mg Alloy Containing Be," *Materials Science and Engineering A*, Vol. 190, 1995, pp. 165-172.
144. Y. Wang and Y. Xiong, "Effects of Beryllium in Al-Si-Mg-Ti Cast Alloys," *Materials Science and Engineering A*, Vol. 280, 2000, pp. 124-127.
145. M. Ravi, U.T.S. Pillai, B.C. Pai, A.D. Damodaran and E.S. Dwarakadasa, "The Effect of Mischmetal Additions on the Structure and Mechanical Properties of a

- 
- Cast Al-7Si-0.3Mg Alloy Containing Excess Iron (up to 0.6 Pct),” *Metallurgical and Materials Transactions A*, Vol. 33A, 2002, pp. 391-400.
146. X. Cao and J. Campbell, “Morphology of  $\beta$ -FeSiAl<sub>5</sub> Phase in Al-Si Cast Alloys,” *Materials Transactions*, Vol. 47 (5), 2006, pp. 1303-1312.
147. S.K. Tang and T. Sritharan, “Morphology of  $\beta$ -AlFeSi Intermetallic in Al-7Si Alloy Castings,” *Materials Science and Technology*, Vol. 14, 1998, pp. 738-742.
148. A.M. Samuel, F.H. Samuel, C. Villeneuve, H.W. Doty and S. Valtierra, “Effect of Trace Elements on  $\beta$ -Al<sub>5</sub>FeSi Characteristics, Porosity and Tensile Properties of Al-Si-Cu (319) Cast Alloys,” *International Journal of Cast Metals Research*, Vol. 14, 2001, pp. 97-120.
149. N. Roy, A.M. Samuel and F.H. Samuel, “Porosity Formation in Al-9 Wt Pct Si-3 Wt Pct Cu Alloy Systems: Metallographic Observations,” *Metallurgical and Materials Transactions A*, Vol. 27A, 1996, pp. 415-429.
150. C.M. Dinnis, J.A. Taylor and A.K. Dahle, “Iron-Related Porosity in Al-Si-(Cu) Foundry Alloys,” *Materials Science and Engineering A*, Vol. 425, 2006, pp. 286-296.
151. M.A. Moustafa, “Effect of Iron Content on the Formation of  $\beta$ -Al<sub>5</sub>FeSi and Porosity in Al-Si Eutectic Alloys,” *Journal of Materials Processing Technology*, Vol. 209 (1), 2009, pp. 605-610.
152. *ASM Handbook Vol. 8, “Mechanical Testing and Evaluation,”* The Materials Information Society, Materials Park, Ohio, U.S.A., 1990.
153. C.D. Lee, “Effects of Microporosity on Tensile Properties of A356 Aluminum Alloy,” *Materials Science and Engineering A*, Vol. 464, 2007, pp. 249-254.
154. H.G. Kang, M. Kida, H. Miyahara and K. Ogi, “Age-Hardening Characteristics of Al-Si-Cu-Base Cast Alloys,” *AFS Transactions*, Vol. 107, 1999, pp. 507-515.
155. G. Wang, Q. Sun, L. Feng, L. Hui, and C. Jing, “Influence of Cu Content on Aging Behavior of AlSiMgCu Cast Alloys,” *Materials & Design*, Vol. 28, 2007, pp. 1001-1005.
156. R.X. Li, R.D. Li, Y.H. Zhao, L.Z. He, C.X. Li, H.R. Guan and Z.Q. Hu, “Age-Hardening Behavior of Cast Al-Si Base Alloy,” *Materials Letters*, Vol. 58, 2004, pp. 2096-2101.

- 
157. W. Reif, J. Dutkiewicz, R. Ciach, S. Yu and J. Krol, "Effect of Ageing on the Evolution of Precipitates in AlSiCuMg Alloys," *Materials Science and Engineering A*, Vol. A234-236, 1997, pp. 165-168.
  158. S. Zafar, N. Ikram, M.A. Shaikh and K.A Shoaib, "Precipitation Hardening," *Journal of Materials Science*, Vol. 25 (5), 1990, pp. 2595-2597.
  159. Y-H. Cho, Y-R. Im, S-W. Kwon and H-C. Lee, "The Effect of Alloying Elements on the Microstructure and Mechanical Properties of Al-12Si Cast Alloys," *Materials Science Forum*, Vol. 426-432, 2003, pp. 339-344.
  160. J. Barresi, M.J. Kerr, H. Wang and M.J. Couper, "Effect of Magnesium, Iron and Cooling Rate on Mechanical Properties of Al-7Si-Mg Foundry Alloys," *AFS Transactions*, Vol. 108, 2000, pp. 563-570.
  161. C.H. Cáceres, C.J. Davidson, J.R. Griffiths and Q.G. Wang, "The Effect of Mg on the Microstructure and Mechanical Behavior of Al-Si-Mg Casting Alloys," *Metallurgical and Materials Transactions A*, Vol. 30A, 1999, pp. 2611-2618.
  162. C. Verdu, H. Cercueil, S. Communal, P. Sainfort and R. Fougères, "Microstructural Aspects of Cast Al-7Si-Mg Alloys," *Materials Science Forum*, Vol. 217-222, 1996, pp. 1449-1454.
  163. Q.G. Wang, C.H. Cáceres and J.R. Griffiths, "Cracking of Fe-Rich Intermetallics and Eutectic Si Particles in an Al-7Si-0.7Mg Casting Alloy," *AFS Transactions*, Vol. 106, 1998, pp. 131-136.
  164. G.E. Nagel, J.P. Mouret and J. Dubrueilh, "A357 Type Alloy with Improved Properties," *AFS Transactions*, Vol. 91, 1983, pp. 157-160.
  165. K.T. Kashyap, S. Murali, K.S. Raman and K.S.S. Murthy, "Casting and Heat Treatment Variables of Al-7Si-Mg Alloy," *Materials Science and Technology*, Vol. 9, 1993, pp. 189-203.
  166. M.M. Haque and M.A. Maleque, "Effect of Process Variables on Structure and Properties of Aluminum-Silicon Piston Alloy," *Journal of Materials Processing Technology*, Vol. 77, 1998, pp. 122-128.
  167. Q.G. Wang, "Microstructural Effects on the Tensile and Fracture Behavior of Aluminum Casting Alloys A356/357," *Metallurgical and Materials Transactions A*, Vol. 34A, 2003, pp. 2887-2899.

- 
168. A. Knuutinen, K. Nogita, S.D. McDonald and A.K. Dahle, "Modification of Al-Si Alloys with Ba, Ca, Y and Yb," *Journal of Light Metals*, Vol. 1, 2001, pp. 229-240.
  169. Q.T. Fang and P.N. Anyalebechi, "Effects of Solidification Conditions on Hydrogen Porosity Formation in Aluminum Alloy Castings," *Light Metals 1988*, The Minerals, Metals & Materials Society, Warrendale, PA, 1988, pp. 477-486.
  170. D.R. Irani and V. Kondic, "Casting and Mold Design Effects on Shrinkage Porosity of Light Alloys," *AFS Transactions*, Vol. 77, 1969, pp. 208-211.
  171. G.K. Sigworth and C.H. Cáceres, "Porosity Formation in Aluminum Alloy Castings under Quasi-Directional Solidification," *International Journal of Cast Metals Research*, Vol. 9, 1997, pp. 331-336.
  172. S.G. Shabestari and J.E. Gruzleski, "The Effect of Solidification Condition and Chemistry on the Formation and Morphology of Complex Intermetallic Compounds in Aluminum-Silicon Alloys," *Cast Metals*, Vol. 6 (4), 1994, pp. 217-224.
  173. O. Vorren, J.E. Evensen and T.B. Pedersen, "Microstructure and Mechanical Properties of AlSi(Mg) Casting Alloys," *AFS Transactions*, Vol. 92, 1984, pp. 459-466.
  174. L.A. Narayanan, F.H. Samuel and J.E. Gruzleski, "Crystallization Behavior of Iron-Containing Intermetallic Compounds in 319 Aluminum Alloy," *Metallurgical and Materials Transactions A*, Vol. 25A, 1994, pp. 1761-1773.
  175. A.N. Lakshmanan, S.G. Shabestari and J.E. Gruzleski, "Microstructure Control of Iron Intermetallics in Al-Si Casting Alloys," *Zeitschrift für Metallkunde*, Vol. 86 1995, pp. 457-464.
  176. J.A. Taylor, "Metal-Related Castability Effects in Aluminum Foundry Alloys," *Cast Metals*, Vol. 8 (4), 1995, pp. 225-252.
  177. *Aluminum Handbook, Vol. 1: Fundamentals and Materials*, First Edition, Aluminum-Verlag Marketing & Kommunikation GmbH, Germany, 1999.
  178. *ASM Handbook Vol. 4, "Heat Treating"*, ASM International, Metals Park, Ohio, U.S.A., 1991.
  179. J.H. Sokolowski, M.B. Djurdjevic, C.A. Kierkus and D.O. Northwood, "Improvements of 319 Aluminum Alloy Casting Durability by High Temperature Solution Treatment," *Journal of Materials Processing Technology*, Vol. 109, 2001, pp. 174-180.

- 
180. F. Paray and J.E. Gruzleski, "Microstructure-Mechanical Property Relationships in a 356 Alloy. Part I: Microstructure," *Cast Metals*, Vol. 7(1), 1994, pp. 29-40.
  181. Z. Li, A.M. Samuel, F.H. Samuel, C. Ravindran, S. Valtierra and H.W. Doty, "Factors Affecting Dissolution of Al<sub>2</sub>Cu Phase in 319 Alloys," *AFS Transactions*, Vol. 111, 2003, pp. 241-254.
  182. N. Crowell and S. Shivkumar, "Solution Treatment Effects in Cast Al-Si-Cu Alloys," *AFS Transactions*, Vol. 103, 1995, pp. 721-726.
  183. <http://www.eaa.net/ea/education/TALAT/lectures/1204.pdf>
  184. R.N. Lumley, I.J. Polmear and P.R. Curtis, "Rapid Heat Treatment of Aluminum High-Pressure Diecastings," *Metallurgical and Materials Transactions A*, Vol. 40A, 2009, pp. 1716-1726.
  185. G. Wang, X. Bian, X. Liu and J. Zhang, "Effect of Mg on Age Hardening and Precipitation Behavior of an AlSiCuMg Cast Alloy," *Journal of Materials Science*, Vol. 39, 2004, pp. 2535-2537.
  186. S. Esmaili, X. Wang, D.J. Lloyd and W.J. Poole, "On the Precipitation-Hardening Behavior of the Al-Mg-Si-Cu Alloy AA6111," *Metallurgical and Materials Transactions A*, Vol. 34A, 2003, pp. 751-763.
  187. S.K. Chaudhury and D. Apelian, "Fluidized Bed Heat Treatment of Cast Al-Si-Cu-Mg Alloys," *Metallurgical and Materials Transactions A*, Vol. 37A, 2006, pp. 2295-2311.
  188. N. Ryum and O. Hunderi, "Precipitates Particle Coarsening," in *Encyclopedia of Materials: Science and Technology*, 2008, pp. 7826-7835.
  189. M. Kahlweit, "Ostwald Ripening of Precipitates," *Advances in Colloid and Interface Science*, Vol. 5 (1), 1975, pp. 1-35.
  190. C.D. Marioara, S.J. Andersen, J. Jansen and H.W. Zandbergen, "The Influence of Temperature and Storage Time at RT on Nucleation of the  $\beta$ " Phases in a 6082 Al-Mg-Si Alloy," *Acta Materialia*, Vol. 51, 2003, pp. 789-796.
  191. G.A. Edwards, K. Stiller, G.L. Dunlop and M.J. Couper, "The Precipitation Sequence in Al-Mg-Si Alloys," *Acta Materialia*, Vol. 46 (11), 1998, pp. 3893-3904.

- 
192. A.K. Gupta, D.J. Lloyd and S.A. Court, "Precipitation Hardening in Al-Mg-Si Alloys with and without Excess Si," *Materials Science and Engineering A*, Vol. 316, 2001, pp. 11-17.
  193. M. Takeda, F. Ohkubo, T. Shirai and K. Fukui, "Stability of Metastable Phases and Microstructures in the Ageing Process of Al-Mg-Si Ternary Alloys," *Journal of Materials Science*, Vol. 33, 1998, pp. 2385-2390.
  194. M. Murayama and K. Hono, "Pre-Precipitate Clusters and Precipitation Processes in Al-Mg-Si Alloys," *Acta Materialia*, Vol. 47 (5), 1999, pp. 1537-1548.

## **APPENDIX**

**APPENDIX A**

**TENSILE PROPERTIES AND QUALITY INDIC**

**Table A.1.** Tensile properties and quality index values for the 359 alloys containing various levels of iron and copper, investigated in the as-cast condition and after applying two solution heat treatment temperatures for 12 h each.

Alloy Code	Solutionizing Temperature	UTS (MPa)	YS (MPa)	E <sub>F</sub> (%)	E <sub>P</sub> (%)	Q (MPa)
1S	As-Cast	194	96	4.9	4.29	297
2S		185	93	4.11	4.03	277
3S		181	95	3.32	3.09	259
4S		208	110	3.5	3.23	290
5S		206	110	3.15	3.1	281
6S		197	111	2.38	2.31	253
7S		220	128	2.62	2.24	283
8S		208	132	1.89	1.46	250
9S		199	133	1.48	1.24	225
1S	490°C	320	278	3.03	2.67	392
2S		296	260	2.5	2.31	355
3S		283	264	0.95	0.49	279
4S		327	287	1.69	1.17	361
5S		300	266	1.33	0.96	319
6S		285	275	0.86	0.43	276
7S		335	292	1.65	1.04	368
8S		324	288	1.16	0.79	334
9S		301	283	0.72	0.29	280
1S	537°C	355	304	3.84	3.34	443
2S		352	314	1.91	1.44	394
3S		349	316	1.59	1.34	380
4S		368	325	2.05	1.56	415
5S		363	329	1.5	1.2	390
6S		360	325	1.28	0.68	376
7S		370	322	1.78	1.34	408
8S		366	328	1.27	0.76	382
9S		363	332	1.12	0.68	371

UTS, YS, E<sub>F</sub>, E<sub>P</sub>, and Q refer to ultimate tensile strength, yield strength, elongation to fracture, plastic elongation to fracture, and the quality index calculated using Equation 1, respectively.

**Table A.2.** Tensile properties and quality index values for the 354 alloys containing various levels of iron, investigated in the as-cast condition and after applying ten solution heat treatment temperatures for 12 h each.

Alloy Code	Solutionizing Temperature	UTS (MPa)	YS (MPa)	E <sub>F</sub> (%)	E <sub>P</sub> (%)	Q (MPa)
10S	As-Cast	226	155	1.50	1.21	253
11S		209	152	1.19	0.81	221
12S		202	147	1.14	0.80	210
10S	490°C	359	324	1.13	0.64	367
11S		335	310	0.94	0.58	331
12S		316	297	0.78	0.36	300
10S	495°C	360	324	1.23	0.97	374
11S		353	318	1.04	0.63	356
12S		340	308	0.87	0.50	331
10S	500°C	374	314	1.43	1.02	397
11S		337	318	0.77	0.37	320
12S		336	322	0.70	0.35	313
10S	505°C	386	337	1.48	0.97	412
11S		351	320	0.86	0.48	341
12S		342	332	0.69	0.29	318
10S	510°C	383	330	1.35	0.95	403
11S		344	324	0.78	0.35	327
12S		337	318	0.74	0.34	317
10S	515°C	396	344	1.52	1.07	423
11S		358	326	0.93	0.48	353
12S		347	336	0.74	0.30	327
10S	520°C	393	341	1.49	0.84	419
11S		369	336	0.92	0.42	363
12S		362	343	0.81	0.39	348
10S	525°C	407	339	2.23	1.78	459
11S		378	341	1.02	0.72	380
12S		369	349	0.82	0.48	356
10S	530°C	339	345	0.63	0.21	309
10S	537°C	350	287	0.66	0.22	322

UTS, YS, E<sub>F</sub>, E<sub>P</sub>, and Q refer to ultimate tensile strength, yield strength, elongation to fracture, plastic elongation to fracture, and the quality index calculated using Equation 1, respectively.

**Table A.3.** Tensile properties and quality index values for the unmodified (1N) and modified (1S) 359 alloys investigated in the as-cast condition and after applying six solution heat treatment times at 537°C for each alloy.

Alloy Code	Solutionizing Time	UTS (MPa)	YS (MPa)	E <sub>F</sub> (%)	E <sub>P</sub> (%)	Q (MPa)
1N	As-Cast	180	88	3.69	3.38	265
	1 h	235	112	5.57	5.21	347
	4 h	241	111	7.26	6.93	371
	8 h	254	121	8.19	7.81	391
	12 h	264	119	10.02	9.63	415
	16 h	267	131	8.28	7.94	404
	24 h	273	138	9.03	8.51	416
1S	As-Cast	184	90	4.94	4.67	288
	1 h	253	113	10.91	10.58	409
	4 h	255	116	12.60	12.26	420
	8 h	264	124	13.21	12.66	432
	12 h	270	123	12.31	11.96	433
	16 h	273	125	13.49	13.09	443
	24 h	276	117	13.51	13.01	446

UTS, YS, E<sub>F</sub>, E<sub>P</sub>, and Q refer to ultimate tensile strength, yield strength, elongation to fracture, plastic elongation to fracture, and the quality index calculated using Equation 1, respectively.  
(Note: "h" refers to hours.)

**Table A.4.** Tensile properties and quality index values for the unmodified (10N) and modified (10S) 354 alloys investigated in the as-cast condition and after applying six solution heat treatment times at 520°C for each alloy.

Alloy Code	Solutionizing Time	UTS (MPa)	YS (MPa)	E <sub>F</sub> (%)	E <sub>P</sub> (%)	Q (MPa)
10N	As-Cast	207	123	1.74	1.46	243
	1 h	245	134	2.74	2.43	310
	4 h	276	146	4.26	3.91	371
	8 h	293	155	5.05	4.67	399
	12 h	291	150	5.81	5.42	406
	16 h	293	153	5.62	5.24	405
	24 h	314	161	7.13	6.72	442
10S	As-Cast	230	144	2.04	1.75	276
	1 h	278	149	4.78	4.42	380
	4 h	290	156	5.85	5.48	405
	8 h	300	157	6.95	6.57	427
	12 h	300	160	7.01	6.60	427
	16 h	298	158	7.14	6.74	426
	24 h	313	168	8.06	7.64	448

UTS, YS, E<sub>F</sub>, E<sub>P</sub>, and Q refer to ultimate tensile strength, yield strength, elongation to fracture, plastic elongation to fracture, and the quality index calculated using Equation 1, respectively.

(Note: "h" refers to hours.)

**Table A.5.** Tensile properties and quality index values for the 359 alloys containing various levels of magnesium.

Alloy Code	UTS (MPa)	YS (MPa)	E <sub>F</sub> (%)	E <sub>P</sub> (%)	Q (MPa)
1SM	366	309	3.99	3.52	456
2SM	377	322	3.47	3.01	458
3SM	381	343	1.88	1.64	423
4SM	381	344	1.82	1.46	420
5SM	383	343	1.77	1.32	421
6SM	385	349	1.48	1.00	410

UTS, YS, E<sub>F</sub>, E<sub>P</sub>, and Q refer to ultimate tensile strength, yield strength, elongation to fracture, plastic elongation to fracture, and the quality index calculated using Equation 1, respectively.

**Table A.6.** Tensile properties and quality index values for the 359 (1S) and 354 (10S) alloys investigated under different solidification rates.

Alloy Code	Specimen Location	UTS (MPa)	YS (MPa)	E <sub>F</sub> (%)	E <sub>P</sub> (%)	Q (MPa)
1S	Level I	344	294	5.63	4.99	456
	Level II	337	292	3.42	2.97	417
	Level III	313	282	1.53	1.25	340
10S	Level I	379	316	2.76	2.45	445
	Level II	344	305	1.36	0.95	364
	Level III	319	297	1.00	0.49	319

Level I, Level II, and Level III refer to the locations in the casting block from where the test specimens were prepared, as shown in Figure 3.3(a). UTS, YS, E<sub>F</sub>, E<sub>P</sub>, and Q refer to ultimate tensile strength, yield strength, elongation to fracture, plastic elongation to fracture, and the quality index calculated using Equation 1, respectively.

**Table A.7.** Tensile properties and quality index values for the 354 (10N) alloy after applying aging treatment at 155°C for various aging times.

<b>Aging Time</b>	<b>UTS (MPa)</b>	<b>YS (MPa)</b>	<b>E<sub>F</sub> (%)</b>	<b>E<sub>P</sub> (%)</b>	<b>Q (MPa)</b>
<b>1 h</b>	338	205	4.91	4.49	441
<b>2 h</b>	346	213	5.58	5.16	458
<b>4 h</b>	379	265	4.68	4.19	479
<b>6 h</b>	377	260	4.31	3.84	472
<b>8 h</b>	384	276	4.00	3.51	474
<b>10 h</b>	406	294	4.44	3.93	503
<b>12 h</b>	397	299	3.37	2.87	476
<b>16 h</b>	411	321	3.11	2.61	485
<b>24 h</b>	418	334	2.57	2.06	480
<b>32 h</b>	424	348	2.71	2.19	489
<b>40 h</b>	419	344	2.45	1.93	478
<b>48 h</b>	418	342	2.39	1.86	474
<b>72 h</b>	423	352	2.27	1.75	476

UTS, YS, E<sub>F</sub>, E<sub>P</sub>, and Q refer to ultimate tensile strength, yield strength, elongation to fracture, plastic elongation to fracture, and the quality index calculated using Equation 1, respectively.

(Note: "h" refers to hours.)

**Table A.8.** Tensile properties and quality index values for the 354 (10N) alloy after applying aging treatment at 170°C for various aging times.

Aging Time	UTS (MPa)	YS (MPa)	E <sub>F</sub> (%)	E <sub>P</sub> (%)	Q (MPa)
1 h	343	223	4.31	3.87	438
2 h	371	270	3.58	3.11	454
4 h	396	317	2.23	1.73	449
6 h	403	326	2.05	1.56	449
8 h	394	324	1.87	1.37	435
10 h	404	335	1.91	1.41	446
12 h	411	348	1.74	1.22	447
16 h	410	352	1.72	1.19	445
24 h	410	360	1.29	0.80	427
32 h	409	360	1.44	0.92	433
40 h	412	373	1.23	0.73	425
48 h	399	364	1.23	0.74	413
72 h	395	360	1.24	0.76	409

UTS, YS, E<sub>F</sub>, E<sub>P</sub>, and Q refer to ultimate tensile strength, yield strength, elongation to fracture, plastic elongation to fracture, and the quality index calculated using Equation 1, respectively.

(Note: "h" refers to hours.)

**Table A.9.** Tensile properties and quality index values for the 354 (10N) alloy after applying aging treatment at 195°C for various aging times.

<b>Aging Time</b>	<b>UTS (MPa)</b>	<b>YS (MPa)</b>	<b>E<sub>F</sub> (%)</b>	<b>E<sub>P</sub> (%)</b>	<b>Q (MPa)</b>
<b>5 min</b>	323	202	4.50	4.08	421
<b>10 min</b>	325	210	3.84	3.44	412
<b>15 min</b>	326	207	3.86	3.46	414
<b>30 min</b>	396	315	2.38	1.89	452
<b>45 min</b>	392	322	1.80	1.32	430
<b>1 h</b>	402	333	1.97	1.45	446
<b>2 h</b>	402	342	1.63	1.13	434
<b>4 h</b>	408	348	1.78	1.29	446
<b>6 h</b>	386	331	1.47	0.98	411
<b>8 h</b>	406	354	1.54	1.03	434
<b>10 h</b>	385	352	1.09	0.61	391
<b>12 h</b>	395	355	1.31	0.81	413
<b>16 h</b>	388	343	1.74	1.26	424
<b>24 h</b>	389	348	1.62	1.15	420
<b>32 h</b>	380	333	1.92	1.44	423
<b>40 h</b>	374	324	1.99	1.53	419
<b>48 h</b>	360	309	2.04	1.58	406
<b>72 h</b>	325	286	1.39	0.97	347

UTS, YS, E<sub>F</sub>, E<sub>P</sub>, and Q refer to ultimate tensile strength, yield strength, elongation to fracture, plastic elongation to fracture, and the quality index calculated using Equation 1, respectively.  
(Note: "min" and "h" refer to minutes and hours, respectively.)

**Table A.10.** Tensile properties and quality index values for the 354 (10N) alloy after applying aging treatment at 220°C for various aging times.

<b>Aging Time</b>	<b>UTS (MPa)</b>	<b>YS (MPa)</b>	<b>E<sub>F</sub> (%)</b>	<b>E<sub>P</sub> (%)</b>	<b>Q (MPa)</b>
<b>5 min</b>	322	189	4.71	4.30	423
<b>10 min</b>	319	195	4.22	3.82	413
<b>15 min</b>	334	222	3.72	3.31	420
<b>30 min</b>	399	325	2.16	1.66	449
<b>45 min</b>	388	328	1.67	1.18	421
<b>1 h</b>	400	332	2.06	1.58	447
<b>2 h</b>	369	316	1.49	1.03	395
<b>4 h</b>	367	326	1.39	0.93	389
<b>6 h</b>	366	320	1.74	1.27	402
<b>8 h</b>	363	310	1.99	1.57	408
<b>10 h</b>	348	293	2.06	1.62	395
<b>12 h</b>	326	264	2.20	1.78	378
<b>16 h</b>	313	245	2.38	1.99	370
<b>24 h</b>	315	245	2.46	2.07	374
<b>32 h</b>	288	219	2.16	1.79	338
<b>40 h</b>	276	186	3.66	3.28	361
<b>48 h</b>	288	207	2.89	2.51	357
<b>72 h</b>	279	188	3.45	3.09	359

UTS, YS, E<sub>F</sub>, E<sub>P</sub>, and Q refer to ultimate tensile strength, yield strength, elongation to fracture, plastic elongation to fracture, and the quality index calculated using Equation 1, respectively.

(Note: "min" and "h" refer to minutes and hours, respectively.)

**Table A.11.** Tensile properties and quality index values for the 354 (10N) alloy after applying aging treatment at 245°C for various aging times.

<b>Aging Time</b>	<b>UTS (MPa)</b>	<b>YS (MPa)</b>	<b>E<sub>F</sub> (%)</b>	<b>E<sub>P</sub> (%)</b>	<b>Q (MPa)</b>
<b>5 min</b>	324	215	3.77	3.37	411
<b>10 min</b>	358	276	2.48	2.02	417
<b>15 min</b>	379	321	1.64	1.17	412
<b>30 min</b>	353	311	1.24	0.81	367
<b>45 min</b>	356	310	1.35	0.92	376
<b>1 h</b>	348	312	1.41	0.96	371
<b>2 h</b>	350	291	1.81	1.36	389
<b>4 h</b>	339	273	1.86	1.44	379
<b>6 h</b>	317	236	2.51	2.09	377
<b>8 h</b>	316	228	2.86	2.45	384
<b>10 h</b>	293	199	2.87	2.45	362
<b>12 h</b>	301	211	3.19	2.80	376
<b>16 h</b>	292	195	3.52	3.13	374
<b>24 h</b>	276	174	3.49	3.11	357
<b>32 h</b>	279	175	3.88	3.52	368
<b>40 h</b>	258	155	3.82	3.45	345
<b>48 h</b>	261	161	3.28	2.93	338
<b>72 h</b>	252	144	4.34	3.97	347

UTS, YS, E<sub>F</sub>, E<sub>P</sub>, and Q refer to ultimate tensile strength, yield strength, elongation to fracture, plastic elongation to fracture, and the quality index calculated using Equation 1, respectively.  
(Note: "min" and "h" refer to minutes and hours, respectively.)

**Table A.12.** Tensile properties and quality index values for the 359 (1N) alloy after applying aging treatment at 155°C for various aging times.

<b>Aging Time</b>	<b>UTS (MPa)</b>	<b>YS (MPa)</b>	<b>E<sub>F</sub> (%)</b>	<b>E<sub>P</sub> (%)</b>	<b>Q (MPa)</b>
<b>1 h</b>	326	208	10.71	10.29	480
<b>2 h</b>	339	245	7.08	6.66	467
<b>4 h</b>	358	273	6.46	6.02	480
<b>6 h</b>	360	279	6.45	6.01	482
<b>8 h</b>	371	293	6.05	5.60	489
<b>10 h</b>	371	299	5.09	4.64	477
<b>12 h</b>	369	301	5.01	4.55	474
<b>16 h</b>	373	313	4.09	3.62	465
<b>24 h</b>	371	303	4.46	4.01	469
<b>32 h</b>	372	317	3.85	3.40	460
<b>40 h</b>	364	314	3.12	2.68	438
<b>48 h</b>	362	298	4.34	3.90	458
<b>72 h</b>	366	309	4.37	3.92	462

UTS, YS, E<sub>F</sub>, E<sub>P</sub>, and Q refer to ultimate tensile strength, yield strength, elongation to fracture, plastic elongation to fracture, and the quality index calculated using Equation 1, respectively.

(Note: "h" refers to hours.)

**Table A.13.** Tensile properties and quality index values for the 359 (1N) alloy after applying aging treatment at 170°C for various aging times.

<b>Aging Time</b>	<b>UTS (MPa)</b>	<b>YS (MPa)</b>	<b>E<sub>F</sub> (%)</b>	<b>E<sub>P</sub> (%)</b>	<b>Q (MPa)</b>
<b>1 h</b>	328	228	6.98	6.55	455
<b>2 h</b>	356	268	5.42	4.96	466
<b>4 h</b>	364	299	4.86	4.41	467
<b>6 h</b>	367	300	5.02	4.58	472
<b>8 h</b>	364	305	3.52	3.06	446
<b>10 h</b>	366	306	5.00	4.55	471
<b>12 h</b>	367	305	5.04	4.58	472
<b>16 h</b>	363	312	3.24	2.80	440
<b>24 h</b>	367	314	3.39	2.93	447
<b>32 h</b>	352	295	4.06	3.62	443
<b>40 h</b>	350	302	3.19	2.77	425
<b>48 h</b>	352	307	2.94	2.52	422
<b>72 h</b>	341	300	2.74	2.32	406

UTS, YS, E<sub>F</sub>, E<sub>P</sub>, and Q refer to ultimate tensile strength, yield strength, elongation to fracture, plastic elongation to fracture, and the quality index calculated using Equation 1, respectively.

(Note: "h" refers to hours.)

**Table A.14.** Tensile properties and quality index values for the 359 (1N) alloy after applying aging treatment at 195°C for various aging times.

<b>Aging Time</b>	<b>UTS (MPa)</b>	<b>YS (MPa)</b>	<b>E<sub>F</sub> (%)</b>	<b>E<sub>P</sub> (%)</b>	<b>Q (MPa)</b>
<b>5 min</b>	295	153	10.82	10.41	450
<b>10 min</b>	291	158	9.00	8.57	434
<b>15 min</b>	306	186	7.71	7.33	439
<b>30 min</b>	360	292	3.56	3.11	443
<b>45 min</b>	358	294	3.51	3.08	439
<b>1 h</b>	361	296	3.25	2.80	438
<b>2 h</b>	351	294	2.81	2.38	418
<b>4 h</b>	342	289	3.26	2.84	419
<b>6 h</b>	327	278	3.43	3.03	407
<b>8 h</b>	327	277	3.46	3.07	407
<b>10 h</b>	304	257	2.71	2.33	369
<b>12 h</b>	306	257	2.93	2.55	376
<b>16 h</b>	286	236	3.38	3.03	365
<b>24 h</b>	274	224	3.77	3.42	360
<b>32 h</b>	259	207	3.74	3.41	345
<b>40 h</b>	247	192	4.21	3.90	341
<b>48 h</b>	240	182	4.33	4.00	336
<b>72 h</b>	210	148	4.54	4.25	309

UTS, YS, E<sub>F</sub>, E<sub>P</sub>, and Q refer to ultimate tensile strength, yield strength, elongation to fracture, plastic elongation to fracture, and the quality index calculated using Equation 1, respectively.  
*(Note: "min" and "h" refer to minutes and hours, respectively.)*

**Table A.15.** Tensile properties and quality index values for the 359 (1N) alloy after applying aging treatment at 220°C for various aging times.

<b>Aging Time</b>	<b>UTS (MPa)</b>	<b>YS (MPa)</b>	<b>E<sub>F</sub> (%)</b>	<b>E<sub>P</sub> (%)</b>	<b>Q (MPa)</b>
<b>5 min</b>	295	172	9.52	9.13	442
<b>10 min</b>	306	191	9.33	8.92	452
<b>15 min</b>	337	263	5.32	4.87	446
<b>30 min</b>	353	301	3.65	3.19	437
<b>45 min</b>	343	298	2.67	2.26	407
<b>1 h</b>	333	285	3.86	3.45	421
<b>2 h</b>	317	272	4.29	3.89	412
<b>4 h</b>	285	237	4.29	3.91	379
<b>6 h</b>	267	215	4.35	3.99	363
<b>8 h</b>	255	201	4.47	4.15	353
<b>10 h</b>	247	189	4.55	4.23	345
<b>12 h</b>	236	183	4.94	4.61	340
<b>16 h</b>	224	169	4.83	4.52	326
<b>24 h</b>	211	156	4.71	4.43	312
<b>32 h</b>	195	139	5.57	5.30	307
<b>40 h</b>	187	130	5.71	5.43	300
<b>48 h</b>	188	132	5.70	5.45	301
<b>72 h</b>	172	114	6.83	6.59	297

UTS, YS, E<sub>F</sub>, E<sub>P</sub>, and Q refer to ultimate tensile strength, yield strength, elongation to fracture, plastic elongation to fracture, and the quality index calculated using Equation 1, respectively.

(Note: “min” and “h” refer to minutes and hours, respectively.)

**Table A.16.** Tensile properties and quality index values for the 359 (1N) alloy after applying aging treatment at 245°C for various aging times.

<b>Aging Time</b>	<b>UTS (MPa)</b>	<b>YS (MPa)</b>	<b>E<sub>F</sub> (%)</b>	<b>E<sub>P</sub> (%)</b>	<b>Q (MPa)</b>
<b>5 min</b>	311	221	7.44	7.04	442
<b>10 min</b>	352	298	3.80	3.34	439
<b>15 min</b>	318	273	3.21	2.79	394
<b>30 min</b>	287	244	4.38	4.01	383
<b>45 min</b>	283	242	3.99	3.62	374
<b>1 h</b>	274	229	4.98	4.62	378
<b>2 h</b>	249	196	4.87	4.53	352
<b>4 h</b>	228	170	5.22	4.91	336
<b>6 h</b>	211	151	5.24	4.94	319
<b>8 h</b>	200	141	5.42	5.14	310
<b>10 h</b>	186	128	6.48	6.21	308
<b>12 h</b>	184	125	6.31	6.04	304
<b>16 h</b>	171	112	6.88	6.62	297
<b>24 h</b>	168	106	7.41	7.18	299
<b>32 h</b>	155	93	8.73	8.47	296
<b>40 h</b>	146	82	10.75	10.53	301
<b>48 h</b>	148	84	10.51	10.29	302
<b>72 h</b>	140	75	11.58	11.38	300

UTS, YS, E<sub>F</sub>, E<sub>P</sub>, and Q refer to ultimate tensile strength, yield strength, elongation to fracture, plastic elongation to fracture, and the quality index calculated using Equation 1, respectively.

(Note: "min" and "h" refer to minutes and hours, respectively.)

---

## **APPENDIX B**

### **CHARACTERISTICS OF EUTECTIC SILICON PARTICLES**

**Table B.1.** Characteristics of eutectic silicon particles of 354 (10S) alloy as functions of solutionizing temperature applied for 12 h.

<b>Solutionizing Temperature</b>	<b>Average Area (<math>\mu\text{m}^2</math>)</b>	<b>SD</b>	<b>Average Length (<math>\mu\text{m}</math>)</b>	<b>SD</b>	<b>Average Aspect Ratio</b>	<b>SD</b>
<b>As-Cast</b>	3.08	7.34	2.60	2.92	1.93	0.83
<b>490°C</b>	6.10	7.10	3.23	2.34	1.70	0.99
<b>495°C</b>	5.36	7.14	3.05	2.31	1.70	1.18
<b>500°C</b>	5.33	7.16	3.01	2.28	1.61	0.76
<b>505°C</b>	6.20	7.51	3.27	2.39	1.69	0.92
<b>510°C</b>	7.07	8.99	3.42	2.62	1.67	0.97
<b>515°C</b>	7.75	9.57	3.49	2.57	1.60	0.83
<b>520°C</b>	7.82	9.76	3.57	2.59	1.67	0.97
<b>525°C</b>	8.08	9.20	3.62	2.45	1.58	0.92

SD refers to standard deviation.

**Table B.2.** Characteristics of eutectic silicon particles of 359 (1S) alloy as functions of solutionizing temperature applied for 12 h.

<b>Solutionizing Temperature</b>	<b>Average Area (<math>\mu\text{m}^2</math>)</b>	<b>SD</b>	<b>Average Length (<math>\mu\text{m}</math>)</b>	<b>SD</b>	<b>Average Aspect Ratio</b>	<b>SD</b>
<b>As-Cast</b>	2.90	6.87	2.27	2.49	1.90	0.71
<b>490°C</b>	5.89	6.63	3.07	2.86	1.77	1.17
<b>537°C</b>	8.19	8.80	3.63	2.35	1.66	1.00

SD refers to standard deviation.

**Table B.3.** Characteristics of eutectic silicon particles of unmodified 354 (10N) alloy as functions of solution heat treatment time applied at 520°C.

Solution Time	Average Area ( $\mu\text{m}^2$ )	SD	Average Length ( $\mu\text{m}$ )	SD	Average Aspect Ratio	SD
As-Cast	7.37	11.90	5.51	5.56	2.74	2.54
1 h	8.19	12.30	5.20	4.59	2.59	1.56
4 h	10.30	12.40	5.29	4.30	2.47	1.41
8 h	10.50	12.60	7.07	5.63	2.32	1.49
12 h	11.90	13.70	5.17	4.00	2.00	1.15
16 h	14.20	18.30	5.49	4.94	2.17	1.52
24 h	15.20	15.40	5.68	4.08	2.06	1.09

SD and h refer to standard deviation and hour, respectively.

**Table B.4.** Characteristics of eutectic silicon particles of modified 354 (10S) alloy as functions of solution heat treatment time applied at 520°C.

Solution Time	Average Area ( $\mu\text{m}^2$ )	SD	Average Length ( $\mu\text{m}$ )	SD	Average Aspect Ratio	SD
As-Cast	1.20	2.51	1.65	1.52	1.90	0.77
1 h	2.57	3.47	2.23	1.64	1.65	0.61
4 h	4.89	6.33	2.90	2.13	1.62	0.68
8 h	6.34	7.67	3.27	2.28	1.60	0.65
12 h	7.21	8.41	3.48	2.37	1.62	0.72
16 h	8.15	9.61	3.67	2.45	1.61	0.72
24 h	12.60	15.90	4.51	3.22	1.66	0.92

SD and h refer to standard deviation and hour, respectively.

**Table B.5.** Characteristics of eutectic silicon particles of unmodified 359 (1N) alloy as functions of solution heat treatment time applied at 537°C.

Solution Time	Average Area ( $\mu\text{m}^2$ )	SD	Average Length ( $\mu\text{m}$ )	SD	Average Aspect Ratio	SD
As-Cast	7.37	12.30	5.97	6.45	3.18	2.32
1 h	8.19	12.30	5.20	4.59	2.59	1.56
4 h	10.90	12.80	5.74	4.97	2.51	1.60
8 h	10.20	10.50	4.89	3.45	2.08	1.06
12 h	11.50	11.60	5.17	3.66	2.12	1.21
16 h	13.10	13.30	5.14	3.39	1.93	1.02
24 h	15.50	15.50	5.99	4.26	2.11	1.12

SD and h refer to standard deviation and hour, respectively.

**Table B.6.** Characteristics of eutectic silicon particles of modified 359 (1S) alloy as functions of solution heat treatment time applied at 537°C.

Solution Time	Average Area ( $\mu\text{m}^2$ )	SD	Average Length ( $\mu\text{m}$ )	SD	Average Aspect Ratio	SD
As-Cast	1.03	2.01	1.59	1.50	1.94	0.82
1 h	2.08	2.39	1.98	1.34	1.60	0.57
4 h	4.02	4.29	2.61	1.67	1.57	0.66
8 h	4.90	5.13	2.86	1.77	1.56	0.98
12 h	5.93	6.63	3.14	2.07	1.61	0.80
16 h	7.70	8.71	3.56	2.34	1.58	0.69
24 h	8.57	9.97	3.71	2.43	1.60	0.71

SD and h refer to standard deviation and hour, respectively.